



LIBRARY Michigan State University

This is to certify that the

dissertation entitled

THERMOSET POLYMER-LAYERED

SILICIC ACID NANOCOMPOSITES presented by

Zhen Wang

has been accepted towards fulfillment of the requirements for

Ph.D. degree in Chemistry

MSU is an Affirmative Action/Equal Opportunity Institution

0-12771

PLACE IN RETURN BOX to remove this checkout from your record. TO AVOID FINES return on or before date due. MAY BE RECALLED with earlier due date if requested.

	DATE DUE	DATE DUE	DATE DUE
	0GT 2 0 2002		
M.A	R & C 2903 ₀ 3		
:			

1/98 c:/CIRC/DateDue.p65-p.14

THERMOSET POLYMER-LAYERED SILICIC ACID NANOCOMPOSITES

By

Zhen Wang

A DISSERTATION

Submitted to
Michigan State University
in partial fulfillment of the requirements
for the degree of

DOCTOR OF PHILOSOPHY

Department of Chemistry

1997

ABSTRACT

THERMOSET POLYMER-LAYERED SILICIC ACID NANOCOMPOSITES

By

Zhen Wang

Nanocomposites are formed when phase mixing occurs on a nanometer length scale. Due to the improved phase morphology and interfacial properties, nanocomposites exhibit mechanical properties superior to conventional composites. Toyota researchers first demonstrated that organoclay could be exfoliated in a nylon-6 matrix to greatly improve the thermal and mechanical properties of the polymer, which has resulted in a practical application in the automobile industry. A great deal of research has been conducted on organic-inorganic hybrid composites in which smectite clays are used as reinforcement agents. However, little work has been devoted to derivatives of other layered inorganic solids. In the present work, the first examples of organic polymer-layered silicic acid nanocomposites have been prepared by formation of a cured epoxy polymer network in the presence of organo cation exchange forms of magadiite.

The exfoliation of silicate nanolayers in the epoxy matrix was achieved by *in-situ* intragallery polymerization during the thermosetting process. In general, the tensile properties, solvent resistance, barrier properties and chemical stability of the polymer matrix are greatly improved by the embedded silicate nanolayers when the matrix is flexible (sub-ambient Tg). The improvement of properties are dependent on the silicate loading, the degree of nanolayer separation and interfacial properties. Interestingly, the exfoliation also affects the polymer elasticity in a favorable way. The mechanism leading to nanocomposite formation is proposed. One exfoliated epoxy-magadiite nanocomposite/composition possessed unique transparent optical properties

The exfoliation chemistry was successfully extended to the other members of the layered silicic acid family. A new approach also was developed to prepare thermoset epoxy polymer-layered silicate nanocomposites in which curing agents can be directly intercalated into the intragallery without the need for alkylammonium ions on the exchange sites. This new development has resulted in a greater improvement in the overall properties of thermoset polymer-clay nanocomposites.

The exfoliation chemistry was extended further to other thermoset silicone polymer systems. The new polysiloxane-layered silicic acid nanocomposites were prepared with promising mechanical properties.

Some fundamental chemistry and physics issues regarding nanocomposite formation were elucidated by this research work, particularly with regard to the relationship of microstructure and interfacial factors to the mechanical properties of the nanocomposites.

To my parents, my sister and my wife for all their love and support.

ACKNOWLEDGMENTS

First and foremost, I would like to thank my advisor, Prof. Thomas J. Pinnavaia for his support and guidance over the years. I am grateful for his patience and inspiration during the experimental work and the shaping of this thesis. I would also like to thank Prof. Smith, Prof. Baker, Prof. Cukier and Prof. Giacin for serving on my committee.

I would like to express my true appreciation to all the Pinnavaia group members, past and present. I would especially like to thank Dr. Tie Lan for his friendship and helpful discussions, Prof. J. Wang for his assistance with TGA measurements, W. Zhang and Dr. Kim for their assistance with N_2 adsorption-desorption measurements, Dr. Massam for revising part of this thesis, Dr. Severin for her assistance with formatting my thesis, and Beth for her help with improving my English skills.

I am grateful to the staff of the MSU Composite Materials & Structures Center for their assistance in obtaining the mechanical testing data. The technical assistance of Dr. Huang of the x-ray powder diffraction facility is also greatly appreciated.

Financial support given by the Department of Chemistry Michigan State University, the Center for Fundamental Materials Research, National Science Foundation and Nanocor is gratefully acknowledged and appreciated.

My deepest gratitude goes to my parents and my sister. From a distance, I have always felt and received their support and encouragement over the last five years.

Finally, I am grateful to my wife Tao for all the love and encouragement she has given me over the years. Her patience and understanding during my over-night lab work were essential for the completion of this work.

TABLE OF CONTENTS

LIST OF TAE	BLESx	i
LIST OF FIG	URESx	iii
CHAPTER 1	INTRODUCTION	
1.1	Nanocomposite Materials	
	1.1.1 Nanocomposite Concept	
	1.1.2 Performance Properties of Nanocomposites	
	1.1.3 Formation of Nanocomposite Materials Through Sol-Gel	
	Approach 2	<u>)</u>
1.2	Polymer-Clay Nanocomposites2	<u>)</u>
	1.2.1 Layered Structures Suited for Nanocomposite Formation	<u>)</u>
	1.2.2 Introduction to Smectite Clay Structure	3
	1.2.3 Organo Clay Structures and Properties	;
	1.2.4 Types of Polymer-Clay Composites	,
	1.2.5 Intercalated Polymer-Clay Nanocomposites	. 1
	1.2.6 Exfoliated Nylon-6-Clay Nanocomposites	.3
	1.2.7 Recent Advances on Polymer-Exfoliated Clay	
	Nanocomposite Formation	6
1.3	Research Objectives	9
	1.3.1 Current Issues and New Directions	9
	1.3.2 Layered Silicic Acid Structures	22
	1.3.3 Research Goals	26
	1.4 References	28
CHAPTER 2	HYBRID ORGANIC-INORGANIC NANOCOMPOSITES FORMED FROM AN EPOXY POLYMER AND A LAYERED	
	SILICIC ACID (MAGADIITE)	3]
2.1	Introduction	R 1

2.2	Experi	mental	32
2.3	Result	s and Discussion	35
	2.3.1	Synthesis of Organo Magadiites	35
	2.3.2	Exfoliation of Magadiite Nanolayers in an Epoxy Polymer	
		Matrix	40
	2.3.3	Performance Properties of Exfoliated Epoxy-Magadiite	
		Nanocomposites	43
2.4	Conclu	asions	52
2.5	Refere	nces	54
CHAPTER 3	MECH	HANISM OF LAYERED SILICIC ACID NANOLAYER	
		LIATION IN EPOXY-MAGADIITE NANOCOMPOSITES	56
	2.2.0		
3.1	Introdu	uction	56
3.2	Experi	mental	57
3.3	Result	s and Discussion	60
	3.3.1	Synthesis of Organo Magadiites With Paraffin Structures	60
	3.3.2	Swelling Properties of Organo Magadiites	65
	3.3.3	Exfoliation of C18A1M-Magadiite in an Epoxy Matrix	69
	3.3.4	Mechanism of Silicate Nanolayer Exfoliation For Organo	
		Magadiites	71
	3.3.5	Effect of Gallery Acidity of Organo Magadiites on	
		Formation of Nanostructures	73
	3.3.6	Relationship Between Nanostructures and Performance	
		Properties	74
	3.3.7	Effect of Secondary Alkylamine and Alkylammonium ions	
		on Mechanical Properties	81
	3.3.8	Effect of Alkylammonium ions on Thermal Stability of	
		Nanocomposites	85
	3.3.9	More Evidences for Morphological Differences Between	
		Intercalated and Exfoliated Nanocomposites	87
3.4	Conclu	isions	
3.5		nces	

CHAPTER 4	HYBE	RID ORGANIC-INORGANIC NANOCOMPOSITES	
	FORM	MED FROM AN EPOXY POLYMER AND LAYERED	
	SILIC	IC ACIDS (KENYAITE AND ILERITE)	92
4.1	Introd	uction	92
4.2	Experimental		93
	4.2.1	Materials	93
	4.2.2	Synthesis of Layered Silicic Acids and Their Derivatives	
	4.2.3	Preparation of Epoxy-Layered Silicic Acid (Kenyaite and	
		Ilerite) Composites	95
	4.2.4	Characterization Methods	96
4.3	Result	ts and Discussion	96
	4.3.1	Exfoliation of Kenyaite Nanolayers in an Epoxy Polymer	
		Matrix	96
		4.3.1.1 Synthesis of Organo Kenyaites	96
		4.3.1.2 Exfoliation of C18-Kenyaite-PF in an Epoxy	
		Polymer Matrix	103
		4.3.1.3 Exfoliation of $C_nH_{2n+1}NH_3^+/C_nH_{2n+1}NH_2$ -kenyaites	
		in an Epoxy Polymer Matrix	106
		4.3.1.4 Effect of Gallery Acidity of Organo Kenyaites on	
		Exfoliation	109
	4.3.2		
		Matrix	112
		4.3.2.1 Synthesis of Organo Ilerites	
		4.3.2.2 Exfoliation of C18-Ilerite in an Epoxy Polymer	
		Matrix	114
	4.3.3	Performance Properties of Exfoliated Epoxy-Kenyaite and	
		Ilerite Nanocomposites	117
		4.3.3.1 Effect of Chain Length on Tensile Properties	
		4.3.3.2 Effect of Extent of Layer Separation on	
		Performance Properties	118
		4.3.3.3 Effect of Nanolayer Thickness on Performance	110
		Properties	121
4.4	Concl	usions	
4.5	Defer		123

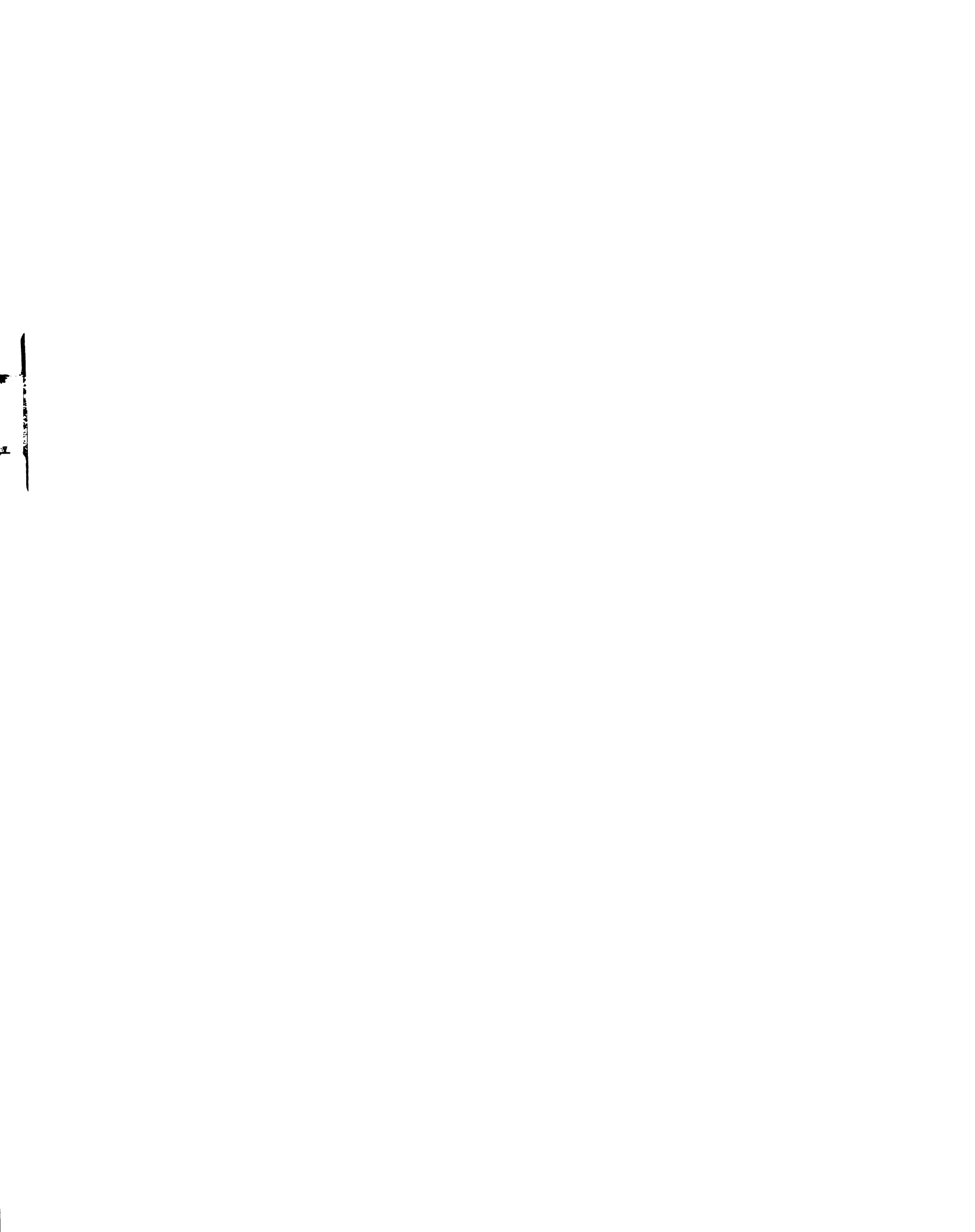
CHAPTER 5	HYBRID ORGANIC-INORGANIC NANOCOMPOSITES	
	FORMED FROM AN EPOXY POLYMER AND AN AMINE	
	CURING AGENT (JEFFAMINE) INTERCALATED IN	
	PROTON FORMS OF LAYERED SILICIC ACIDS	127
5.1	Introduction	127
5.2	Experimental	130
	5.2.1 Materials	130
	5.2.2 Synthesis of Layered Silicic Acids and Their Derivatives	130
	5.2.3 Preparation of Epoxy-Layered Silicic Acid Composites	
	Using Jeffamine-H-Layered Silicic Acid Intercalates	136
	5.2.4 Characterization Methods	136
5.3	Results and Discussion	137
	5.3.1 Synthesis of Jeffamine-H-Layered Silicic Acid Intercalates	137
	5.3.2 Exfoliation of Layered Silicic Acid Nanolayers in an Epoxy	
	Polymer Matrix Using Jeffamine-H-Layered Silicic Acid Intercalates	1.40
	5.3.3 Performance Properties of Exfoliated Epoxy-Layered	172
	Silicic Acid Nanocomposites Prepared by the Proton	
	Exchanged Pathway	161
5.4	Conclusions	
5.5	References	
3.3	References	1 / 1
CHAPTER 6	HYBRID NANOCOMPOSITES FORMED FROM AN	
	ORGANOFUNCTIONAL POLY(DIMETHYLSILOXANE)	
	POLYMER AND PROTON FORMS OF LAYERED SILICIC	
	ACIDS; AND THEIR USE FOR THE FORMATION OF HIGH	
	SURFACE AREA SILICAS	173
6.1	Introduction	173
6.2	Experimental	175
	6.2.1 Materials	175
	6.2.2 Synthesis of Layered Silicic Acids	176
	6.2.3 Preparation of PDMS-Layered Silicic Acid Composites	177
	6.2.4 Characterization Methods	
6.3	Results and Discussion	179

	6.3.1	Synthesis of PDMS-H-Layered Silicic Acid Intercalates179
	6.3.2	Exfoliation of Layered Silicic Acid Nanolayers in a Cured
		PDMS Matrix 182
	6.3.3	Performance Properties of Exfoliated PDMS-Layered
		Silicic Acid Nanocomposites
6.4	Concl	usions
6.5	Refer	ences

LIST OF TABLES

Table 1.1	Polymers Reported to Form Intercalated Polymer-Clay Nanocomposites	12
Table 1.2	Mechanical and Thermal Properties of Nylon 6-Clay Composites	14
Table 2.1	Intercalates Formed by Reaction of Na+-Magadiite with C ₁₈ H ₃₇ NH ₃ +Cl ⁻ and C ₁₈ H ₃₇ NH ₂	36
Table 2.2	Chemical and Solvent Resistance of Epoxy-Exfoliated Magadiite Nanocomposites Prepared From C18-magadiite-PF (9.1 wt %). Values are the Immersion Weight Gain (wt %) after a Certain Period.	50
Table 3.1	Intercalates Formed by Reaction of Na ⁺ -magadiite with $CH_3(CH_2)_{17}NH_{3-n}(CH_3)_n^+Cl^-$ and $CH_3(CH_2)_{17}NH_{2-n}(CH_3)_n$ (n = 0, 1, 2) or $CH_3(CH_2)_{17}N(CH_3)_3^+Br^-$ (n = 3)	63
Table 3.2	Basal Spacings (d ₀₀₁ , Å) for CH ₃ (CH ₂) ₁₇ NH _{3-n} (CH ₃) _n ⁺ -magadiite Paraffin Structures Under Air-dried Conditions and Solvated by Epoxy Resin (EPON 828), Poly(oxypropyleneamine) (D-2000) Curing Agent, and a Stoichiometric Mixture of These Polymer Precursors.	66
Table 4.1	Intercalates Formed by Reaction of K+-Kenyaite with $C_nH_{2n+1}NH_3$ +Cl ⁻ and $C_nH_{2n+1}NH_2$	100
Table 4.2	Effect of Chain Length of CH ₃ (CH ₂) _{n-1} NH ₃ +/CH ₃ (CH ₂) _{n-1} NH ₂ Gallery Surfactant on Tensile Properties of Epoxy-Kenyaite Nanocomposites. The organo kenyaite loading is 15 wt % for each composite.	118
Table 4.3	Chemical and Solvent Resistance of Epoxy-Layered Silicic Acid Nanocomposites Prepared From C18-magadiite-PF (9.1 wt %), C18-kenyaite-PF (10.4 wt %) and C18-ilerite (10.0 wt %). Values are the Immersion Weight Gains (wt %) after a Certain Period	124
Table 5.1	Synthesis of Alkali-Metal Forms of Layered Silicic Acids	131

Table 5.2	Synthesis of JEFFAMINE-H-Magadiite Intercalates Useful for Preparation of Epoxy-Exfoliated Layered Silicic Acid Nanocomposites	133
Table 5.3	Synthesis of JEFFAMINE-H-Kenyaite Intercalates Useful for Preparation of Epoxy-Exfoliated Layered Silicic Acid Nanocomposites	134
Table 5.4	Synthesis of JEFFAMINE-H-Ilerite Intercalates Useful for Preparation of Epoxy-Exfoliated Layered Silicic Acid Nanocomposites	135
Table 5.5	Basal Spacings (Å) of As-Synthesized Intercalates Formed From Layered Silicic Acids and JEFFAMINE D-Series and T-Series	146
Table 5.6	Synthesis Conditions for Formation of Powdered Forms of As- Synthesized JEFFAMINE-H-Layered Silicic Acid Intercalates	148
Table 5.7	Average Silicate Layer Separation (Å) for Regularly Exfoliated Epoxy-Magadiite Nanocomposites Prepared form D2000-H-magadiite Intercalates	156
Table 5.8	Chemical and Solvent Resistance of Epoxy-Exfoliated Layered Silicic acid Nanocomposites Prepared From D2000-H-silicic acid intercalates. The silicate (SiO ₂) loadings for each composite are 4.4 wt %, 6.4 wt % and 6.6 wt % for ilerite, magadiite and kenyaite respectively. Values are the Immersion Weight Gain (wt %) after Certain Uptake Periods.	169
Table 6.1	Synthesis of DMSA12-H-layered Silicic Acid Intercalates	178



LIST OF FIGURES

Figure 1.1	The layered framework of smectite clays. Each layer consists of two tetrahedral sheets cross-linking a central octahedral sheet. $M^{n+} \cdot xH_2O$ represents the interlayer exchangeable cation with its coordination water molecules. Each silicate nanolayer (sheet) has a 200 nm $\sim 2~\mu m$ of length in a x b dimensions, and about 1 nm of layer thickness.
Figure 1.2	Orientations of alkylammonium ions in the galleries of layered silicates with different layer charge densities
Figure 1.3	Schematic illustrations of (A) a conventional; (B) an intercalated; and (C) an exfoliated polymer-clay nanocomposites. The clay layers adopt an aggregated, intercalated, and exfoliated morphology, respectively, in each type of composite. The clay interlayer spacing is fixed in an intercalated nanocomposite, on the other hand, the average gallery height is determined by clay silicate loading in an exfoliated nanocomposite.
Figure 1.4	Schematic illustration of (A) a disordered exfoliated and (B) an ordered exfoliated polymer-clay nanocomposites. The onium ion is represented by and the polymer chain by (Polym.). he is the average gallery height for the exfoliated polymer-clay nanocomposites. ho is the gallery height expected for a lipid-like bilayer of onium ions.
Figure 1.5	Injection-molded NCH (nylon 6-clay hybrid) timing belt cover15
Figure 1.6	Proposed model for the torturous zigzag diffusion path in an exfoliated polymer-clay nanocomposite when used as a gas barrier18
Figure 1.7	Proposed model for the fracture of (A) a glassy and (B) a rubbery polymer-clay exfoliated nanocomposite with increasing strain
Figure 1.8	Interfacial interactions in a polymer-layered silicate nanocomposite: (A) Electrostatic binding of onium ion to the clay surfaces; (B) "Dissolution" of the alkyl chains into the polymer matrix by van der Waals forces; (C) Physical sorption of polymer to the siloxane oxygen atoms of the basal surfaces; (D) Polymer sorption to hydroxyl-terminated edge sites

^k igure 1.9	Magadiite structure postulated by Garces et al. The presence of a bilayer of interlayer water molecules is based on the basal spacing of 15.6 Å for Na ⁺ -magadiite
Figure 1.10	Schematic representation (edge-view) of the layered silicic acids. The silicate layers are formed by sharing of apical oxygen atoms between tetrahedral SiO ₄ sheets for ilerite, magadiite and kenyaite. The thickness of the layers differs depending on the degree of cross-linking between stacked sheets
Figure 2.1	X-ray powder diffraction patterns of (A) air-dried Na ⁺ -magadiite; (B) CH ₃ (CH ₂) ₁₇ NH ₃ ⁺ -magadiite with a lateral monolayer (LM) structure. Patterns (C) and (D) are for mixed CH ₃ (CH ₂) ₁₇ NH ₃ ⁺ /CH ₃ (CH ₂) ₁₇ NH ₂ -magadiite with a paraffin (PF) and a lipid bilayer (BL) gallery structure, respectively. The LM structure contains no free amine (0.45 onium ions per Si ₁₄ O ₂₉ formula unit), whereas PF and BL structures contain neutral primary amine molecules, in addition to primary onium ions
Figure 2.2	Thermogravimetric analysis curves of (A) air-dried Na ⁺ -magadiite; (B) CH ₃ (CH ₂) ₁₇ NH ₃ ⁺ -magadiite with a lateral monolayer (LM) structure. Patterns (C) and (D) are for mixed CH ₃ (CH ₂) ₁₇ NH ₃ ⁺ /CH ₃ (CH ₂) ₁₇ NH ₂ -magadiite with a paraffin (PF) and a lipid bilayer (BL) gallery structure, respectively
Figure 2.3	X-ray diffraction pattern of the initial mixture product in an effort to obtain C18-magadiite-PF. The mixture was formed when Na+magadiite was ion exchanged by CH ₃ (CH ₂) ₁₇ NH ₃ +/CH ₃ (CH ₂) ₁₇ NH ₂ followed by ethanol washing. The tabulated values in the insert are d ₀₀₁ values for the lipid bilayer and paraffin phases. 439
Figure 2.4	X-ray diffraction patterns of C18-magadiite-PF in different physical states: (A) pristine organo magadiite; (B) 10 wt % organo magadiite solvated by epoxide resin (EPON 828) at 75 °C for 90 min
Figure 2.5	X-ray diffraction patterns of products prepared by reaction of (A) C18-magadiite-PF (15 wt % loading) with epoxide resin and poly(oxypropyleneamine) curing agent at an epoxide group to amine group molar ratio of 2:1. Reaction conditions were as follows: (B) 25 °C, 60 min; (C) 75 °C, 5 min; (D) 75 °C, 15 min; (E) 75 °C, 3 h; (F) 75 °C, 3 h and 125 °C, 5 min; (G) 75 °C, 3 h and 125 °C, 10 min. The 00l lines marked with an asterisk are from the initial paraffin structure of the organo magadiite
Figure 2.6	X-ray diffraction pattern of a cured epoxy polymer-magadite nanocomposite prepared from C18-magadite-PF. The organo silicate content was 15 wt % Polymer curing was carried out at 75

	°C for 3 h, and followed by 3 h at 125 °C
<i>Fig</i> ure 2.7	Comparison of the tensile strengths of an epoxy-exfoliated magadiite nanocomposite prepared from C18-magadiite-PF and conventional magadiite composites prepared from Na ⁺ -magadiite and C18-magadiite-LM. The inorganic silicate loading was determined by calcining the composites in air at 650 °C for 4 hours using a heating rate of 2 °C/min. The onium ion and amine content of the organo magadiite was counted as contributing to the stoichiometry of epoxide cross-linking
Figure 2.8	X-ray diffraction patterns of products prepared by reaction of (A) C18-magadiite-BL (15 wt % loading) with epoxide resin and poly(oxypropyleneamine) curing agent at an epoxide group to amine group molar ratio of 2:1. Reaction conditions were as follows: (B) 75 °C, 60 min; (C) 75 °C, 120 min. The inset is a pattern for the cured epoxy polymer-magadiite nanocomposite prepared from C18-magadiite-BL. The marked sharp lines in pattern (B) are derived from the octadecylamine
Figure 2.9	Effect of octadecylammonium and octadecylamine on the tensile modulus of epoxy-exfoliated magadiite nanocomposites prepared from C18-magadiite-PF. The solid line is for composites formed by including the onium ion and neutral amine content of the organo magadiite as a curing agent for epoxide crosslinking and reducing the amount of poly(oxypropyleneamine) accordingly; the dash line is for composites formed by disregarding the crosslinking reactivity of the gallery onium ion and amine in the initial intercalate and curing the resin with 1 equiv of poly(oxypropyleneamine). The values given in parenthesis for curve B are the molar fractions of excess alkylamine functional groups contributed by the onium ions and free amine relative to poly(oxypropyleneamine).
Figure 2.10	Effect of octadecylammonium and octadecylamine on the strain-at- break values of epoxy-exfoliated magadiite nanocomposite prepared from C18-magadiite-PF. The dashed line is for composites formed by not counting onium ion and amine content of the organo magadiite as contributing to the stoichiometry for epoxide crosslinking, the solid line is reversed. The values in parenthesis give the amount of excess amine curing agent due to the organo magadiite component.
Figure 2.11	Chemical reagent and solvent uptake of (A) 30% sulfuric acid; (B) 5% acetic acid; (C) methanol; and (D) toluene by epoxy-exfoliated magadiite nanocomposites prepared from C18-magadiite-PF (9.1 wt %)
Figure 2.12	Comparison of the optical properties among (A) a pristine epoxy polymer; (B) an epoxy-exfoliated magadiite nanocomposite prepared form C18-magadiite-PF; (C) an epoxy-exfoliated smectite clay nanocomposite prepared from CH ₂ (CH ₂) ₁ -NH ₂ + ion-

	thickness of each sample is ~ 1 mm. Polymer curing was carried out at 75 °C for 3 h, and followed by 3 h at 125 °C	53
Figure 3.1	X-ray powder diffraction patterns of air-dried Na ⁺ -magadiite and $CH_3(CH_2)_{17}NH_{3-n}(CH_3)_n$ ⁺ -intercalated magadiites (n = 0, 1, 2, 3). The organo magadiites have paraffin-like gallery structures with onium ion and free amine compositions given in Table 1	62
Figure 3.2	Effect of washing on the formation of C18A1M-magadiite. The product in Pattern (A) was obtained by centrifuging the secondary alkylammonium exchanged reaction mixture without further treatment. The product in pattern (B) was formed when the onium ion exchanged reaction mixture was washed with an equal volume of ethanol. The paraffin phase in pattern (C) was obtained by washing the product of pattern (B) with 50% EtOH	64
Figure 3.3	X-ray diffraction patterns of products prepared by reaction of C18A2M-magadiite (15 wt % loading) with a stoichiometric mixture of epoxide resin and poly(oxypropyleneamine) curing agent under the reaction conditions as follows: (A) 75 °C, 10 min; (B) 75 °C, 90 min; (C) 75 °C, 120 min; (D) 75 °C, 3 h and 125 °C, 20 min.	67
Figure 3.4	X-ray diffraction patterns of products prepared by reaction of C18A3M-magadiite (20 wt % loading) with a stoichiometric mixture of epoxide resin and poly(oxypropyleneamine) curing agent under the reaction conditions as follows: (A) 75 °C, 10 min; (B) 75 °C, 30 min; (C) 75 °C, 45 min.	68
Figure 3.5	X-ray diffraction patterns of products prepared by reaction of C18A1M-magadiite (15 wt % loading) with a stoichiometric mixture of epoxide resin and poly(oxypropyleneamine) curing agent (epoxide group to amine group molar ratio of 2:1). Reaction conditions were as follows: (A) 25 °C, 30 min; (B) 75 °C, 10 min; (C) 75 °C, 15 min; (D) 75 °C, 30 min; (E) 75 °C, 60 min; (F) 75 °C, 70 min; (G) 75 °C, 90 min.	70
Figure 3.6	Proposed pathway for epoxy-magadiite exfoliated nanocomposite formation: (A) An organo magadiite with paraffin-like gallery structure of onium ions and neutral amine (see Table 3.1 for compositions). (B) An intercalate formed when long chain alkylammoniums reorienting from a paraffin to a lipid bilayer orientation to accommodate the co-intercalation of epoxide and curing agent. (C) The gallery height exceeds the value characteristic of a lipid bilayer due to the rapid intragallery polymerization rate. The silicate platelets start to tilt. The chain formation (gelation) is the main reaction for the epoxide and amino groups at this stage of the process. (D) Silicate nanolayers are completely exfoliated in a fully cross-linked epoxy polymer network.	72
	characteristic of a lipid bilayer due to the rapid intragallery polymerization rate. The silicate platelets start to tilt. The chain formation (gelation) is the main reaction for the epoxide and amino groups at this stage of the process. (D) Silicate nanolayers are	

Figure 3.7	X-ray diffraction patterns of cured epoxy polymer-magadiite nanocomposites prepared from $CH_3(CH_2)_{17}NH_{3-n}(CH_3)_n^+$ -magadiites with a paraffin gallery structure (cf. Table 3.1). The organo magadiite loading is 15 wt % (n = 0) or 20 wt % (n = 1, 2,
	3). Polymer curing was carried out at 75 °C for 3 h, followed by 3
	h at 125 °C. The primary and secondary onium ions (n = 0, 1) give highly exfoliated (disordered) nanocomposites (d > 90 Å). The tertiary onium ion derivative (n = 2) also gives an exfoliated nanocomposite, but the layer separation is highly ordered (d = 78 Å). The quaternary onium ion exchange form (n = 3) forms an intercalated nanocomposite (d = 41 Å)
Figure 3.8	A comparison of the tensile strengths of epoxy-magadiite nanocomposites prepared from CH ₃ (CH ₂) ₁₇ NH _{3-n} (CH ₃) _n ⁺ -magadiites. The magadiite silicate loading (expressed on wt % SiO ₂) was determined by calcining the composites in air at 650 °C
	for 4 hours using a heating rate of 2 °C/min. The secondary alkylammonium (n = 2) and the free amine content of CH ₃ (CH ₂) ₁₇ NH ₂ CH ₃ +-magadiite was counted as contributing to the stoichiometry for epoxide cross-linking at magadiite loadings > 10 wt %.
Figure 3.9	X-ray diffraction patterns of CH ₃ (CH ₂) _{n-1} N(CH ₃) ₃ +-magadiites in different physical states: (A) organo magadiite; (B) intercalated magadiite (10 wt %) in an cured epoxy nanocomposite
Figure 3.10	A comparison of the tensile strengths of epoxy-magadiite intercalated nanocomposites prepared from CH ₃ (CH ₂) _{n-1} N(CH ₃) ₃ +-magadiites. The magadiite silicate loading was determined by calcining the composites in air at 650 °C for 4 hours using a heating rate of 2 °C/min.
Figure 3.11	Toluene uptake by nanocomposites prepared from $CH_3(CH_2)_{17}NH_{3-n}(CH_3)_n^+$ -magadiites (n = 1, 2, 3). The tabulated values in the insert are equilibrium data determined by the immersion weight gain after 24 hr. The loading of organomagadiite is 10 wt % for each epoxy-magadiite composite80
Figure 3.12	A comparison of (A) the tensile strengths and (B) the tensile moduli between epoxy-magadiite exfoliated nanocomposites prepared from C18A1M-magadiite and C18-magadiite-PF, and epoxy-smectite clay exfoliated nanocomposite prepared from CH ₃ (CH ₂) ₁₇ NH ₃ ⁺ ion-exchange montmorillonite (from Wyoming). The silicate loading was determined by calcining the composites in air at 650 °C for 4 hours using a heating rate of 2 °C/min

Figure 3.13	Effect of methyloctadecylammonium and methyloctadecylamine on (A) the tensile strengths; (B) the tensile moduli; (C) the strainat-break values of epoxy-exfoliated magadiite nanocomposites prepared from C18A1M-magadiite. The solid line is for composites formed by including the secondary onium ion and neutral amine content of the organo magadiite as curing agents for epoxide cross-linking and reducing the amount of poly(oxypropyleneamine) (D-2000) accordingly; the dash line is for composites formed at an epoxy-D-2000 stoichiometry that disregards the reactivity of the gallery secondary onium ion and amine in the initial intercalate. The values in parenthesis for the dash curves are the molar fraction of excess secondary amine functional groups relative to D-2000.	83
Figure 3.14	Comparison of the stain-at-break values among the exfoliated epoxy-magadiite nanocomposites prepared from C18A1M-magadiite, the intercalated nanocomposites prepared from C18A3M-magadiite, and the conventional composites prepared from C18-magadiite-LM with a lateral monolayer structure	84
Figure 3.15	Thermogravimetric analysis curves for (A) epoxy-exfoliated magadiite nanocomposite prepared from C18A1M-magadiite and (B) intercalated nanocompsoite formed from C18A3M-magadiite. The loading of organo magadiite is 20 wt % for each epoxy-magadiite nanocomposite. Curves (C) and (D) are for the pristine organo magadiites of C18A1M-magadiite and C18A3M-magadiite, respectively. The analysis was carried out in N ₂ atmosphere with a	97
	heating rate of 5 °C/min	86
Figure 3.16	X-ray powder diffractions for the silica formed from upon calcination of (A) the exfoliated nanocomposite prepared form C18A-magadite-PF; and (B) the intercalated nanocomposite prepared from C18A3M-magadite. The expanded inset for the d ₀₀₁ peaks was obtained using a step scan mode. The calcination condition is at 650 °C for 4 h in air using a heating rate of 2 °C/min	88
Figure 3.17	N ₂ adsorption-desorption isotherms for the silicas obtained by calcination of an epoxy-exfoliated magadiite nanocomposite prepared from C18-magadiite-PF (top curve) and an intercalated nanocomposite prepared from C18A3M-magadiite (bottom curve). The organo magadiite loading for each composite is 10 wt %. The calcination was carried out at 650 °C for 4 hr in air using a heating rate of 2 °C/min	80
Figure 4.1	X-ray powder diffraction patterns of air-dried K+-kenyaite and CH ₃ (CH ₂) _{n-1} NH ₃ +/CH ₃ (CH ₂) _{n-1} NH ₂ -kenyaites. The gallery structures and compositions are given in Table 4.1.	89
Figure 4.2	Thermogravimetric analysis curves for air-dried K+-kenyaite and CH ₃ (CH ₂) _{n-1} NH ₃ +/CH ₃ (CH ₂) _{n-1} NH ₂ -kenyaites. The gallery	

	structures and compositions derived from these curves are give in Table 4.1	101
Figure 4.3	X-ray powder diffraction patterns of (A) C8-kenyaite-GB (gauche block structure) obtained by applying a film of the wet product on a glass slide right after centrifuging the reaction mixture; (B) airdried C8-kenyaite-GB with a less ordered gauche block gallery structure; (C) CH ₃ (CH ₂) ₇ NH ₃ +-kenyaite with a lateral bilayer	
	gallery structure obtained by thorough washing of the C8-kenyaite-GB to remove excess amine	102
Figure 4.4	X-ray diffraction patterns of (A) pristine C18-kenyaite-PF and (B-E) the partially cured composites prepared by reaction of C18-kenyaite-PF (14.6 wt % loading) with a stoichiometric mixture of epoxide resin (EPON 828) and poly(oxypropyleneamine) (Jeffamine D-2000) curing agent. The primary alkylammonium and the free amine content of C18-kenyaite-PF was counted as contributing to the stoichiometry for epoxide cross-linking. Reaction conditions were as follows: (B) 25 °C, 60 min; (C) 75 °C, 30 min; (D) 75 °C, 40 min; (E) 75 °C, 120 min.	104
Figure 4.5	X-ray diffraction pattern of a cured epoxy polymer-kenyaite nanocomposite prepared from C18-kenyaite-PF. The organo kenyaite loading was 14.6 wt %. Polymer curing was carried out at 75 °C for 3 h, and followed by 3 h at 125 °C. The sharp lines are the in-plane reflections of the exfoliated kenyaite layers	105
Figure 4.6	XRD patterns of partially cured composites prepared by reaction of $CH_3(CH_2)_{n-1}NH_3+/CH_3(CH_2)_{n-1}NH_2$ -kenyaites (n = 6, 8, 10, 12 and 18) with a stoichiometric mixture of epoxide resin and poly(oxypropyleneamine) curing agent. The organo kenyaite loading is 15 wt % for n = 6, 10, 12, 18, and 30 wt % for n = 8. The reactions were carried out at 25 °C for 5 min to 60 min for n ≤ 12, and at 75 °C, 30 min for n = 18. The sharp lines in the patterns for n = 10, 12 are attributed to phase-segregated amine.	
Figure 4.7	X-ray diffraction patterns of cured epoxy-kenyaite nanocomposites prepared from CH ₃ (CH ₂) _{n-1} NH ₃ +/CH ₃ (CH ₂) _{n-1} NH ₂ -kenyaites (n = 6, 8, 10, 12 and 18). The organo kenyaite loading for each composite was 15 wt %. Polymer curing was carried out at 75 °C for 3 h, and followed by 3 h at 125 °C	108
Figure 4.8	X-ray powder diffraction patterns of $CH_3(CH_2)_{17}NH_{3-n}(CH_3)_n^+$ - kenyaites (n = 1, 2, 3). All of the organo kenyaites have paraffin- like gallery structures	110
Figure 4.9	X-ray diffraction patterns of cured epoxy polymer-kenyaite nanocomposites prepared from $CH_3(CH_2)_{17}NH_{3-n}(CH_3)_n^+$ -kenyaites with a paraffin gallery structure. The organo kenyaite loading was 20 wt % (n = 1, 3) and 10 wt % (n = 2). Polymer	

	curing was carried out at 75 °C for 3 h, followed by 3 h at 125 °C. The secondary onium ions (n = 1) give highly exfoliated (disordered) nanocomposites (d > 90 Å). The tertiary onium ion derivative (n = 2) also gives an exfoliated nanocomposite, but the layer separation is highly ordered (d = 72 Å). The quaternary onium ion exchange form (n = 3) forms an intercalated nanocomposite (d = 44 Å)
Figure 4.10	X-ray powder diffraction patterns of air-dried (A) Na ⁺ -ilerite; (B) H ⁺ -ilerite; and (C) CH ₃ (CH ₂) ₁₇ NH ₃ ⁺ -ilerite (C18-ilerite)
Figure 4.11	X-ray diffraction patterns of the partially cured composites prepared by reaction of C18-ilerite (15 wt % loading) with a stoichiometric mixture of epoxide resin and poly(oxypropyleneamine) curing agent. The primary alkylammonium and the free amine content of C18-ilerite was counted as contributing to the stoichiometry for epoxide cross-linking. Reaction conditions were as follows: (A) 25 °C, 20 min; (B) 75 °C, 40 min; (C) 75 °C, 100 min; (D) 75 °C, 150 min
Figure 4.12	X-ray diffraction pattern of a cured epoxy polymer-ilerite nanocomposite prepared from C18-ilerite. The organo ilerite loading was 15 wt %. Polymer curing was carried out at 75 °C for 3 h, and followed by 3 h at 125 °C. The sharp peaks at 3.69 Å and 1.87 Å are the in-plane reflections of ilerite. The broad peaks at $2\Theta = 20^{\circ}$, 42° are due to the polymer matrix
Figure 4.13	A comparison of the tensile strengths of epoxy-kenyaite nanocomposites prepared from CH ₃ (CH ₂) ₁₇ NH _{3-n} (CH ₃) _n ⁺ -kenyaites. The kenyaite silicate loading (expressed on wt % SiO ₂) was determined by calcining the composites in air at 650 °C for 4 h using a heating rate of 2 °C/min. The secondary alkylammonium and the free amine content of CH ₃ (CH ₂) ₁₇ NH ₂ CH ₃ ⁺ -kenyaite (n = 2) was counted as contributing to the stoichiometry for epoxide cross-linking
Figure 4.14	Toluene uptake curves for nanocomposites prepared from CH ₃ (CH ₂) ₁₇ NH _{3-n} (CH ₃) _n +-kenyaites (n = 1, 2, 3). The tabulated values in the insert are equilibrium data obtained from the immersion weight gain after 24 hr. The loading of organokenyaite is 10 wt % for each epoxy-kenyaite composite
Figure 4.15	Comparison of (A) tensile strengths and (B) tensile moduli for epoxy-exfoliated ilerite nanocomposites prepared from C18-ilerite and epoxy-intercalated ilerite composites prepared from C18A3M-ilerite. The primary onium ion and amine content of the organo ilerite was counted as contributing to the stoichiometry of epoxide

`'gure 4.16	A comparison of the tensile strengths between epoxy-magadite and epoxy-kenyaite nanocomposites prepared from (A) primary; (B) secondary; (C) tertiary; (D) quaternary alkylammonium exchanged CH ₃ (CH ₂) ₁₇ NH _{3-n} (CH ₃) _n +-layered silicic acids	123
Figure 5.1	XRD patterns of air-dried proton exchanged forms of layered silicic acids: (A) H+-ilerite; (B) H+-magadiite; (C) H+-kenyaite	138
Figure 5.2	XRD patterns for the as-synthesized (unwashed) intercalates formed from H ⁺ -magadiite and poly(oxypropyleneamines): (A) Jeffamine D-series; and (B) Jeffamine T-series	140
Figure 5.3	XRD patterns for the as-synthesized intercalates (unwashed) formed from H ⁺ -kenyaite and poly(oxypropyleneamines): (A) Jeffamine D-series; and (B) Jeffamine T-series	141
Figure 5.4	XRD patterns for the as-synthesized (unwashed) intercalates formed from H ⁺ -ilerite and poly(oxypropyleneamines) Jeffamine T-series.	142
Figure 5.5	XRD patterns of the intercalates formed from H ⁺ -kenyaite and the poly(oxypropyleneamine) Jeffamine D4000: (A) as-synthesized (unwashed); (B) washed one time with ethanol; and (C) washed multiple times with ethanol	144
Figure 5.6	TGA curves for H-kenyaite and D4000-H-kenyaite intercalates with different basal spacings (cf. Figure 5.5)	145
Figure 5.7	XRD patterns of (A) the initial D2000-H-magadiite intercalate and the nanocomposites formed at 20 wt % D2000-H-magadiite intercalate loading by reaction of stoichiometric mixtures of epoxide and the poly(oxypropyleneamine) under the following reaction conditions: (B) 25 °C, 60 min; (C) 75 °C, 60 min; (D) 75 °C, 120 min; (E) 75 °C, 150 min.	150
Figure 5.8	XRD patterns of (A) the initial D2000-H-kenyaite intercalate and the nanocomposites formed at 20 wt % D2000-H-kenyaite intercalate loading by reaction of stoichiometric mixtures of epoxide and the poly(oxypropyleneamine) under the following reaction conditions: (B) 25 °C, 2 min; (C) 25 °C, 10 min; (D) 75 °C, 30 min.	151
Figure 5.9	XRD patterns of (A) the initial D2000-H-ilerite intercalate and the nanocomposites formed at 20 wt % D2000-H-ilerite intercalate loading by reaction of stoichiometric mixtures of epoxide and the poly(oxypropyleneamine) under the following reaction conditions: (B) 25 °C, 5 min; (C) 75 °C, 5 min; (D) 75 °C, 135 min.	152
Figure 5.10	XRD patterns for the epoxy-layered silicic acid nanocomposites formed from the following intercalates: (A) D2000-H-ilerite; (B) D2000-H-magadite: (C) D2000-H-kenyajte. The D2000 layered	

	silicic acid intercalate loadings are 20 wt %, 10 wt % and 15 wt % for ilerite, magadiite and kenyaite, respectively. The intercalated curing agent was counted as contributing to the stoichiometry for epoxide cross-linking.	154
Figure 5.11	XRD patterns of cured epoxy-magadiite nanocomposites (curing conditions: at 75 °C for 3 h, and followed by 3 h at 125 °C) prepared from D2000-H-magadiite intercalates. The D2000-H-magadite intercalate loadings were as follows: (A) 5 wt %; (B) 10 wt %; (C) 20 wt %; (D) 30 wt %; (E) 40 wt %; and (F) 50 wt %	155
Figure 5.12	XRD patterns for the silica formed from upon calcination of (A) D2000-H-magadiite intercalate with a 54.6 Å basal spacing and containing 50 wt % H-magadiite; and (B) an exfoliated epoxymagadiite nanocomposite prepared form the D2000-H-magadiite intercalate with a 44.0 Å basal spacing and containing 5 wt % H-magadiite. The expanded insert for the d ₀₀₁ peaks was obtained using a step scan mode. The calcinations were carried out at 650 °C for 4 h in air using a heating rate of 2 °C/min.	157
Figure 5.13	N ₂ adsorption-desorption isotherms for the silicas obtained by calcination of an epoxy-exfoliated magadiite nanocomposite prepared from D2000-H-magadiite intercalate with a 44.0 Å basal spacing and containing 5 wt % H-magadiite (top curve); and the D2000-H-magadiite intercalate with a 54.6 Å basal spacing containing 50 wt % H-magadiite (bottom curve). The calcinations were carried out at 650 °C for 4 h in air using a heating rate of 2 °C/min.	159
Figure 5.14	Possible types of morphologies for silicate nanolayer aggregates formed upon calcination. The card house structure is predominant for the magadiite recovered by calcination of an exfoliated epoxymagadiite nanocomposite. Restacked layers are more predominant in the magadiite obtained by calcination of a well ordered D2000-H-magadiite intercalate.	160
Figure 5.15	Comparison of tensile properties for exfoliated nanocomposites prepared from D2000-H-magadiite intercalates and organo magadiite intercalates with a paraffin structure (C18-magadiite-PF and C18A1M-magadiite)	162
Figure 5.16	Comparison of methanol uptake curves for epoxy-exfoliated magadiite nanocomposites prepared from C18-magadiite-PF intercalates and D2000-H-magadiite intercalates. The tabulated values are the loadings (wt %) of C18-magadiite-PF intercalate and D2000-H-magadiite intercalate for each composite.	164
Figure 5.17	Comparison of toluene uptake curves for epoxy-exfoliated magadiite nanocomposites prepared from C18-magadiite-PF intercalates and D2000-H-magadiite intercalates. The tabulated values are the loadings (wt %) of C18-magadiite-PF intercalate and D2000-H-magadiite intercalate for each composite.	165

Figure 5.18	Comparison of methanol and toluene uptake at equilibrium vs. magadiite silicate (SiO ₂) loading for epoxy-exfoliated magadiite nanocomposites prepared form C18-magadiite-PF and D2000-H-magadiite intercalates.	166
Figure 5.19	Tensile properties for the epoxy-kenyaite nanocomposites prepared from D2000-H-kenyaite intercalates before and after having been swollen in toluene. In the solvent swelling experiment the nanocomposites were soaked in toluene for 12 h, and subsequently dried in air for 24 h before the tensile properties were measured	167
Figure 5.20	A comparison of the tensile strength vs. silicate loading for epoxy- layered silicic acid nanocomposites prepared from D2000-H- layered silicic acid intercalates.	168
Figure 6.1	XRD patterns of intercalates formed by reaction of aminopropyl terminated polydimethylsiloxane (DMSA12) and (A) H-ilerite; (B) H-magadiite; and (C) H-kenyaite in ethanol/H ₂ O (cf. Table 6.1) and air-dried without washing.	181
Figure 6.2	XRD patterns of (A) the initial DMSA12-H-kenyaite intercalate and the partially cured composites formed at 15 wt % H-kenyaite loading by reaction of a stoichiometric mixture of DMSA12 and DMSE12 under the following reaction conditions: (B) 50 °C, 30 min; (C) 50 °C, 22 h; (D) 50 °C, 24 h and 125 °C, 10 min. The pattern (E) is for the fully cured PDMS-kenyaite composite that was cured first at 50 °C for 24 h and then at 125 °C for 6 h	183
Figure 6.3	XRD patterns of the cured PDMS-exfoliated layered silicic acid nanocomposites prepared from the intercalates formed between DMSA12 and (A) H-magadiite; and (B) H-kenyaite. The H-silicic acid loading for each composite is 10 wt %. Polymer curing was carried out at 50 °C for 24 h, and followed by 6 h at 125 °C	184
Figure 6.4	XRD patterns for the silica-intercalated kenyaites obtained by calcination of the PDMS-exfoliated kenyaite nanocomposites at 540 °C for 10 h with a heating rate of 1 °C/min. The H-kenyaite loading was (A) 8.2 wt %; and (B) 15 wt %. Pattern (C) is for the DMSA12-H-kenyaite intercalate after the same calcination conditions.	186
Figure 6.5	N ₂ adsorption-desorption isotherm for the silica residue obtained by calcining the PDMS-exfoliated kenyaite nanocomposite prepared from a DMSA12-H-kenyaite intercalate. The H-kenyaite loading was 8.2 wt %. The calcination was carried out at 540 °C for 10 hr in air using a heating rate of 1 °C/min.	187
Figure 6.6	XRD patterns of kenyaite intercalates: (A) DMSA12-H-kenyaite (36.5 Å); (B) a PDMS-intercalated kenyaite (10 wt % loading of H-kenyaite) nanocomposite (72.8 Å)	189

Figure 6.7	Comparison of BET surface area for the silica residues obtained by calcining exfoliated PDMS-kenyaite nanocomposites with different loadings (wt %) of H-kenyaite. The open circle is the surface area for the silica residue obtained by calcining an intercalated PDMS-kenyaite nanocomposite with a 10 wt %	
	loading of H-kenyaite. The calcination was carried out at 540 °C	
	for 10 hr in air using a heating rate of 1 °C/min	190
Figure 6.8	Toluene uptake by the exfoliated PDMS-kenyaite nanocomposites prepared from DMSA12-H-kenyaite intercalates. The tabulated values in the insert are equilibrium data determined by the immersion weight gain after 24 hr. The H-kenyaite loadings for the composites are 5 wt % and 10 wt %.	192
Figure 6.9	Thermogravimetric analysis curves for (A) a pristine PDMS polymer; and (B) an exfoliated PDMS-kenyaite nanocomposite. The loading of H-kenyaite for the composite is 10 wt $\%$. The analysis was carried out in N_2 atmosphere with a heating rate of 5	
	°C/min.	193

Chapter 1

INTRODUCTION

1.1 Nanocomposite Materials

1.1.1 Nanocomposite Concept

Nanostructured hybrid organic-inorganic composites have attracted great attention from both a fundamental research and applications point of view.¹⁻⁴ In general, composite materials are formed when at least two distinctly dissimilar materials are mixed to form a monolith. The overall properties of a composite material are determined not only by the parent components, but also by the composite phase morphology and interfacial properties.² The fiber-reinforced polymer composites are very typical and successful examples of this composite concept. A nanocomposite is formed when phase mixing occurs on a nanometer length scale. For conventional composites, phase mixing occurs on a macroscopic (µm) length scale. Nanocomposites are usually superior to conventional composites owing to their unique phase morphology and improved interfacial properties.

1.1.2 Performance Properties of Nanocomposites

Improvement of strength, stiffness and toughness are the primary characteristic structural properties of organic-inorganic nanocomposites. Desirable properties such as barrier properties, thermal stability, moisture stability, solvent resistance and fire retardancy generally accompany the reinforcement benefit. When special inorganic building blocks and/or polymer materials are applied, the secondary characteristics of

EC:01

in is

yen

113

Tich

onie

1

E.

şh_{iệ},

improvement such as optical transparency, dielectric strength, nonlinear optical properties, quantum confinement effects and electrical conductivity can also be observed.²

1.1.3 Formation of Nanocomposite Materials Through Sol-Gel Approach

One approach to preparing organic-inorganic nanocomposites is by the sol-gel processing method.⁵⁻⁸ In this method the inorganic phase is formed by the hydrolysis and condensation of metal oxide precursors (Scheme 1) in the presence of preformed polymer or polymer precursors which can be polymerized simultaneously. The size of inorganic building blocks is controllable and the interfacial properties can be improved by introducing covalent bonding between organic and inorganic phases. However, the solgel approach is limited by the evolution of volatile by-product and shrinkage when the hybrid is molded at elevated temperature. The controlling of microstructure formation also needs great effort to be achieved and phase segregation is another issue that has to be solved especially when a high loading of the inorganic phase is involved.

Scheme 1

Hydrolysis:

$$M(OR)_4 + H_2O \longrightarrow (RO)_3M-OH + ROH$$

Condensation:
 $-M-OH + HO-M - M-O-M + H_2O$
and/or
 $-M-OH + RO-M - M-O-M + ROH$
 $M = Si, Al, Ti, Zr$

1.2 Polymer-Clay Nanocomposites

1.2.1 Layered Structures Suited for Nanocomposite Formation

Inorganic materials with structures that can be broken down into nanoscale building blocks are attractive alternatives to the sol-gel approach in the preparation of

hybrid organic-inorganic nanocomposites. Lamellar structures become good candidates because of their diverse intercalation chemistry and platy morphology. Layered structures such as MoS₂, V₂O₅, FeOCl, layered phosphates and layered silicates are all plausible inorganic materials which have potential applications in the field of organic-inorganic nanocomposites.^{3,9-11}

Clay silicate nanolayers have a chemically stable siloxane surface with a high surface area. They also possess high aspect ratios and high strength which are very important indexes for use as reinforcing agents when compared with conventional fibers. 12 More importantly, their interlayer surface is easily modified by ion-exchange reaction and the gallery can be intercalated by organic cations or polymer precursors. All of these technical factors along with the economic considerations suggest that layered silicate clays are particularly well suited to the design of platelet-reinforced organic-inorganic nanocomposites.

1.2.2 Introduction to Smectite Clay Structure

Clays are 2-dimensional layered silicates of particle size < 2 µm. The 2:1 micatype silicates consist of 10 Å-thick layers stacked face-face to form turbostratic tactoids. Each silicate nanolayer (~ 2000 Å diameter) is made up of a central sheet of edge-shared octahedra sandwiched by two sheets of corner-shared SiO₄ (Si can be replaced by Al) tetrahedral layers. The substitution of metal ions in the octahedral or tetrahedral layer by low valence metal ions (e.g., Si⁴⁺ by Al³⁺; Al³⁺ by Mg²⁺ or Fe²⁺; Mg²⁺ by Li⁺) results in negative charges to the clay layers which are neutralized by gallery cations, such as Na⁺, K⁺ or Ca²⁺. A typical smectite clay structure is represented in Figure 1.1.¹² The hydrophilic inorganic cations in the galleries can be replaced by ion exchange reaction with both inorganic and organic cations. Many polymers, both hydrophilic and hydrophobic, have been intercalated into the clay gallery.^{13,14}

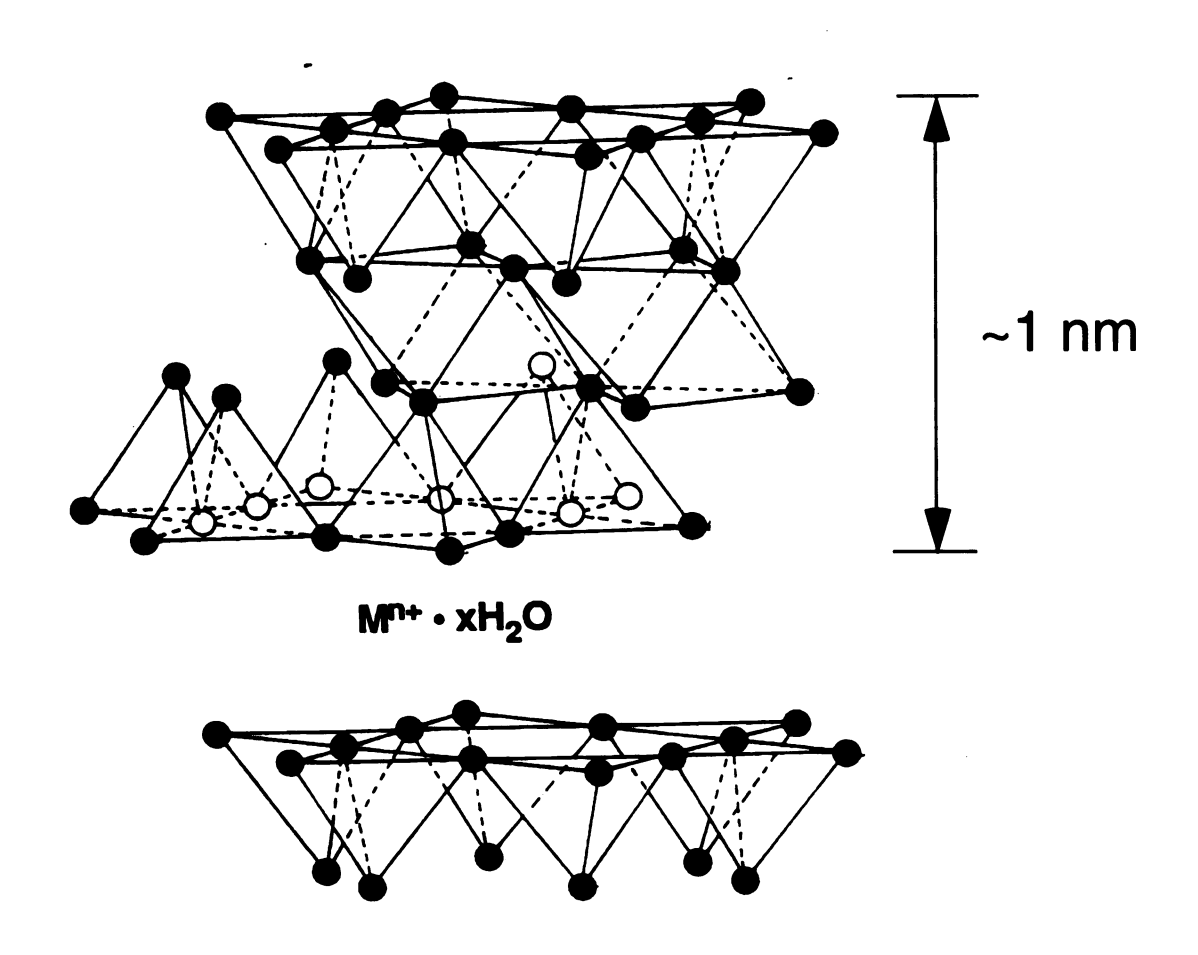


Figure 1.1 The layered framework of smectite clays. Each layer consists of two tetrahedral sheets cross-linking a central octahedral sheet. $M^{n+}\cdot xH_2O$ represents the interlayer exchangeable cation with its coordination water molecules. Each silicate nanolayer (sheet) has a 200 nm ~ 2 μ m of length in a x b dimensions, and about 1 nm of layer thickness.

1.2.3 Organo Clay Structures and Properties

The intercalation chemistry of layered silicate clays plays an important role in the formation of polymer-clay nanocomposites. Because many thermoplastic and thermoset polymers or their precursors are hydrophobic, the hydrophilic inorganic clay surface usually has to be modified to accommodate the incoming organic species. Generally, an organic cation exchange reaction is used to form a hydrophobic organo clay. Depending in part on the layer charge density of silicate clays and the dynamic size of organic cations, the structures adopted by organo clay are quite different. A schematic illustration of intragallery structures for organo clays is represented in Figure 1.2, wherein primary alkylammonium ions are used as intragallery cations. When long chain alkylammonium ions are the exchange cations, the alkyl chain axes will lie parallel to the siloxane surface for low charge density clays and a paraffin structure is preferred for high charge density clays.¹⁵ When the onium ion chain length becomes shorter, the chain orientation changes from a paraffin to a lateral monolayer structure for the same charge density clay. Interestingly, when additional neutral organic molecules such as alkylamines co-occupy the gallery along with the cationic surfactant, which are needed to balance the layer charge, a lipid-like structure (Figure 1.2 F-H) is formed for some layered silicate clays. 16

For most short chain organo clays, the intragallery region is not swellable by a polymer or polymer precursor due to strong electrostatic forces between the layers and the exchange cations. The driving force for swelling may be balanced by the intragallery electrostatic forces. Depending on the nature of the organic cations, mixed organic/inorganic exchanged clays can be formed. Normally, multiple exchanged reactions can overcome this competitive binding of inorganic ions to the exchange sites to give a completely organic cation exchanged product. The presence of metal ions on even a small fraction of the exchange sites can significantly affect the swelling properties of organo clays in some cases, especially when a very hydrophobic system is involved. 17

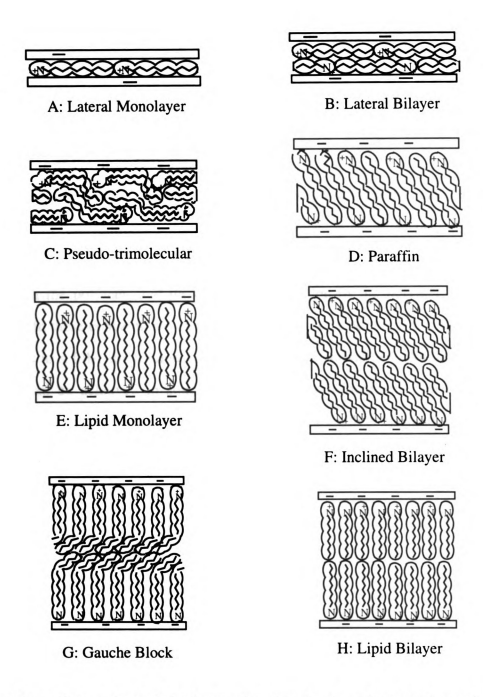
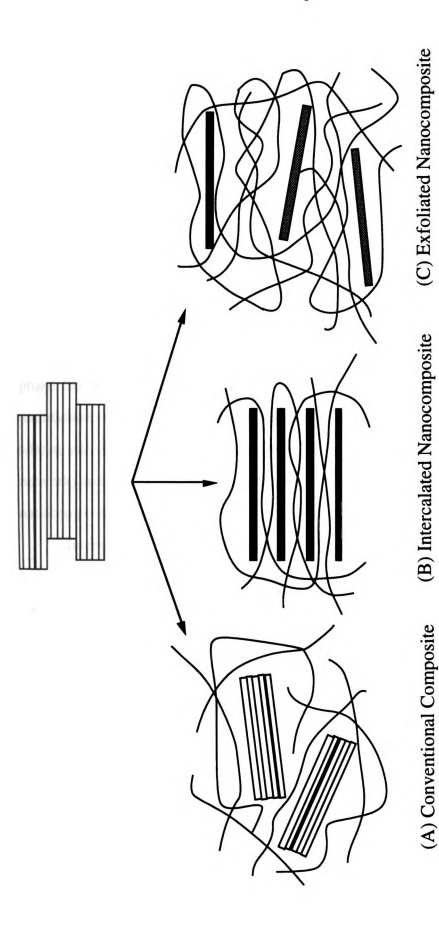


Figure 1.2 Orientations of alkylammonium ions in the galleries of layered silicates with different layer charge densities. 15.16

For long chain organo clays that are swellable, the alkyl chains can rearrange their orientation to accommodate the incoming intercalated species. Depending on the mobility of intragallery organic cations, the increased gallery space can be varied. For instance, quaternary alkylammonium exchanged clay can only provide a limited gallery space for the incoming organo species, because a lipid-like monolayer (Figure 1.2E) is the optimal structure that can be formed.

1.2.4 Types of Polymer-Clay Composites

From a structural point of view, polymer-clay composites can be generally classified into "conventional composites" and "nanocomposites". In a conventional composite, as illustrated in Figure 1.3A, the registry of clay tactoids are retained when mixed with the polymer, and there is no intercalation of the polymer into the clay structure. In these conventional composites the clay plays no major functional role and acts mainly as a filler for volumetric and economic considerations. An improvement in modulus can be achieved in some cases, but this reinforcement benefit is usually accompanied by a sacrifice in other properties such as strength or elasticity.



Schematic illustrations of (A) a conventional; (B) an intercalated; and (C) an exfoliated polymer-clay nanocomposites. interlayer spacing is fixed in an intercalated nanocomposite, on the other hand, the average gallery height is determined by clay The clay layers adopt an aggregated, intercalated, and exfoliated morphology, respectively, in each type of composite. The clay silicate loading in an exfoliated nanocomposite. Figure 1.3

Two types of polymer-clay nanocomposites are possible. Intercalated nanocomposites (Figure 1.3B) are formed when one or a few molecular layers of polymer are inserted into the clay galleries with fixed interlayer spacings. The polymer occupies the clay gallery in a crystallographically regular fashion, regardless of the overall ratio of clay to polymer. When the extragallery polymer phase is not considered, the clay component can be described as an intercalation compound with definite composition and structure.

In contrast, an exfoliated polymer-clay nanocomposite is a new phase formed between polymer and layered silicate nanolayers (Figure 1.3C). The individual 10 Å-thick clay layers are separated in a continuous polymer matrix by average distances that depend on loading. From a microstructural point of view, the domain size of the polymer phase has been dramatically reduced, and the registry of silicate layers is no longer maintained in most cases. Due to these structural factors, the interactions between silicate nanolayers are weak in relation to the interactions between polymer chains (or network) and layered silicate. So, a nonadditive behavior for the exfoliated polymer-clay nanocomposites is observed.

Interestingly, the interlayer spacing for an exfoliated nanocomposite may be uniform (ordered) or variable (disordered). Structural differences between these two phases are schematically illustrated in Figure 1.4. It is noteworthy to point out that an ordered exfoliated polymer-clay nanocomposite is formed when a synthetic layered silicate clay is involved. The mechanistic reason behind this particular structural feature will be discussed in more detail in chapter 3.

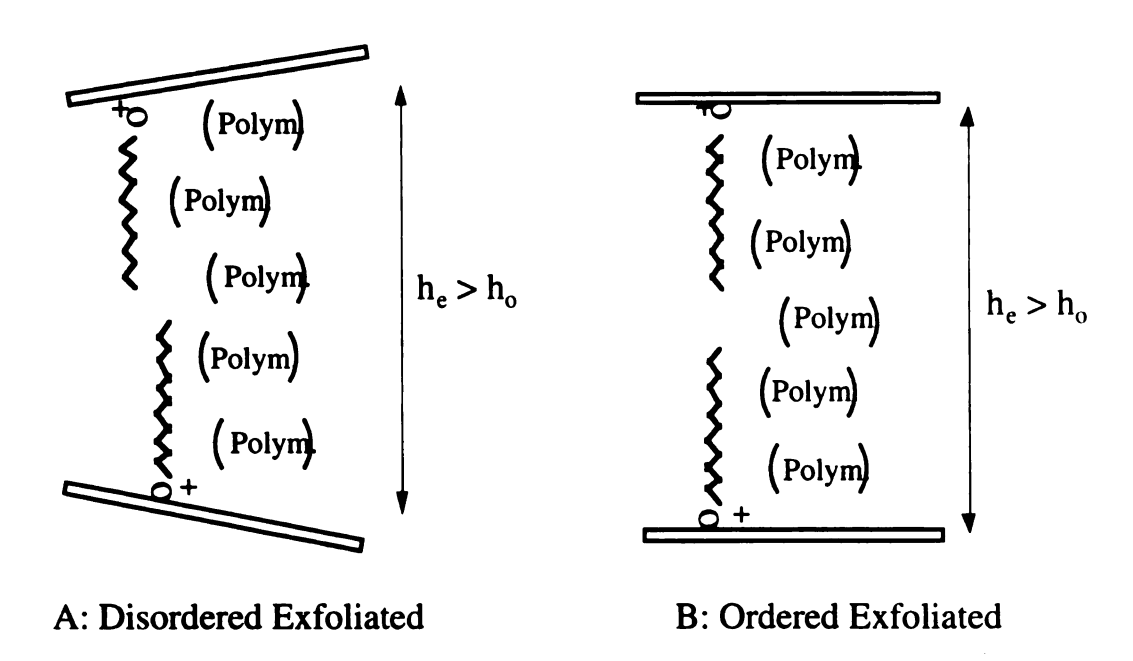


Figure 1.4 Schematic illustration of (A) a disordered exfoliated and (B) an ordered exfoliated polymer-clay nanocomposites. The onium ion is represented by and the polymer chain by (Polym.). he is the average gallery height for the exfoliated polymer-clay nanocomposites. ho is the gallery height expected for a lipid-like bilayer of onium ions.

1.2.5 Intercalated Polymer-Clay Nanocomposites

Polymer-intercalated clay phases have been known for decades. ^{13,14} But their potential as reinforcing and electrically conducting phases in nanocomposite structures has only recently been recognized. ^{19,20} So, the field of synthesis of intercalated polymer-clay nanocomposites is still very active. Table 1.1 lists the typical polymers that have been reported to be intercalated into clay galleries. The polymer can be either hydrophilic or hydrophobic. When oligomers are used, the polymer can be formed by radical, ionic and redox polymerization. The improvement of dielectric strength, nonlinear optical properties, quantum confinement effect and electrical conductivity are of major interest.

Intercalated polymer-clay nanocomposites can be readily synthesized by direct polymer intercalation ¹⁴ or by *in situ* intercalative polymerization of monomers. ^{13,21} For these preformed hydrophilic polymers such as poly(vinyl alcohol), poly(vinyl acetate) and poly(ethylene oxide), the intercalation can be performed in aqueous solution, wherein clay layers exist in a highly swollen or exfoliated state. An organic solvent can be used when a hydrophobic polymer is involved. The removal of the solvent, especially if it is toxic, is a major limitation of this approach. Molten polymers, such as nylon-6, poly(\varepsilon\)-caprolactone), and polystyrene have been reported recently that can be intercalated into organo clay galleries without the facilitation of solvent, ²⁷ however this method can not be applied to a very hydrophobic thermoplastic polymer such as polyethylene or polypropylene, and thermoset polymers.

Table 1.1 Polymers Reported to Form Intercalated Polymer-Clay Nanocomposites

oligomers/polymers	formula	ref.
Poly(ε-caprolactam)	$(CH_2(CH_2)_4 - C - N)_n$	13
Poly(ε-caprolactone)	$ \begin{pmatrix} CH_2(CH_2)_4 - C - O \end{pmatrix}_{n} $	21
Polystyrene	-(CH₂−CH-) _n Ph	25
Poly(methyl methacrylate)	(CH_2-CH_3) (CH_2-CH_3)	24
Poly(vinyl alcohol)	+ сн ₂ −сн) п он	23
Poly(ethylene oxide)	$+ CH_2-CH_2-O \rightarrow_n$	20
Polyaniline	(K) h)	19
Polypyrrole	(N)	26
Polythiophene	tist,	26

In situ intercalative polymerization method is a very successful and more general approach to prepare an intercalative polymer-clay nanocomposite. First at all, the polymer precursors (monomers or oligomers) are adsorbed or intercalated into clay galleries. Then, the intercalated polymer precursors are polymerized inside clay gallery. Solvent can also be involved when necessary in the entire process such as the formation of PMMA-intercalated clay nanocomposites.²⁴ In most cases, organo clay is intercalated by the polymer precursors at the liquid state (at the molten state for crystalline monomers), and the initial viscosity of the system is optimized by the nonviscous organic species to form a homogenous intercalated phase. Another advantage of this approach is that the intragallery cations can perform as a catalyst to initiate the polymerization, so that a driving force for the monomer diffusion exists which can play a very important role to achieve a high degree of homogeneity. This method works very well for both thermoplastic and thermoset polymer systems. The limitation of this approach is that a suitable polymer precursor for this specific intercalation reaction is not always available.

1.2.6 Exfoliated Nylon-6-Clay Nanocomposites

Owing to the platy morphology of the silicate layers and the improved microscopic homogeneity, the exfoliated clay nanocomposites can exhibit dramatically improved properties that are not available for the conventional and the intercalated composite materials. Toyota researchers first demonstrated that organo clays exfoliated in a thermoplastic nylon-6 polymer matrix greatly improved the thermal, mechanical, barrier and even the flame retardant properties of the polymer.²⁸⁻³¹

By replacing the hydrophilic exchange cations of Na⁺-montmorillonite with a hydrophobic ammonium cations of ω -amino acid they were able to conduct the ring opening polymerization of ε -caprolactam in the interlayer gallery region. The intercalative polymerization process resulted in almost complete delamination (exfoliation) of the stacked clay layers into the nylon-6 polymer matrix. The overall

performance properties of the nylon-6-clay nanocomposites substantially exceeded the composites prepared by the conventional method.³² For instance, the exfoliation of only 4.2 wt % montmorillonite clay in nylon-6 increased the tensile strength and modulus, respectively, from 69 MPa and 1.1 GPa for the pristine polymer to 107 MPa and 2.1 GPa for the composite. More importantly, the thermal and rheological properties of the nylon-6 were improved dramatically by exfoliation. An increase in heat distortion temperature from 65 °C for nylon-6 to 145 °C for the nylon-6-clay hybrid was achieved with as low as 4.2 wt % clay loading. The performance properties of nylon-6-clay nanocomposites are summarized in Table 1.2. This spectacular improvement in heat distortion temperature has made it possible to extend the commercial use of this relatively cheap polymer to high temperature environments, such as specialized under-the-hood applications in the automobile industry. A picture for the timing belt cover made of nylon-6-clay hybrid is shown in Figure 1.5.

Table 1.2 Mechanical and Thermal Properties of Nylon 6-Clay Composites³²

Composite Type	wt % Clay	Tensile Strength (MPa)	Tensile Modulus (GPa)	Impact (kJ/m ²)	HDT (°C) at 18.5 kg/cm ²
"Nanoscopic" (Exfoliated)	4.2	107	2.1	2.8	145
"Micro" (Tactoids)	5.0	61	1.0	2.2	89
Pristine Polymer	0	69	1.1	2.3	65

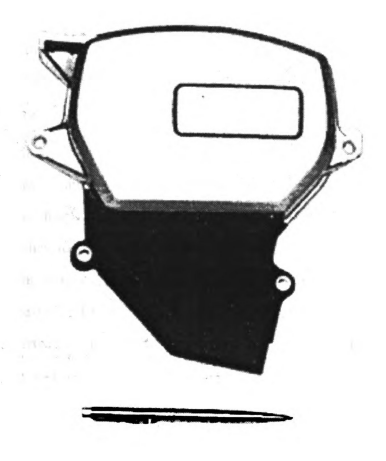


Figure 1.5 Injection-molded NCH (nylon 6-clay hybrid) timing belt cover.³²

1.2.7 Recent Advances on Polymer-Exfoliated Clay Nanocomposite Formation

Over the pass few years, this revolutionary nanocomposite chemistry has been successfully extended to other polymer systems such as polyimide, ³³ acrylonitrile rubber, ³⁴ polyether, ³⁵ epoxy ^{36,37} and polysiloxane. ³⁸ Among these, the epoxy-clay nanocomposites with a sub-ambient Tg exhibited exceptionally strong reinforcing effects. For instance, 7.5 vol. % of the exfoliated 10 Å-thick silicate layers improve the strength of the polymer matrix by more than 10-fold. Mass transport studies of polyimide-clay nanocomposites revealed a great reduction in the permeability of small gases, e.g., CO₂, O₂, H₂O, and the organic vapor ethyl acetate. ³⁹ More recently, silicate nanolayers have been dispersed in a very hydrophobic polymer, such as polypropylene. ^{40,41} Although, the barrier properties of this polypropylene-clay nanocomposite have not yet been reported, the application of this nanocomposite in the field of packaging is very promising.

Approaches to the exfoliation of clay nanolayers have been investigated by several different research groups using both thermoplastic and thermoset polymers. However, the desired exfoliated polymer-clay nanocomposites are much more difficult to prepare. Nevertheless, *in situ* polymerization is still a very powerful approach to preparing exfoliated polymer-clay nanocomposites.⁴² In this approach, a strong driving force, which can be a chemical potential and/or a mechanical force such as the shear blending, has to be applied in order to achieve the exfoliated phase of the silicate nanolayers. The driving force of polymerization to overcome the intragallery electrostatic forces can be especially effective. In utilizing this driving force, controlling the relative intra- and extragallery polymerization rates is perhaps the key factor. For instance, the acidic intragallery cations can function as catalyst centers and cause the intragallery polymerization rate to be competitive with the extragallery polymerization rate. This competitive polymerization results in the exfoliation of the silicate nanolayers in a monolithic polymer matrix. However, the rapidly increasing viscosity of the

polymerizing media can prevent the silicate nanolayers from exfoliating to a high extent. If the migration of the polymer precursors into clay galleries is slow early, then an intercalated clay nanocomposite will be formed, which is always not as a good performer as an exfoliated polymer-clay nanocomposite.

The mechanisms and factors governing the reinforcement of barrier and mechanical properties of polymer-clay nanocomposites were illustrated by some researchers. For instance, the larger aspect ratios and the turbostratic stacking fashion of the exfoliated clay platelets significantly increase the transportation path (Figure 1.6) for the gas molecules, and simultaneously reduce the permeability.⁴³ Some results also revealed that the improvement of mechanical properties is quite dependent on the glass transition temperature of the pristine polymer used. For the polymer matrix with a sub-ambient Tg, the reinforcement by the exfoliated clay is more significant than the high Tg system. A theory of platelet alignment under strain was used to explain this spectacular improvement which is illustrated in Figure 1.7.³⁶

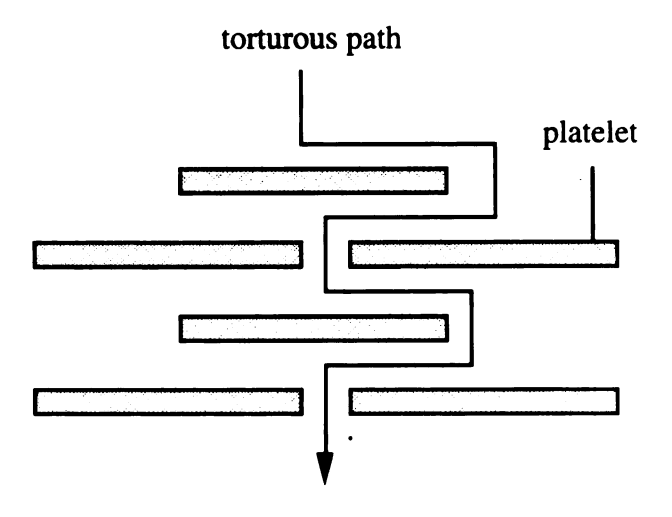


Figure 1.6 Proposed model for the torturous zigzag diffusion path in an exfoliated polymer-clay nanocomposite when used as a gas barrier.⁴³

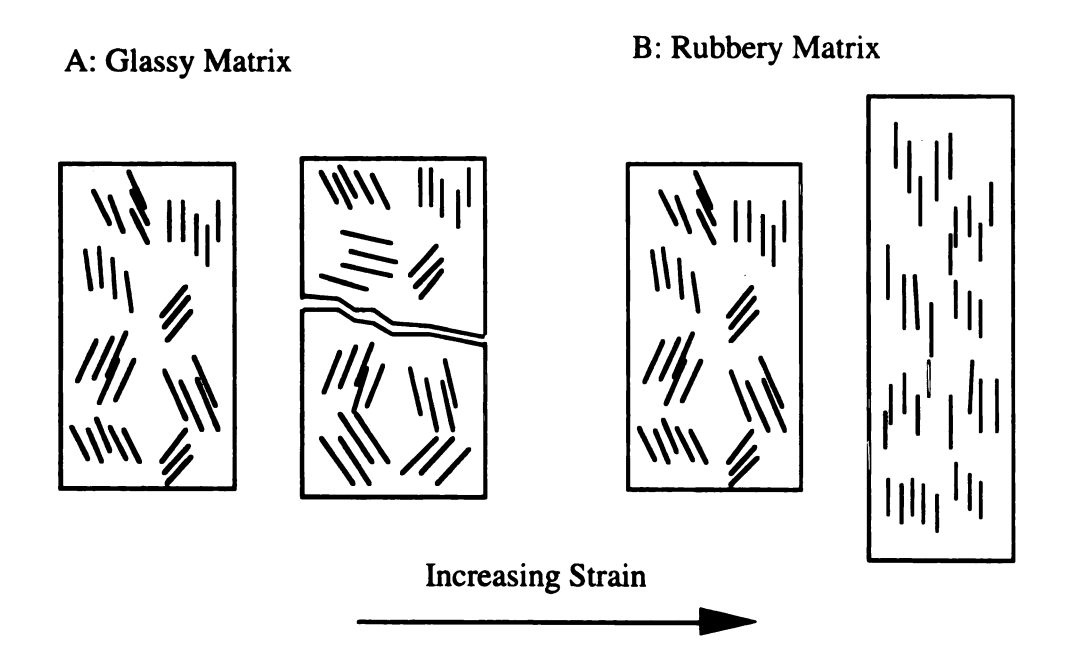


Figure 1.7 Proposed model for the fracture of (A) a glassy and (B) a rubbery polymer-clay exfoliated nanocomposite with increasing strain.³⁶

1.3 Research Objectives

1.3.1 Current Issues and New Directions

The breakthrough represented by nylon-6-clay nanocomposite introduced a new concept in the field of organic-inorganic nanocomposites. However, some of the fundamental chemistry and physics issues regarding nanocomposite formation are not well elucidated. For instance, what are the most effective aspect ratios of silicate nanolayers? What extent of exfoliation is needed for optimized mechanical properties? Is the extent of layer exfoliation totally controllable? The mechanisms responsible for the unprecedented reinforcement properties of this exciting new class of nanocomposite materials are not well understood, because the models developed for the conventional fiber-reinforced composites can not be simply transferred into this new field. New models for nanostructural composites, which can be used to explain the issues, such as the effect of nanolayer exfoliation on polymer elasticity, are needed.

The importance of interfacial properties of organic-inorganic composites, which can govern composite performance properties, has been realized. The suitable interface is almost a prerequisite to achieve a nanostructural phase, otherwise a segregated conventional phase will be formed. However, several factors can play important roles in determining the performance properties, especially the mechanical behavior for the composites. A general model ¹⁷ is proposed by Pinnavaia et al. for the possible interactions occurring at polymer-clay interfaces which is schematically illustrated in Figure 1.8. Earlier work has revealed that the physical adsorption of the polymer to the siloxane-like oxygen atoms of the clay (ie. Type C interactions) are more important in governing the mechanical behavior of the composite than the interactions between the alkyl chains and polymer network (ie. Type B interactions). This result suggests that exfoliated forms of layered silicate clays would be good reinforcement agents for epoxy matrices even in the absence of onium-exchange cations on the gallery surfaces. However, it is not easy to investigate the effect of only one interfacial factor while the

ì

other factors are maintained unchanged. So, expanding the exfoliated chemistry developed for semctite clays to other layered inorganic materials is essential in order to help address these issues.

The majority of engineering thermoplastic and thermoset polymers have not yet been fully explored for nanocomposite formation. Benefits similar to those obtained for nylon-6 should be possible for other polymer systems through nanolayer reinforcement. A deeper understanding of the fundamental chemistry and physics regarding nanocomposite formation, the relation between structure and properties, and the interfacial factors governing the mechanical behavior will help to advance nanocomposite science and technology.

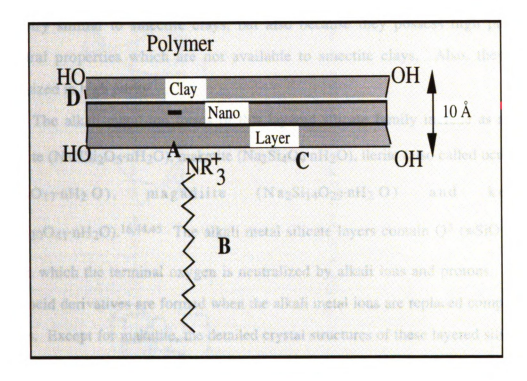


Figure 1.8 Interfacial interactions in a polymer-layered silicate nanocomposite: (A) Electrostatic binding of onium ion to the clay surfaces; (B) "Dissolution" of the alkyl chains into the polymer matrix by van der Waals forces; (C) Physical sorption of polymer to the siloxane oxygen atoms of the basal surfaces; (D) Polymer sorption to hydroxyl-terminated edge sites.¹⁷

1.3.2 Layered Silicic Acid Structures

Although, a great deal of research has been conducted on organic-inorganic hybrid composites in which smectite clays are used as reinforcement agents, layered silicic acids have drawn little attention in this field. Layered silicic acids are potentially good candidates not only because they have platy phase morphology and intercalation chemistry similar to smectite clays, but also because they possess high purity and structural properties which are not available to smectite clays. Also, they can be synthesized in high purity.

The alkali-metal-ion forms of this layered silicate family include as members kanemite (NaHSi₂O₅·nH₂O), makatite (Na₂Si₄O₉·nH₂O), ilerite (also called octosilicate, Na₂Si₈O₁₇·nH₂O), magadiite (Na₂Si₁₄O₂₉·nH₂O) and kenyaite (Na₂Si₂₀O₄₁·nH₂O). ^{16,44,45} The alkali metal silicate layers contain Q³ (≡SiO⁻) silicon sites in which the terminal oxygen is neutralized by alkali ions and protons. Layered silicic acid derivatives are formed when the alkali metal ions are replaced completely by protons. Except for makatite, the detailed crystal structures of these layered silicates are still unknown. In the makatite structure, continuous sheets of edged-shared Q³ tetrahedra are condensed to form six-memberred rings. A proposed structure for magadiite, ⁴⁷ which possesses a layer thickness (11.2 Å) similar to smectite clay (9.6 Å), is shown in Figure 1.9. In general, the structure of these layered silicates is built up of one or more sheets of SiO₄ tetrahedra.

Most of the alkali-metal forms of layered silicic acids can be easily synthesized by hydrothermal methods. By changing the ratio of starting sodium hydroxide, amorphous silica and water, and by controlling the reaction conditions, such as reaction temperature and time, these alkali-metal layered silicates can be prepared with different layer thickness.

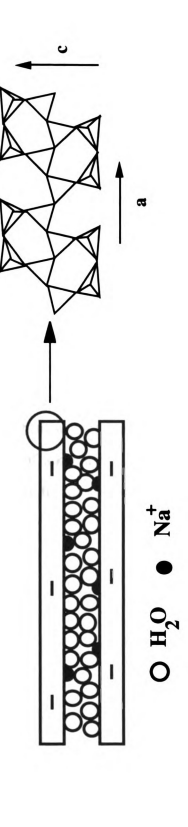


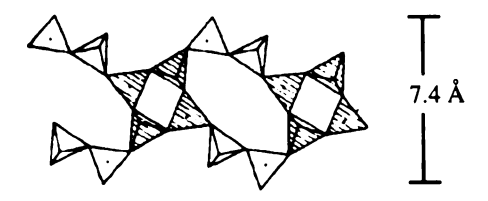
Figure 1.9 Magadiite structure postulated by Garces et al.⁴⁷ The presence of a bilayer of interlayer water molecules is based on the basal spacing of 15.6 Å for Na+-magadiite.

The intercalation chemistry of layered silicic acid is very similar to smectite clays. The alkali ions are exchangeable, and the intragalleries can be intercalated by various organic molecules ^{16,48,49} and even pillared by inorganic pillaring agents. ^{50,51} However, the physical states of silicate layers in aqueous solution are quite different. The layers of Na⁺-smectite clay are exfoliated in water, whereas the layers of layered silicic acids are stacked in an aqueous suspension. The special properties of layered silicates, which are not available to smectite clays include the presence of basal plane hydroxyl groups ^{52,53} and the variable thickness of the silicate layers ⁴⁶ from 5.0 Å for makatite to 17.7 Å for kenyaite, as shown in Figure 1.10.

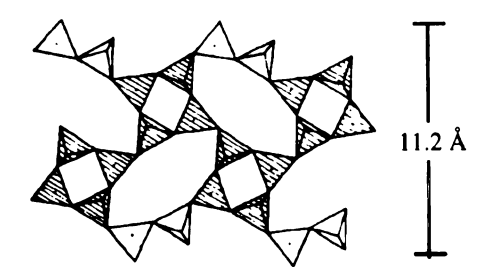
Much research has been conducted on transforming layered silicic acids into catalysts and pillared microporous derivatives or molecular sieves. 50.51 A few examples have been reported using layered silicic acids for nanocomposite formation. This limited knowledge is mainly due to a lack of structural information and a complete knowledge of the intercalation chemistry for layered silicic acids. For instance, the conditions needed for the synthesis of alkylammonium exchanged layered silicic acids are much more restrictive than those for the synthesis of smectite clay analogs.



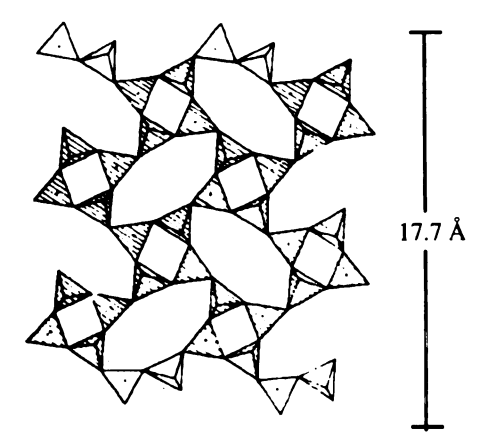
Makatite: $Na_2Si_4O_8(OH)_2 \times H_2O$



Ilerite: Na₂Si₈O₁₆(OH)₂ xH₂O



Magadiite: Na₂Si₁₄O₂₈(OH)₂·xH₂O



Kenyaite: $Na_2Si_{20}O_{41}(OH)_2xH_2O$

Figure 1.10 Schematic representation (edge-view) of the layered silicic acids.⁴⁶ The silicate layers are formed by sharing of apical oxygen atoms between tetrahedral SiO₄ sheets for ilerite, magadiite and kenyaite. The thickness of the layers differs depending on the degree of cross-linking between stacked sheets.

1.3.3 Research Goals

The active hydroxyl sites of layered silicic acids may provide enhanced bonding to gallery intercalants. Also, the variable layer thickness may provide insights on the relationship between nanocomposite properties and aspect ratios. Although a large number of organic compounds have been intercalated into layered silicic acid derivatives, the exfoliation of this family of materials in a polymer matrix has not yet been achieved. In the present work we will first extend the exfoliation chemistry developed for smectite clays in an epoxy matrix to include the layered silicate magadiite with a layer thickness of 11.2 Å. The chemistry elucidated for magadiite is likely to be applicable to other members of this mineral family for the formation of polymer-inorganic nanolayer composites.

Some fundamental chemistry and physics issues regarding nanocomposite formation will be elucidated to some degree by this research work. The main focus will be on the relationship of microstructures and properties, and the interfacial factors which govern the mechanical properties of nanocomposites. The interactions between the silicate phase and the polymer phase will be emphasized over the other interactions. New polymer systems, especially other thermoset polymers, are also of interest in this work.

Epoxy-clay nanocomposites prepared by *in situ* intercalative polymerization starting from an organo clay compromise the mechanical performance properties of the resulting composites. New approaches to polymer-layered silicate nanocomposites will be also explored in the present work so that greatly improved mechanical properties can be achieved using proton exchanged forms of layered silicic acids.

Once the exfoliation chemistry of layered silicic acids has been established, then long term future work can be proposed. Since the layered silicic acids possess active functional hydroxyl groups for potential covalent linking to the polymer phase, a great opportunity is provided to investigate the potential benefit of covalent interfacial forces

between organic and inorganic phases in improving the mechanical properties of polymer-inorganic nanolayer composites.

The polymer-layered silicic acid nanocomposites described in the present work are characterized by X-ray powder diffraction, which is the most powerful technique to determine the orientation and stacking of layers and the average basal spacing between silicate layers. Tensile tests will be used to obtain the mechanical properties of the composite materials. Sample coupons with a dog-bone shape will be prepared by the molding methods. The performance properties will be further characterized in terms of chemical stability, solvent resistance and thermal stability. The technique of surface area measurement by N₂ adsorption-desorption will also be used to deepen our understanding of the phase morphology of silicate nanolayers.

1.5 References

- 1. Schmidt, H. J. Non-Cryst. Solids 1985, 73, 681.
- 2. Novak, B. M. Adv. Mater. 1993, 5, 422.
- 3. Giannelis, E. P. *JOM* **1992**, 44, 28.
- 4. Messersmith, P. B.; Stupp, S. I. J. Mater. Res. 1992, 7, 2599.
- 5. Schubert, U.; Husing, N.; Lorenz, A. Chem. Mater. 1995, 7, 2010.
- 6. Judeinstein, P.; Sanchez, C. J. Mater. Chem. 1996, 6, 511.
- 7. Corriu, R. J. P.; Leclercq, D. Angew. chem. Int. Ed. Engl. 1996, 35, 1420.
- 8. Ellsworth, M. W.; Novak, B. M. Chem. Mater. 1993, 5, 839.
- 9. Kanatzidis, M. G.; Bissessur, R.; DeGroot, D. C.; Schindler, J. L.; Kannewurf, C. R. Chem. Mater. 1993, 5, 595.
- 10. Kanatzidis, M. G.; Wu, C.-G.; Marco, H. O.; Kannewurf, C. R. J. Am. Chem. Soc., 1989, 111, 4139.
- 11. Kanatzidis, M. G.; Wu, C.-G.; Marco, H. O.; Kannewurf, C. R.; Kostikas, A.; Papaefthymion, V. Adv. Mater. 1990, 2, 364.
- 12. Pinnavaia, T. J. Science 1983, 220, 365.
- 13. Kato, C.; Kuroda, K.; Misawa, M. Clays Clay Miner. 1979, 27, 129.
- 14. Theng, B. K. G. Formation and Properties of Clay-Polymer Complexes, Elsevier: New York, 1979.
- 15. Lagaly, G. Solid State Ionics 1986, 22, 43.
- 16. Lagaly, G.; Beneke, K.; Weiss, A. Am. Mineral. 1975, 60, 642.
- 17. Shi, H.; Lan, T.; Pinnavaia, T. J. Chem. Mater. 1996, 8, 1584.
- 18. Lan, T.; Pinnavaia, T. J. Mater. Res. Soc. Symp. Proc. 1996, 435, 79.
- 19. Mehrotra, V.; Giannelis, E. P. Solid State Ionics 1992, 51, 115.
- 20. Ruiz-Hitzky, E. Adv. Mater. 1993, 5, 334.
- 21. Messersmith, P. B.; Giannelis, E. P. Chem. Mater. 1993, 5, 1064.
- 22. Kyoyani, T.; Sonobe, N.; Tomita, A. Nature 1988, 331, 331.
- 23. Greenland, D. J. J. Colloid Sci. 1963, 18, 647.
- 24. Lee, D. C.; Jang, L. W. J. Appl. Polym. Sci. 1996, 61, 1117.

- 25. Akelah, A.; Moet, A. J. Mater. Sci. 1996, 31, 3589.
- 26 Oriakhi, C. O.; Lerner, M. M. Mater. Res. Bull. 1995, 30, 723.
- 27. Vaia, R. A.; Jandt, K. D.; Kramer, E. J.; Giannelis, E. P. Chem. Mater. 1996, 8, 2628.
- 28. Usuki, A.; Kawasumi, M.; Kojima, Y.; Okada, A.; Kurauchi, T.; Kamingaito, O. *J. Mater. Res.* **1993**, 8, 1174.
- 29. Usuki, A.; Kojima, Y.; Kawasumi, M.; Okada, A.; Fukushima, Y.; Kurauchi, T.; Kamigaito, O. J. Mater. Res. 1993, 8, 1179.
- 30. Kojima, Y.; Usuki, A.; Kawasumi, M.; Okada, A.; Fukushima, Y.; Kurauchi, T.; Kamigaito, O. J. Mater. Res. 1993, 8, 1185.
- 31. Kojima, Y.; Usuki, A.; Kawasumi, M.; Okada, A.; Kurauchi, T.; Kamigaito, O. J. Appl. Polym. Sci. 1993, 49, 1259.
- 32. Okada, A.; Usuki, A. Mater. Sci. Eng. 1995, C3, 109.
- 33. Yano, K.; Usuki, A.; Okada, A.; Kurauchi, T.; Kamigaito, O. J. Polym. Sci., Part A: Polym. Chem. 1993, 31, 2493.
- 34. Kojima, Y.; Fukumori, K.; Usuki, A.; Okada, A.; Kurauchi, T. J. Mater. Sci. Lett. 1993, 12, 889.
- 35. Wang, M. S.; Pinnavaia, T. J. Chem. Mater. 1994, 6, 468.
- 36. Lan, T.; Pinnavaia, T. J. Chem. Mater. 1994, 6, 2216.
- 37. Messersmith, P. B.; Giannelis, E. P. Chem. Mater. 1994, 6, 1719.
- 38. Burnside, S. D.; Giannelis, E. P. Chem. Mater. 1995, 7, 1597.
- 39. Gu, J. M.S. Thesis, Michigan State University, 1997.
- 40. Kurokawa, Y.; Yasuda, H.; Oya, A. J. Mater. Sci. lett. 1996, 15, 1481.
- 41. Usuki, A.; Kato, M.; Okada, A.; Kurauchi, T. J. Appl. Polym. Sci. 1997, 63, 137.
- 42. Pinnavaia, T. J.; Lan, T.; Wang, Z.; Shi, H.; Kaviratna, P. D. ACS Symp. Ser. 1996, 622, 250.
- 43. Lan, T. Ph.D. Thesis, Michigan State University, 1997.
- 44. Beneke, K.; Lagaly, G. Am. Mineral. 1977, 62, 763.
- 45. Beneke, K.; Lagaly, G. Am. Mineral. 1983, 68, 818.
- 46. Schwieger, W.; Heidemann, D.; Bergk, K. H. Revue de Chimie Minérale 1985, 12, 639.

- 47. Garces, J. M.; Rocke, S. C.; crowder, C.E.; Hasha, D. L. Clays Clay Miner. 1988, 36, 409.
- 48. Sugahara, Y.; Sugimoto, K.; Yanagisawa, T.; Nomizu, Y.; Kuroda, K.; Kato, C. Yogyo Kyokai Shi 1987, 95, 117.
- 49. Yanagisawa, T.; Yokoyama, C.; Kuroda, K.; Kato, C. Bull. Chem. Soc. Jpn. 1990, 63, 47.
- 50. Dailey, J. S.; Pinnavaia, T. J. Chem. Mater. 1992, 4, 855.
- 51. Wong, S. T.; Cheng, S. Chem. Mater. 1993, 5, 770.
- 52. Rojo, J. M.; Ruiz-Hitzky, E.; Sanz, J. Inorg. Chem. 1988, 27, 2785.
- 53. Pinnavaia, T. J.; Johnson, I. D.; Lipsicas, M. J. Solid State Chem. 1986, 63, 118.

Chapter 2

HYBRID ORGANIC-INORGANIC NANOCOMPOSITES FORMED FROM AN EPOXY POLYMER AND A LAYERED SILICIC ACID (MAGADIITE)

2.1 Introduction

Toyota researchers first demonstrated that organo clays exfoliated in a thermoplastic nylon-6 polymer matrix greatly improved the thermal, mechanical, barrier and even the flame retardant properties of the polymer. These composites are now used in under-the-hood applications in the automobile industry.¹⁻⁴ Although considerable research has been conducted on organic-inorganic hybrid composites in which smectite clays are used as reinforcement agents,⁵⁻⁸ relatively little work has been devoted to derivatives of layered silicic acids that possess layered morphology and ion-exchange properties similar to smectite clays. The alkali-metal-ion forms of this layered silicate family include as members kanemite (NaHSi₂O₅·nH₂O), makatite (Na₂Si₄O₉·nH₂O), ilerite (Na₂Si₈O₁₇·nH₂O), magadiite (Na₂Si₁₄O₂₉·nH₂O) and kenyaite (Na₂Si₂₀O₄₁·nH₂O).⁹⁻¹¹ The detailed crystal structures of these layered silicates are still unknown, except for makatite.¹² In general, the structure of these layered silicates is built up of one or more sheets of SiO₄ tetrahedra with an abundant hydroxyl siloxane surface.^{13,14}

The alkali-metal silicate layers contain Q³ (≡SiO⁻) silicon sites in which the terminal oxygen is neutralized by alkali ions and protons. The alkali ions are exchangeable, and the intragalleries can be intercalated by various organic molecules and even pillared by inorganic pillaring agents. Layered silicic acid derivatives are

formed when the alkali-metal ions are replaced completely by protons. The special properties of layered silicic acids include their basal plane hydroxyl groups and the variable thickness of the silicate layers (from 5.0 Å for makatite to 17.7 Å for kenyaite).¹² The active hydroxyl sites may provide enhanced bonding to the gallery intercalates. Also, the variable layer thickness may provide insights into the relationship between nanocomposite properties and aspect ratios. Although a large number of organic compounds have been intercalated into layered silicic acid derivatives,^{9,17,18} the exfoliation of this family of materials in a polymer matrix has not yet been achieved.

In the present work we will extend the exfoliation chemistry of smectite clay in an epoxy matrix to include the layered silicate magadiite with a layer thickness of 11.2 Å. The chemistry elucidated for magadiite is likely to be applicable to other members of this mineral family for the formation of polymer-inorganic nanolayer composites.

2.2 Experimental

Materials. The epoxide resin used to for epoxy-magadiite hybrid composite formation was poly(bisphenol A-co-epichlorohydrin) (Shell, EPON 828), with MW ~377:

$$\begin{array}{c} CH_{2}-CHCH_{2}O \\ \hline \\ CH_{3} \\ \hline \\ CH_{3} \\ \hline \end{array} \begin{array}{c} OCH_{2}CHCH_{2}O \\ \hline \\ CH_{3} \\ \hline \end{array} \begin{array}{c} CH_{3} \\ \hline \\ CH_{3} \\ \hline \end{array} \begin{array}{c} CH_{3} \\ \hline \\ CH_{3} \\ \hline \end{array} \begin{array}{c} OCH_{2}CH-CH_{2} \\ \hline \\ CH_{3} \\ \hline \end{array} \begin{array}{c} OCH_{2}CH-CH_{2} \\ \hline \end{array}$$

$$n = 0 (88\%); n = 1 (10\%); n = 2 (2\%).$$

The curing agent was poly(propylene glycol) bis(2-aminopropyl ether) (Huntsman Chemical, JEFFAMINE D-2000), with MW ~2000:

$$H_2NCHCH_2 = OCH_2CH = NH_2$$
 $CH_3 = CH_3$
 $X=33.1$

The above monomers afford a rubbery-like epoxy polymer matrix with a sub-ambient Tg of -40 °C. All the other chemicals used in this work were purchased from Aldrich Chemical Co. and used without further purification.

Synthesis of Na⁺-magadiite. Na⁺-magadiite was synthesized according to the published methods. A suspension of 60.0 g of amorphous silica gel (1.0 mol) in 300 mL of 1.11 M NaOH solution (0.33 mol) was heated at 150 °C for 42 h with stirring in a Teflon-lined stainless steel 1.0 L Parr reactor. The suspension containing Na⁺-magadiite was centrifuged, and the solid product was washed twice with 600 mL of deionized water to remove excess NaOH, and air-dried at room temperature.

Synthesis of Organo Magadiites. Primary long chain alkylammonium exchanged C18-magadiite-PF was prepared by the following approach. An aqueous suspension containing 15.0 g of Na⁺-magadiite was combined with ethanol/water solution containing 0.141 mol of alkylammonium chloride and alkylamine in a 6:1 molar ratio to form a suspension in 1.0 L of 1:1 (v:v) ethanol/water total solution. The suspension was stirred at 65 °C for 48 hours. The pH of the reaction mixture was in the range of 8 - 9. The product mixture was added to an equal volume of ethanol and centrifuged. The wet solid product was washed consecutively with one 750-mL portion of 50 % EtOH, two 750-mL portions of 25 % EtOH and then with water until free of Cl-, and air-dried.

Octadecylamine-solvated octadecylammonium exchanged magadiite (C18-magadiite-BL) was prepared using Lagaly's method. An aqueous suspension containing 4.0 g of Na⁺-magadiite was combined with ethanol/water solution containing 2.63 x 10⁻² mol of alkylammonium chloride and alkylamine in a 3:2 molar ratio to form a suspension in 400 mL of 1:9 (v:v) ethanol/water total solution. The suspension was stirred at 65 °C for 48 hours. The pH of the reaction mixture was in the range > 9. The product mixture was added to 200 mL of ethanol and centrifuged. The wet solid product was washed with one 250-mL portion of 10 % EtOH and then with water until free of Cl⁻, and air-dried.

Octadecylammonium exchanged magadiite (C18-magadiite-LM) with a lateral monolayer structure could be prepared by two methods. (1) C18-magadiite-PF or C18-magadiite-BL was washed with ethanol extensively until a lateral monolayer phase

appeared (characterized by XRD) and air-dried. (2) An aqueous suspension containing 4.0 g of Na⁺-magadiite was combined with ethanol/water solution containing 2.25 x 10⁻² mol of alkylammonium chloride to form a suspension in 400 mL of 3:2 (v:v) ethanol/water total solution. The suspension was stirred at 65 °C for 48 hours. The pH of the reaction mixture was maintained in the range of 6 - 7 by adding 0.1 M HCl solution. The product mixture was added to an equal volume of ethanol and centrifuged. The wet solid product was washed with ethanol extensively until a lateral monolayer phase appeared and free of Cl⁻.

All of the air-dried organo magadiite was ground to a powder with a particle size smaller than 270 mesh (53 μ m) and stored for further use.

Preparation of Epoxy-Magadiite Composites. Equivalent amounts of epoxide resin and poly(oxypropyleneamine) curing agent were mixed at room temperature for 30 min. The desired amount of organo magadiite was added to the epoxide-poly(oxypropyleneamine) mixture and stirred for another 60 min. This mixture was outgassed in a vacuum oven and poured into a stainless steel mold for curing at 75 °C for 3 h and, subsequently, at 125 °C for an additional 3 h.

X-ray Powder Diffraction (XRD). XRD patterns were recorded on a Rigaku rotaflex 200B diffractometer equipped with a rotating anode, Cu K_{α} x-ray radiation (λ = 1.541838 Å) and a curved crystal graphite monochromator. The x-ray was operated at 45 KV and 100 mA. Diffraction patterns were collected with 0.01° 2θ interval between 1 and 10° 2θ using a scanning rate of 2° 2θ per minute, and DS and SS slit widths of 1/6. Samples of epoxy-solvated magadiite or uncured epoxy-magadiite composites were prepared by applying thin films on glass slides. Cured composite specimens were prepared by mounting a flat rectangular sample into an aluminum holder.

Thermal Analysis. Thermogravimetric analyses (TGA) were performed using a Cahn TG System 121 thermogravimetric analyzer. Samples were heated to 750 °C at a heating rate of 5 °C/min under N₂ atmosphere.

Mechanical Measurement. Tensile testing was performed at ambient temperature according to ASTM procedure D3039 using a SFM-20 United Testing System.

Chemical and Solvent Resistance. The resistance of the composite materials to solvent swelling was obtained according to ASTM procedure D543. The specimens were immersed in the desired reagent and removed periodically to measured the weight gain until equilibrium was reached.

2.3 Results and Discussion

2.3.1 Synthesis of Organo Magadiites

Intercalation chemistry has played a very important role in the formation of polymer-clay nanocomposites. 1,20 Most polymer precursors require a hydrophobic environment to be intercalated into the clay galleries. Our first goal was to synthesize suitable organo magadiites which can be used to prepare epoxy-magadiite nanocomposites. Na+-magadiite has been reported to undergo ion-exchange reaction with primary alkylammonium ions. However, a lipid-like bilayer is the most favored intragallery structure. The lipid-like bilayer is formed from neutral amine and the necessary amount of alkylammonium needed to balance the negative charge of the silicate layer (cf. Figure 1.2H). The presence of a large amount of neutral amine with mono-functional end groups is not suitable in the chemistry of epoxy polymer curing. In this work, we have developed a new approach to synthesize a paraffin-like intercalated phase of organo magadiite by using long chain primary alkylammonium surfactants and a neutral amine as gallery guests.

The Na⁺ form of the magadiite was converted to a previously unknown mixed CH₃(CH₂)₁₇NH₃⁺-CH₃(CH₂)₁₇NH₂ intercalate by ion exchange reaction in the presence of neutral amine. A basal spacing of 38.2 Å was consistent with the paraffin structure of onium ions and neutral amine with an inclined angle about 65°. This intercalated paraffin-like phase was designated C18-magadiite-PF. Elemental analysis and TGA

results indicated that the sodium ions were completely replaced by onium ions. This product also contained a small fraction of neutral primary amine which was essential for forming the paraffin structure, in addition to the primary onium ions.

Two previously known organo magadiite intercalates were also synthesized for comparison purposes. One was an organo magadiite with a 63.1 Å basal spacing, prepared using Lagaly's method. The gallery of this organo magadiite contains a lipid-like bilayer structure of onium ions and neutral amine molecules. The sample was designated C18-magadiite-BL. This product should be regarded as octadecylamine-solvated octadecylammonium magadiite which contains near 100% neutral amine, except the alkylammonium fraction needed to balance the negative charge of the silicate layer. The other known organo magadiite phase was a 14.0 Å phase intercalated by a lateral monolayer of CH₃(CH₂)₁₇NH₃+ ions. This monolayer phase was denoted C18-magadiite-LM. In this lateral monolayer structure the onium ion chains lie parallel to the interlayer siloxane surface.

The unit cell compositions, basal spacings and gallery structures for the three organo magadiite derivatives are summarized in Table 2.1. The powder XRD patterns and TGA curves for each phase, along with that for Na⁺-magadiite are given in Figure 2.1 and Figure 2.2 respectively.

Table 2.1 Intercalates Formed by Reaction of Na⁺-Magadiite with C₁₈H₃₇NH₃⁺Cl⁻ and C₁₈H₃₇NH₂

material	intragallery composition ^a	gallery	d ₀₀₁
designation	per Si ₁₄ O ₂₉ ²⁻ unit cell	structure	(Å)
C18-magadiite-LM	$(C_{18}H_{37}NH_{3}^{+})_{0.45}H^{+}_{1.55}$	lateral monolayer	14.0
C18-magadiite-PF	$(C_{18}H_{37}NH_3^+)_2(C_{18}H_{37}NH_2)_{0.48}$	paraffin	38.2
C18-magadiite-BL	$(C_{18}H_{37}NH_3^+)_2(C_{18}H_{37}NH_2)_{1.83}$	lipid bilayer	63.1

^aThe compositions were determined by CHN and Si analyses.

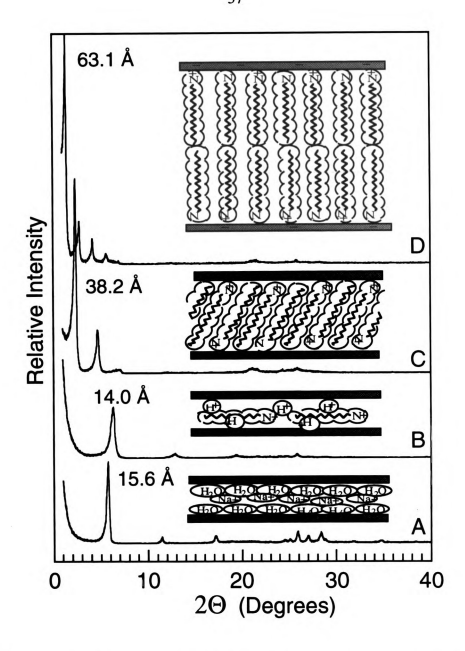


Figure 2.1 X-ray powder diffraction patterns of (A) air-dried Na*-magadiite; (B) CH₃(CH₂)₁₇NH₃*-magadiite with a lateral monolayer (LM) structure. Patterns (C) and (D) are for mixed CH₃(CH₂)₁₇NH₃*/CH₃(CH₂)₁₇NH₂-magadiite with a paraffin (PF) and a lipid bilayer (BL) gallery structure, respectively. The LM structure contains no free amine (0.45 onium ions per Si₁₄O₂₉ formula unit), whereas PF and BL structures contain neutral primary amine molecules, in addition to primary onium ions.

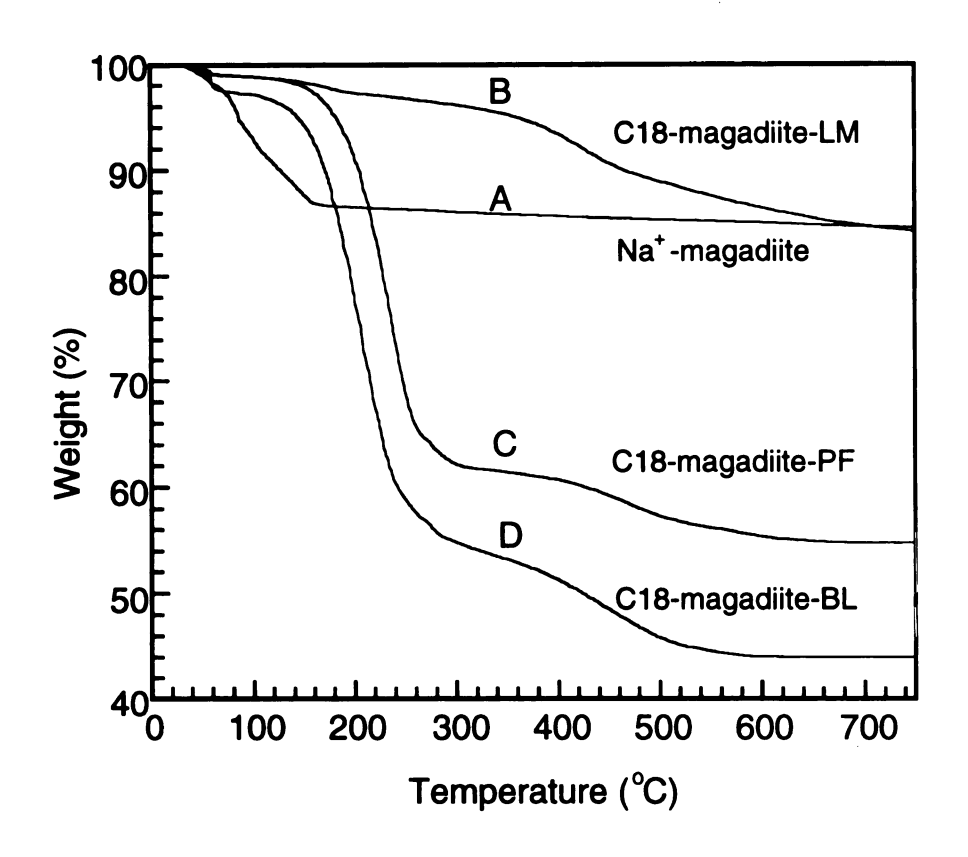


Figure 2.2 Thermogravimetric analysis curves of (A) air-dried Na⁺-magadiite; (B) CH₃(CH₂)₁₇NH₃⁺-magadiite with a lateral monolayer (LM) structure. Patterns (C) and (D) are for mixed CH₃(CH₂)₁₇NH₃⁺/CH₃(CH₂)₁₇NH₂-magadiite with a paraffin (PF) and a lipid bilayer (BL) gallery structure, respectively.

It is noteworthy that the initial product obtained by the ion exchange reaction for C18-magadiite-PF is a mixture of the lipid bilayer and the paraffin magadiite phases with its XRD pattern shown in Figure 2.3. To obtain this paraffin phase it is essential to execute washing according to the conditions specified in the experimental section. Otherwise, most of the organo species will be removed from the gallery by the ethanol washing process, resulting in the formation of C18-magadiite-LM with a lateral monolayer structure.

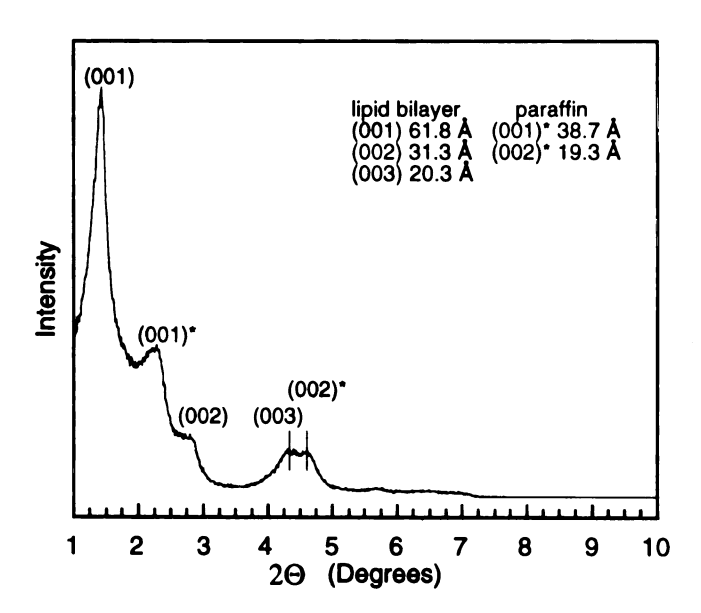


Figure 2.3 X-ray diffraction pattern of the initial mixture product in an effort to obtain C18-magadiite-PF. The mixture was formed when Na⁺-magadiite was ion exchanged by CH₃(CH₂)₁₇NH₃⁺/CH₃(CH₂)₁₇NH₂ followed by ethanol washing. The tabulated values in the insert are d₀₀₁ values for the lipid bilayer and paraffin phases.

2.3.2 Exfoliation of Magadiite Nanolayers in an Epoxy Polymer Matrix

Owing to the strong intragallery electrostatic interactions in C18-magadiite-LM, this structure can not be further intercalated by epoxide resin or even by small polymer precursor molecules such as \varepsilon-caprolactam. However, both C18-magadiite-PF and C18-magadiite-BL with 38.2 Å and 63.1 Å basal spacing are readily swelled by polymer precursors and can be used to form hybrid composites. C18-magadiite-PF is much preferred over the BL analog due to a much smaller amount of neutral amine (cf. Table 2.1), which can participate and interfere with the desired thermoset curing process. Unless otherwise indicated, all of the following experiments were carried out by using C18-magadiite-PF as a reinforcement agent. All effort to form a paraffin-like intercalate with onium ions and amines with chain length shorter than C16 resulted in intercalates with a lipid bilayer or lateral monolayer structure.

C18-magadiite-PF when mixed with epoxide resin at 75 °C undergoes a 4.3 Å increase in basal spacing from 38.2 Å to 42.5 Å shown in Figure 2.4. This indicates that the gallery onium ions change their orientation from an inclined to a vertical orientation to accommodate epoxide penetration into the gallery. Furthermore, the X-ray diffraction patterns in Figure 2.5 show the gallery can also be expanded by co-intercalation of the epoxide and poly(oxypropyleneamine) mixtures. At room temperature, the gallery is only partially solvated due to the slow gallery diffusion of those macromolecules. This results in the presence of a 63 Å intercalate and the unintercalated initial phase. At elevated temperature (75 °C), the gallery is totally solvated within 15 minutes to form an intercalate with a very sharp d₀₀₁ peak near 63 Å. This latter value is consistent with the reorientation of the onium ions into a bilayer structure when solvated by the resin and the curing agent (Compare Figure 2.5A and 2.5D). The broadening of the first order peak upon further heating at 75 °C (Figure 2.5E) suggests that the gallery is further expanded by cross-linking polymerization. Upon further heating at 125 °C, the gallery continues to

undergo expansion and the solvated phase basal spacing of 63 Å is replaced by the nearly amorphous phase characteristic of the exfoliated composite (Figure 2.5F and 2.5G).

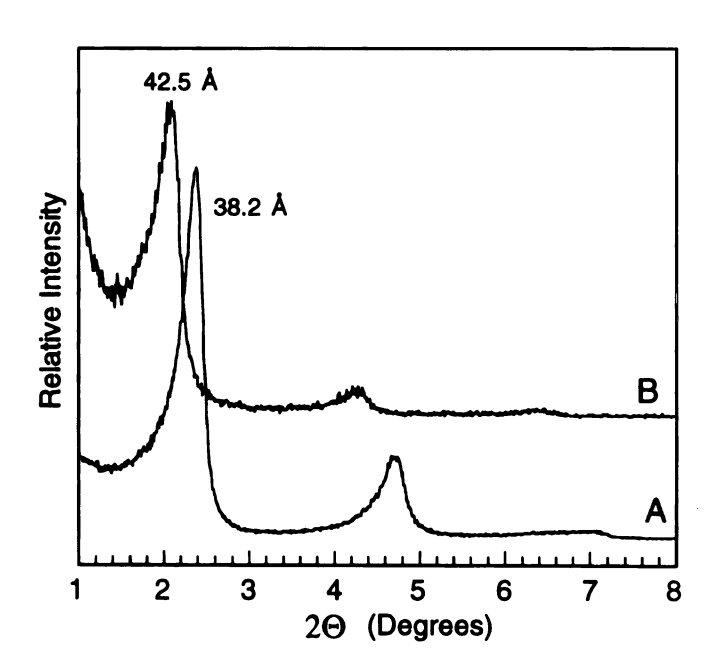


Figure 2.4 X-ray diffraction patterns of C18-magadiite-PF in different physical states:
(A) pristine organo magadiite; (B) 10 wt % organo magadiite solvated by epoxide resin (EPON 828) at 75 °C for 90 min.

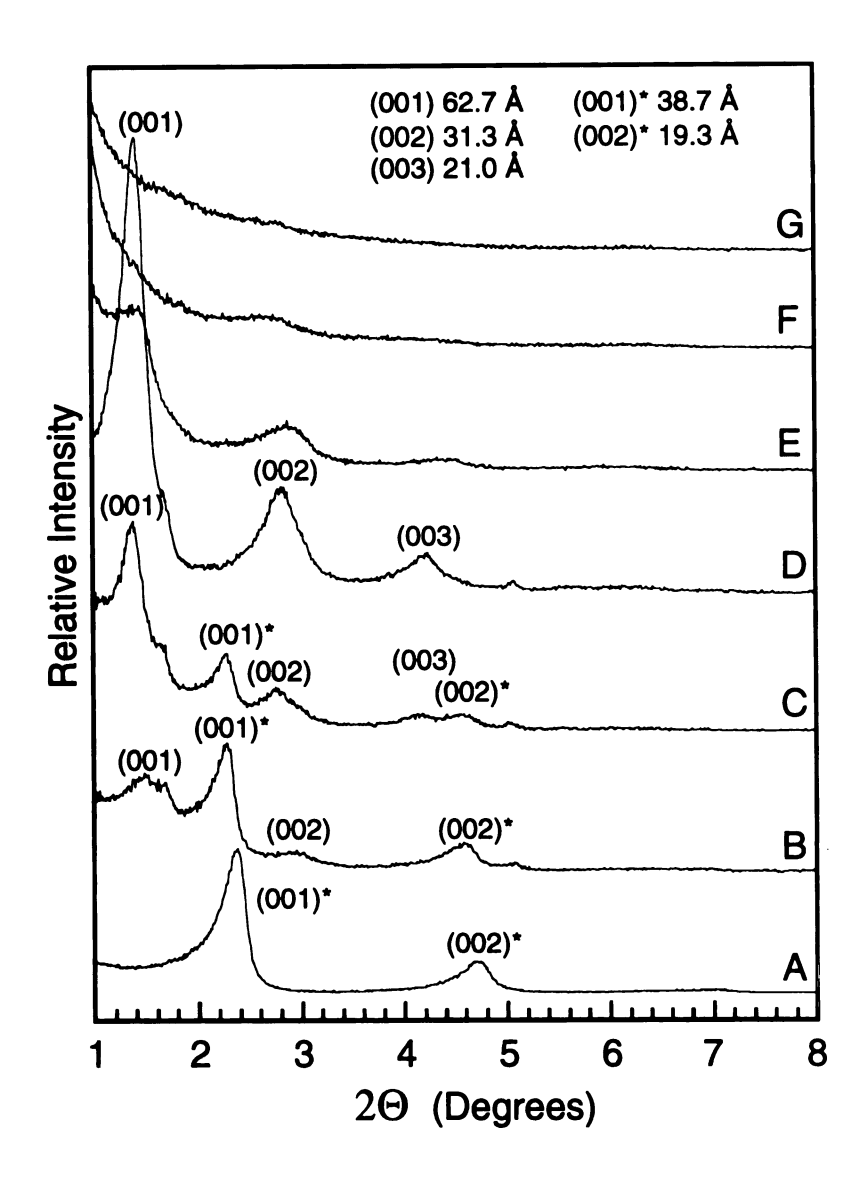


Figure 2.5 X-ray diffraction patterns of products prepared by reaction of (A) C18-magadiite-PF (15 wt % loading) with epoxide resin and poly(oxypropyleneamine) curing agent at an epoxide group to amine group molar ratio of 2:1. Reaction conditions were as follows: (B) 25 °C, 60 min; (C) 75 °C, 5 min; (D) 75 °C, 15 min; (E) 75 °C, 3 h; (F) 75 °C, 3 h and 125 °C, 5 min; (G) 75 °C, 3 h and 125 °C, 10 min. The 00l lines marked with an asterisk are from the initial paraffin structure of the organo magadiite.

The X-ray diffraction pattern of epoxy-exfoliated magadiite composite completely cured at 125 °C for 3 h is shown in Figure 2.6. The absence of the 00l diffraction peaks provides strong evidence that the silicate layers of magadiite have been exfoliated in the thermoset curing process. However, the magadiite 2-dimensional structure is still retained in the exfoliated state, as indicated by a d₀₁₄ reflection at 3.4 Å. As indicated by the XRD data in Figure 2.5, the key to achieving an exfoliated composite structure is to first load the magadiite gallery with mobile onium ions and amine guest species and then expand the gallery region to a "critical gallery height" by replacing the amine with epoxide and poly(oxypropyleneamine) precursors. This expansion of the gallery by the precursors allows the intragallery and extragallery curing of the polymer to occur at comparable cross-linking rates.

2.3.3 Performance Properties of Exfoliated Epoxy-Magadiite Nanocomposites

The benefit of magadiite exfoliation in polymer reinforcement is illustrated by the tensile strength vs loading curves in Figure 2.7. The tensile strengths of the exfoliated magadiite nanocomposites are superior to the conventional composites prepared from both Na⁺-magadiite and C18-magadiite-LM. In obtaining these curves we adjusted the stoichiometry of epoxide and poly(oxypropyleneamine) by including the intragallery onium ion and amine as curing agents. The results are very predictable. Since the single silicate nanolayers have been dispersed into the polymer matrix, the exfoliated nanocomposite is more or less microscopically homogeneous relative to the macroscopic homogeneity of the conventional composites. Thus each nanolayer of the exfoliated composite contributes to the reinforcement effect.

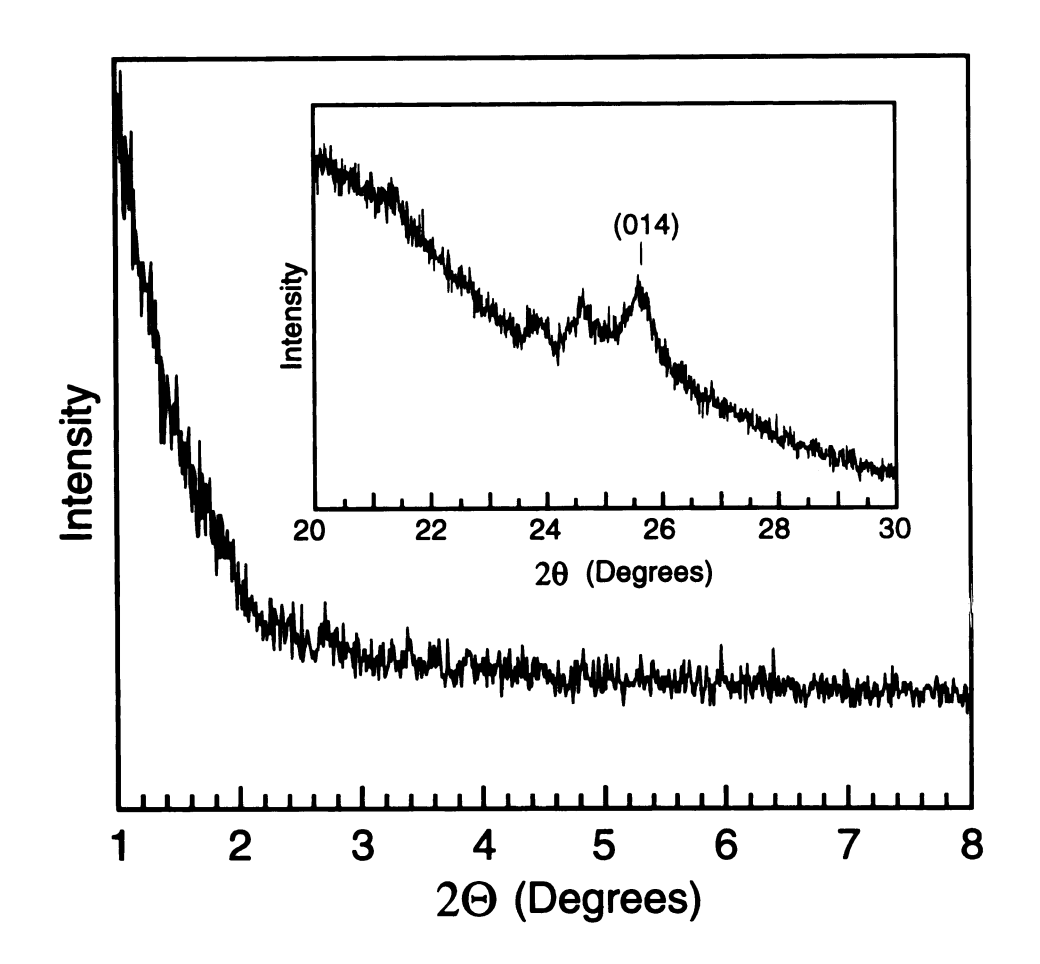


Figure 2.6 X-ray diffraction pattern of a cured epoxy polymer-magadiite nanocomposite prepared from C18-magadiite-PF. The organo silicate content was 15 wt %. Polymer curing was carried out at 75 °C for 3 h, and followed by 3 h at 125 °C.

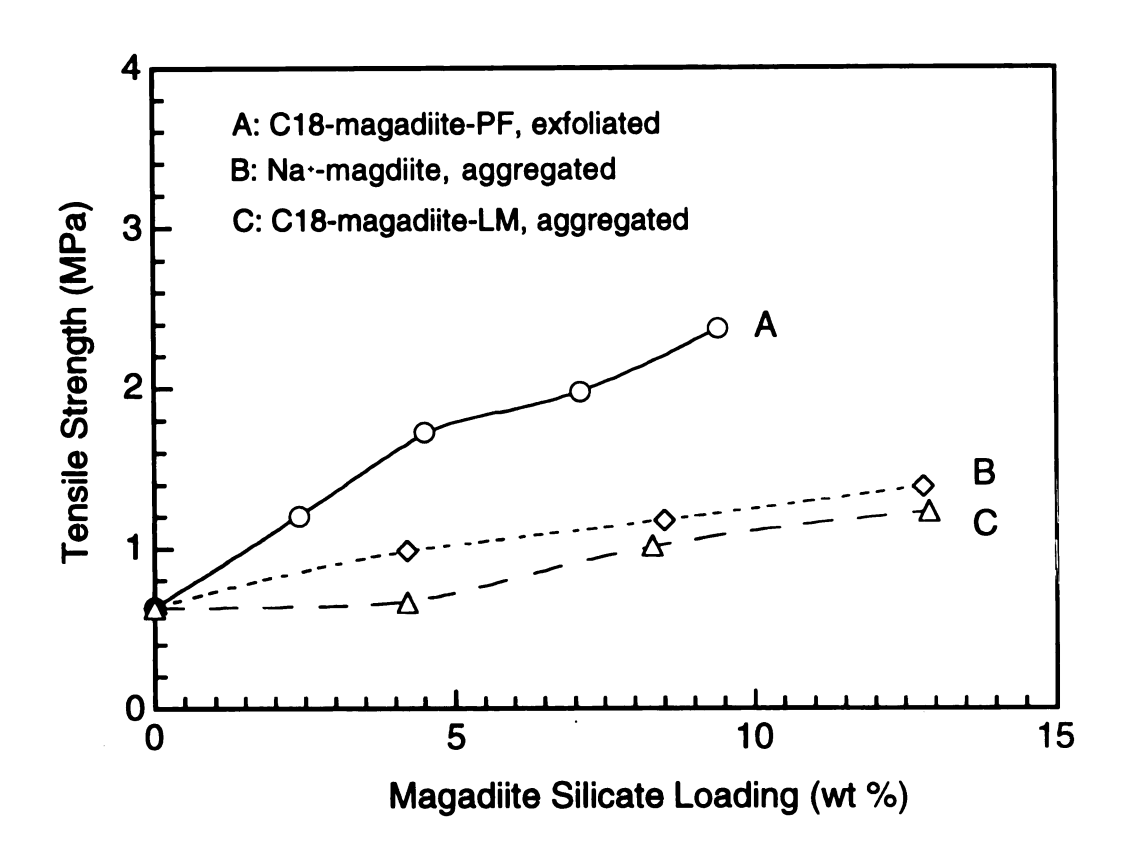


Figure 2.7 Comparison of the tensile strengths of an epoxy-exfoliated magadiite nanocomposite prepared from C18-magadiite-PF and conventional magadiite composites prepared from Na⁺-magadiite and C18-magadiite-LM. The inorganic silicate loading was determined by calcining the composites in air at 650 °C for 4 hours using a heating rate of 2 °C/min. The onium ion and amine content of the organo magadiite was counted as contributing to the stoichiometry of epoxide cross-linking.

Examples of epoxy hybrid composites based on smectite clay intercalates have been reported previously. 21,22 In comparison to the results obtained for epoxy-smectite clay nanocomposites, the reinforcement provided by magadiite is not as significant at higher loading. The difference in the charge density between magadiite and smectite results in a different loading of alkylammonium ions. It is quite likely that the onium exchange ions function as curing agents in the process of polymer cross-linking. This hypothesis was supported by an experiment wherein C18-magadiite-BL was swelled by epoxide and poly(oxypropyleneamine). The series of sharp XRD reflections present at the swelling stage disappear upon complete curing (Figure 2.8). This result signifies that C18-magadiite-BL can also be exfoliated in an epoxy polymer matrix. Therefore, it was necessary to investigate the effect of alkylammonium ion chain length on the mechanical behavior of our nanocomposites.

The dashed line (Curve B) in Figure 2.9 shows the results obtained if we do not compensate for the alkylammonium and alkylamine content of the organo magadite curing agent and use the stoichiometry amounts of epoxide resin and poly(oxypropyleneamine). The tensile moduli of the resulting nanocomposites exhibit a maximum. At low organo magadite loading, the effect was minimal due to reinforcement contribution of the layers, but at high loading, the effect of the gallery onium ion and amine is significant. Although the polymer network maintains its continuity, the excess amine weakens the composite and reduces the benefit derived from exfoliation of the silicate layers. However, we still obtain some benefit from the effect of excess alkylamine in nanocomposite formation. The strain-at-break is significantly improved by the excess alkylamine provided by the organo magadite (Figure 2.10). A very elastic nanocomposite with higher tensile strength and modulus is obtained. Significantly, this plasticizing effect can not be achieved by adding an excess of poly(oxypropyleneamine) in the absence magadite reinforcement.

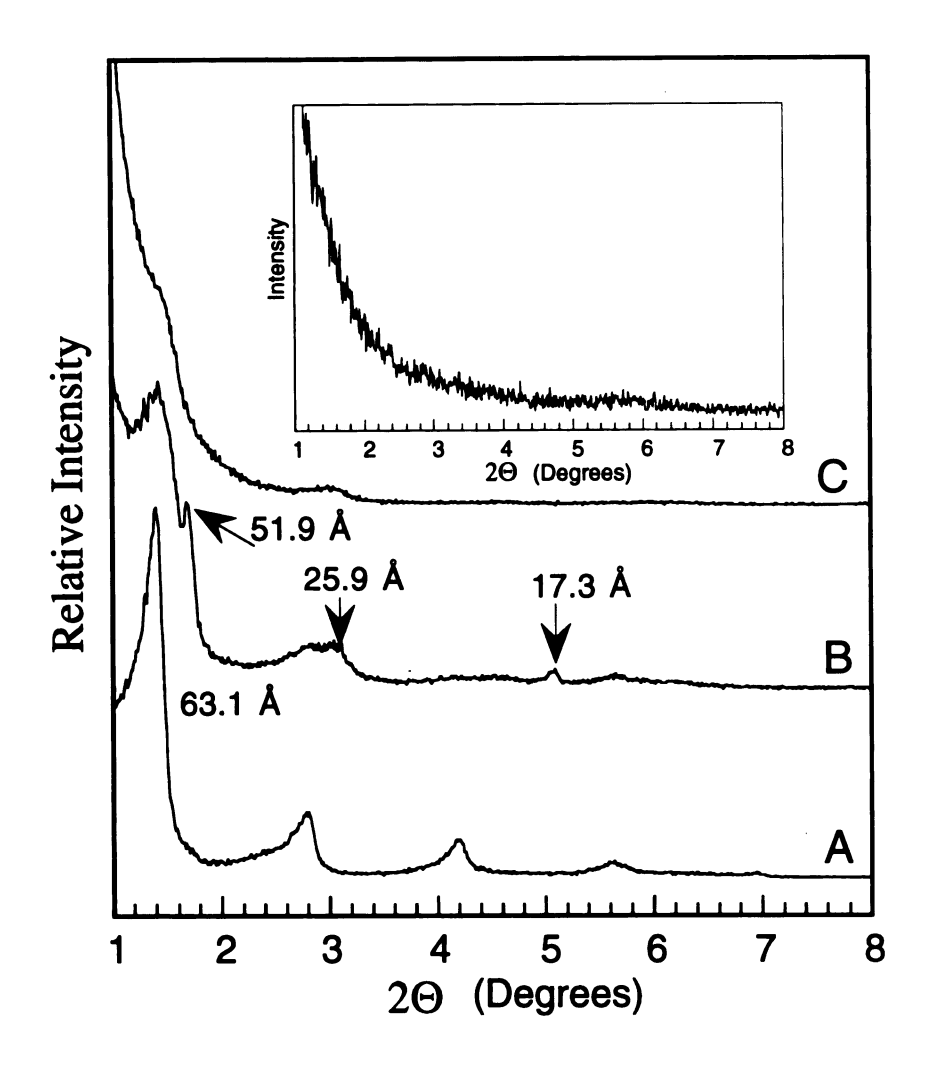


Figure 2.8 X-ray diffraction patterns of products prepared by reaction of (A) C18-magadiite-BL (15 wt % loading) with epoxide resin and poly(oxypropyleneamine) curing agent at an epoxide group to amine group molar ratio of 2:1. Reaction conditions were as follows: (B) 75 °C, 60 min; (C) 75 °C, 120 min. The inset is a pattern for the cured epoxy polymer-magadiite nanocomposite prepared from C18-magadiite-BL. The marked sharp lines in pattern (B) are derived from the octadecylamine.

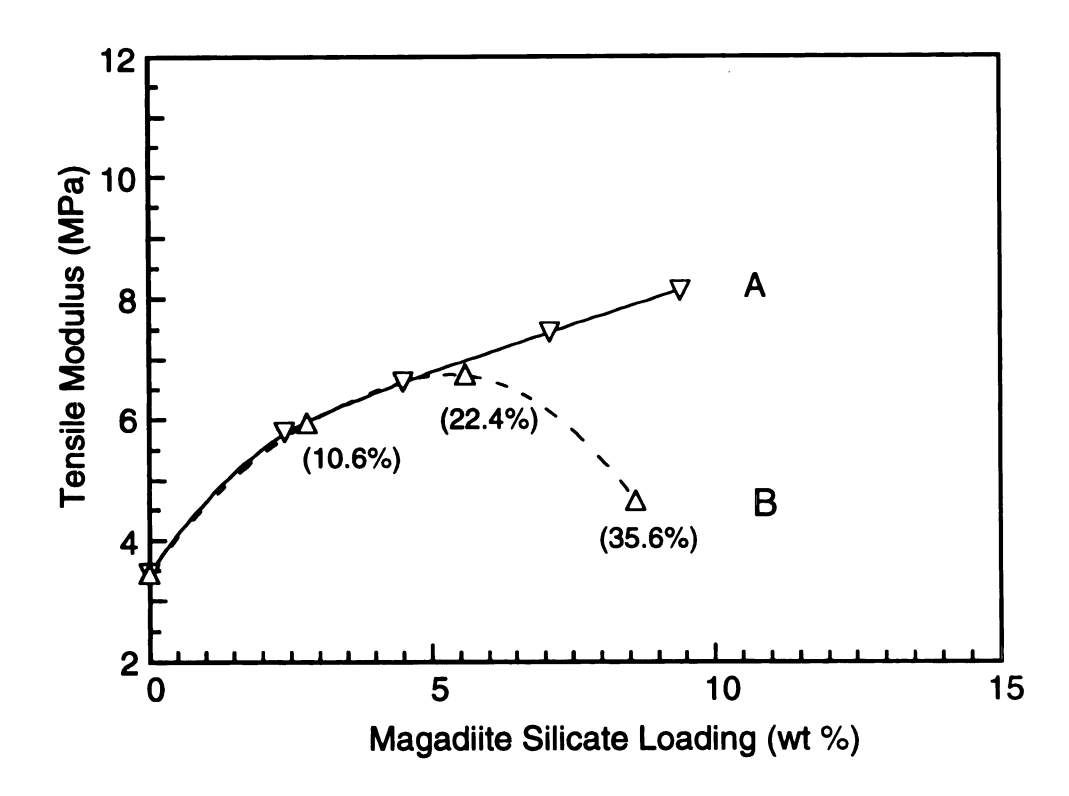


Figure 2.9 Effect of octadecylammonium and octadecylamine on the tensile modulus of epoxy-exfoliated magadiite nanocomposites prepared from C18-magadiite-PF. The solid line is for composites formed by including the onium ion and neutral amine content of the organo magadiite as a curing agent for epoxide crosslinking and reducing the amount of poly(oxypropyleneamine) accordingly; the dash line is for composites formed by disregarding the cross-linking reactivity of the gallery onium ion and amine in the initial intercalate and curing the resin with 1 equiv of poly(oxypropyleneamine). The values given in parenthesis for curve B are the molar fractions of excess alkylamine functional groups contributed by the onium ions and free amine relative to poly(oxypropyleneamine).

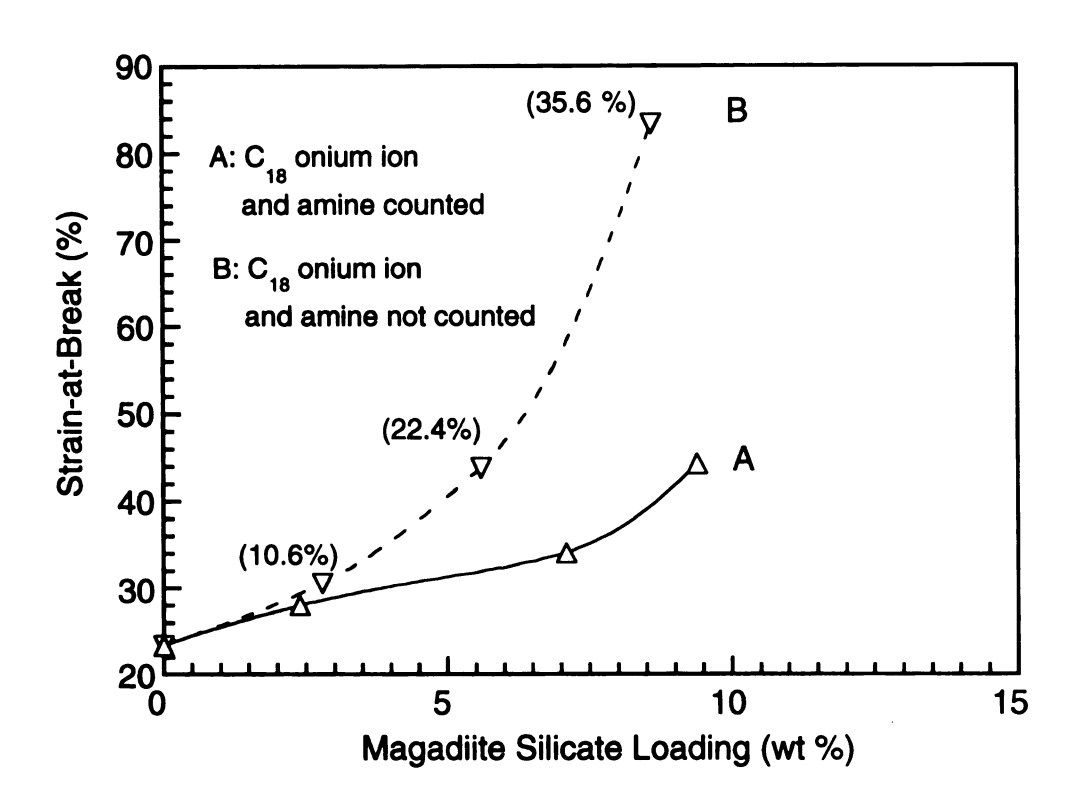


Figure 2.10 Effect of octadecylammonium and octadecylamine on the strain-at-break values of epoxy-exfoliated magadiite nanocomposite prepared from C18-magadiite-PF. The dashed line is for composites formed by not counting onium ion and amine content of the organo magadiite as contributing to the stoichiometry for epoxide crosslinking, the solid line is reversed. The values in parenthesis give the amount of excess amine curing agent due to the organo magadiite component.

The exfoliated nanocomposites are superior not only in their tensile properties. We also measured the chemical stability and solvent resistance for the exfoliated nanocomposites prepared from C18-magadiite-PF. The results are listed in Table 2.2.

Table 2.2 Chemical and Solvent Resistance of Epoxy-Exfoliated Magadiite Nanocomposites Prepared From C18-magadiite-PF (9.1 wt %). Values are the Immersion Weight Gain (wt %) after a Certain Period.

materials	10%	distilled	30%	5%	methanol ^b	toluenec
	NaOHa	H ₂ Oa	H ₂ SO ₄ ^a	acetic acida		
pristine polymer	1.6	2.5	16.7	13.4	76.5	189
C18-magadiite-PF	1.5	1.6	7.2	9.6	58.5	136

aweight gain after 15 days. bweight gain after 48 hr. cweight gain after 24 hr.

Since the pristine epoxy polymer has already offered good inertness to basic and aqueous solution uptake, we do not expect an impressive improvement for nanocomposites in these two cases. For inorganic acid and organic acid solutions, the exfoliated nanocomposite containing 9.1 wt % C18-magadiite-PF did show a significant reduction in uptake. The uptake of methanol and toluene was reduced substantially for the exfoliated nanocomposites. On the other hand, we observed that the barrier to solvent uptake by conventional and intercalated composites was not as significant as for the exfoliated nanocomposite. These barrier properties parallel tensile properties. Figure 2.11 shows the kinetic solvent uptake data for the nanocomposites prepared from C18-magadiite-PF relative to the pristine epoxy polymer.

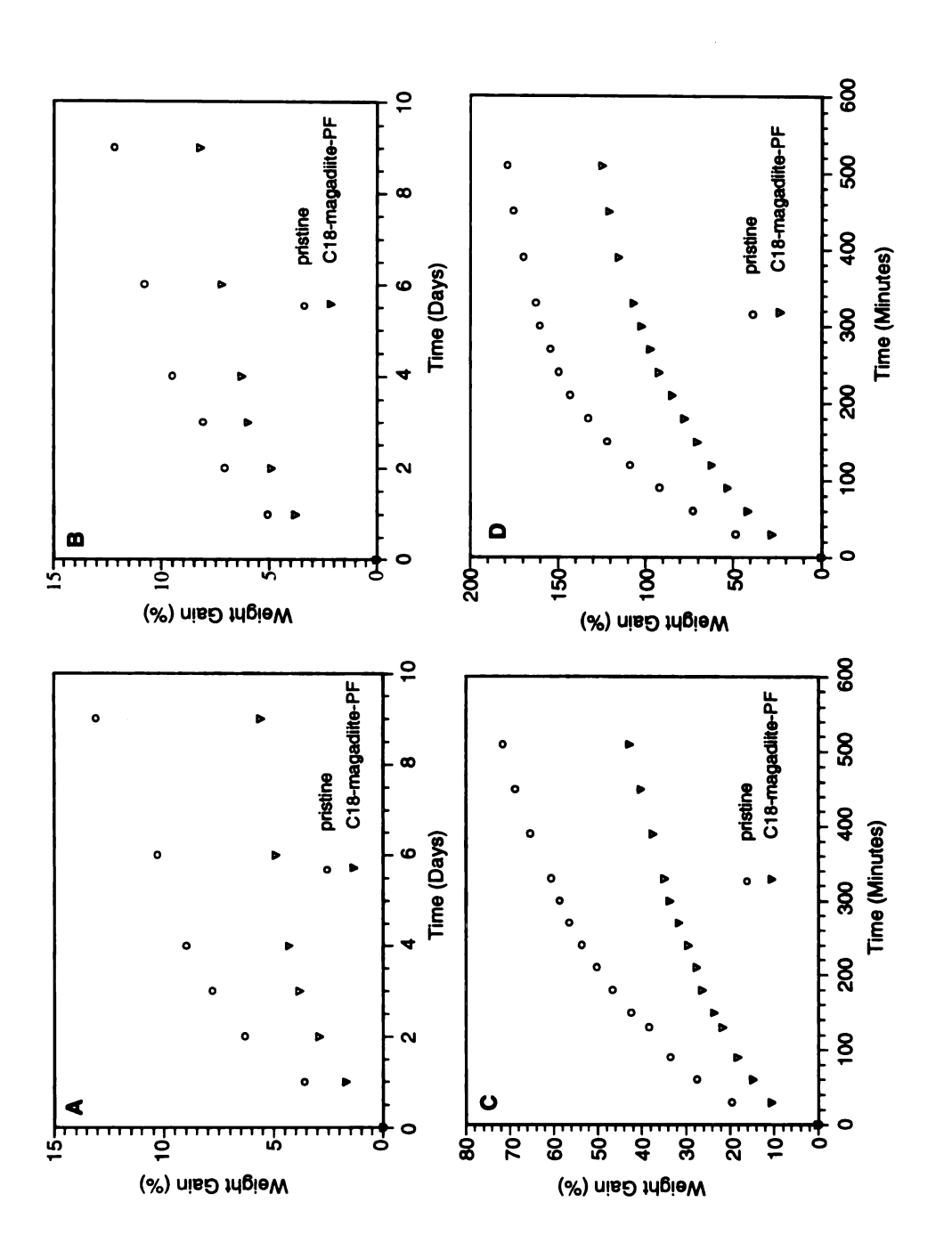


Figure 2.11 Chemical reagent and solvent uptake of (A) 30% sulfuric acid; (B) 5% acetic acid; (C) methanol; and (D) toluene by epoxy-exfoliated magadiite nanocomposites prepared from C18-magadiite-PF (9.1 wt %).

The most significant result we derive from the epoxy-magadiite system relative to epoxy-smectite nanocomposite is the unique transparent optical properties. As shown in Figure 2.12, the magadiite composites are much more transparent than the corresponding smectite composites at the same loading. This result suggests that the refraction index of magadiite nearer matches that of the organic matrix or that the magadiite is fully exfoliated more than the smectite clay. Future studies will address the transparent properties, which represent a significant milestone in the development of polymer-clay nanocomposites.

2.4 Conclusions

In conclusion, three organo magadiite intercalates have been synthesized. The lateral monolayer intercalate, which contains only intercalated onium ions and no free amine, is not organophilic enough to be intercalated by epoxy monomer and curing agent. The lipid bilayer intercalate can be exfoliated into the epoxy matrix, but the high gallery concentrations of onium ion and free amine compromise the properties of the matrix by participating in the curing process. Thus, the reinforcing benefit of the nanolayers is diminished. The paraffin intercalate is best suited for exfoliation into an epoxy matrix, because the gallery concentration of onium ion and free amine is sufficient to impart a hydrophobic environment and allow monomer intercalation without greatly disrupting the integrity of the polymer network. The transparent properties of the composites, together with the barrier film properties of these materials should make them especially attractive for packaging materials and protective films.

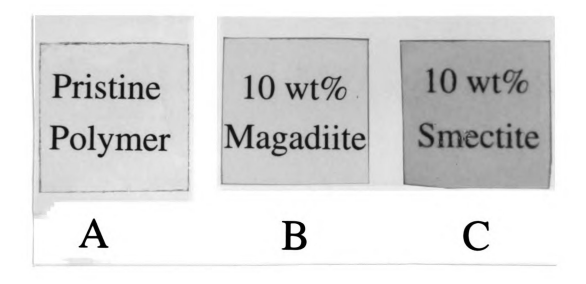


Figure 2.12 Comparison of the optical properties among (A) a pristine epoxy polymer; (B) an epoxy-exfoliated magadiite nanocomposite prepared form C18-magadiite-PF; (C) an epoxy-exfoliated smectite clay nanocomposite prepared from $CH_3(CH_2)_{17}NH_3^+$ ion-exchange montmorillonite (from Wyoming, cf. reference 21). The thickness of each sample is ~ 1 mm. Polymer curing was carried out at 75 °C for 3 h, and followed by 3 h at 125 °C.

2.5 References

- 1. Usuki, A.; Kawasumi, M.; Kojima, Y.; Okada, A.; Kurauchi, T.; Kamingaito, O. *J. Mater. Res.* **1993**, 8, 1174.
- 2. Usuki, A.; Kojima, Y.; Kawasumi, M.; Okada, A.; Fukushima, Y.; Kurauchi, T.; Kamigaito, O. J. Mater. Res. 1993, 8, 1179.
- 3. Kojima, Y.; Usuki, A.; Kawasumi, M.; Okada, A.; Fukushima, Y.; Kurauchi, T.; Kamigaito, O. J. Mater. Res. 1993, 8, 1185.
- 4. Okada, A.; Usuki, A. Mater. Sci. Eng. 1995, C3, 109.
- 5. Messersmith, P. B.; Giannelis, E. P. Chem. Mater. 1993, 5, 1064.
- 6. Wang, M. S.; Pinnavaia, T. J. Chem. Mater. 1994, 6, 468.
- 7. Lan, T.; Kaviratna, P. D.; Pinnavaia, T. J. Chem. Mater., 1995, 7, 2144.
- 8. Giannelis, E. P. Adv. Mater. 1996, 8, 29.
- 9. Lagaly, G.; Beneke, K.; Weiss, A. Am. Mineral. 1975, 60, 642.
- 10. Beneke, K.; Lagaly, G. Am. Mineral. 1977, 62, 763.
- 11. Beneke, K.; Lagaly, G. Am. Mineral. 1983, 68, 818.
- 12. Schwieger, W.; Heidemann, D.; Bergk, K. H. Revue de Chimie Minérale 1985, 12, 639.
- 13. Rojo, J. M.; Ruiz-Hitzky, E.; Sanz, J. *Inorg. Chem.* **1988**, 27, 2785.
- 14. Pinnavaia, T. J.; Johnson, I. D.; Lipsicas, M. J. Solid State Chem. 1986, 63.
- 15. Dailey, J. S.; Pinnavaia, T. J. Chem. Mater. 1992, 4, 855.
- 16. Wong, S. T.; Cheng, S. Chem. Mater. 1993, 5, 770.
- 17. Ruiz-Hitzky, E.; Rojo, J. M. Nature 1980, 287, 28.
- 18. Sugahara, Y.; Sugimoto, K.; Yanagisawa, T.; Nomizu, Y.; Kuroda, K.; Kato, C. Yogyo Kyokai Shi 1987, 95, 117.
- 19. Fletcher, R. A.; Bibby, D. M. Clays Clay Miner. 1987, 35, 318.
- 20. Fukushima, Y.; Okada, A.; Kawasumi, M.; Kurauchi, T.; Kamigaito, O. *Clay Miner.* **1988**, 23, 27.
- 21. Lan, T.; Kaviratna, P. D.; Pinnavaia, T. J. Chem. Mater., 1994, 6, 573.

22. Messersmith, P. B.; Giannelis, E. P. Chem. Mater. 1994, 6, 1719.

Chapter 3

MECHANISM OF LAYERED SILICIC ACID NANOLAYER EXFOLIATION IN EPOXY-MAGADIITE NANOCOMPOSITES

3.1 Introduction

The breakthrough represented by nylon-6-clay nanocomposites presages the development of a new area of composite science and technology based on organic polymer-inorganic nanolayer interactions. ¹⁻³ In the passed few years, this revolutionary nanocomposite chemistry has been successfully extended to the other polymer systems such as polyimide, ^{4,5} epoxy ^{6,7} and polysiloxane. ⁸ Among these, the epoxy-clay nanocomposites with a sub-ambient Tg exhibited exceptionally strong reinforcing effects. For instance, 7.5 vol. % of the exfoliated 10 Å-thick silicate layers improve the strength of polymer matrix stronger by more than 10-fold. ⁹

Approaches to the exfoliation of clay nanolayers have been investigated by several different research groups using both thermoplastic and thermoset polymers.^{3,10-12} The hydrophilic inorganic clay surface usually has to be modified to accommodate the incoming organic precursors. Generally, an organic cation exchanged reaction is used to form a hydrophobic organo clay. Then, the organo clay is intercalated by polymer precursors which are either organic monomers or prepolymers. In situ intercalative polymerization is a very successful approach for the preparation of exfoliated polymer-clay nanocomposites.¹³⁻¹⁵ In this approach, the acidic intragallery cations function as catalyst centers and cause the intragallery polymerization rate to be competitive with the extragallery polymerization rate. This competitive polymerization results in the

exfoliation of the silicate nanolayers in a monolithic polymer matrix. However, this exfoliation chemistry has only been developed for smectite clay, few other layered inorganic materials have demonstrated this similar chemistry. It is recognized that clay nanolayer exfoliation generally improves mechanical properties, 7,9,16 quantitative studies of the relationship between performance properties and the degree of clay layer exfoliation are unavailable. In order to facilitate the development and practical utilization of this new family of nanocomposite materials, several fundamental chemistry and physics issues regarding nanocomposite formation need to be elucidated.

In last chapter, we have successfully extended the exfoliation chemistry developed for smectite clays to magadiite, a typical member of layered silicic acid family. Layered silicic acids possess some special properties, which are not available to smectite clays, so another modeling system has been provided to address the issues relative to the exfoliation. Optimistically, the exfoliation of layered silicic acids in polymer matrices may contribute further understanding of the nanolayer exfoliation processes, the relationships between the structure, composition, and performance properties, and the basic physics behind the reinforcement.

3.2 Experimental

Materials. The epoxide resin used to for epoxy-magadiite hybrid composite formation was poly(bisphenol A-co-epichlorohydrin) (Shell, EPON 828), with MW ~377:

CH₂- CHCH₂O
$$\leftarrow$$
 CH₃ OCH₂CHCH₂O \rightarrow CH₃ OCH₂CH-CH₂O \rightarrow CH₃OCH₂CH-CH₂O \rightarrow CH₃OCH₂OCH₂CH-CH₂O \rightarrow CH₃OCH₂CH-CH₂O \rightarrow CH₃OCH₂CH-CH₂O \rightarrow CH₃OCH₂CH-CH₂O \rightarrow CH₃OCH₂CH-CH₂O \rightarrow CH₃OCH₂OCH

The curing agent was poly(propylene glycol) bis(2-aminopropyl ether) (Huntsman Chemical, JEFFAMINE D-2000), with MW ~2000:

$$H_2NCHCH_2 = OCH_2CH = NH_2$$
 $CH_3 = CH_3$
 $X=33.1$

The above monomers afford a rubbery-like epoxy polymer matrix with a sub-ambient Tg of -40 °C. All the other chemicals used in this work were purchased from Aldrich Chemical Co. and used without further purification.

Synthesis of Na⁺-magadiite. Na⁺-magadiite was synthesized according to the published methods.¹⁷ A suspension of 60.0 g of amorphous silica gel (1.0 mol) in 300 mL of 1.11 M NaOH solution (0.33 mol) was heated at 150 °C for 42 h with stirring in a Teflon-lined stainless steel 1.0 L Parr reactor. The suspension containing Na⁺-magadiite was centrifuged, and the solid product was washed twice with 600 mL of deionized water to remove excess NaOH, and air-dried at room temperature.

Synthesis of Organo Magadiite. Quaternary alkylammonium exchanged magadiites were prepared in general by the reaction of 10.0 g of Na⁺-magadiite with 800 mL of 0.117 M CH₃(CH₂)_{n-1}N(CH₃)₃+Br⁻ (n = 12, 16, 18) aqueous solution at 65 °C for 48 hr. The products were centrifuged and washed by deionized water until free of Br⁻. For reaction with n = 12, 16, the reaction was stopped after 24 hr, and resumed for an additional 24 hr after the mother liquor had been replaced with a fresh solution of onium ions. This treatment could be repeated until free of the Na⁺-magadiite phase, which could be checked by the x-ray diffraction technique.

Primary, secondary and tertiary long chain alkylammonium exchanged CH₃(CH₂)₁₇NH_{3-n}(CH₃)_n+-magadiites (n = 0, 1, 2) were prepared by the following approach. An aqueous suspension containing 15.0 g of Na⁺-magadiite was combined with ethanol/water solution containing 0.141 mol of alkylammonium chloride and alkylamine in a 6:1 molar ratio to form a suspension in 1.0 L of 1:1 (v:v) ethanol/water total solution. This suspension was stirred at 65 °C for 48 hours. The pH of the reaction mixture was in the range of 8 - 9. The product mixture was added to an equal volume

ethanol and centrifuged. The wet solid product was washed consecutively with one 750-mL portion of 50 % EtOH, two 750-mL portions of 25 % EtOH and then with water until free of Cl⁻, and air-dried. The air-dried organo magadiite was ground to a powder with a particle size smaller than 270 mesh (53 µm) and stored for further use.

Preparation of Epoxy-Magadiite Composites. Equivalent amounts of epoxide resin and poly(oxypropyleneamine) curing agent were mixed at room temperature for 30 min. The desired amount of organo magadiite was added to the epoxide-poly(oxypropyleneamine) mixture and stirred for another 60 min. This mixture was outgassed in a vacuum oven and poured into a stainless steel mold for curing at 75 °C for 3 h and, subsequently, at 125 °C for an additional 3 h.

X-ray Powder Diffraction (XRD). XRD patterns were recorded on a Rigaku rotaflex 200B diffractometer. Samples of wet solid organo magadiite products, epoxysolvated magadiites, and uncured epoxy-magadiite composites were prepared by applying thin films on glass slides. Cured composite specimens were prepared by mounting a flat rectangular sample into an aluminum holder.

Chemical Analysis. CHN analysis is determined by combustion of samples in an oxygen atmosphere at 980 °C. Na and Si are determined by ICP analysis.

Thermal Analysis. Thermogravimetric analyses (TGA) were performed using a Cahn TG System 121 thermogravimetric analyzer. Samples were heated to 750 °C at a heating rate of 5 °C/min under N₂ atmosphere.

Surface Area Measurement. N_2 adsorption-desorption isotherms were determined on a ASAP 2010 Sorptometer at liquid N_2 temperature using a static sorption mode. Samples were outgassed at 150 °C and 10⁻⁵ Torr for 12 h. Surface areas were determined using BET plots.

Mechanical Measurement. Tensile testing was performed at ambient temperature according to ASTM procedure D3039 using a SFM-20 United Testing System.

Chemical and Solvent Resistance. The resistance of the composite materials to solvent swelling was obtained according to ASTM procedure D543. The specimens were immersed in the desired reagent and removed periodically to measured the weight gain until equilibrium was reached.

3.3 Results and Discussion

3.3.1 Synthesis of Organo Magadiites With Paraffin Structures

In the approach of *in situ* intercalative polymerization for the synthesis of polymer-clay nanocomposites, the intragallery acidic catalytic centers play a very important role to afford a competitive intragallery polymerization rate.⁶ By using onium ions of different Brönsted acidity, it is possible to achieve a series of polymer-layered silicate nanocomposites with different degree of layer separation.

Recently, we developed a new approach to paraffin-like intercalated phases of organo magadiite using long chain primary alkylammonium surfactants and a neutral amine as gallery guests. This significantly reduced the amount of neutral amine needed to form the intercalate. In the present work, we have extended this new synthesis approach to prepare the other organo magadites with paraffin-like gallery structures using long chain secondary and tertiary alkylammonium ions in place of primary onium ions. A quaternary alkylammonium ion exchanged magadiite was also prepared using the previous known method. 18 Figure 3.1 shows the powder x-ray diffraction patterns for $CH_3(CH_2)_{17}NH_{3-n}(CH_3)_n^+$ -magadite (n = 0, 1, 2, 3). Table 3.1 lists their intragallery compositions, d₀₀₁ basal spacings and gallery structures. The primary and secondary alkylammonium exchanged magadiites with n = 0 and 1, require a small amount of neutral amine to achieve this particular paraffin-like structure. We also find that when amine head groups are bigger, less neutral amine is needed for achieving this paraffinlike structure. Consequently, the tertiary alkylammonium exchanged magadiite is more truly an ion exchanged product without additional neutral amine molecules. Due to the hydrophobic nature of $CH_3(CH_2)_{17}NH_{3-n}(CH_3)_n^+$ (n = 0, 1, 2) salts and their amine

analogue, the sodium ions are rarely retained in these paraffin structures as judged by both elemental analysis and TGA results. The residue of sodium ions in the gallery for the quaternary alkylammonium exchanged magadiite can be overcome by applying multiple ion-exchange reactions. The small fraction of protons existed in C18A3M-magadiite is due to multiple washing by water in an effort to remove the extra salts. It is noteworthy that the initial products obtained by ion-exchange reaction with $CH_3(CH_2)_{17}NH_{3-n}(CH_3)_n^+$ -magadiite (n = 0, 1) are a mixture of lipid bilayer and paraffin phases as shown in Figure 3.2 (also see Figure 2.3). The washing process can unify the phases existing in reaction media, however, this process has to be adjusted so that a lateral monolayer structure can be avoided except for n = 3. It is has been proved that organo magadiites with the lateral monolayer structure are not expandable by polymer precursors due to the high electrostatic interactions between their silicate nanolayers and the exchange cations.

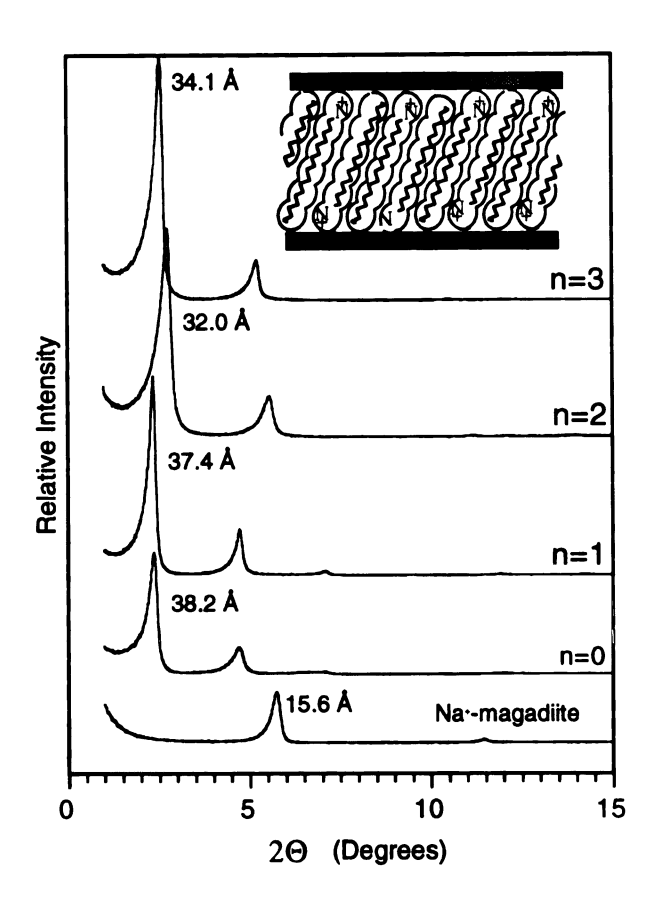


Figure 3.1 X-ray powder diffraction patterns of air-dried Na⁺-magadite and $CH_3(CH_2)_{17}NH_{3-n}(CH_3)_n$ ⁺-intercalated magadites (n = 0, 1, 2, 3). The organo magadites have paraffin-like gallery structures with onium ion and free amine compositions given in Table 1.

Intercalates Formed by Reaction of Na+-magadiite with CH₃(CH₂)₁₇NH_{3-n}(CH₃)_n+Cl⁻ and CH₃(CH₂)₁₇NH₂₋ $_{n}(CH_{3})_{n}$ (n = 0, 1, 2) or $CH_{3}(CH_{2})_{17}N(CH_{3})_{3}^{+}Br^{-}$ (n = 3) Table 3.1

u	material designation	organo species existing	intragallery composition ^a	gallery	d ₀₀₁
		in reaction	per Si ₁₄ O ₂₉ ² - unit cell	structure (Å)	(Å)
0	0 C18-magadiite-PF	C ₁₈ bNH ₃ + & C ₁₈ NH ₂	(C ₁₈ NH ₃ +) _{2.0} (C ₁₈ NH ₂) _{0.48}	paraffin	38.2
-	C18A1M-magadiite	C ₁₈ NH ₂ Me ⁺ & C ₁₈ NHMe	C ₁₈ NH ₂ Me ⁺) _{2.0} (C ₁₈ NHMe) _{0.30}	paraffin	37.4
7	C18A2M-magadiite	C ₁₈ NHMe ₂ + & C ₁₈ NMe ₂	$(C_{18}NHMe_2^+)_{2.0}$	paraffin	32.0
3	C18A3M-magadiite	nagadiite C ₁₈ NMe ₃ +	$(C_{18}NMe_3^+)_{1.62}Na^+_{0.12}H^+_{0.26}$	paraffin 34.1	34.1

^a The compositions were determined by elemental analysis and TGA measurement.

^b C₁₈=CH₃(CH₂)₁₇

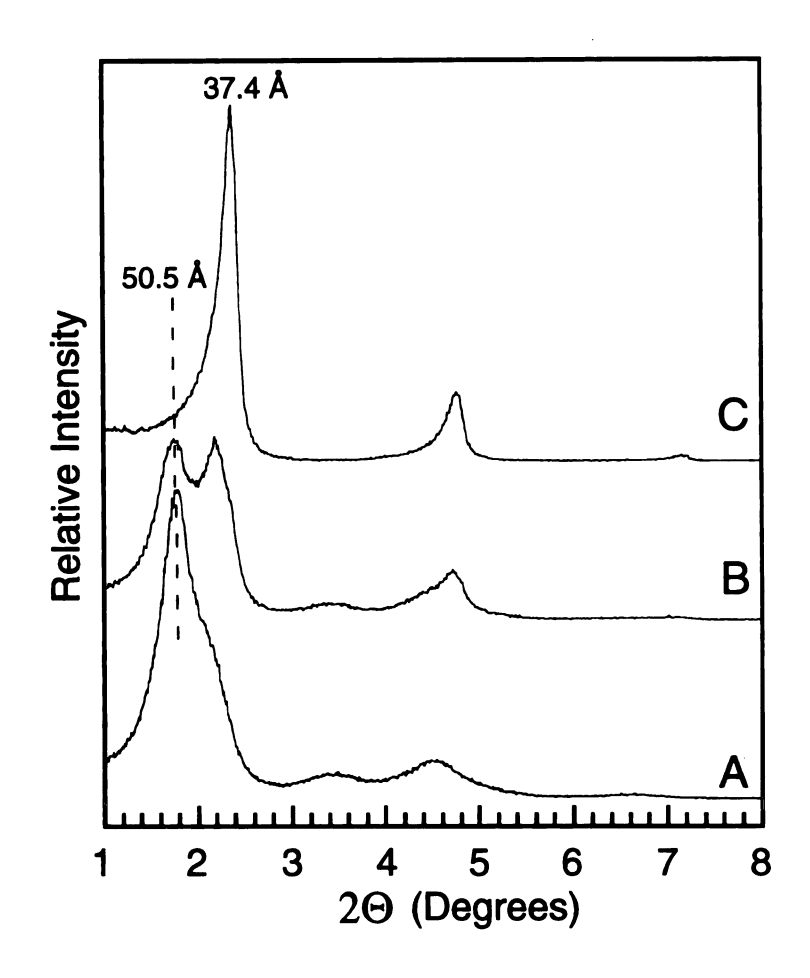


Figure 3.2 Effect of washing on the formation of C18A1M-magadiite. The product in Pattern (A) was obtained by centrifuging the secondary alkylammonium exchanged reaction mixture without further treatment. The product in pattern (B) was formed when the onium ion exchanged reaction mixture was washed with an equal volume of ethanol. The paraffin phase in pattern (C) was obtained by washing the product of pattern (B) with 50% EtOH.

3.3.2 Swelling Properties of Organo Magadiites

All of the paraffin structures described in Table 3.1 can be intercalated by epoxide resin at 75 °C to give intercalates with about 42 Å basal spacings (Table 3.2). In this epoxide intercalation reaction, the onium ions reorient from an inclined angle to a perpendicular orientation so that extra intragallery space is formed to accommodate the intercalated epoxide resin. The solvation of these paraffin structures by the poly(oxypropyleneamine) (D-2000) curing agent gives products with different gallery structures. For instance, C18-magadiite-PF and C18A1M-magadiite can be intercalated by the D-2000 curing agent. For C18-magadite-PF, the basal spacing increases from 38.2 Å to 63.3 Å; whereas for C18A1M-magadiite, the basal spacing increases from 37.4 Å to 52.4 Å initially. This intercalation process is facilitated by the proton transfer reaction between the curing agent and gallery onium ion. However, the solvation of C18A2M-magadite and C18A3M-magadite by D-2000 is not thermodynamically favored due to the lower acidity of the onium ions and the presence of metal ions for C18A3M-magadiite. The co-intercalation of the mixture of epoxide resin and D-2000 curing agent was quite successful for all of the organo magadiites. The different increased basal spacings are derived from the solvation abilities of D-2000 curing agent and epoxide resin. All these solvation results are summarized in Table 3.2 and verified by our XRD studies. The XRD results for the co-intercalation of C18A2M-magadiite and C18A3M-magadiite by the mixture of epoxide resin and D-2000 curing agent at an elevated temperature are shown in Figure 3.3 and Figure 3.4, respectively.

Table 3.2 Basal Spacings $(d_{001}, Å)$ for $CH_3(CH_2)_{17}NH_{3-n}(CH_3)_n^+$ -magadiite Paraffin Structures Under Air-dried Conditions and Solvated by Epoxy Resin (EPON 828), Poly(oxypropyleneamine) (D-2000) Curing Agent, and a Stoichiometric Mixture of These Polymer Precursors

n	air-dried	epoxy	D-2000	epoxy & D-2000
		solvated	solvated	solvated
0	38.2	42.5	63.3	62.7
1	37.4	41.9	52.4	51.4
2	32.0	42.5	32.4	43.1
3	34.1	41.7	34.2	39.1

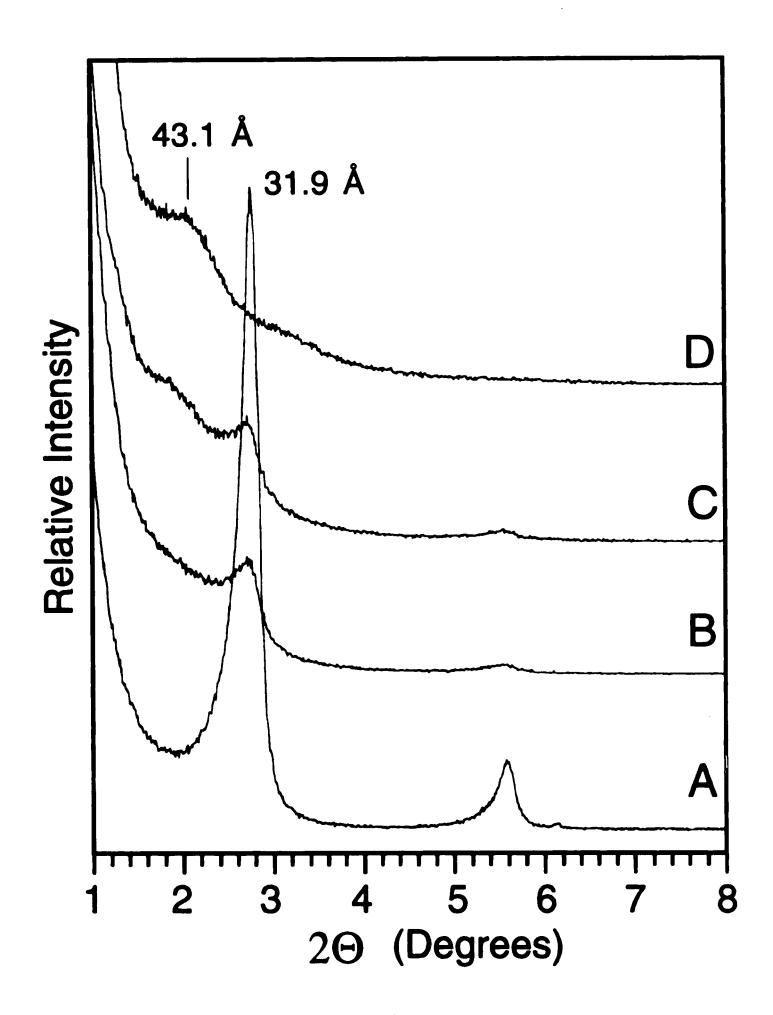


Figure 3.3 X-ray diffraction patterns of products prepared by reaction of C18A2M-magadiite (15 wt % loading) with a stoichiometric mixture of epoxide resin and poly(oxypropyleneamine) curing agent under the reaction conditions as follows: (A) 75 °C, 10 min; (B) 75 °C, 90 min; (C) 75 °C, 120 min; (D) 75 °C, 3 h and 125 °C, 20 min.

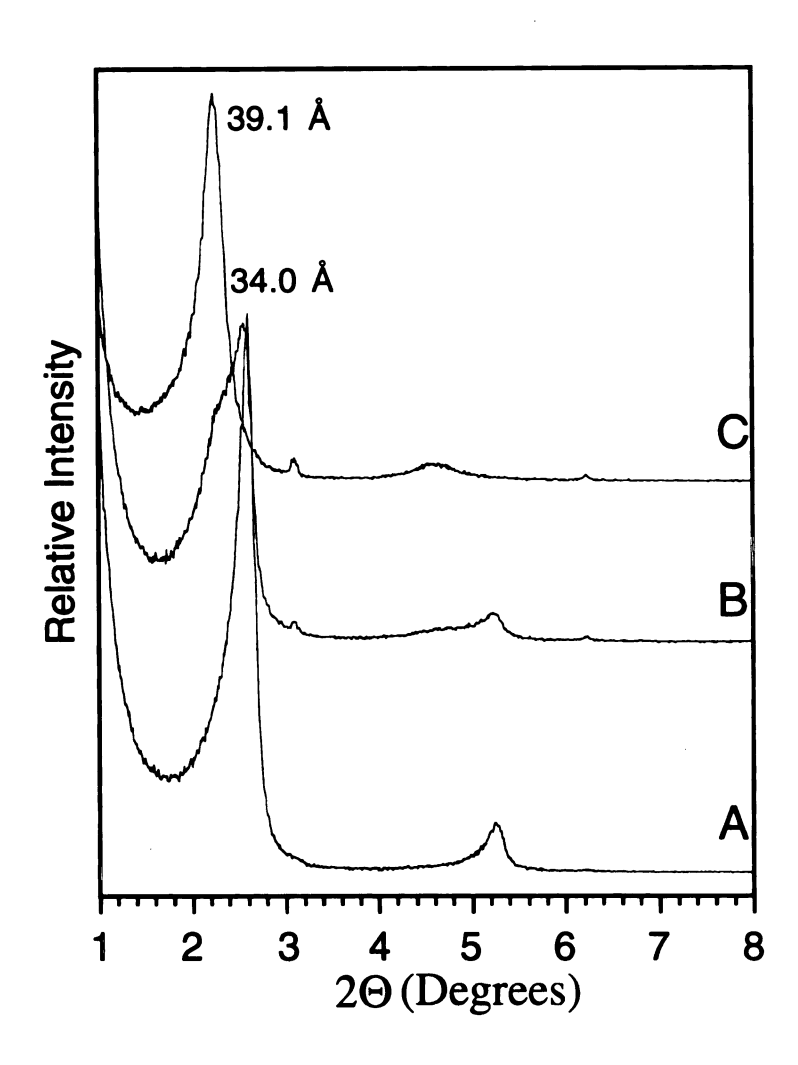


Figure 3.4 X-ray diffraction patterns of products prepared by reaction of C18A3M-magadiite (20 wt % loading) with a stoichiometric mixture of epoxide resin and poly(oxypropyleneamine) curing agent under the reaction conditions as follows: (A) 75 °C, 10 min; (B) 75 °C, 30 min; (C) 75 °C, 45 min.

3.3.3 Exfoliation of C18A1M-Magadite in an Epoxy Matrix

The co-intercalation of C18A1M-magadiite by a 2:1 molar mixture of epoxy resin and curing agent as a function of time is investigated by XRD (Figure 3.5). The solvation of C18A1M-magadiite by resin and curing agent is initially very slow at room temperature (Figure 3.5A), since the viscosity of the system is high and diffusion process is very low. Upon heating at 75 °C, the C18A1M-magadiite is rapidly solvated as evidenced by a broad x-ray peak at low angle (Figure 3.5B). This two-phase mixture is quickly replaced by a single d₀₀₁ peak at 51.4 Å (Figure 3.5C) corresponding to the onium ions totally reoriented as an inclined bilayer conformation to accommodate the intercalated epoxy resin and curing agent. The 51.4 Å peak is eventually replaced by another peak at 57.0 Å (Figure 3.5D) to provide more intragallery space, presumably through more extension of alkyl chains. Finally, a phase with 62.7 Å basal spacing appears, corresponding to the onium ions with a lipid bilayer orientation (Figure 3.5E). This phase is crucial to achieving an exfoliated state instead of an intercalated state of the layer silicates. In this phase, the organo onium ions adopt an optimized orientation to afford maximum intragallery space for the intercalated species. The interactions between silicate nanolayers and polymer precursors are balanced by the electrostatic forces between silicate layers. Beyond this stage, the interactions between intercalates and silicate layers are more favored than electrostatic interactions between silicate layers. This hypothesis is supported by the following XRD results. Figure 3.5F indicates that the platelets do not have to keep their original stacking registry when intragallery region has been expanded beyond that critical region. The final x-ray amorphous phase (Figure 3.5G) suggests that an exfoliated state had been achieved in which silicate layer exfoliated dispersed in organic matrix. Our previous results have showed that the primary alkylammonium exchanged C18-magadiite-PF also goes through this intercalation-exfoliation process with slight difference.

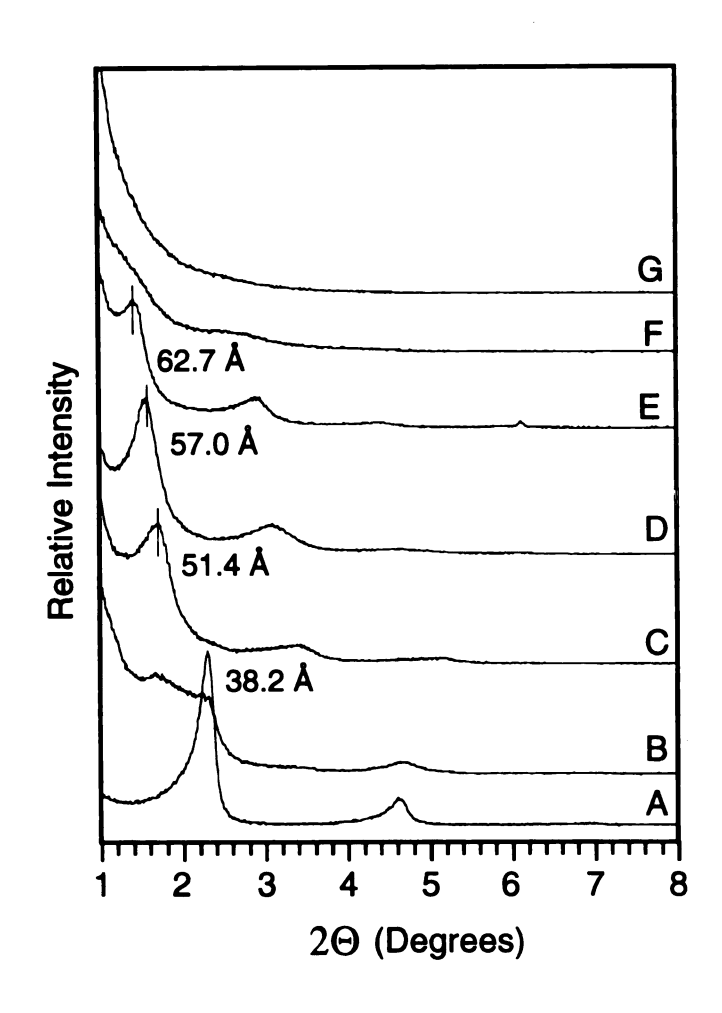
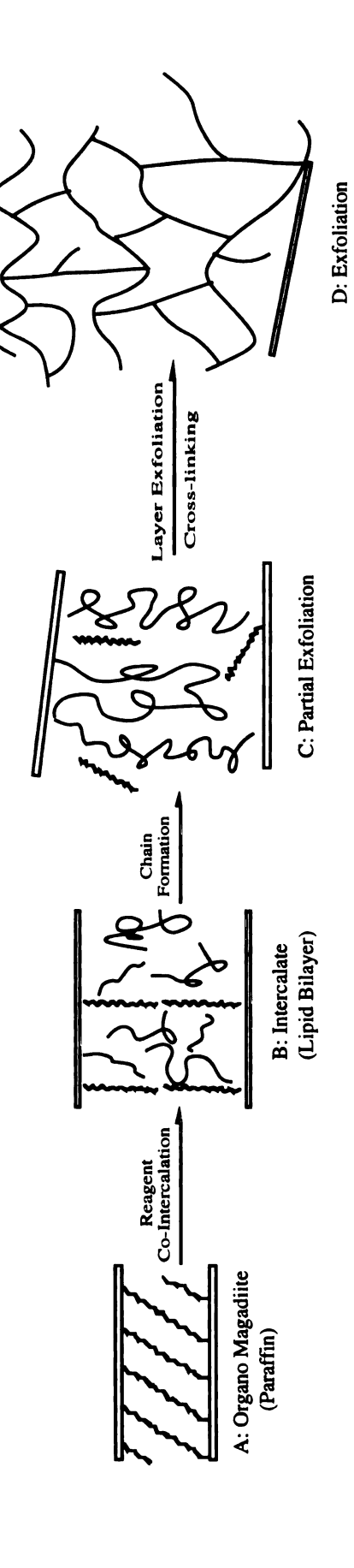


Figure 3.5 X-ray diffraction patterns of products prepared by reaction of C18A1M-magadiite (15 wt % loading) with a stoichiometric mixture of epoxide resin and poly(oxypropyleneamine) curing agent (epoxide group to amine group molar ratio of 2:1). Reaction conditions were as follows: (A) 25 °C, 30 min; (B) 75 °C, 10 min; (C) 75 °C, 15 min; (D) 75 °C, 30 min; (E) 75 °C, 60 min; (F) 75 °C, 70 min; (G) 75 °C, 90 min.

3.3.4 Mechanism of Silicate Nanolayer Exfoliation For Organo Magadiites

Figure 3.6 illustrates a pathway for the formation of an epoxy-exfoliated magadiite nanocomposite formed from an acidic CH₃(CH₂)₁₇NH_{3-n}(CH₃)_n+-magadiite with n = 0, 1. The organophilic magadite with a paraffin-like structure (Figure 3.6A) is the starting point which can be easily co-intercalated by stoichiometric ratio of the epoxide resin and D-2000 curing agent at an elevated temperature. An intercalate is formed with the gallery height expected from a lipid-like bilayer formation of onium ions (Figure 3.6B). The intragallery acidic onium ions catalyze the epoxide polymerization to afford a competitive intragallery polymerization rate relative to extragallery rate, so the gallery will expand beyond a bilayer region (Figure 3.6C). The relative rates of reagent intercalation, chain formation and network cross-linking must be controlled to form the final epoxy-magadiite exfoliated nanocomposite (Figure 3.6D). It is seems that the intercalation is thermodynamically favored especially at elevated temperature, because the overall exfoliation process requires an entropy increase. The onium ion protons play an essential role in this *in-situ* polymerization process to satisfy all these requirements. The D-2000 curing agent has a mild reactivity to give chain formation privilege over cross-linking formation, in another word, the gel time is also an important factor to decide the morphology of the final product.



like gallery structure of onium ions and neutral amine (see Table 3.1 for compositions). (B) An intercalate formed when long chain Proposed pathway for epoxy-magadiite exfoliated nanocomposite formation: (A) An organo magadiite with paraffinalkylammoniums reorienting from a paraffin to a lipid bilayer orientation to accommodate the co-intercalation of epoxide and curing agent. (C) The gallery height exceeds the value characteristic of a lipid bilayer due to the rapid intragallery polymerization rate. The silicate platelets start to tilt. The chain formation (gelation) is the main reaction for the epoxide and amino groups at this stage of the process. (D) Silicate nanolayers are completely exfoliated in a fully cross-linked epoxy polymer network. Figure 3.6

3.3.5 Effect of Gallery Acidity of Organo Magadiites on Formation of Nanostructures

The XRD patterns (Figure 3.7) of the cured composites prepared from $CH_3(CH_2)_{17}NH_{3-n}(CH_3)_n^+$ -magadite (n = 0, 1, 2, 3) show that three kinds of nanocomposite structures have been prepared. Two exfoliated epoxy-magadiite nanocomposites have been obtained from C18-magadiite-PF and C18A1M-magadiite for which the galleries are occupied by acidic primary or secondary alkylammonium/alkylamine with a paraffin structure. These exfoliated nanocomposites are characterized by the absence of XRD peaks at low angle. An intercalated nanocomposite is obtained from quaternary alkylammonium exchanged C18A3Mmagadiite, wherein the galleries are non-acidic. The formation of an intercalated nanocomposite for this exchange derivative is quite expected because of the absence of protons to catalyze the intragallery polymerization reaction and the strong interaction of the quaternary alkylammonium ions with the silicate surface. Interestingly, an ordered exfoliated nanocomposite is achieved by using C18A2M-magadiite with mild Brönsted acidity. In this ordered exfoliated nanocomposite, the registry of the silicate nanolayer stacking is sufficient to give x-ray scattering along 00l, but the gallery height is far larger than the value expected for an intercalated nanocomposite with a bilayer of long chain onium ions (cf., Figure 1.4). This result further supports our previous hypothesis concerning the exfoliation of silicate nanolayers. Because tertiary alkylammonium ions provide weak acidity to catalyze the intragallery epoxy polymerization, the gallery expansion will be mainly determined by the initial monomer loading in the gallery. Further expansion to the exfoliated state is precluded by the high viscosity and slow diffusion of additional monomers into the gallery. Our x-ray results show that the 2dimensional structure of magaditie is retained for all nanocomposite structures, as indicated by the several strong in-plane peaks. It is noteworthy that the ordered exfoliated nanocomposite is generally limited to synthetic layered silicates. The

homogenous distribution of layer charges in a synthetic clay results in a homogeneous intragallery polymerization rate. Most nature clays with a heterogeneous charge distribution will give broad x-ray peaks at low angle, because intragallery polymerization rate is not uniform from gallery to gallery.

3.3.6 Relationship Between Nanostructures and Performance Properties

It is interesting to note the relationship between mechanical performance and the extent of layer separation for epoxy-magadite nanocomposites. The mechanical properties for the epoxy nanocomposites prepared from C18-magadiite-PF have investigated in chapter 2. A comparison of tensile properties for the nanocomposites prepared form $CH_3(CH_2)_{17}NH_{3-n}(CH_3)_n$ +-magadities (n = 1, 2, 3) is shown in Figure 3.8. The tensile strengths for all three types of nanocomposites show a dependence on magadiite silicate loading. However, the silicate loading is substantially more effective for the exfoliated nanocomposites than the intercalated nanocomposites. The intercalated nanocomposites give a trend similar to the conventional composites even they have multiple molecular layers of epoxy polymer inserted into magadiite galleries. It is also known that the loading percentage of reinforcing agents will not be quite effective for phase segregated composites. This suggests that the tensile reinforcement properties for nanocomposites will not become additive until the layer separation has reached a certain threshold or at least part of silicate nanolayers reached that stage. The ordered exfoliated nanocomposites prepared from C18A2M-magadiite behave more or less like the disordered exfoliated nanocomposites prepared from C18A1M-magadiite. However, the performance of ordered exfoliated nanocomposites is not as quite good as the disordered exfoliated nanocomposites. The average layer separation for disordered exfoliated nanocomposites is more than 100 Å and substantially larger than 78 Å for the ordered exfoliated nanocomposites. We can conclude that the tensile properties are dependent on the extent of layer separation. There is a structural reason for this effect. For an ideal exfoliated polymer-layered silicate nanocomposite, the average distance between silicate nanolayers will be dependent on the silicate loading. Therefore, alternation of the organic and inorganic phases in an exfoliated nanocomposite is more uniform than in an intercalated nanocomposite. From a microscopic point of view, the homogeneity of an exfoliated nanocomposite is higher than an intercalated nanocomposite. This improved homogeneity for exfoliated nanocomposites optimizes a strong molecular interactions between the silicate layers and the polymer network. So, the improved interfacial properties of exfoliated nanocomposites is an important feature of this superior tensile performance. To further illustrate the importance of layer separation on properties, we prepared a series of intercalated nanocomposites with different layer separation (Figure 3.9). By simple variation the chain lengths of quaternary alkylammoniums, the basal spacing of intercalated nanocomposites can differ from 35.5 Å to 41.3 Å. Figure 3.10 showed that all of these intercalated nanocomposites exhibit a similar dependence on silicate loading. This consequence suggests that a dramatic improvement in tensile properties will not happen until the layer separation greatly exceeds the value for a onium ion bilayer in the galleries.

The relationship between properties and extent of layer separation is further demonstrated in Figure 3.11. The results show that both kinetic and equilibrium solvent uptake data for the nanocomposites prepared from $CH_3(CH_2)_{17}NH_{3-n}(CH_3)_n^+$ -magadiite (n = 1, 2, 3) relied on their nanophase morphology. These results further prove that the properties of polymer-layered silicate nanocomposites are closely linked to the extent of layer separation.

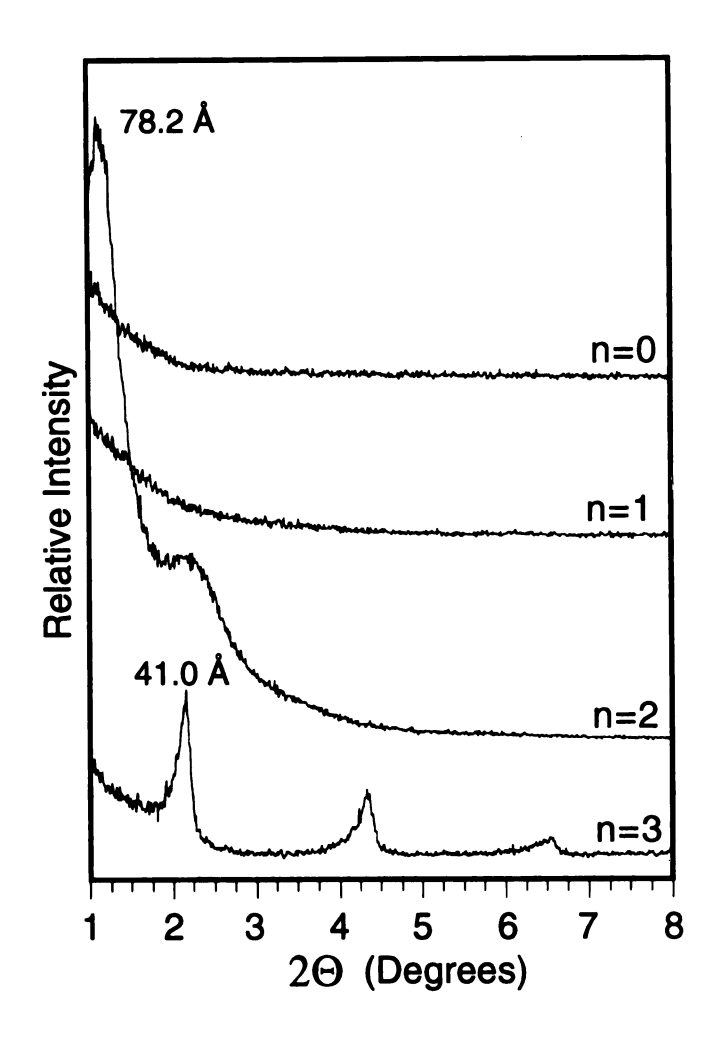


Figure 3.7 X-ray diffraction patterns of cured epoxy polymer-magadiite nanocomposites prepared from $CH_3(CH_2)_{17}NH_{3-n}(CH_3)_n^+$ -magadiites with a paraffin gallery structure (cf. Table 3.1). The organo magadiite loading is 15 wt % (n = 0) or 20 wt % (n = 1, 2, 3). Polymer curing was carried out at 75 °C for 3 h, followed by 3 h at 125 °C. The primary and secondary onium ions (n = 0, 1) give highly exfoliated (disordered) nanocomposites (d > 90 Å). The tertiary onium ion derivative (n = 2) also gives an exfoliated nanocomposite, but the layer separation is highly ordered (d = 78 Å). The quaternary onium ion exchange form (n = 3) forms an intercalated nanocomposite (d = 41 Å).

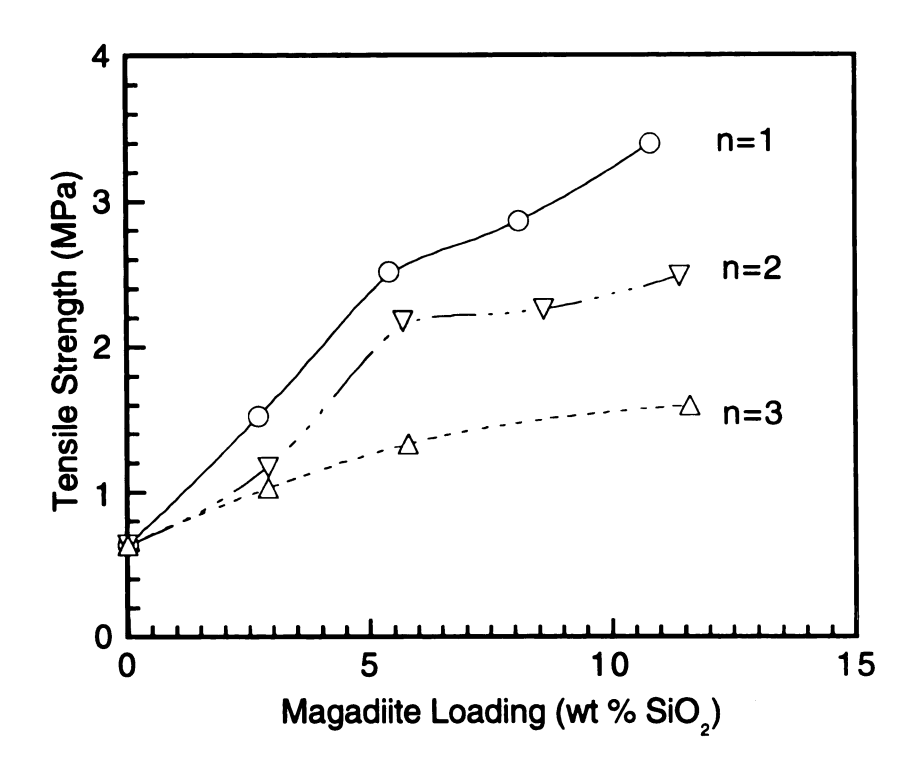
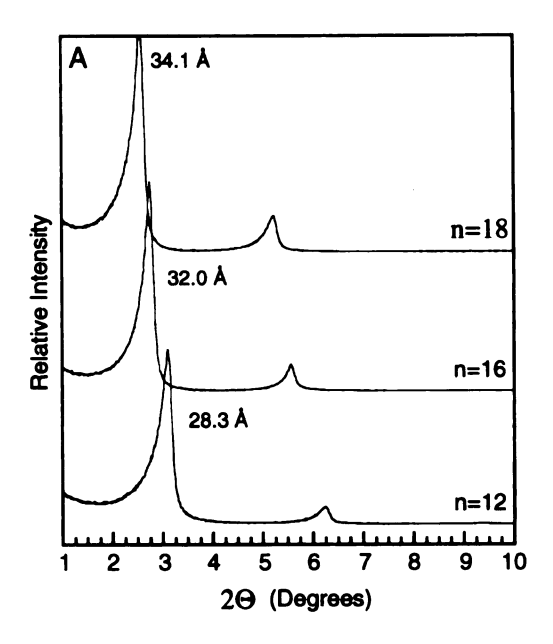


Figure 3.8 A comparison of the tensile strengths of epoxy-magadiite nanocomposites prepared from $CH_3(CH_2)_{17}NH_{3-n}(CH_3)_n^+$ -magadiites. The magadiite silicate loading (expressed on wt % SiO_2) was determined by calcining the composites in air at 650 °C for 4 hours using a heating rate of 2 °C/min. The secondary alkylammonium (n = 2) and the free amine content of $CH_3(CH_2)_{17}NH_2CH_3^+$ -magadiite was counted as contributing to the stoichiometry for epoxide cross-linking at magadiite loadings > 10 wt %.



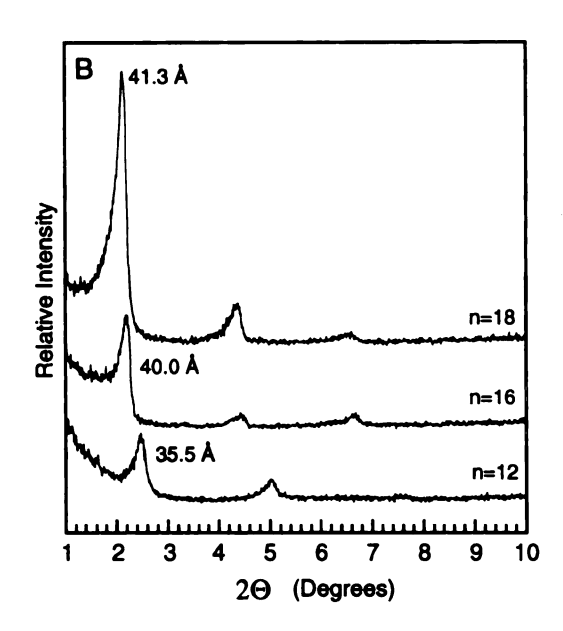


Figure 3.9 X-ray diffraction patterns of $CH_3(CH_2)_{n-1}N(CH_3)_3^+$ -magadiites in different physical states: (A) organo magadiite; (B) intercalated magadiite (10 wt %) in an cured epoxy nanocomposite.

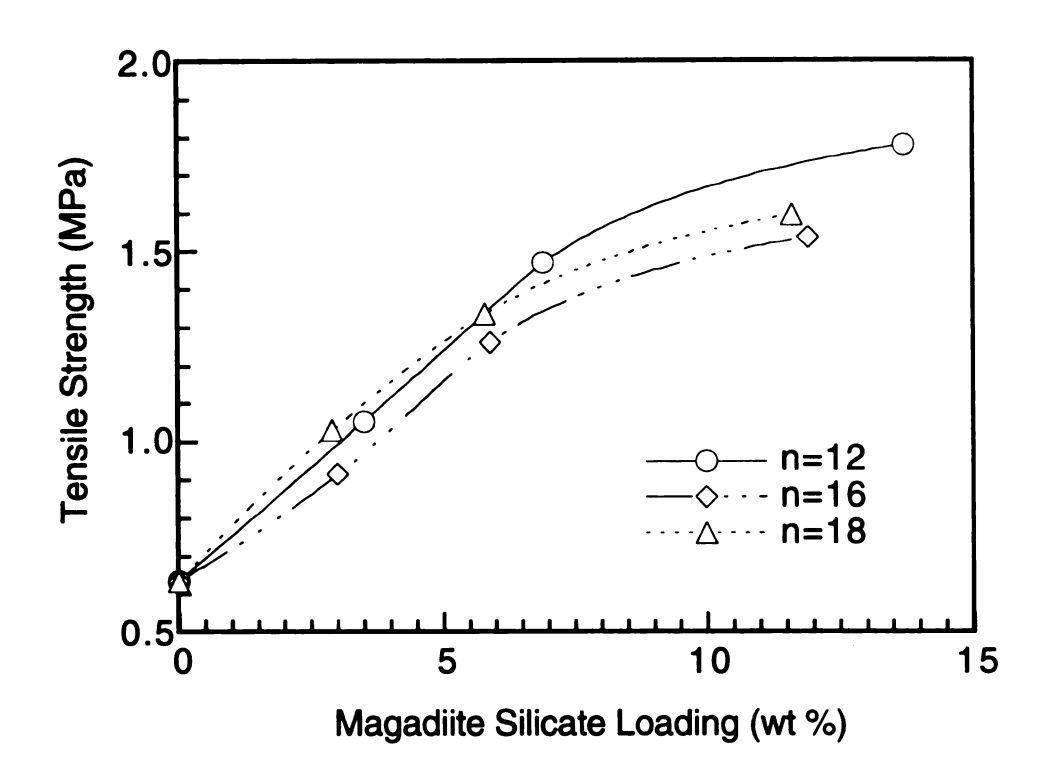


Figure 3.10 A comparison of the tensile strengths of epoxy-magadiite intercalated nanocomposites prepared from CH₃(CH₂)_{n-1}N(CH₃)₃+-magadiites. The magadiite silicate loading was determined by calcining the composites in air at 650 °C for 4 hours using a heating rate of 2 °C/min.

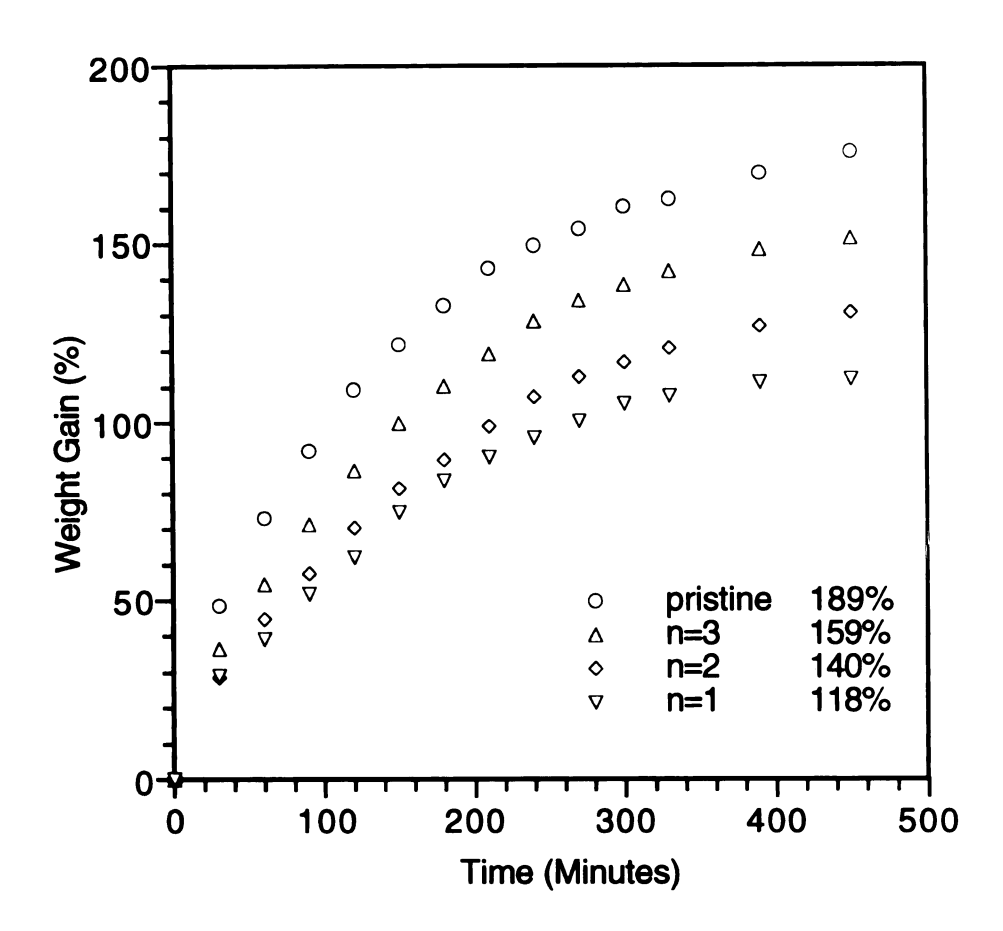
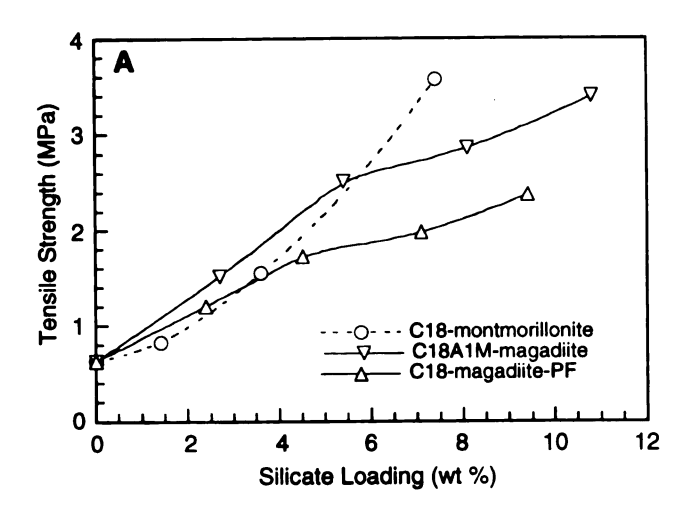


Figure 3.11 Toluene uptake by nanocomposites prepared from $CH_3(CH_2)_{17}NH_3$. $_n(CH_3)_n^+$ -magadiites (n = 1, 2, 3). The tabulated values in the insert are equilibrium data determined by the immersion weight gain after 24 hr. The loading of organo-magadiite is 10 wt % for each epoxy-magadiite composite.

3.3.7 Effect of Secondary Alkylamine and Alkylammonium ions on Mechanical Properties

The comparison of the tensile properties for epoxy-magadiite and epoxy-exfoliated smectite clay exfoliated nanocomposites is shown in Figure 3.12. At low silicate loading, they show similar reinforcing performance. At high silicate loading, the epoxy-smectite clay nanocomposites are better than magadiite in terms of tensile strength and modulus. The difference in the charge density between magadiite and montmorillonite will result in different loading of onium ions. Our previous studies have shown that the gallery alkylammonium exchange cations and alkylamine are incorporated into epoxy network to form dangling polymer chains. The formation of these dangling chains compromises the advantages of silicate layer exfoliation, particularly, at high magadiite loading. Both the primary and secondary ammonium and become involved in the cross-linking reaction.

The effect of methyloctadecylamine on tensile properties is shown in Figure 3.13. The dashed line shows that both the tensile strengths and the moduli will exhibit a maximum if we do not compensate for the curing by the gallery species by reducing the amount of D-2000 curing agent. Interestingly, the polymer elasticity is affected in a favor way (Figure 3.14A) for the epoxy-magadiite exfoliated nanocomposites. The effect of intercalation on the elasticity for the epoxy-magadiite intercalated nanocomposites is not as significant as exfoliation (Figure 3.14B). This unique behavior is totally opposite from conventional composites in which a reinforcement in modulus is accompanied by a sacrifice in the polymer elasticity (Figure 3.14C).



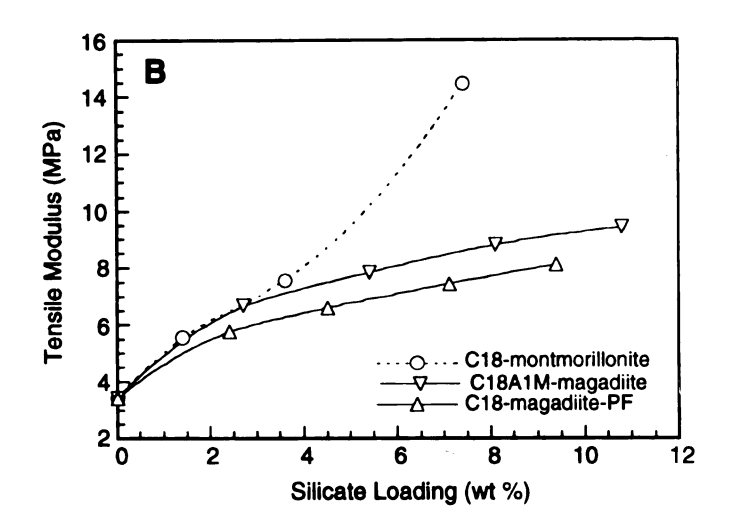


Figure 3.12 A comparison of (A) the tensile strengths and (B) the tensile moduli between epoxy-magadiite exfoliated nanocomposites prepared from C18A1M-magadiite and C18-magadiite-PF, and epoxy-smectite clay exfoliated nanocomposite prepared from CH₃(CH₂)₁₇NH₃⁺ ion-exchange montmorillonite (from Wyoming). The silicate loading was determined by calcining the composites in air at 650 °C for 4 hours using a heating rate of 2 °C/min.

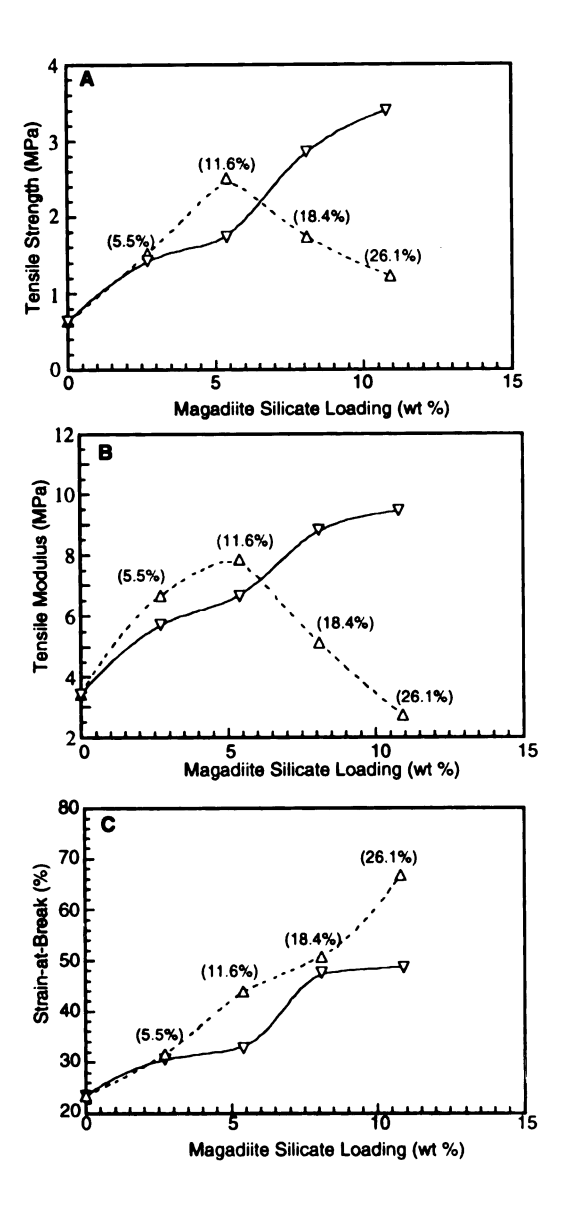


Figure 3.13 Effect of methyloctadecylammonium and methyloctadecylamine on (A) the tensile strengths; (B) the tensile moduli; (C) the strain-at-break values of epoxy-exfoliated magadiite nanocomposites prepared from C18A1M-magadiite. The solid line is for composites formed by including the secondary onium ion and neutral amine content of the organo magadiite as curing agents for epoxide cross-linking and reducing the amount of poly(oxypropyleneamine) (D-2000) accordingly; the dash line is for composites formed at an epoxy-D-2000 stoichiometry that disregards the reactivity of the gallery secondary onium ion and amine in the initial intercalate. The values in parenthesis for the dash curves are the molar fraction of excess secondary amine functional groups relative to D-2000.

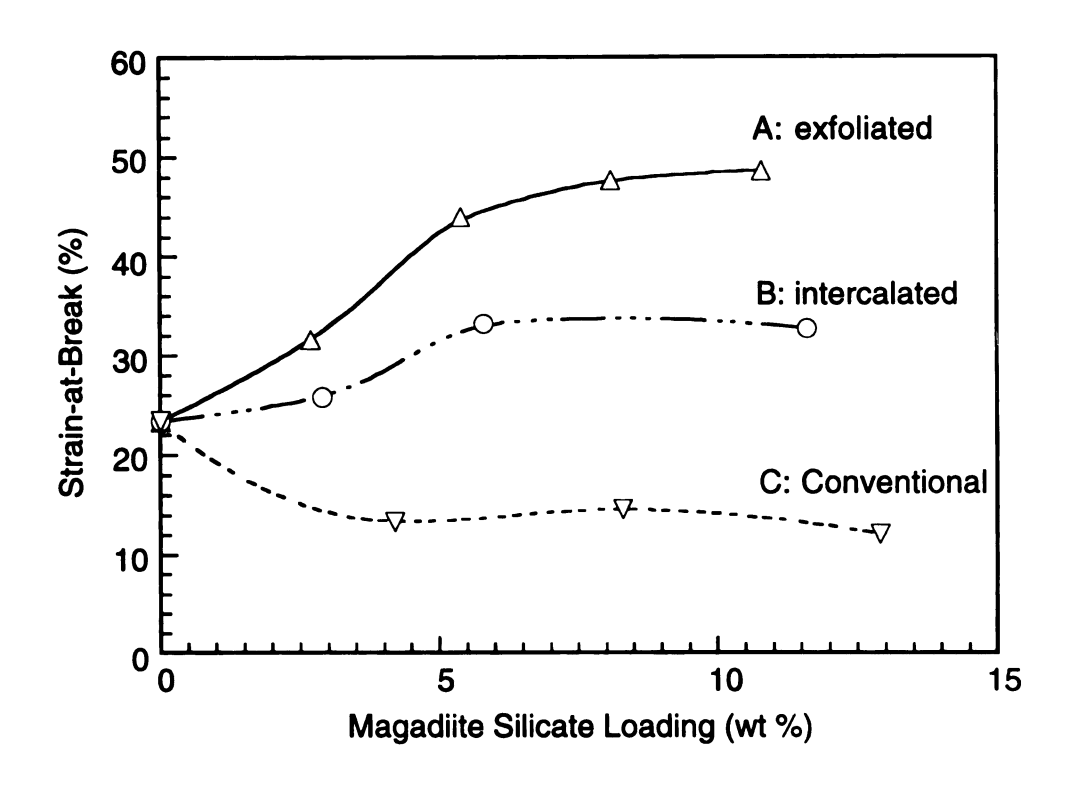


Figure 3.14 Comparison of the stain-at-break values among the exfoliated epoxymagadiite nanocomposites prepared from C18A1M-magadiite, the intercalated nanocomposites prepared from C18A3M-magadiite, and the conventional composites prepared from C18-magadiite-LM with a lateral monolayer structure.

3.3.8 Effect of Alkylammonium Ions on Thermal Stability of Nanocomposites

We also have investigated by TGA methods the effect of long chain alkylammonium on the thermal stability of the nanocomposites prepared from $CH_3(CH_2)_{17}NH_{3-n}(CH_3)_n^+$ -magadiites (n = 0, 1, 2, 3). Figure 3.15 compares the behavior for the exfoliated nanocomposite prepared from C18A1M-magadiite and the intercalated nanocomposite prepared from C18A3M-magadiite. The exfoliated nanocomposite prepared from C18-magadiite-PF is similar to C18A1M-magadiite, and the exfoliated nanocomposite prepared from C18A2M-magadiite is similar to C18A3Mmagadiite. The thermal stability for the exfoliated nanocomposites prepared from C18magadiite-PF and C18A1M-magadiite is as good as pristine epoxy polymer. This has also been observed in the case of nylon 6-clay exfoliated nanocomposites. The lower temperature weight lose for the intercalated nanocomposite is attributed to the decomposition of isolated quaternary alkylammonium cations from the cross-linked polymer network. An analogous weight lose is observed for C18A3M-magadiite (Figure 3.15D). The TGA results also verify that the gallery onium ions are incorporated into the polymer network; otherwise the exfoliated C18A1M-magadiite nanocomposite should show a similar low temperature decomposition of onium ions as Figure 3.15C.

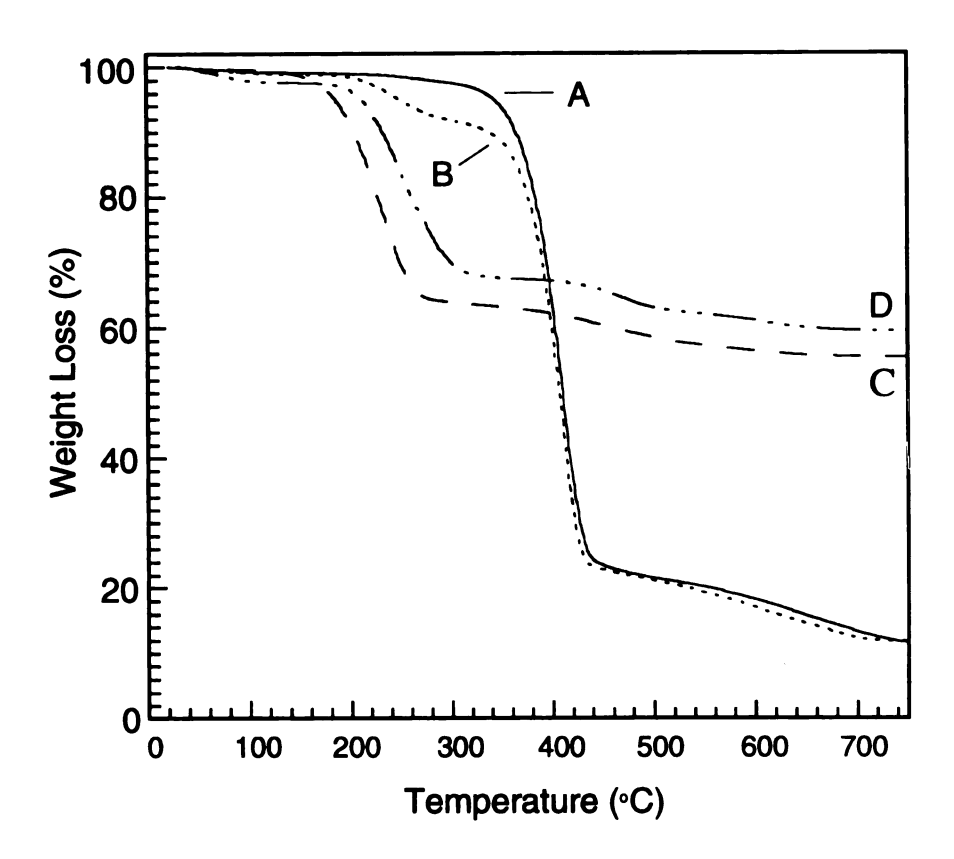


Figure 3.15 Thermogravimetric analysis curves for (A) epoxy-exfoliated magadiite nanocomposite prepared from C18A1M-magadiite and (B) intercalated nanocomposite formed from C18A3M-magadiite. The loading of organo magadiite is 20 wt % for each epoxy-magadiite nanocomposite. Curves (C) and (D) are for the pristine organo magadiites of C18A1M-magadiite and C18A3M-magadiite, respectively. The analysis was carried out in N₂ atmosphere with a heating rate of 5 °C/min.

3.3.9 More Evidences for Morphological Differences Between Intercalated and Exfoliated Nanocomposites

It is interesting to note the differences between intercalated and exfoliated nanocomposites using the other techniques such as surface area measurement by N₂ adsorption-desorption. The intercalated nanocomposite prepared from C18A3Mmagadiite and the exfoliated nanocomposite prepared from C18-magadiite-PF were calcined at 650 °C for 4 hours. The X-ray results (Figure 3.16) showed strong in-plane magadiite peaks in both cases. However, the layer restacking upon calcination was quite different in these two cases. The silica from the intercalated nanocomposite showed a narrow d₀₀₁ peak coheres the d₀₀₁ peak for the exfoliated nanocomposite was a very broad shoulder, which indicated less restacking order. The N₂ adsorption-desorption measurements for calcined residues of the exfoliated and the intercalated nanocomposites, shown in Figure 3.17, verify the above XRD results. A much larger texture porosity and surface area were observed for the magadiite recovered form the exfoliated nanocomposite than from the intercalated nanocomposite. Most of the exfoliated silicate nanolayers will retain their exfoliated morphology to form the familiar card-house structure upon calcination. The card-house structure will result in a significant increase in texture porosity and surface area, in addition to a very broad 001 XRD reflection. These latter experiments allow us to explore the overall phase morphology for intercalated and exfoliated nanocomposites. The results help us to deepen understanding the relationship between nanophase morphology and properties.

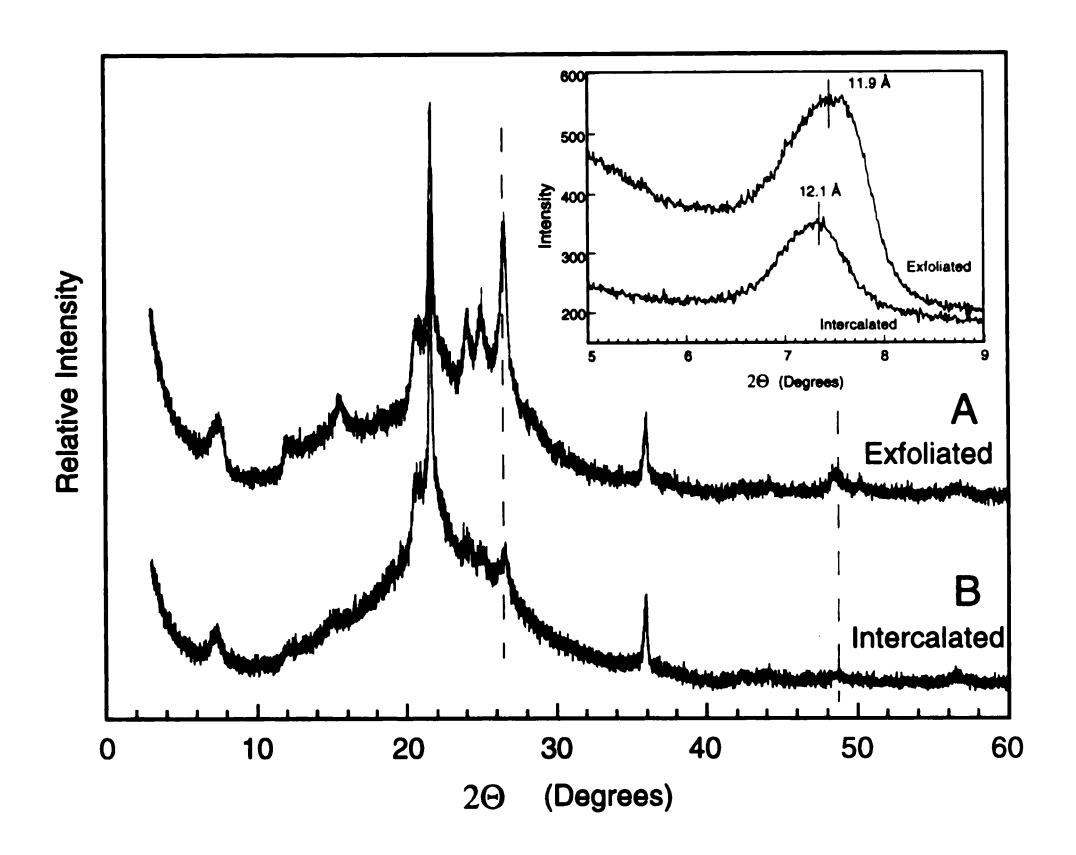


Figure 3.16 X-ray powder diffractions for the silica formed from upon calcination of (A) the exfoliated nanocomposite prepared form C18A-magadiite-PF; and (B) the intercalated nanocomposite prepared from C18A3M-magadiite. The expanded inset for the d_{001} peaks was obtained using a step scan mode. The calcination condition is at 650 °C for 4 h in air using a heating rate of 2 °C/min.

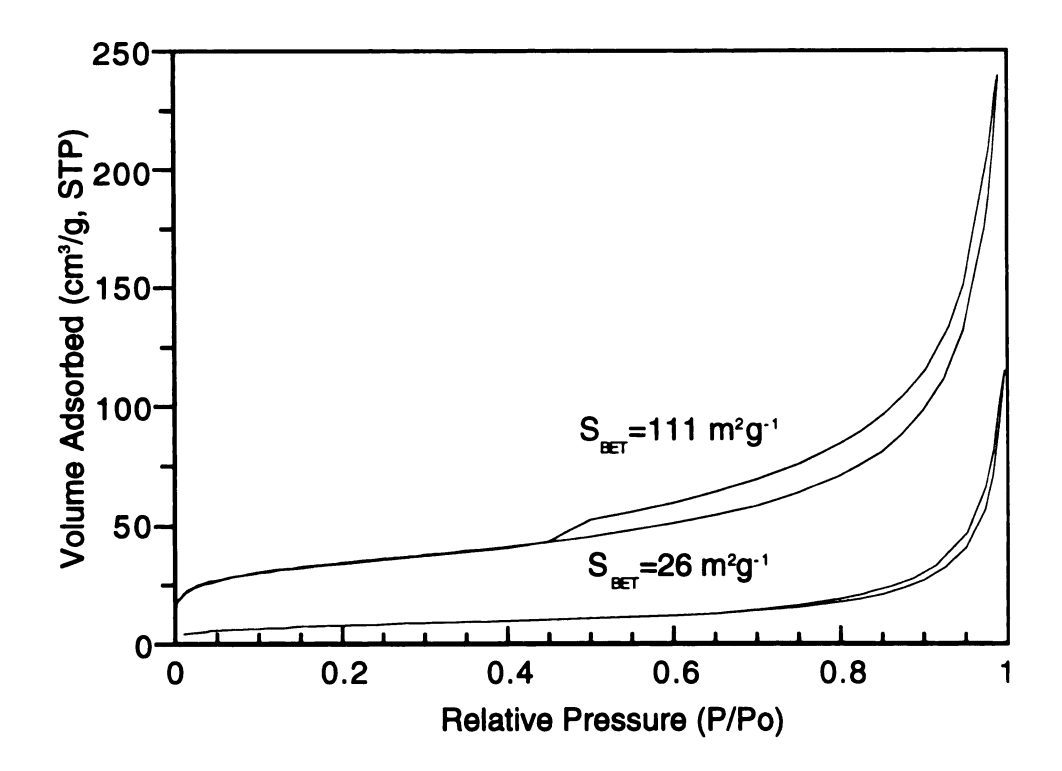


Figure 3.17 N_2 adsorption-desorption isotherms for the silicas obtained by calcination of an epoxy-exfoliated magadiite nanocomposite prepared from C18-magadiite-PF (top curve) and an intercalated nanocomposite prepared from C18A3M-magadiite (bottom curve). The organo magadiite loading for each composite is 10 wt %. The calcination was carried out at 650 °C for 4 hr in air using a heating rate of 2 °C/min.

3.4 Conclusions

Organo magadiites intercalated by RNH_{3-n}(CH₃)_n+ forms of onium ions with paraffin-like structures allow us to prepare a series of epoxy-magadiite nanocomposites with different extent of layer separation. The mechanism leading to exfoliation of magadiite nanolayers is understood by investigating the swelling properties of the each intercalate. The dependence of the performance properties of epoxy-magadiite nanocomposites on magadiite loading and the extent of layer separation are the two major factors governing the mechanical properties of the composites. The exfoliated nanocomposites are superior to intercalated and conventional composites for their overall performance due to their specific phase morphology and improved interfacial properties. However, the exfoliated nanocomposites are more difficult to form than intercalated nanocomposites. By optimizing reaction condition, the exfoliation chemistry will be likely to be extended to the other members of layered silicic acid family, and more sophisticated polymer systems.

3.5 References

- 1. Fukushima, Y.; Okada, A.; Kawasumi, M.; Kurauchi, T.; Kamigaito, O. Clay Miner. 1988, 23, 27.
- 2. Usuki, A.; Kojima, Y.; Kawasumi, M.; Okada, A.; Fukushima, Y.; Kurauchi, T.; Kamigaito, O. J. Mater. Res. 1993, 8, 1179.
- 3. Okada, A.; Usuki, A. Mater. Sci. Eng. 1995, C3, 109.
- 4. Yano, K.; Usuki, A.; Okada, A.; Kurauchi, T.; Kamigaito, O. J. Polym. Sci., Part A: Polym. Chem. 1993, 31, 2493.
- 5. Lan, T.; Kaviratna, P. D.; Pinnavaia, T. J. Chem. Mater. 1994, 6, 573.
- 6. Lan, T.; Kaviratna, P. D.; Pinnavaia, T. J. Chem. Mater., 1995, 7, 2144.
- 7. Messersmith, P. B.; Giannelis, E. P. *Chem. Mater.* **1994**, 6, 1719.
- 8. Burnside, S. D.; Giannelis, E. P. Chem. Mater. 1995, 7, 1597.
- 9. Lan, T.; Pinnavaia, T. J. Chem. Mater. 1994, 6, 2216.
- 10. Messersmith, P. B.; Giannelis, E. P. J. Polym. Sci., Part A: Polym. Chem. 1995, 33, 1047.
- 11. Pinnavaia, T. J.; Lan, T.; Wang, Z.; Shi, H.; Kaviratna, P. D. ACS Symp. Ser. 1996, 622, 250.
- 12. Vaia, R. A.; Jandt, K. D.; Kramer, E. J.; Giannelis, E. P. Chem. Mater., 1996, 8, 2628.
- 13. Kato, C.; Kuroda, K.; Misawa, M. Clays Clay Miner. 1979, 27, 129.
- 14. Fukushima, Y.; Inagaki, S. J. Inclusion Phenom. 1987, 5, 473.
- 15. Messersmith, P. B.; Giannelis, E. P. Chem. Mater. 1993, 5, 1064.
- 16. Kojima, Y.; Usuki, A.; Kawasumi, M.; Okada, A.; Fukushima, Y.; Kurauchi, T.; Kamigaito, O. J. Mater. Res. 1993, 8, 1185.
- 17. Fletcher, R. A.; Bibby, D. M. Clays Clay Miner. 1987, 35, 318.
- 18. Sugahara, Y.; Sugimoto, K.; Yanagisawa, T.; Nomizu, Y.; Kuroda, K.; Kato, C. Yogyo Kyokai Shi 1987, 95, 117.

Po. che

Chapter 4

HYBRID ORGANIC-INORGANIC NANOCOMPOSITES FORMED FROM AN EPOXY POLYMER AND LAYERED SILICIC ACIDS (KENYAITE AND ILERITE)

4.1 Introduction

Layered silicic acids have drawn little attention in the field of organic-inorganic composites. Even less work has been done for members other than magadiite for this layered inorganic family of silicates in efforts to use them as reinforcements. In the last two chapters, we have fully investigated the exfoliation chemistry of magadiite. It should in principle be possible to realize similar benefits for other layered silicic acids based on nanolayer reinforcement.

The family of layered silicic acids includes five members in as-synthesized Na⁺-exchanged form: kanemite (NaHSi₂O₅·nH₂O), makatite (Na₂Si₄O₉·nH₂O), ilerite (Na₂Si₈O₁₇·nH₂O), magadiite (Na₂Si₁₄O₂₉·nH₂O) and kenyaite (Na₂Si₂₀O₄₁·nH₂O). ¹⁻³ They all can be easily synthesized by hydrothermal methods. By changing the ratio of starting materials such as sodium hydroxide, amorphous silica and water, and by controlling the reaction conditions such as reaction temperature and time, one can produce these alkali-metal-ion layered silicates with similar layer structure, but with different layer thickness. ⁴⁻⁶ The variable aspect ratios of the silicate nanolayers provide us extra opportunities to elucidate some issues governing the mechanical properties of the polymer-layered silicate nanocomposites. In this chapter, we extend the exfoliation chemistry developed for magadiite to the other members of this layered inorganic family.

At the same time, we address the fundamental issues regarding nanocomposite formation, such as the nanolayer exfoliation processes, the relationships between structure, composition, and performance properties, and the basic physics behind the reinforcement.

4.2 Experimental

4.2.1 Materials

The epoxide resin used to for epoxy-magadiite hybrid composite formation was poly(bisphenol A-co-epichlorohydrin) (Shell, EPON 828), with MW ~377:

$$CH_{2}$$
- $CHCH_{2}O$ CH_{3} OCH_{2} CHC $H_{2}O$ CH_{3} OCH_{2} CHC $H_{2}O$ CH_{3} OCH_{2} CHC $H_{2}O$ CH_{3} OCH_{2} CHC $H_{2}O$ CH_{3} OCH_{2} CH- CH_{2} OCH_{2} CH- OCH_{2} OCH_{2} CH- OCH_{2} OCH

The curing agent was poly(propylene glycol) bis(2-aminopropyl ether) (Huntsman Chemical, JEFFAMINE D-2000), with MW ~2000:

$$H_2NCHCH_2 = OCH_2CH = NH_2$$
 $CH_3 \qquad CH_3$
 $x=33.1$

4.2.2 Synthesis of Layered Silicic Acids and Their Derivatives

Synthesis of K*-kenyaite. K*-kenyaite was synthesized according to published methods.⁵ A suspension of 75.0 g of amorphous silica gel (1.25 mol) in 300 mL of 1.39 M KOH solution (0.42 mol) was heated at 140 °C for 72 h with stirring in a Teflon-lined stainless steel 1.0 L Parr reactor. The suspension containing K*-kenyaite was centrifuged, and the solid product was washed twice with 600 mL of deionized water to remove excess KOH, and air-dried at room temperature.

Synthesis of Na⁺-ilerite. Na⁺-ilerite was synthesized according to published methods.⁶ A suspension of 142.9 g of amorphous silica gel (2.38 mol) in 300 mL of 3.97 M NaOH solution (1.19 mol) was heated at 105 °C for 9 days with stirring in a Teflon-lined stainless steel 1.0 L Parr reactor. The suspension containing Na⁺-ilerite was

centrifuged, and the solid product was washed three times with 700 mL of deionized water to remove excess NaOH, and air-dried at room temperature.

Synthesis of H*-ilerite. H*-ilerite was obtained by titration of synthetic Na*-ilerite with dilute hydrochloric acid. A 500 mL of aqueous suspension containing 15.0 g of Na*-ilerite was titrated by 0.1 M HCl at a rate of 3 mL/min to lower the pH to 1.9. The suspension with pH = 1.9 was stirred for 24 hours. H*-ilerite was separated by centrifugation and washed with deionized water until free of Cl*, and then air-dried at room temperature.

Synthesis of Organo Kenyaites. $C_nH_{2n+1}NH_3^+/C_nH_{2n+1}NH_2$ -kenyaite (n = 6, 8) was prepared by the following approach. An aqueous suspension containing 15.0 g of K⁺-kenyaite was combined with an aqueous solution containing 0.102 mol of $C_nH_{2n+1}NH_3^+Cl^-$ to form a suspension in 1.0 L of total solution. The suspension was stirred at 50 °C for 24 hours. The pH of the reaction mixture was in the range of 7 - 8. The product mixture was centrifuged and the wet solid product was washed once with 500 mL of H_2O and then air-dried.

 $C_nH_{2n+1}NH_3^+/C_nH_{2n+1}NH_2$ -kenyaite (n = 10, 12) was prepared by the following approach. An aqueous suspension containing 15.0 g of K⁺-kenyaite was combined with ethanol/water solution containing 0.102 mol of $C_nH_{2n+1}NH_3^+Cl^-$ to form a suspension in 1.0 L of 7:1 (n = 10) or 3:1 (n = 12) (v/v) ethanol/water total solution. The suspension was stirred at 50 °C for 24 hours. The pH of the reaction mixture was in the range of 7 - 8. The product mixture was centrifuged. The wet solid product was washed once with 500 mL of H_2O and then air-dried.

Primary, secondary and tertiary long chain alkylammonium exchanged $CH_3(CH_2)_{17}NH_{3-n}(CH_3)_n+/CH_3(CH_2)_{17}NH_{2-n}(CH_3)_n$ -kenyaites (n = 0, 1, 2) were prepared by the following approach. An aqueous suspension containing 15.0 g of K+kenyaite was combined with ethanol/water solution containing 0.102 mol of alkylammonium chloride and alkylamine in a 4:1 molar ratio to form a suspension in 1.0

L of 1:1 (v:v) ethanol/water total solution. The suspension was stirred at 65 °C for 24 hours. The pH of the reaction mixture was in the range of 8 - 9. The product mixture was added to an equal volume ethanol and centrifuged. The wet solid product was washed consecutively with two 750-mL portions of 50 % EtOH, one 750-mL portion of 30 % EtOH and then with water until free of Cl⁻, and air-dried.

Quaternary alkylammonium exchanged CH₃(CH₂)₁₇N(CH₃)₃+-kenyaite was prepared by the reaction of 10.0 g of K+-kenyaite with 800 mL of 5.08 x 10⁻² M CH₃(CH₂)₁₇N(CH₃)₃+Br⁻ aqueous solution at 65 °C for 48 hr. The product was centrifuged and washed with deionized water until free of Br⁻, and then air-dried.

All of the air-dried organo kenyaites were ground to a powder with a particle size smaller than 270 mesh (53 μ m) and stored for further use.

Synthesis of Organo Ilerites (Octosilicates). Quaternary alkylammonium exchanged CH₃(CH₂)₁₇N(CH₃)₃+-ilerite was prepared by the reaction of 10.0-g quantity of air-dried Na+-ilerite with 31.2 g (7.95 x 10⁻² mol) of CH₃(CH₂)₁₇N(CH₃)₃+Br⁻ in 800 mL of 3:5 (v:v) ethanol/water solution at 65 °C for 48 hr. The reaction mixture was centrifuged and the wet solid product was washed with three 750-mL portions of 50 % EtOH and then with water until free of Br⁻, and air-dried.

CH₃(CH₂)₁₇NH₃+-ilerite, abbreviated C18-ilerite, was obtained by conversion of the H+ form of ilerite to CH₃(CH₂)₁₇NH₂-ilerite intercalate in the presence of neutral amine. A 2.0-g quantity of air-dried H+-ilerite was added to 100 mL of 1:4 (v:v) ethanol/water solution containing 1.8 g (6.68 x 10⁻³ mol) of CH₃(CH₂)₁₇NH₂ and stirred at 50 °C for 4.5 hr. The final product was obtained by evaporation of the ethanol/water solvent and air-dried.

4.2.3 Preparation of Epoxy-Layered Silicic Acid (Kenyaite and Ilerite)

Composites

Equivalent amounts of epoxide resin and poly(oxypropyleneamine) curing agent were mixed at room temperature for 30 min. The desired amount of organo layered

silicate was added to the epoxide-poly(oxypropyleneamine) mixture and stirred for another 60 min. This mixture was outgassed in a vacuum oven and poured into a stainless steel mold for curing at 75 °C for 3 h and, subsequently, at 125 °C for an additional 3 h.

4.2.4 Characterization Methods

X-ray Powder Diffraction (XRD). XRD patterns were recorded on a Rigaku rotaflex 200B diffractometer. Diffraction patterns were collected with 0.01° 2θ interval between 1 and 10° 2θ using a scanning rate of 2° 2θ per minute, and DS and SS slit widths of 1/6. Samples of epoxy-solvated layered silicic acids or uncured epoxy-layered silicic acid composites were prepared by applying thin films on glass slides. Cured composite specimens were prepared by mounting a flat rectangular sample into an aluminum holder.

Thermal Analysis. Thermogravimetric analyses (TGA) were performed using a Cahn TG System 121 thermogravimetric analyzer. Samples were heated to 750 °C at a heating rate of 5 °C/min under N₂ atmosphere.

Mechanical Measurement. Tensile testing was performed at ambient temperature according to ASTM procedure D3039 using a SFM-20 United Testing System.

Chemical and Solvent Resistance. The resistance of the composite materials to solvent swelling was obtained according to ASTM procedure D543. The specimens were immersed in the desired reagent and removed periodically to measured the weight gain until equilibrium was reached.

4.3 Results and Discussion

4.3.1 Exfoliation of Kenyaite Nanolayers in an Epoxy Polymer Matrix

4.3.1.1 Synthesis of Organo Kenyaites

The synthesis of swellable organo kenyaites was our first goal in our effort to prepare epoxy-kenyaite nanocomposites. Our starting layered inorganic solid was the K⁺

form of kenyaite which has a better crystallinity and contains less impurities in term of amorphous silica or quartz than the Na⁺ form of kenyaite.^{3,7} Kenyaite has been reported to undergo ion-exchange reaction with primary $C_nH_{2n+1}NH_3+Cl^-$ ($n=10,\ 12$) and quaternary $CH_3(CH_2)_{n-1}N(CH_3)_3+X^-$ ($n=10,\ 12,\ X=Cl,\ Br$) ammonium ions.³ In the present work we studied the intercalation of primary alkylammonium/alkylamine mixtures of the type $C_nH_{2n+1}NH_3+Cl^-/C_nH_{2n+1}NH_2$ ($n=6,\ 8,\ 10,\ 12,\ 18$). The solvent used for the intercalation reaction was varied from an aqueous solution for $n=6,\ 8$ to an ethanol/water solution for $n=10,\ 12,\ 18$, the concentration of ethanol was varied from 12.5 % to 50% (volume), depending on the chain length of the alkylammonium involved. For the long chain alkylammonium, the intercalation method used for kenyaite intercalation is the same as that previously described in Chapter 2 & 3 for the preparation of organo magadiite.

Figure 4.1 shows the powder x-ray diffraction patterns for kenyaites intercalated by mixtures of protonated and neutral primary amines with chain length n=6, 8, 10, 12, 18. Table 4.1 lists the intragallery compositions, d_{001} basal spacings and gallery structures. For chain length with n=6, the intercalated alkylammonium forms only a lateral monolayer structure. This result also agrees with the well-known intercalation chemistry of 2:1 smectite clays. 8,9 For n=8, 10, 12, the basal spacings increase from 19.6 Å for K-kenyaite to ~ 40 Å for the organo kenyaites. On the basis of the observed spacings, we propose that the intragallery alkylammonium/alkylamine chains have a gauche-block structure, wherein the alkyl chains adopt a bilayer arrangement with a mixed *trans* and *cis* conformation of the chains (cf. Figure 1.2G). This conformational arrangement of the chains is consistent with Lagaly's model with only a slight difference. 10 Our long chain alkylammonium (n=18) exchanged kenyaite showed a different gallery structure from those with n=6, 8, 10, 12. The 43.1 Å basal spacing for air-dried $CH_3(CH_2)_{17}NH_3+/CH_3(CH_2)_{17}NH_2$ -kenyaite was consistent with the paraffin structure of the intercalated alkyl chains, and is designated to C18-kenyaite-PF. The

TGA results given in Figure 4.2 and Table 4.1 show that all these primary alkylammonium exchanged kenyaites, except for n = 6 must contain a mixture of protonated and neutral amine in order to explain the observed gallery structures.

It is noteworthy that the broad d₀₀₁ peak at 35.9 Å for CH₃(CH₂)₇NH₃+/CH₃(CH₂)₇NH₂-kenyaite (Figure 4.3B) most likely arises due to the evaporation of the neutral amine molecules from the gallery. This short chain amine possesses a relatively high vapor pressure. However, the wet and as-synthesized CH₃(CH₂)₇NH₃+/CH₃(CH₂)₇NH₂-kenyaite gave a high intensity and narrow peak at 35.9 Å as shown in Figure 4.3A. Excessive washing resulted in the formation of another kind of gallery structure with a 23.1 Å basal spacing (Figure 4.3C). The gallery height of 5.4 Å (layer thickness of kenyaite is 17.7 Å) is consistent with a lateral bilayer structure of alkyl chains (see Figure 1.2A). As we have already demonstrated for the intercalation chemistry of organo magadiites with a lateral monolayer structure, the organo kenyaites with lateral monolayer and lateral bilayer structures are not expandable by epoxy resin and other polymer precursors due to the high electrostatic interactions between the onium ions and the silicate nanolayers.

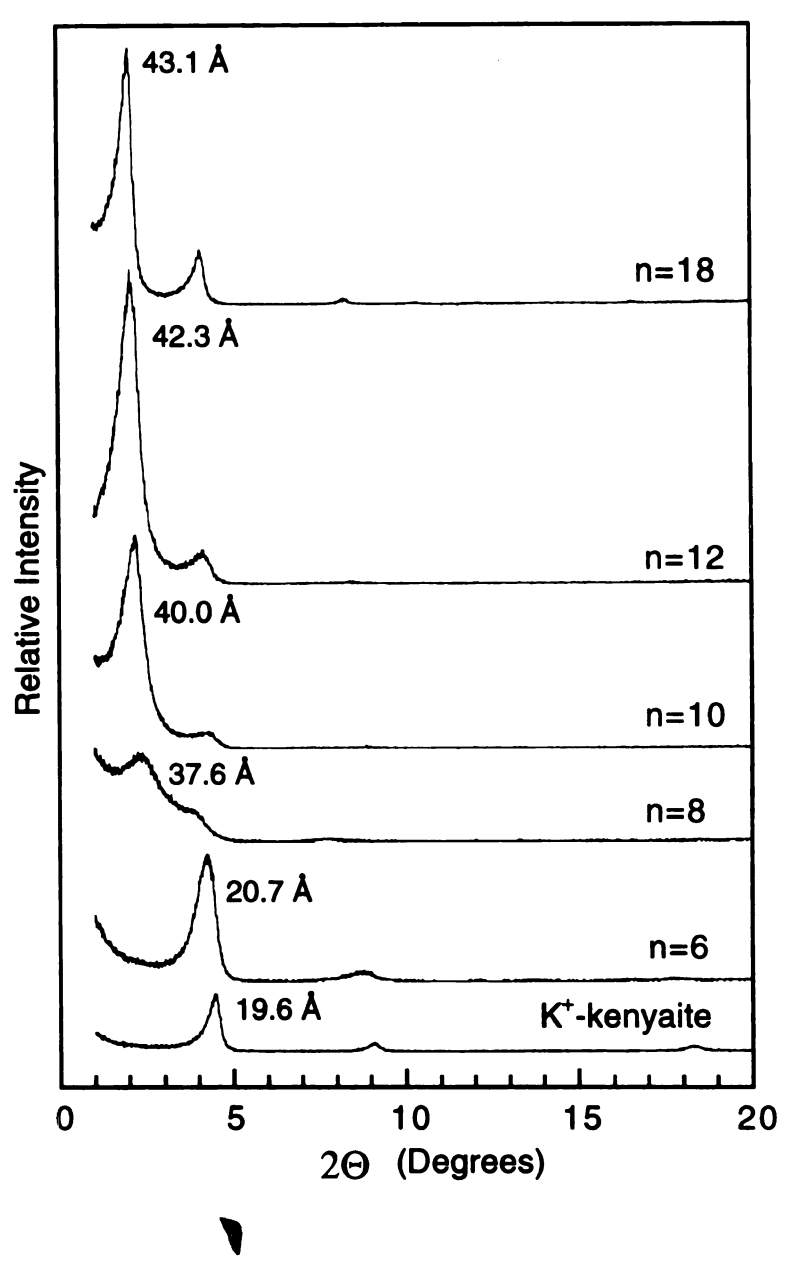


Figure 4.1 X-ray powder diffraction patterns of air-dried K⁺-kenyaite and $CH_3(CH_2)_{n-1}NH_3^+/CH_3(CH_2)_{n-1}NH_2$ -kenyaites. The gallery structures and compositions are given in Table 4.1.

Intercalates Formed by Reaction of K+-Kenyaite with C_nH_{2n+1}NH₃+Cl⁻ and C_nH_{2n+1}NH₂ Table 4.1

material intragallery composition gallery dool paraffin designation per Si ₂₀ O ₄₁ ² - unit cell structure (Å) monol 6 C6-kenyaite-LM (C ₆ H ₁₃ NH ₃ +) _{1.25} H ⁺ _{0.75} lateral monolayer 20.7 30.8 C8-kenyaite-GB (C ₈ H ₁₇ NH ₃ +) ₂ (C ₈ H ₁₇ NH ₂) _{0.29} gauche blockb 37.6 33.0 10 C10-kenyaite-GB (C ₁₀ H ₂₁ NH ₃ +) ₂ (C ₁₀ H ₂₁ NH ₂) _{1.00} gauche block 40.0 35 12 C12-kenyaite-GB (C ₁ ,H ₂ ,NH ₃ +) ₂ (C ₁ ,H ₂ ,NH ₃) _{1.00} gauche block 42.3 38.0						calculated d ₀₀₁ values (Å) ^a	doorvalu	ies (Å)a
structure (A) 1 lateral monolayer 20.7 gauche block 37.6 gauche block 40.0 gauche block 42.3	=	material	intragallery composition	gallery	d 001	paraffin-like gauche lipid-like	ganche	lipid-like
lateral monolayer 20.7 gauche block ^b 37.6 gauche block 40.0 gauche block 42.3	:	designation	per Si ₂₀ O ₄₁ ²⁻ unit cell	structure	(A)	monolayer	block	bilayer
gauche block 37.6 gauche block 40.0 gauche block 42.3	9	C6-kenyaite-LM	$(C_6H_{13}NH_3^+)_{1.25}H^+_{0.75}$	lateral monolayer	20.7	30.4	32.4	38.0
gauche block 40.0 gauche block 42.3	∞	C8-kenyaite-GB	(C ₈ H ₁₇ NH ₃ ⁺) ₂ (C ₈ H ₁₇ NH ₂) _{0.29}	gauche block ^b	37.6	33.0	36.6	43.1
gauche block 42.3	10	C10-kenyaite-GB	(C ₁₀ H ₂₁ NH ₃ +) ₂ (C ₁₀ H ₂₁ NH ₂) _{0.96}	gauche block	40.0	35.5	39.3	48.2
- \(\frac{1}{2} - \frac{1}{2} - \fracc{1}{2} - \frac{1}{2} - \frac{1}{2} - \frac{1}{2} - \frac{1}{2}	12	C12-kenyaite-GB	$(C_{12}H_{25}NH_3^+)_2(C_{12}H_{25}NH_2)_{1.00}$	gauche block	42.3	38.0	43.5	53.3
paraffin 43.1	18	C18-kenyaite-PF	(C ₁₈ H ₃₇ NH ₃ +) ₂ (C ₁₈ H ₃₇ NH ₂) _{0.90}	paraffin	43.1	45.7	53.1	68.5

silicate layer and an all trans configuration for the paraffin-like monolayer and lipid-like bilayer structures, or a mixed trans and cis configuration for the gauche block structure. The following expressions, taken from Lagaly (ref. 10), were used to calculate the expected basal spacings for each type of structure: Monolayer: $d_{001}(A) = 19.8 + 3 + 1.27n$; Bilayer: $d_{001}(A) = 19.8 + 3 + 2.1.27n$; Gauche block: $d_{001}(A) = 19.8 + 3 + x/4.1.45 + n/2.1.27$ (x = 3n for n = 8, 12; x ^aBasal spacings are calculated assuming the alkylammonium/alkylamine adopt a vertical orientation relative to the = 3n-2 for n = 6, 10, 18), where 19.8 Å is the d_{001} value for NH₄⁺-kenyaite, 3.0 Å is size of the methyl groups normal to the silicate layer, and 1.27 Å is the distance increase upon adding one -CH₂- unit to the alkyl chain.

^bSee Figure 1.2G for an illustration of the gauche block structure.

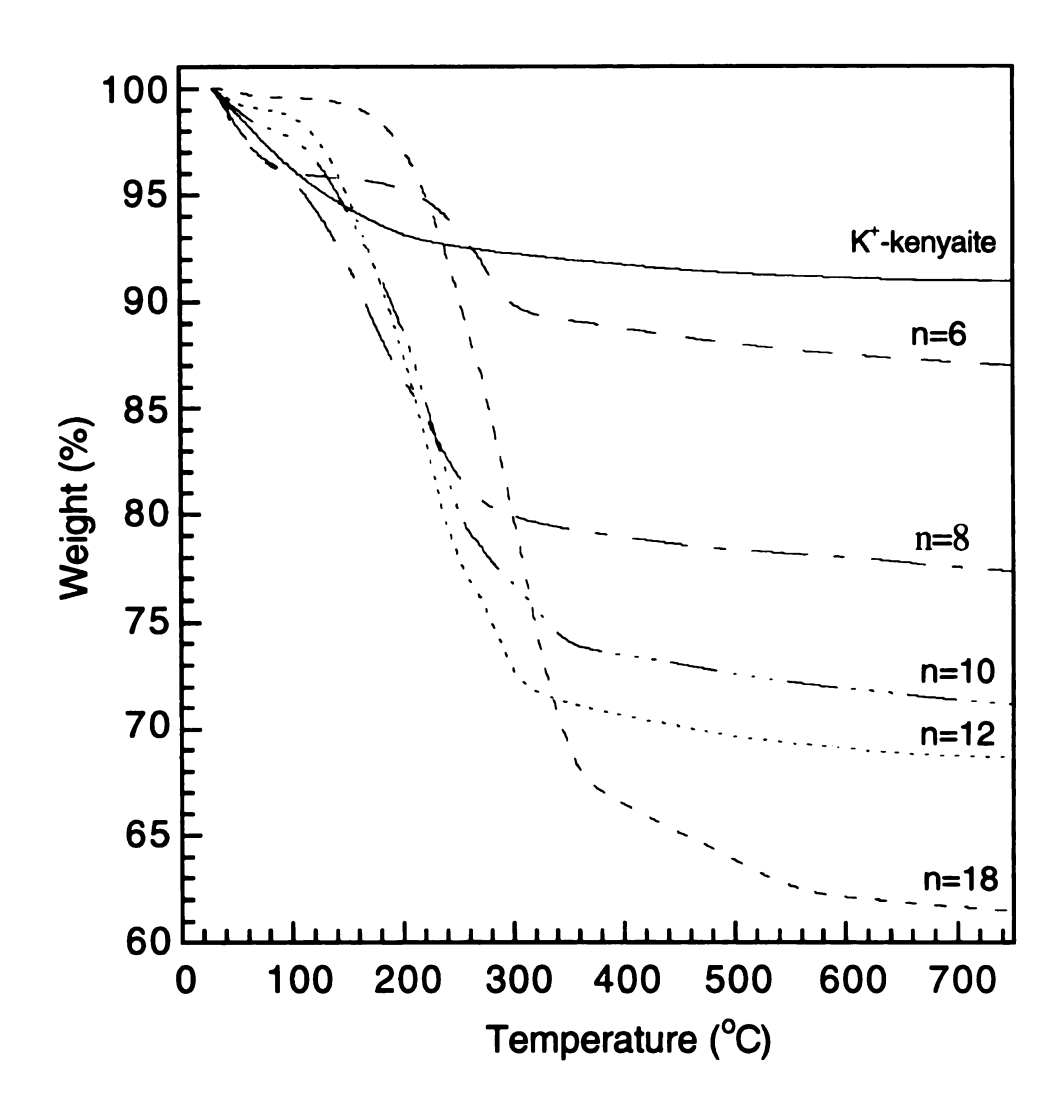


Figure 4.2 Thermogravimetric analysis curves for air-dried K⁺-kenyaite and $CH_3(CH_2)_{n-1}NH_3^+/CH_3(CH_2)_{n-1}NH_2$ -kenyaites. The gallery structures and compositions derived from these curves are give in Table 4.1.

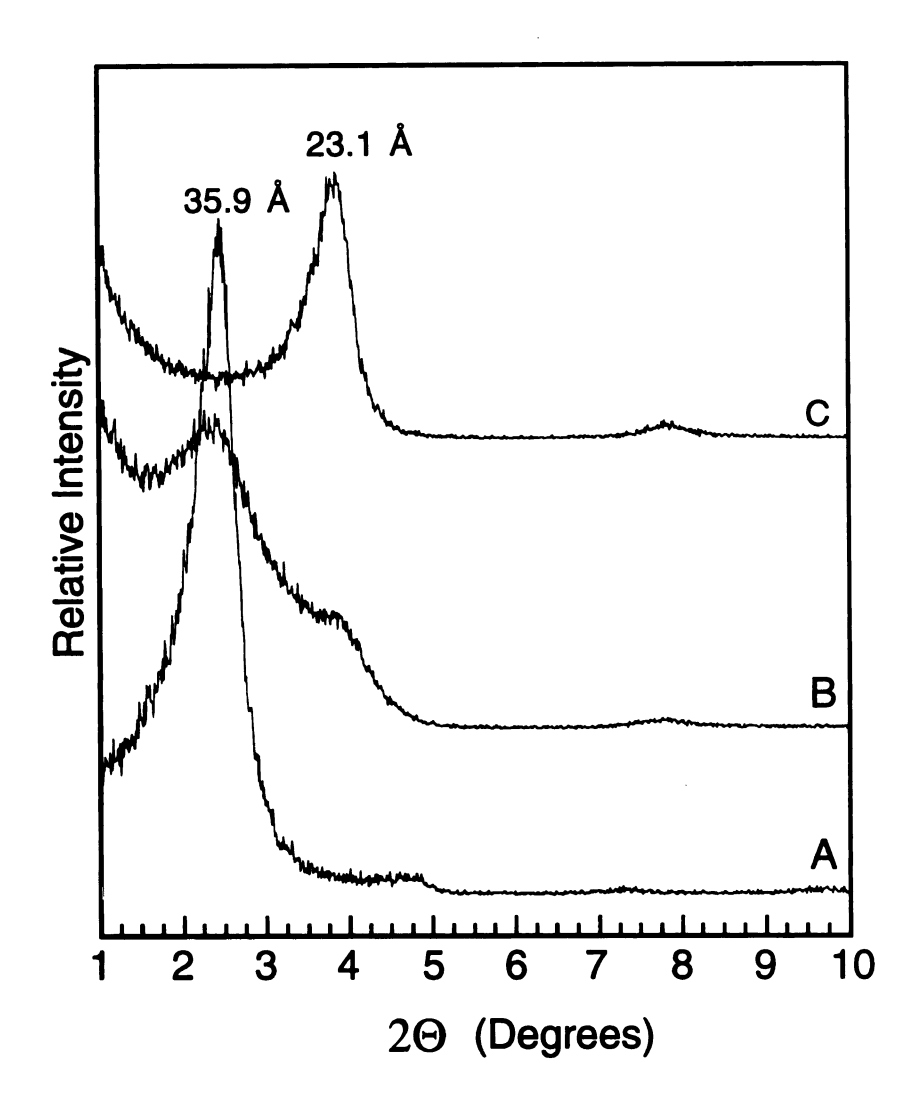


Figure 4.3 X-ray powder diffraction patterns of (A) C8-kenyaite-GB (gauche block structure) obtained by applying a film of the wet product on a glass slide right after centrifuging the reaction mixture; (B) air-dried C8-kenyaite-GB with a less ordered gauche block gallery structure; (C) CH₃(CH₂)₇NH₃+-kenyaite with a lateral bilayer gallery structure obtained by thorough washing of the C8-kenyaite-GB to remove excess amine.

4.3.1.2 Exfoliation of C18-Kenyaite-PF in an Epoxy Polymer Matrix

The intercalation of C18-kenyaite-PF by a mixture of epoxy resin and curing agent as a function of time was investigated by XRD (Figure 4.4). The solvation of C18kenyaite-PF by a stoichiometric mixture of resin and curing agent was initially very slow at room temperature, because the viscosity of the system is high and the diffusion process is very slow. The 46.7 Å spacing for the solvated intercalate (Figure 4.4B) is consistent with the perpendicular orientation of onium ions and amine molecules with a paraffin monolayer structure (cf. Table 4.1). The intercalation may be limited primarily to the epoxide resin only at this stage, because the change in intragallery spacing is very small and the spacing agrees with that for epoxide solvation without the presence of the curing agent. Upon heating at 75 °C, the C18-kenyaite-PF is rapidly solvated, as evidenced by a sharp increase in spacing to a value of 62.8 Å (Figure 4.4C). The 62.8 Å peak is replaced by another peak at 69.0 Å (Figure 4.4D) corresponding to the onium ions with a lipid bilayer orientation (cf. Table 4.1). As we have discussed in Chapter 2 & 3, the formation of this intermediate phase is crucial for achieving an exfoliated state instead of an intercalated state for the silicate nanolayers. In this phase, the organic onium ions adopt an orientation that allows optimal intragallery space for the intercalated species. Curing beyond this stage allows the exfoliated state of silicate nanolayers to be achieved, as shown in the XRD Figure 4.4E. The final x-ray amorphous phase (Figure 4.5) suggests that an epoxy-exfoliated kenyaite nanocomposite has been achieved. The formation of an epoxy-exfoliated kenyaite nanocomposite supports the pathway that we have previously proposed for the exfoliation of organo magadiites in an epoxy polymer matrix, even though the layer thickness increases from 11.2 Å for magadite to 17.7 Å for kenyaite.

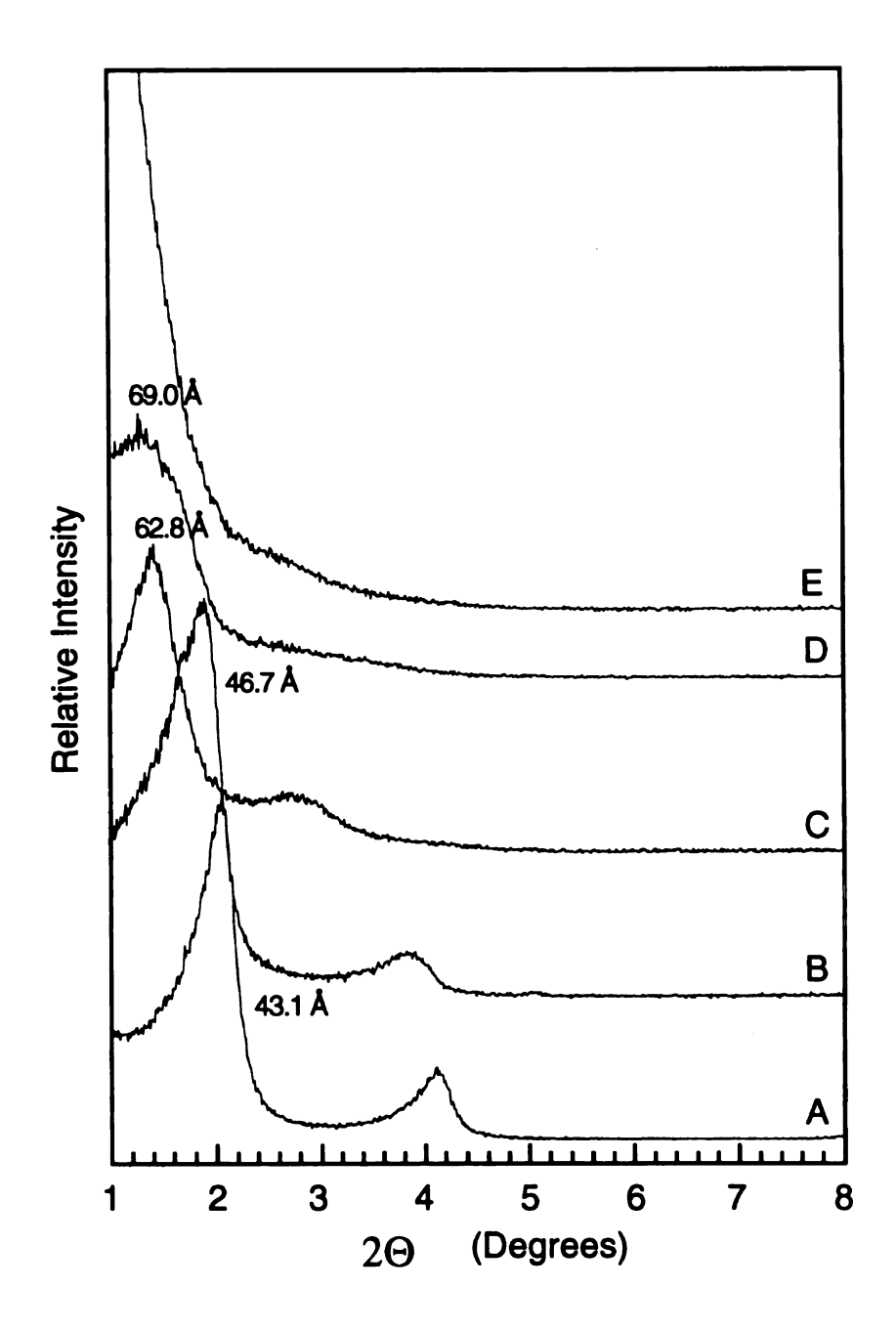


Figure 4.4 X-ray diffraction patterns of (A) pristine C18-kenyaite-PF and (B-E) the partially cured composites prepared by reaction of C18-kenyaite-PF (14.6 wt % loading) with a stoichiometric mixture of epoxide resin (EPON 828) and poly(oxypropyleneamine) (Jeffamine D-2000) curing agent. The primary alkylammonium and the free amine content of C18-kenyaite-PF was counted as contributing to the stoichiometry for epoxide cross-linking. Reaction conditions were as follows: (B) 25 °C, 60 min; (C) 75 °C, 30 min; (D) 75 °C, 40 min; (E) 75 °C, 120 min.

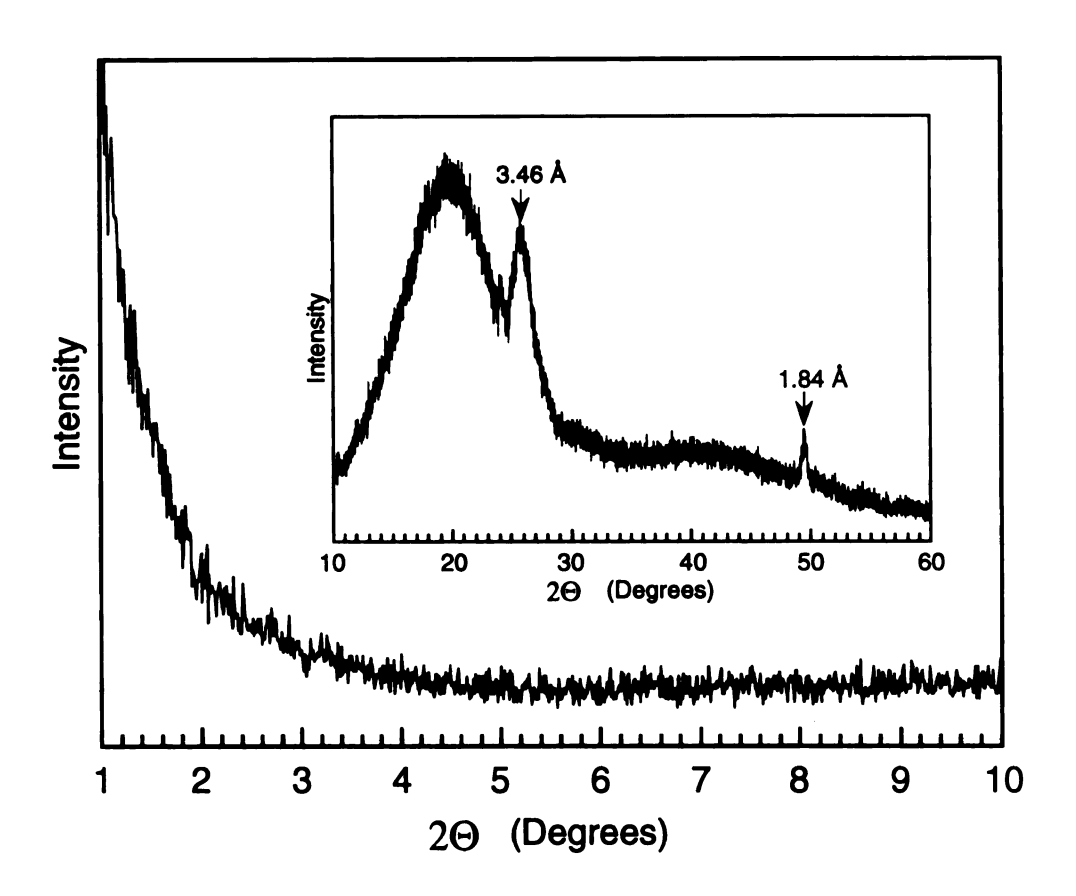


Figure 4.5 X-ray diffraction pattern of a cured epoxy polymer-kenyaite nanocomposite prepared from C18-kenyaite-PF. The organo kenyaite loading was 14.6 wt %. Polymer curing was carried out at 75 °C for 3 h, and followed by 3 h at 125 °C. The sharp lines are the in-plane reflections of the exfoliated kenyaite layers.

4.3.1.3 Exfoliation of $C_nH_{2n+1}NH_3^+/C_nH_{2n+1}NH_2$ -kenyaites in an Epoxy Polymer Matrix

The intercalation of $C_nH_{2n+1}NH_3^+/C_nH_{2n+1}NH_2$ -kenyaites (n = 6, 8, 10, 12) by a stoichiometric mixture of epoxide resin and curing agent was also investigated by XRD (Figure 4.6). The intercalation of the resin/curing agent mixture was very successful for chain length $n \ge 8$. The basal spacings for n = 8, 10 and 12 all exceeded the values that the lipid-like bilayer structures can afford (cf. Table 4.1). The sharp x-ray peaks for n = 10, 12 arise from the phase segregated extragallery amine molecules. This result suggests that the pristine intragallery alkylammonium/alkylamine molecules have lost their original registry and preferred orientations after the co-intercalation of epoxide resin and poly(oxypropyleneamine) curing agent. The alkylammonium ions can undergo proton transfer reaction and, consequently, the small mobile amine molecules can be excluded from intragallery region to provide extra intragallery space for the intercalation and intragallery polymerization.

The XRD patterns of fully cured epoxy-kenyaite nanocomposites prepared from $C_nH_{2n+1}NH_3^+/C_nH_{2n+1}NH_2$ -kenyaites (n = 6, 8, 10, 12, 18) are shown in Figure 4.7. The absence of the 00l diffraction peaks for n > 6 provides strong evidence that the silicate nanolayers of kenyaite have been exfoliated during the thermosetting process. A small contraction in d-spacing is observed for the resulting aggregated epoxy-kenyaite composite prepared from C6-kenyaite-LM. This is probably due to the loss of interlayer water molecules during the thermosetting process. The low angle background scattering for the epoxy-kenyaite nanocomposites prepared from $C_nH_{2n+1}NH_3^+/C_nH_{2n+1}NH_2$ -kenyaites (n = 8 and 10) is more intense than for C18-kenyaite-PF. This suggests that the extent of nanolayer exfoliation for the nanocomposites prepared from different intercalates may vary due to the nature of alkylammonium ions. This issue will be discussed in detail latter.

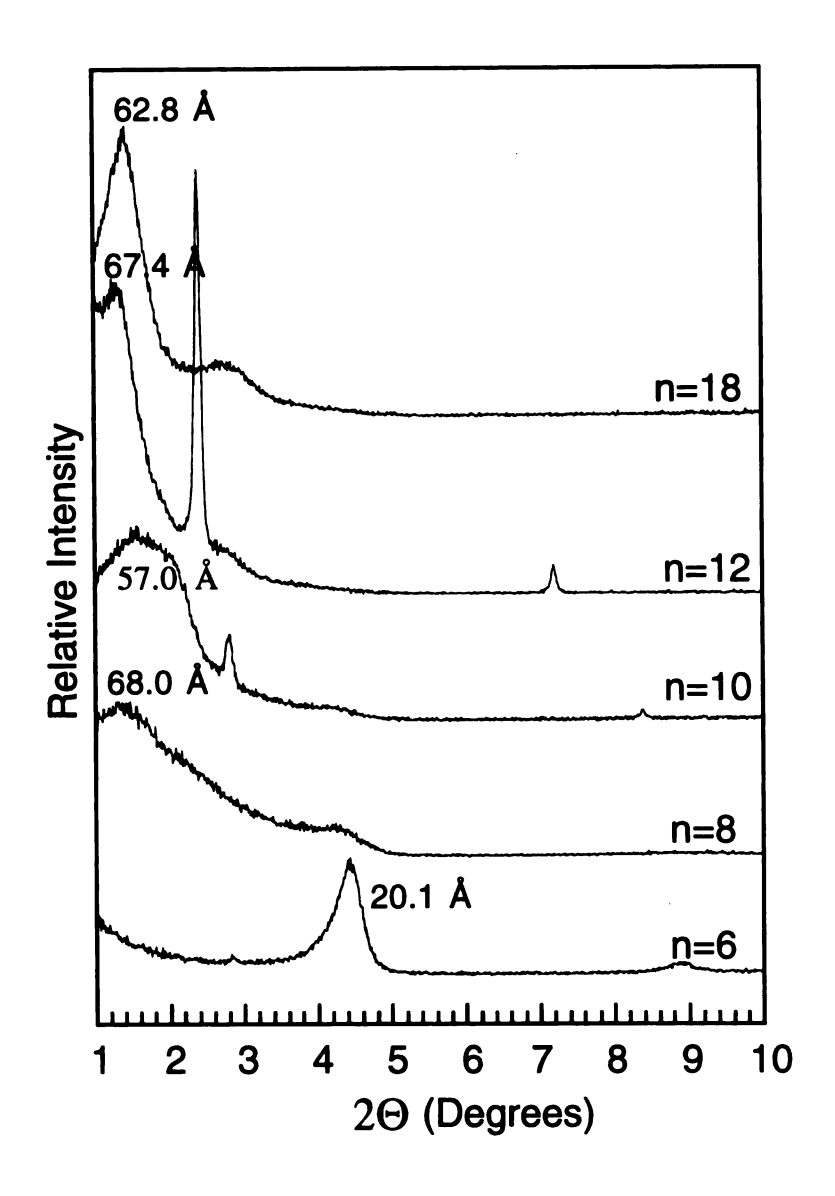


Figure 4.6 XRD patterns of partially cured composites prepared by reaction of $CH_3(CH_2)_{n-1}NH_3$ +/ $CH_3(CH_2)_{n-1}NH_2$ -kenyaites (n = 6, 8, 10, 12 and 18) with a stoichiometric mixture of epoxide resin and poly(oxypropyleneamine) curing agent. The organo kenyaite loading is 15 wt % for n = 6, 10, 12, 18, and 30 wt % for n = 8. The reactions were carried out at 25 °C for 5 min to 60 min for n \leq 12, and at 75 °C, 30 min for n = 18. The sharp lines in the patterns for n = 10, 12 are attributed to phase-segregated amine.

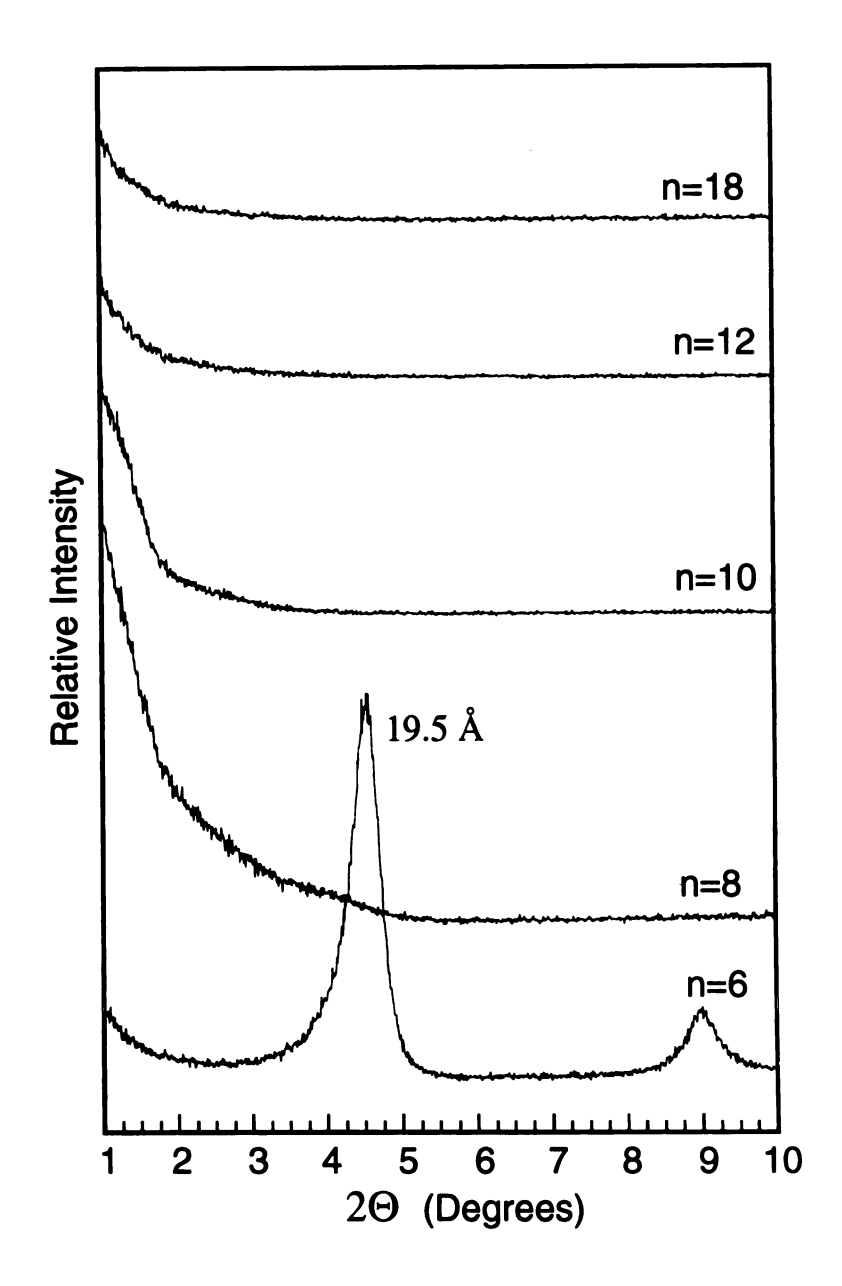


Figure 4.7 X-ray diffraction patterns of cured epoxy-kenyaite nanocomposites prepared from $CH_3(CH_2)_{n-1}NH_3+/CH_3(CH_2)_{n-1}NH_2$ -kenyaites (n = 6, 8, 10, 12 and 18). The organo kenyaite loading for each composite was 15 wt %. Polymer curing was carried out at 75 °C for 3 h, and followed by 3 h at 125 °C.

4.3.1.4 Effect of Gallery Acidity of Organo Kenyaites on Exfoliation

Organo kenyaites with paraffin-like gallery structures were prepared by intercalation of long chain secondary and tertiary alkylammonium ions in place of primary onium ions. The methodology used to achieve intercalation was the same as described above for C18-kenyaite-PF. A quaternary alkylammonium ion exchanged kenvaite was also prepared using the previous reported method of Lagaly. 10 Figure 4.8 shows the XRD patterns of $CH_3(CH_2)_{17}NH_{3-n}(CH_3)_n^+$ -kenyaite (n = 1, 2, 3). The XRD patterns (Figure 4.9) of the cured composites prepared from these intercalates show that three kinds of nanocomposite structures have been achieved. A disordered exfoliated, an ordered exfoliated and an intercalated epoxy-kenyaite nanocomposites were obtained for n = 1, 2, 3, respectively. The different gallery acidities provided by onium ions resulted in the different intragallery polymerization rates, which is the decisive factor governing the final morphology of silicate nanolayers in the polymer matrix. This dependence of gallery exfoliation on onium ion acidity was also shown in the system of $CH_3(CH_2)_{17}NH_{3-n}(CH_3)_n^+$ -magadite (n = 1, 2, 3), which was fully investigated in Chapter 3. So, we have developed a general approach, wherein by varying the Brönsted acidity of the intragallery catalytic centers, it is possible to control the extent of intragallery separation. Interestingly, the extent of layer separation for the intercalated and ordered exfoliated composites is slightly less for epoxy-kenyaite nanocomposites than for magadiite. This difference in the extent of exfoliation may reflect differences in layer charge density.

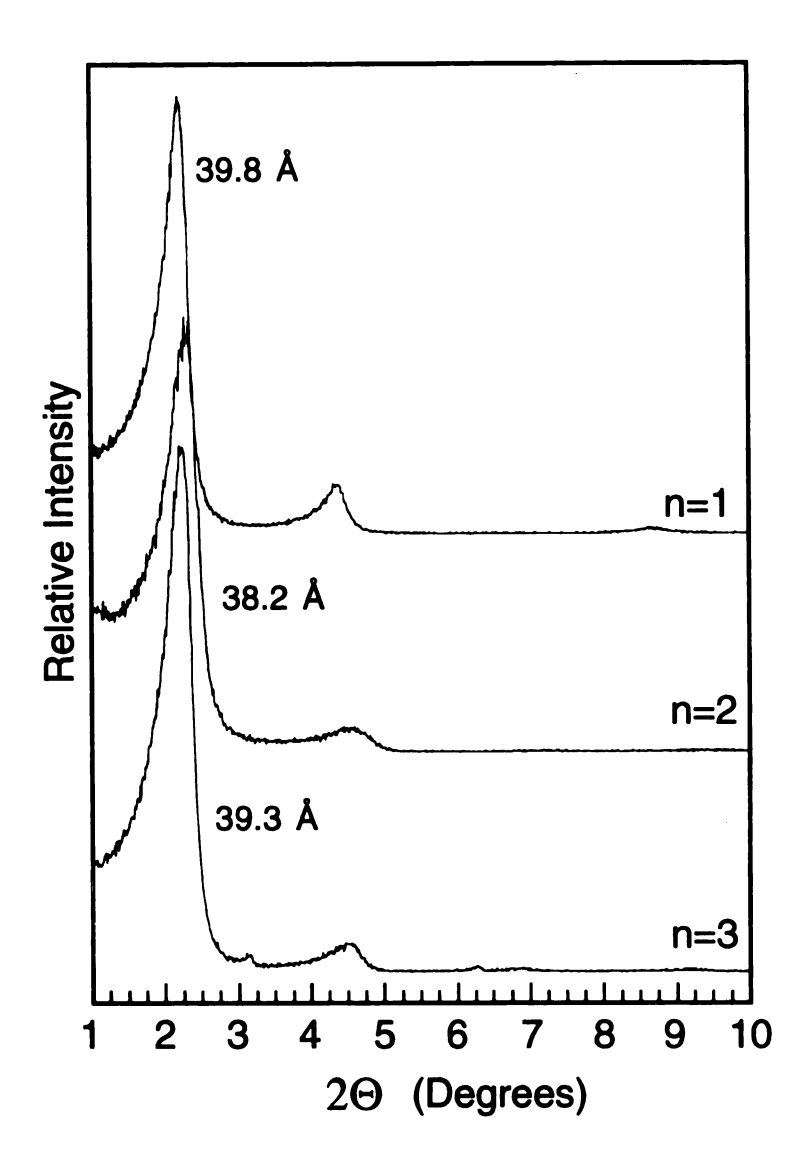


Figure 4.8 X-ray powder diffraction patterns of $CH_3(CH_2)_{17}NH_{3-n}(CH_3)_n^+$ -kenyaites (n = 1, 2, 3). All of the organo kenyaites have paraffin-like gallery structures.

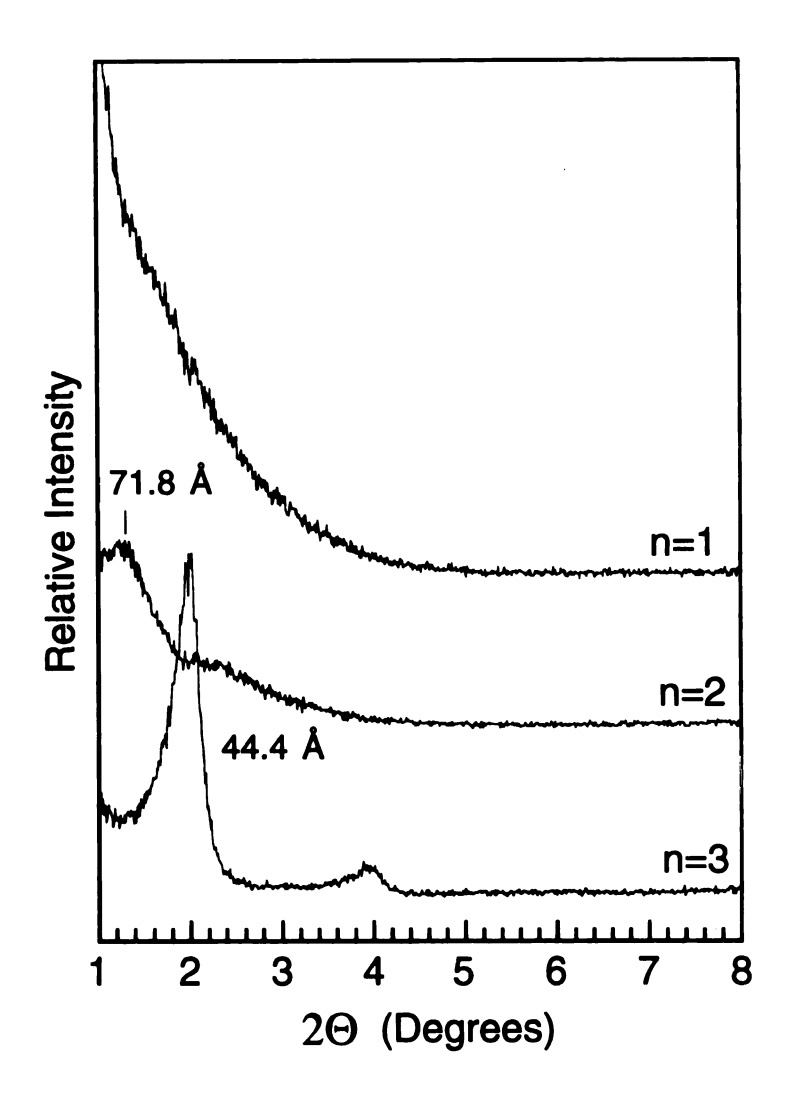


Figure 4.9 X-ray diffraction patterns of cured epoxy polymer-kenyaite nanocomposites prepared from $CH_3(CH_2)_{17}NH_{3-n}(CH_3)_n^+$ -kenyaites with a paraffin gallery structure. The organo kenyaite loading was 20 wt % (n = 1, 3) and 10 wt % (n = 2). Polymer curing was carried out at 75 °C for 3 h, followed by 3 h at 125 °C. The secondary onium ions (n = 1) give highly exfoliated (disordered) nanocomposites (d > 90 Å). The tertiary onium ion derivative (n = 2) also gives an exfoliated nanocomposite, but the layer separation is highly ordered (d = 72 Å). The quaternary onium ion exchange form (n = 3) forms an intercalated nanocomposite (d = 44 Å).

4.3.2 Exfoliation of Ilerite Nanolayers in an Epoxy Polymer Matrix

4.3.2.1 Synthesis of Organo Ilerites

The Na⁺ form of ilerite has been reported only in a few cases to undergo cation-exchange reaction by quaternary or short chain primary alkylammonium ions.⁶ Our effort to convert Na⁺-ilerite to long chain alkylammonium exchanged ilerite with a paraffin structure was not successful using our previously developed method for converting Na⁺-magadiite and K⁺-kenyaite to their organic analogs. However, it was possible to convert Na⁺-ilerite into organo intercalates with very high basal spacings from 61 Å - 75 Å. The variable interlayer spacings and the orientations of intragallery onium ions are not understood. Our results showed that washing processes removed some of the intragallery organic species and lowered the amine content. However, a single phase with a paraffin gallery structure was very difficult to achieve.

A new approach was developed to achieve organo ilerite intercalate with a reasonable content of intragallery long chain onium ions. Na⁺-ilerite was fist converted into the proton exchanged form, then the H-ilerite was reacted with small amount of neutral amine. The experimental section provides specific details for the synthesis of this CH₃(CH₂)₁₇NH₃⁺-ilerite which is designated as C18-ilerite. The XRD patterns for both the inorganic forms and the organic form of ilerite are shown in Figure 4.10. The basal spacing of 36.4 Å is consistent with a perpendicular monolayer of alkyl chains. The XRD pattern show no peaks for the neutral amine phase. Our TGA results shows that the molar ratio of CH₃(CH₂)₁₇NH₂ to Si₈O₁₇²⁻ unit is about 1.6. It is very reasonable to assume the amine molecules have been transferred into gallery region by the acid-base reaction.

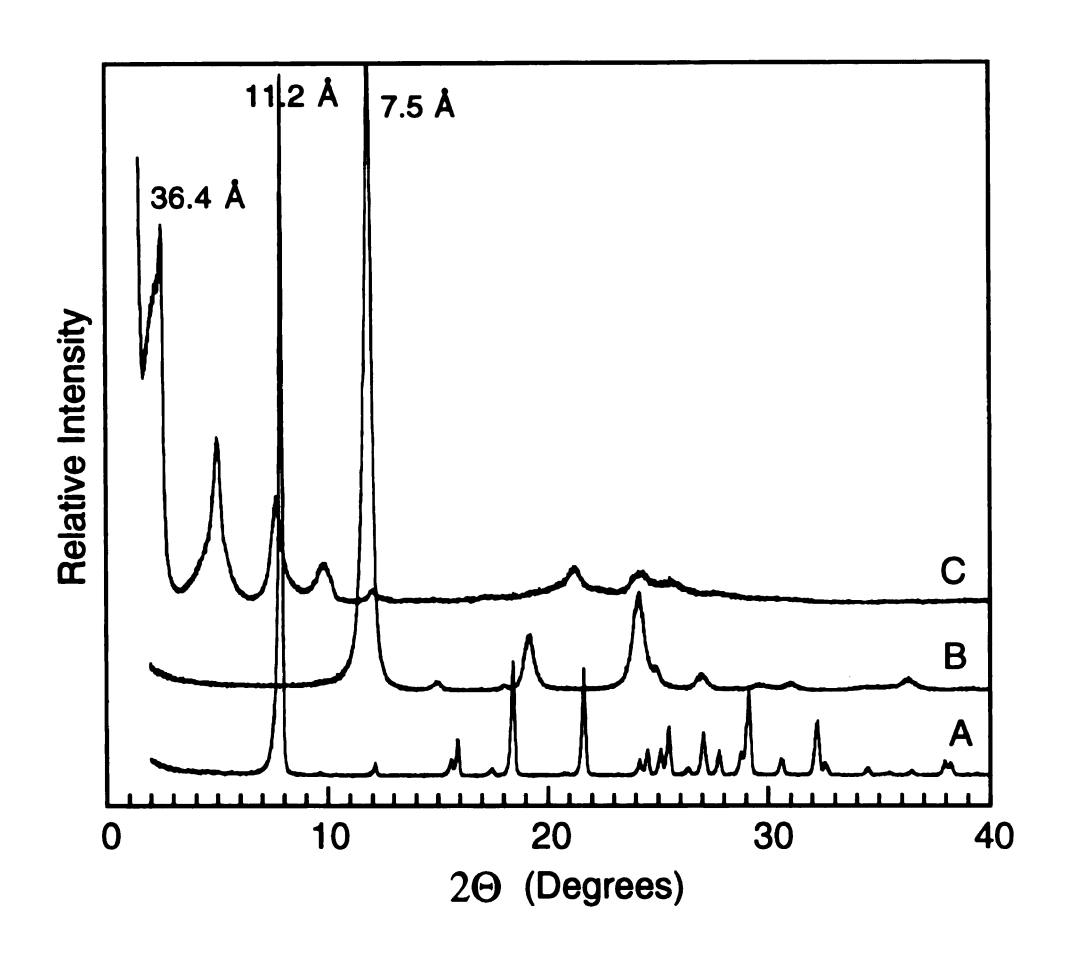


Figure 4.10 X-ray powder diffraction patterns of air-dried (A) Na⁺-ilerite; (B) H⁺-ilerite; and (C) CH₃(CH₂)₁₇NH₃⁺-ilerite (C18-ilerite).

4.3.2.2 Exfoliation of C18-Ilerite in an Epoxy Polymer Matrix

The co-intercalation of C18-ilerite by a stoichiometric mixture of epoxide resin and curing agent as a function of time was investigated by XRD (Figure 4.11). At 25 °C, the C18-ilerite is partially solvated, as evidenced by a broad x-ray peak at low angle (Figure 4.11A). This two-phase mixture was quickly replaced by a single d₀₀₁ peak at 60.1 Å (Figure 4.11B) corresponding to an orientation of the onium ions with a lipid-like bilayer structure to afford an optimal intragallery space for the intercalated epoxide resin and curing agent. Figure 4.11 C and D indicate that the intragallery region has been expanded beyond that the critical height which the lipid-bilayer structure can afford. The final x-ray amorphous phase (Figure 4.12) suggests that an exfoliated epoxy-ilerite nanocomposite has been obtained. The ilerite 2-dimensional structure is still retained in the exfoliated state, as indicated by strong high angle in-plane peaks. The formation pathway for the epoxy-exfoliated ilerite nanocomposites shows a similarity to magadiite and kenyaite.

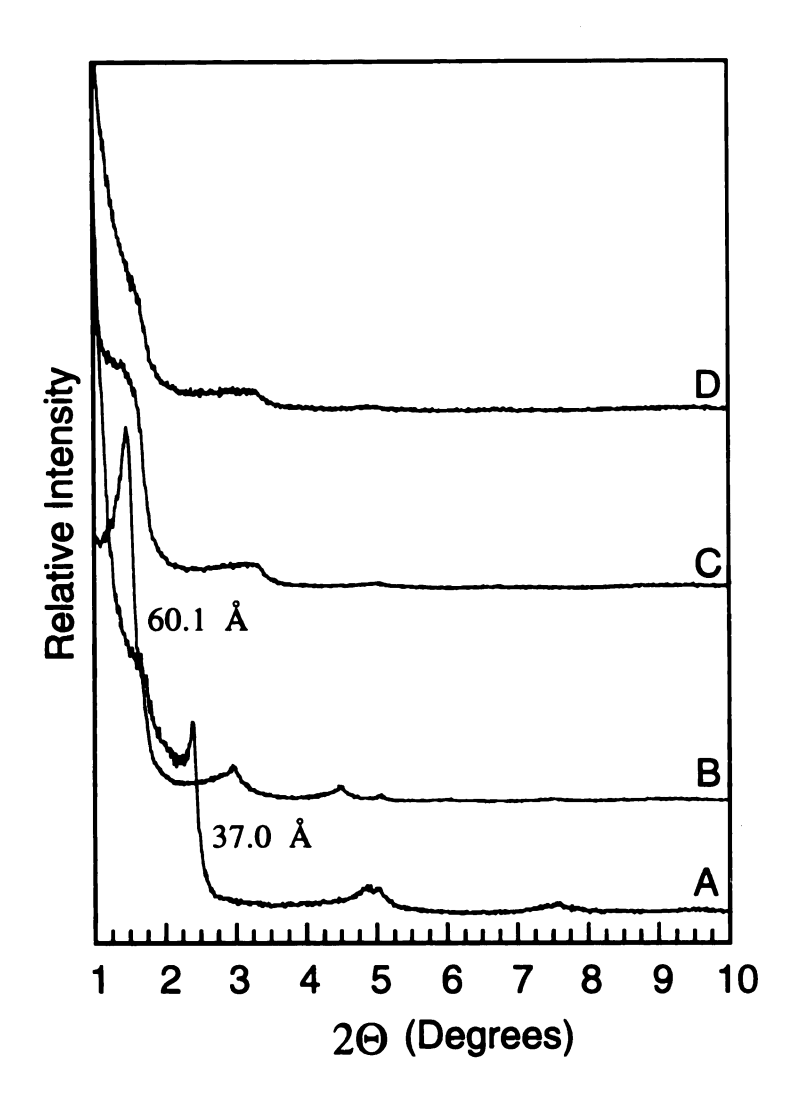


Figure 4.11 X-ray diffraction patterns of the partially cured composites prepared by reaction of C18-ilerite (15 wt % loading) with a stoichiometric mixture of epoxide resin and poly(oxypropyleneamine) curing agent. The primary alkylammonium and the free amine content of C18-ilerite was counted as contributing to the stoichiometry for epoxide cross-linking. Reaction conditions were as follows: (A) 25 °C, 20 min; (B) 75 °C, 40 min; (C) 75 °C, 100 min; (D) 75 °C, 150 min.

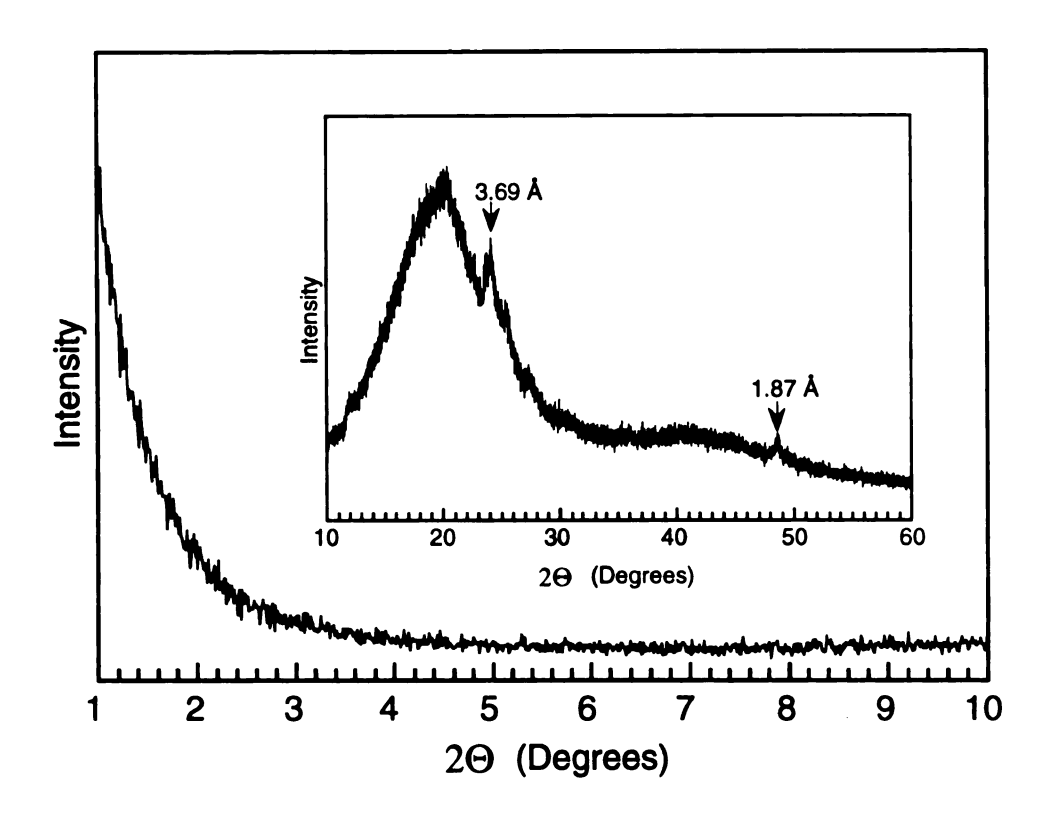


Figure 4.12 X-ray diffraction pattern of a cured epoxy polymer-ilerite nanocomposite prepared from C18-ilerite. The organo ilerite loading was 15 wt %. Polymer curing was carried out at 75 °C for 3 h, and followed by 3 h at 125 °C. The sharp peaks at 3.69 Å and 1.87 Å are the in-plane reflections of ilerite. The broad peaks at $2\Theta = 20^{\circ}$, 42° are due to the polymer matrix.

4.3.3 Performance Properties of Exfoliated Epoxy-Kenyaite and Ilerite Nanocomposites

4.3.3.1 Effect of Chain Length on Tensile Properties

It was interesting to know the benefits of kenyaite and ilerite nanolayer exfoliation in the epoxy polymer matrices. Table 4.2 illustrates the tensile properties of epoxy-exfoliated kenvaite nanocomposites prepared from the $C_nH_{2n+1}NH_3^+/C_nH_{2n+1}NH_2$ -kenyaites (n = 8, 10, 12, 18). All of the exfoliated nanocomposites have shown a tremendous increase in tensile strength. Even the tensile elongation at break is improved when the matrix has a sub-ambient T_g. However, the composites prepared from the intercalates with a chain length $n \le 12$ behave not as good as C18-kenyaite-PF (n = 18) at the same organo kenyaite loading. As we have demonstrated before, $C_nH_{2n+1}NH_2$ amines with mono-functional end groups can be incorporated into a cross-linked epoxy network to form the dangling chains. This is the major factor in deciding the improvement properties for each composite. From the thermogravimetric analysis we recognized that for the $C_{10}H_{21}NH_3^+/C_{10}H_{21}NH_2$ -kenyaite intercalate, has been loaded with 20.7% more amino groups than C18-kenyaite-PF. Therefore, there are more dangling chains in the composite prepared from C₁₀H₂₁NH₃+/C₁₀H₂₁NH₂-kenyaite than C18-kenyaite-PF. Consequently, the benefit of nanolayer exfoliation was compromised more when the short chain onium exchanged kenyaites (n = 8, 10, 12) are used to form the epoxy-kenyaite nanocomposites. Also, there are other factors that govern the performance properties of the final composites. All of the nanocomposites prepared from $C_nH_{2n+1}NH_3^+/C_nH_{2n+1}NH_2$ -kenyaites show amorphous XRD patterns, but the patterns for the composites prepared from short chain onium exchange kenyaits show greater low angle background scattering than C18kenyaite-PF. This suggests that the degree of exfoliation in latter case is higher. The extent of layer separation always governs the overall performance properties of the

polymer-layered silicate nanocomposites, and in some cases is more decisive than the number of dangling network chains caused by the amine intercalated.

Table 4.2 Effect of Chain Length of CH₃(CH₂)_{n-1}NH₃+/CH₃(CH₂)_{n-1}NH₂
Gallery Surfactant on Tensile Properties of Epoxy-Kenyaite
Nanocomposites. The organo kenyaite loading is 15 wt % for each composite.

chain length n =	pristine polymer	8	10	12	18
tensile strength (MPa)	0.63	1.63	1.94	1.74	2.63
elongation at break (%)	23.4	28.2	38.8	39.8	41.6

4.3.3.2 Effect of Extent of Layer Separation on Performance Properties

A comparison of tensile properties for the nanocomposites prepared form $CH_3(CH_2)_{17}NH_{3-n}(CH_3)_n^+$ -kenyaites (n = 1, 2, 3) is shown in Figure 4.13. Although, the tensile strengths for all three types of nanocomposites (cf. Figure 4.9) show a dependence on kenyaite silicate loading, the silicate loading is substantially more effective for the exfoliated nanocomposites (n = 1) than the ordered exfoliated (n = 2) and the intercalated nanocomposites (n = 3). This result further supports the conclusion that the tensile properties are closely linked to the extent of layer separation and the effective behavior for the exfoliated silicate nanolayers. The structural reason behind this effect has been discussed in detail in Chapter 3. Figure 4.14 shows the dependence of solvent uptake for the nanocomposites prepared from $CH_3(CH_2)_{17}NH_{3-n}(CH_3)_n^+$ -kenyaites (n = 1, 2, 3) on their nanophase morphology.

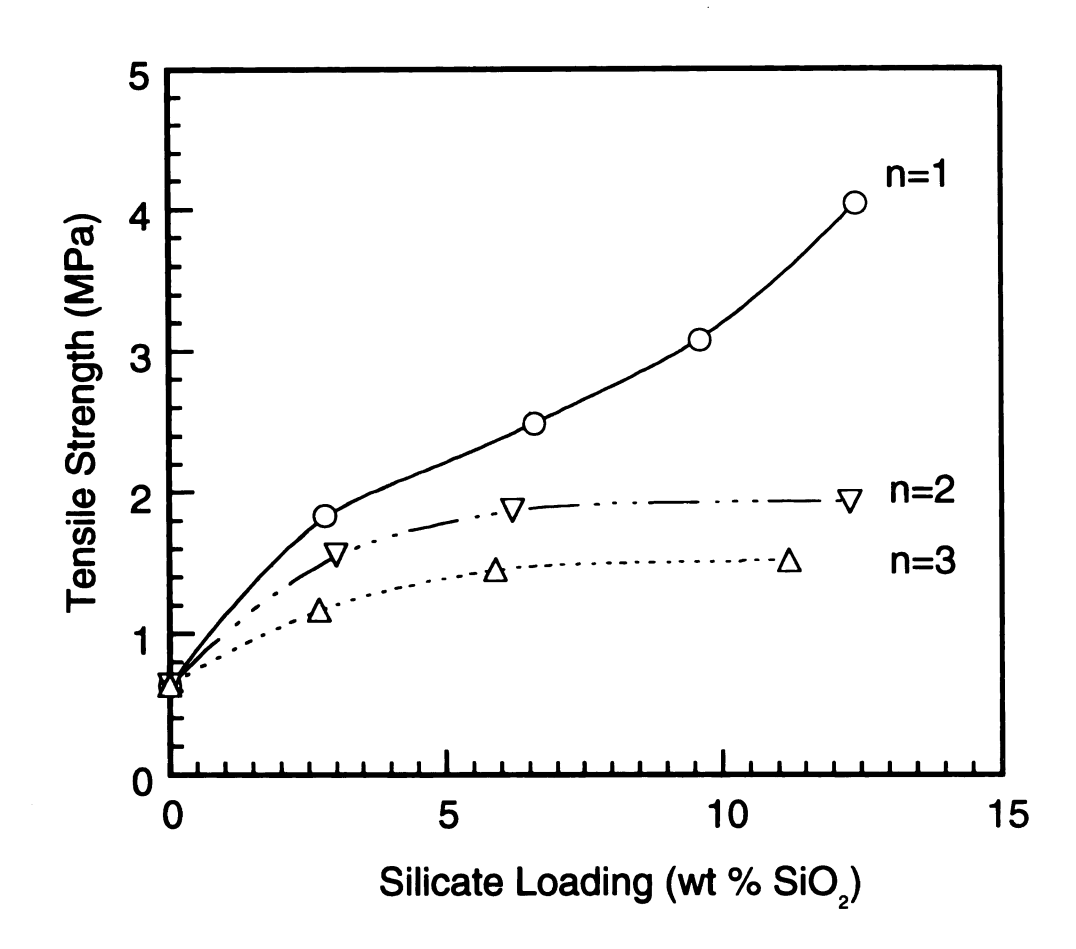


Figure 4.13 A comparison of the tensile strengths of epoxy-kenyaite nanocomposites prepared from $CH_3(CH_2)_{17}NH_{3-n}(CH_3)_n^+$ -kenyaites. The kenyaite silicate loading (expressed on wt % SiO_2) was determined by calcining the composites in air at 650 °C for 4 h using a heating rate of 2 °C/min. The secondary alkylammonium and the free amine content of $CH_3(CH_2)_{17}NH_2CH_3^+$ -kenyaite (n = 2) was counted as contributing to the stoichiometry for epoxide cross-linking.

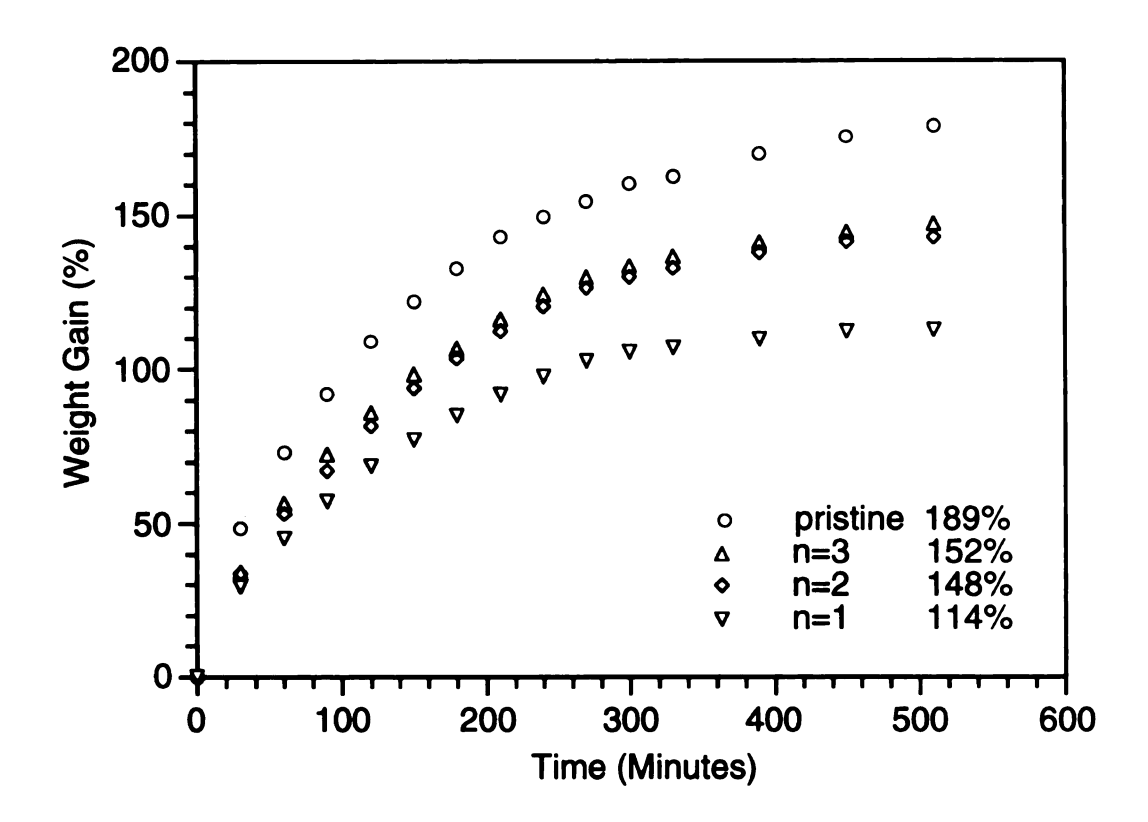


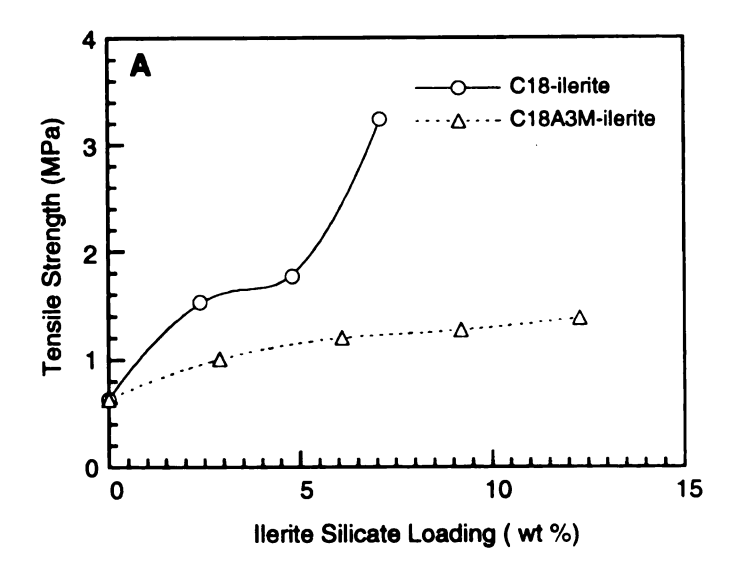
Figure 4.14 Toluene uptake curves for nanocomposites prepared from $CH_3(CH_2)_{17}NH_{3-n}(CH_3)_n^+$ -kenyaites (n = 1, 2, 3). The tabulated values in the insert are equilibrium data obtained from the immersion weight gain after 24 hr. The loading of organo-kenyaite is 10 wt % for each epoxy-kenyaite composite.

The mechanical performance properties of epoxy-ilerite nanocomposites was also investigated. An intercalated epoxy-ilerite nanocomposite(d-spacing = 39.0 Å) was prepared from C18A3M-ilerite, which is a quaternary CH₃(CH₂)₁₇N(CH₃)₃+ ion exchanged ilerite with a 29.5 Å basal spacing. A comparison of tensile properties between the exfoliated and intercalated epoxy-ilerite nanocomposites is shown in Figure 4.15. The exfoliated nanocomposites performed better in the terms of tensile strength and tensile modulus. All of kenyaite and ilerite results show the exceptional performance, owing primarily to the presence of exfoliated silicate nanolayers.

4.3.3.3 Effect of Nanolayer Thickness on Performance Properties

After we have extended the intercalation and exfoliation chemistry to the other members of the layered silicic acid family, there remains an important question: Which member in term of nanolayer thickness is more suitable for nanocomposite formation and optimal performance properties?

A comparison of the dependence of tensile properties on layered silicate loading for all three types nanocomposites (exfoliated, ordered exfoliated and intercalated) is shown in Figure 4.16 for magadiite and kenyaite. Interestingly, the curves for magadiite and kenyaite for each type of composite are almost identical in terms of slope and value at the same loading. We also measured the chemical stability and resistance to solvent swelling for the exfoliated nanocomposites prepared from C18-magadiite-PF, C18-kenyaite-PF and C18-ilerite. The results are given in Table 4.3. Since the silicate (SiO₂) loading determined by calcination is difficult to control in equal for each case, each composite possess only a closed silicate loading. Nevertheless, all of these composites showed a similar performance. The effect of different layer thickness is hardly to be distinguished based on solvent uptake experiment.



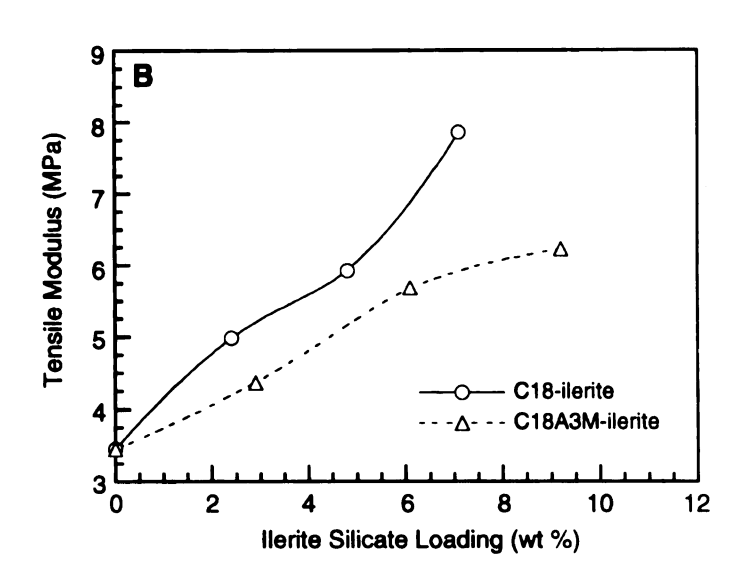
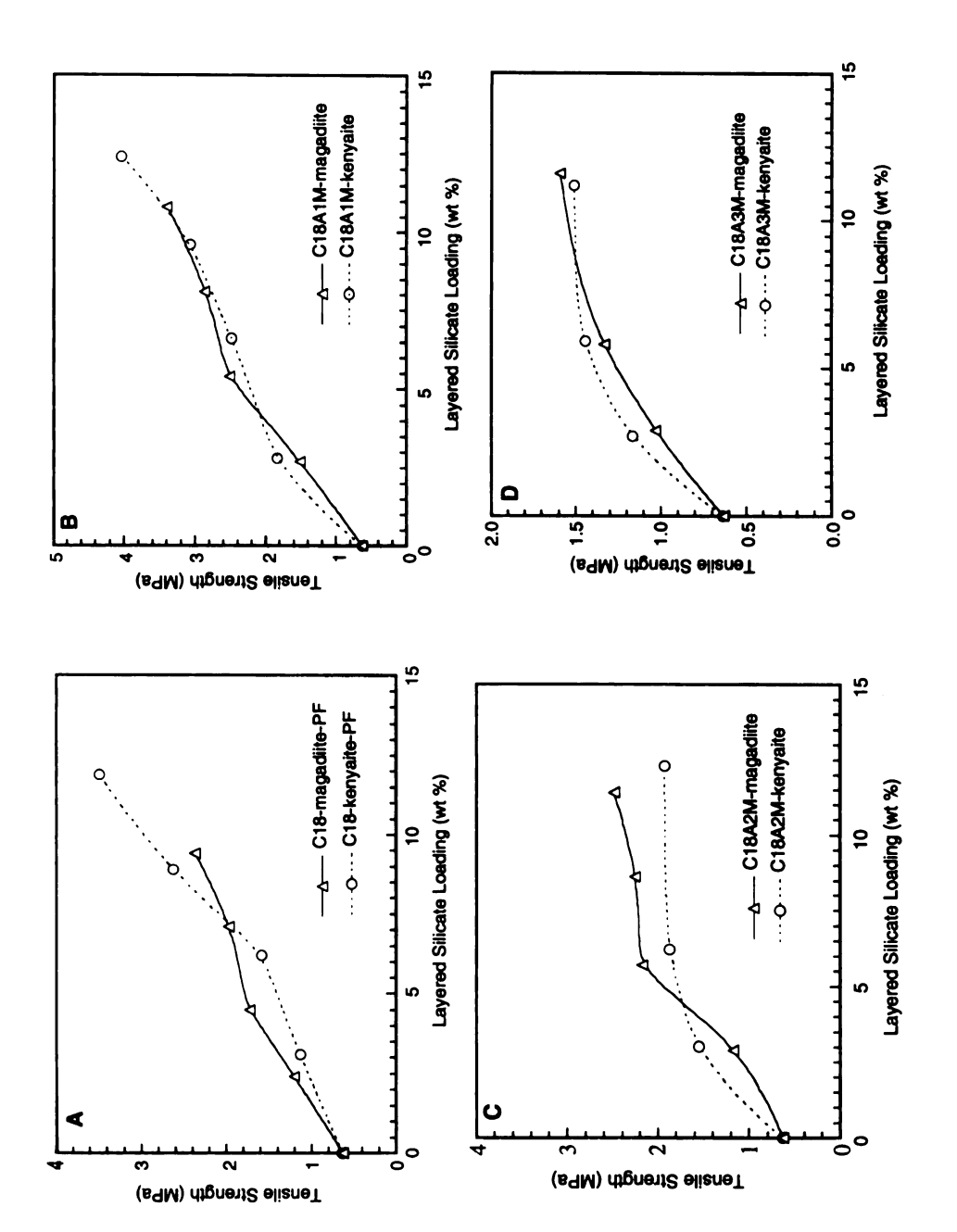


Figure 4.15 Comparison of (A) tensile strengths and (B) tensile moduli for epoxy-exfoliated ilerite nanocomposites prepared from C18-ilerite and epoxy-intercalated ilerite composites prepared from C18A3M-ilerite. The primary onium ion and amine content of the organo ilerite was counted as contributing to the stoichiometry of epoxide cross-linking.



A comparison of the tensile strengths between epoxy-magadiite and epoxy-kenyaite nanocomposites prepared from (A) primary; (B) secondary; (C) tertiary; (D) quaternary alkylammonium exchanged CH₃(CH₂)₁₇NH_{3-n}(CH₃)_n+-layered silicic acids. Figure 4.16

Table 4.3 Chemical and Solvent Resistance of Epoxy-Layered Silicic Acid Nanocomposites Prepared From C18-magadiite-PF (9.1 wt %), C18-kenyaite-PF (10.4 wt %) and C18-ilerite (10.0 wt %). Values are the Immersion Weight Gains (wt %) after a Certain Period.

materials	10% NaOHa	distilled H ₂ O ^a		5% acetic acida	methanol ^b	toluenec
pristine polymer	1.6	2.5	16.7	13.4	76.5	189
C18-magadiite-PF	1.5	1.6	7.2	9.6	58.5	136
C18-kenyaite-PF	1.7	2.1	8.1	9.1	57.1	132
C18-ilerite	2.4	2.6	8.0	10.7	56.6	133

a Weight gain after 15 days. b Weight gain after 48 hr. c Weight gain after 24 hr.

Additional factors could govern the overall performance properties of the composites prepared from different layered silicic acids, such as the aspect ratios, the amine loading (which can form dangling chains), the amount of amorphous silica presented (which probably always accompanies the crystalline products), and the degree of nanolayer exfoliation. At this stage, we can conclude only that all of the organo layered silicic acid nanolayers exhibit similar composite performance properties when their silicate nanolayers are exfoliated in epoxy matrix with a sub-ambient $T_{\rm g}$.

4.4 Conclusions

The exfoliation chemistry of magadiite was successfully extended to the other members of the layered silicic acid family. The mechanism leading to the exfoliation of silicate nanolayers for magadiite is shared by kenyaite and ilerite. The approach developed for organo layered silicic acids, which allows control of the extent of nanolayer separation, make it possible to investigate the relationship between the nanolayer properties and material performance properties. Factors such as silicate loading, extent of nanolayer separation and the degree of cross-linking also govern the performance of composites prepared from organo kenyaites and ilerites. A large amount of alkylamine should be avoided in the synthesis of polymer-layered silicic acid nanocomposites to minimize the fraction of dangling chain in the polymer network. The overall performance properties of the nanocomposites prepared from different organo layered silicic acids show no significant dependence on the nanolayer thickness.

4.5 References

- 1. Lagaly, G.; Beneke, K.; Weiss, A. Am. Mineral. 1975, 60, 650.
- 2. Beneke, K.; Lagaly, G. Am. Mineral. 1977, 62, 763.
- 3. Beneke, K.; Lagaly, G. Am. Mineral. 1983, 68, 818.
- 4. Fletcher, R. A.; Bibby, D. M. Clays Clay Miner. 1987, 35, 318.
- 5. Beneke, K.; Kruse, H. H.; Lagaly, G. Z. anorg. allg. Chem. 1984, 518, 65.
- 6. Kosuge, K.; Tsunashima, A. J. Chem. Soc., Chem. Commun. 1995, 2427.
- 7. Beneke, K.; Lagaly, G. Am. Mineral. 1989, 74, 224.
- 8. Lan, T.; Kaviratna, P. D.; Pinnavaia, T. J. Chem. Mater. 1995, 7, 2144.
- 9. Shi, H.; Lan, T.; Pinnavaia, T. J. Chem. Mater. 1996, 8, 1584.
- 10. Lagaly, G.; Beneke, K.; Weiss, A. Am. Mineral. 1975, 60, 642.

Chapter 5

HYBRID ORGANIC-INORGANIC NANOCOMPOSITES FORMED FROM AN EPOXY POLYMER AND AN AMINE CURING AGENT (JEFFAMINE) INTERCALATED IN PROTON FORMS OF LAYERED SILICIC ACIDS

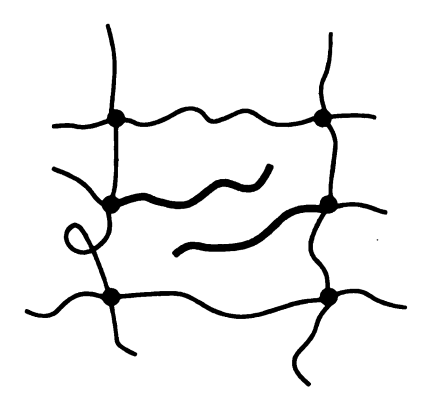
5.1 Introduction

A great deal of research has been conducted on organic-inorganic hybrid composites in which layered silicate clays are used as reinforcement agents.¹⁻¹¹ Layered silicate clays become good candidates not only because their silicate nanolayers have a chemically stable siloxane surface, high aspect ratios and high strength, but more importantly,¹² because the rich intercalation chemistry of clay silicates can be used to facilitate exfoliation of silicate nanolayers into the polymer network.¹³⁻¹⁵ The exfoliation can optimize the interfacial contact between the organic and inorganic phases for improved nanocomposite properties.¹⁶

Approaches to the exfoliation of clay nanolayers have been investigated by several different research groups using both thermoplastic and thermoset polymers. 7.17-20 Most polymer precursors require a hydrophobic environment for intercalation into clay galleries. The hydrophilic inorganic clay surface usually has to be modified first to accommodate the incoming organic precursors. Generally, an organic cation exchanged reaction is used to form a hydrophobic organo clay. Then, the organo clay is intercalated by polymer precursors which are either organic monomers or prepolymers. Direct intercalation of a preformed polymer into the clay galleries by melt processing is also possible. 21

The most commonly used organic species for clay cation exchange reaction are ammonium ions of the type R₁R₂R₃R₄N⁺, wherein the R groups contain 1-18 carbon atoms and up to three R groups are replaced by protons. An intercalated nanocomposite is likely to be formed when only non-acidic quaternary alkylammonium ions are used. The overall performance properties of the intercalated polymer-clay nanocomposites are inferior to their exfoliated analogs. In most cases, the presence of long chain $(n \ge 8)$ alkyl groups and strong intragallery acidity is required to form an exfoliated polymer-clay nanocomposite; otherwise, the resulted organo cation exchange clay products are not sufficiently hydrophobic to facilitate the intercalation of the incoming polymer precursors.8 However, the introduction of larger alkyl groups will simultaneously cause a steric or structural problem, because most of the organic cations can not be incorporated into the polymer network and will independently occupy space in the polymer matrix without contributing positive structural properties. When onium ions dilute the polymer network structure, especially for high charge density layered silicate clays with high surface concentrations of organo species loaded, the advantages of silicate nanolayer exfoliation will be compromised. Although, some organic cations can have functional groups for cross-linking into the polymer chains with minimal loss of performance properties, unteathered onium ions act as a plasticizer and performance is not as good as a homopolymer matrix.

As discussed in Chapters 2, 3 and 4, primary alkylammonium exchanged layered silicic acids have been successfully used as the starting layered hosts to form epoxy-exfoliated layered silicic acid nanocomposites. The mono-functional amino groups cause the formation of a significant number of dangling chains and lower the extent of network formation as illustrated schematically bellow:



Although, onium ions derived from aliphatic diamines would minimize dangling chain formation, clays interlayered by such onium ions form lateral monolayers, which is the most favorable structure, and the strong intragallery bonding prevents swelling by the polymer precursors.

The proton exchanged forms of layered silicic acids can be obtained easily by the treatment of alkali-metal forms of layered silicic acids using a dilute acid.²²⁻²⁷ The H⁺ forms of layered silicic acids have a layered structure similar to their alkali-metal exchange forms, and can be used as acid catalysts and as absorbents for alkylamine.^{28,29} The present work demonstrates that poly(oxypropyleneamine) curing agents acting as strong bases can form onium ions by a simple acid-base reaction in the galleries of a silicate clay. Thus, these curing agents can be intercalated into silicate galleries to form an intercalate that functions as an alkylammonium exchange layered silicic acid.

$$\begin{array}{c|c} \hline \hline \hline H^+ & H^+ & H^+ \\ \hline \hline \end{array} + \begin{array}{c} \hline \\ NH_2 \\ \hline \end{array}$$

A new approach to the preparation of thermoset polymer-layered silicic acid nanocomposites is discussed based on this chemistry, thus eliminating the need to pre-intercalated the layered silicate galleries with undesired onium ions. This new processing development has resulted in a greater improvement of the overall performance properties of polymer-layered silicic acid nanocomposites.

5.2 Experimental

5.2.1 Materials

The epoxide resin used to for epoxy-layered silicic acid hybrid composite formation was poly(bisphenol A-co-epichlorohydrin) (Shell, EPON 828), with MW ~377:

$$\begin{array}{c} \begin{array}{c} \begin{array}{c} \begin{array}{c} \begin{array}{c} \begin{array}{c} CH_3 \\ \end{array} \end{array} \\ \begin{array}{c} CH_2\text{-} CHCH_2O \end{array} \end{array} \\ \begin{array}{c} \begin{array}{c} CH_3 \\ \end{array} \end{array} \\ \begin{array}{c} OCH_2CHCH_2O \end{array} \end{array} \\ \begin{array}{c} \begin{array}{c} CH_3 \\ \end{array} \\ \begin{array}{c} CH_3 \end{array} \\ \begin{array}$$

DGEBA type, n = 0 (88%); n = 1 (10%); n = 2 (2%).

The curing agent was poly(oxypropyleneamine) (Huntsman Chemical, JEFFAMINE D-series and T-series):

The above monomers can afford epoxy polymer matrices with a broad T_g range from a sub-ambient T_g of -40 °C (D-2000) to a T_g above room temperature of 95 °C (T-403). All the other chemicals used in this work were purchased from Aldrich Chemical Co. and used without further purification.

5.2.2 Synthesis of Layered Silicic Acids and Their Derivatives

Synthesis of Alkali-Metal Forms of Layered Silicic Acids. Alkali-metal forms of layered silicic acids were synthesized by hydrothermal methods.³⁰⁻³² In general, a suspension of amorphous silica gel was added to a MOH solution (M = Na or K) and heated at a temperature above 100 °C for a few days with stirring in a Teflon-lined Parr

reactor. The suspension containing the alkali-metal form of layered silicic acid was centrifuged, and the solid product was washed with deionized water to remove excess MOH, and air-dried at room temperature. The synthesis conditions used for each layered silicic acid are specified in Table 5.1.

Table 5.1 Synthesis of Alkali-Metal Forms of Layered Silicic Acids

materials	d ₀₀₁ (Å)	MOH ^a :SiO ₂ :H ₂ O molar ratio	temp (°C)	time (h)	H ₂ O washings vol (mL) x times
Na+-magadiite	15.6	1:3:50	150	42	600 x 2
K+-kenyaite	19.6	1:3:40	140	72	600 x 2
Na+-ilerite	11.2	1:2:14	105	216	700 x 3

 $^{^{}a}M = Na$ (magadiite and ilerite), K (kenyaite)

Synthesis of Proton Forms of Layered Silicic Acids. H⁺ forms of layered silicic acids were obtained by titration of synthetic alkali-metal forms of layered silicic acids with dilute a hydrochloric acid.²³ A 500-mL of aqueous suspension containing 15.0 g of layered silicic acid (magadiite, kenyaite and ilerite) was titrated with 0.1 M HCl at a rate of 3 mL/min to lower the pH to 1.9. For kenyaite the final pH was 1.8. The suspensions at pH = 1.9 (1.8 for kenyaite) were stirred for 24 hours (48 h for kenyaite). The proton exchange forms of layered silicic acids were separated by centrifugation and washed with deionized water until free of Cl⁻, and then air-dried at room temperature.

Synthesis of Jeffamine-H-Layered Silicic Acid Intercalates. An ethanol solution containing the Jeffamine (D2000, D4000, T3000 and T5000) was added to an aqueous suspension of the H+ form of the layered silicic acid and stirred at 60 °C for a certain period. The products were separated by centrifugation and air-dried. The ratios of Jeffamine to H-layered silicic acid, the solvent composition, reaction time, and post

reaction washing process used for each synthesis, along with the basal spacings for airdried products for each intercalate, are specified in Table 5.2-5.4. The powdered products for composite preparation were ground, and the fine particles were collected and stored for further use.

The intercalates formed between Jeffamine D400 or T403 and the H-layered silicic acids were synthesized by the following method. An aqueous solution containing Jeffamine was combined with an aqueous suspension of a layered silicic acid to form a mixture containing 3 g of Jeffamine in 80 mL of water per gram of layered silicic acid. The reaction is carried at 50 °C for 24 h. The reaction mixture was centrifuged, and the product was washed twice with an equal volume of water and air-dried.

Synthesis of JEFFAMINE-H-Magadiite Intercalates Useful for Preparation of Epoxy-Exfoliated Layered Silicic Acid Nanocomposites Table 5.2

intercalates d ₀₀₁ (Å) ph	d ₀₀₁ (Å)	physical state	Jeffamine (g)/g solvent (v/v) rxn time of H-magadiite EtOH/H ₂ O (h)	solvent (v/v) EtOH/H ₂ O	rxn time (h)	rxn temp (°C)	washing with EtOH/H ₂ O (v/v)
D2000-H-magadiite 54.6	54.6	sticky pwd	3.00	40/60	24	09	none
	44.0	pwd	3.60	20/20	12	09	25/25
T3000-H-magadiite	57.7	sticky pwd	3.85	30/30	12	09	none
	39.4	pwd	3.00	45/45	24	99	40/10
T5000-H-magadiite	80.7	gel	3.00	35/35	18	09	none
	53.2	pwd	4.28	45/45	24	09	35/15

Synthesis of JEFFAMINE-H-Kenyaite Intercalates Useful for Preparation of Epoxy-Exfoliated Layered Silicic Acid Nanocomposites Table 5.3

intercalates d ₀₀₁ (Å)	d ₀₀₁ (Å)	physical state	Jeffamine (g)/g of H-kenyaite	solvent (v/v) EtOH/H ₂ O	rxn time (h)	rxn temp (°C)	washing with EtOH/H ₂ O (v/v)
D2000-H-kenyaite	65.4	sticky pwd	3.00	30/70	12	09	none
	47.8	pwd	3.00	20/20	12	8	15/35
D4000-H-kenyaite	97.2	gel	3.50	20/20	12	09	none
	0.69	pwd	3.50	40/40	24	99	25/25
T3000-H-kenyaite	66.1	gel	3.00	35/65	12	9	none
	43.3	pwd	3.8	40/40	12	99	25/25
T5000-H-kenyaite	85.0	gel	3.0	40/40	12	99	none
	59.7	pwd	3.0	40/40	12	9	25/25

Table 5.4 Synthesis of JEFFAMINE-H-Ilerite Intercalates Useful for Preparation of Epoxy-Exfoliated Layered Silicic Acid Nanocomposites

intercalates	d ₀₀₁ (Å)	physical state	Jeffamine (g)/g of H-ilerite	solvent (v/v) rxn time rxn temp EtOH/ H_2O (h) (oC)	rxn time (h)	rxn temp (°C)	washing
D2000-H-ilerite	0.89	sticky pwd	1.57	30/20	9	09	no
	52.9	pwd	1.35	20/50	12	09	ou
D4000-H-ilerite	52.0	sticky pwd	1.60	30/50	12	99	no
T3000-H-ilerite	65.4	pwd	1.20	25/50	12	99	no
T5000-H-ilerite	71.1	sticky pwd	1.60	30/50	12	9	no

5.2.3 Preparation of Epoxy-Layered Silicic Acid Composites Using Jeffamine-H-Layered Silicic Acid Intercalates

Stoichiometric amounts of epoxide resin and Jeffamine curing agent in the form of the free amine and the Jeffamine-H-layered silicate intercalate were mixed at 25 °C. This mixture was prepared by adding the desired amount of Jeffamine-H-layered silicic acid intercalates to an epoxide-Jeffamine curing agent mixture at 25 °C and stirring for 30 min. The Jeffamine in intercalated form was counted as contributing to the stoichiometry for epoxide cross-linking. This mixture was outgassed in a vacuum oven and poured into a stainless steel mold for curing at 75 °C for 3 h and, subsequently, at 125 °C for an additional 3 h.

5.2.4 Characterization Methods

X-ray Powder Diffraction (XRD). XRD patterns were recorded on a Rigaku rotaflex 200B diffractometer equipped with a rotating anode, Cu K_{α} x-ray radiation (λ = 1.541838 Å) and a curved crystal graphite monochromator. The x-ray was operated at 45 KV and 100 mA. Diffraction patterns were collected with 0.01° 2θ interval between 1 and 10° 2θ using a scanning rate of 2° 2θ per minute, and DS and SS slit widths of 1/6. For patterns obtained at starting angle of 0.5° 2θ , a SS width of 0.05 was used instead of 1/6. XRD patterns at high angles were collected using DS and SS slit widths of 1. The samples of gel-like Jeffamine intercalated H-layered silicic acids or uncured epoxylayered silicic acid composites were prepared by applying thin films on glass slides. Cured composite specimens were prepared by mounting a flat rectangular sample into an aluminum holder.

Thermal Analysis. Thermogravimetric analyses (TGA) were performed using a Cahn TG System 121 thermogravimetric analyzer. Samples were heated to 750 °C at a heating rate of 5 °C/min under N₂ atmosphere.

Surface Area Measurement. N₂ adsorption-desorption isotherms were determined on a ASAP 2010 Sorptometer at liquid N₂ temperature using a static sorption mode. Samples were outgassed at 150 °C and 10⁻⁵ Torr for 12 h. Surface areas were determined using BET plots.

Mechanical Measurement. Tensile testing was performed at ambient temperature according to ASTM procedure D3039 using a SFM-20 United Testing System.

Chemical and Solvent Resistance. Resistance to solvent swelling was obtained according to ASTM procedure D543. The specimens were immersed in the desired reagent and removed periodically to measured the weight gain until equilibrium was reached.

5.3 Results and Discussion

5.3.1 Synthesis of Jeffamine-H-Layered Silicic Acid Intercalates

Alkali-metal forms of layered silicic acids can be easily converted to their proton analogs using the titration technique. Figure 5.1 shows the x-ray diffraction patterns for each H+ form of layered silicic acid. The proton forms normally contain less structural water molecules than their alkali-metal forms. The presence of the interlayer water molecules is very important to prevent the silicate layers from cross-linking. The proton forms can undergo very similar intercalation chemistry as their alkali forms as long as they are not converted into anhydrous forms by high temperature treatment.²³

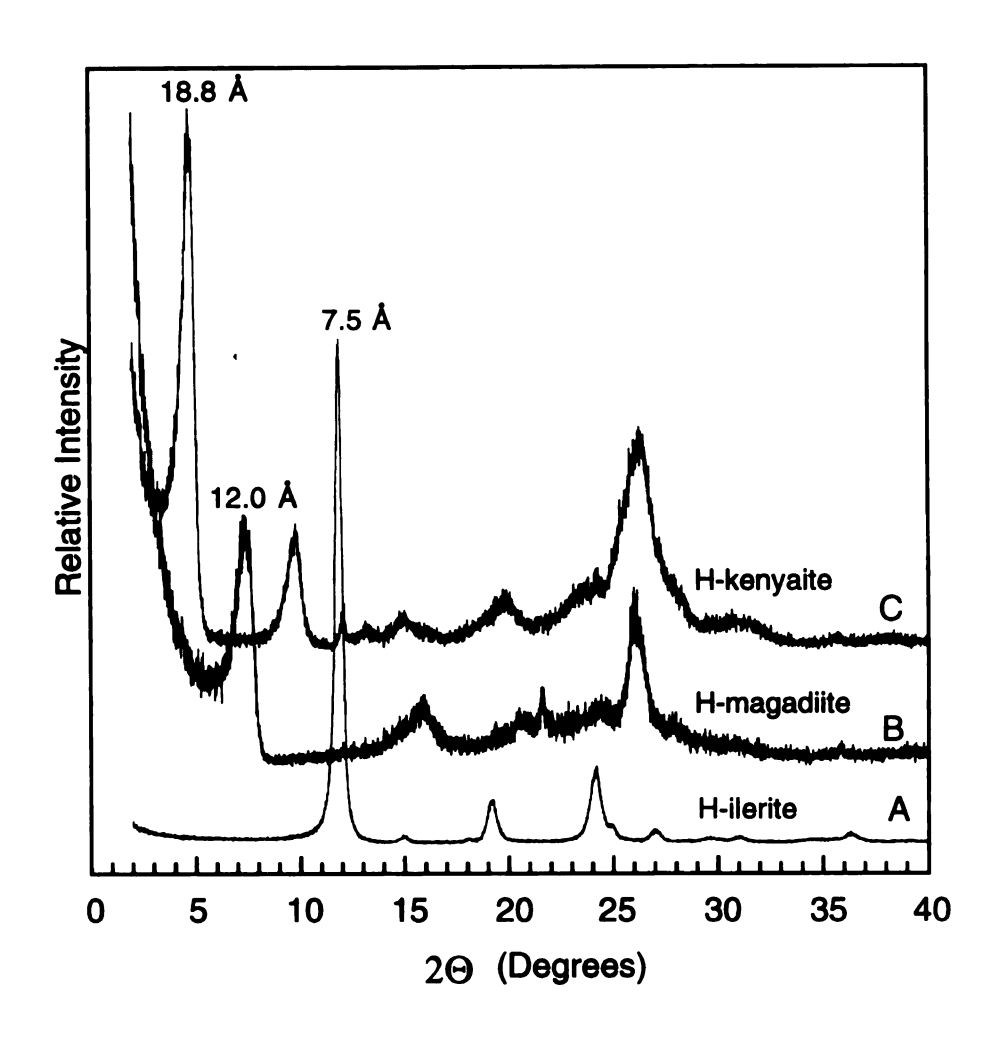


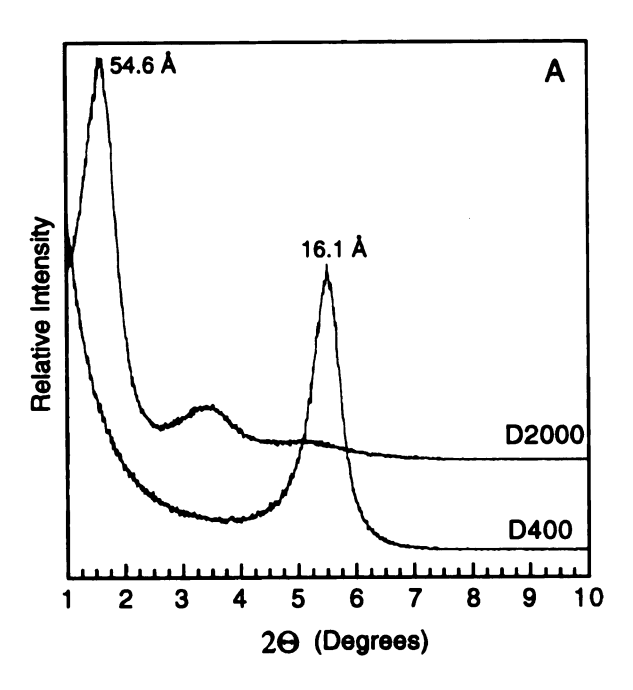
Figure 5.1 XRD patterns of air-dried proton exchanged forms of layered silicic acids:

(A) H⁺-ilerite; (B) H⁺-magadiite; (C) H⁺-kenyaite.

Our efforts to synthesize Jeffamine intercalated layered silicic acids were very successful. Because the higher molecular weight Jeffamines are immiscible with aqueous solution, a co-solvent of water and ethanol was generally necessary to obtain these particular types of intercalates. The amount of ethanol used was dependent on the solubility of Jeffamine curing agent; however, a high volume percentage of ethanol was avoided. The synthesis conditions given in Table 5.2-5.4 provide only typical reaction conditions for the synthesis of each intercalate. However, the range for ethanol can be varied form 0% for D400 and T403 to 50% (vol.) for a higher molecular weight Jeffamine. Also, the reaction can be completed in 4 h to 24 h at an elevated temperature over a broad range form 35 °C to 75 °C.

Interestingly, two kinds of intercalates can be formed between high molecular weight Jeffamines and layered silicic acids. As-synthesized intercalates normally exhibited high basal spacings and a gel-like physical state. The post synthesis washing of the products with a mixture of ethanol and water removes part of the intercalated Jeffamine from gallery and results in a powered form with decreased basal spacings.

Figure 5.2-5.4 show XRD patterns for some of the intercalates formed between layered silicic acids and Jeffamines. Basically, the basal spacings are dependent on the molecular weight and functionality (number of amino end groups) of the Jeffamine, or, more precisely, on the equivalent weight. For instance, Jeffamine D2000 and T3000 give very similar gallery height when they are intercalated into the galleries of layered silicic acids. If we subtract the layer thickness for the different member of the layered silicic acids from the observed d-spacings (especially in the cases of magadiite and kenyaite), the obtained intercalates normally have a very similar gallery height. Apparently, each negative charge in the layer occupies an equal surface area, independent of the difference in layer thickness.



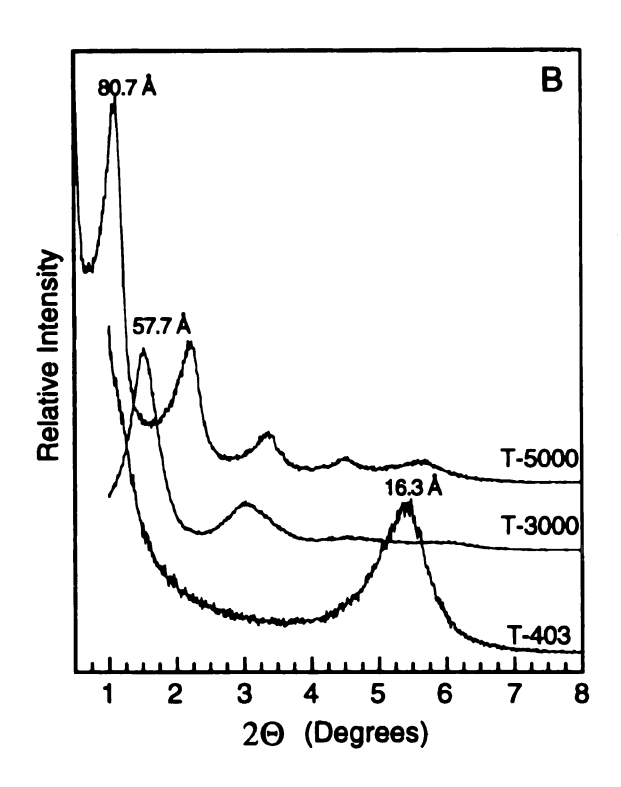
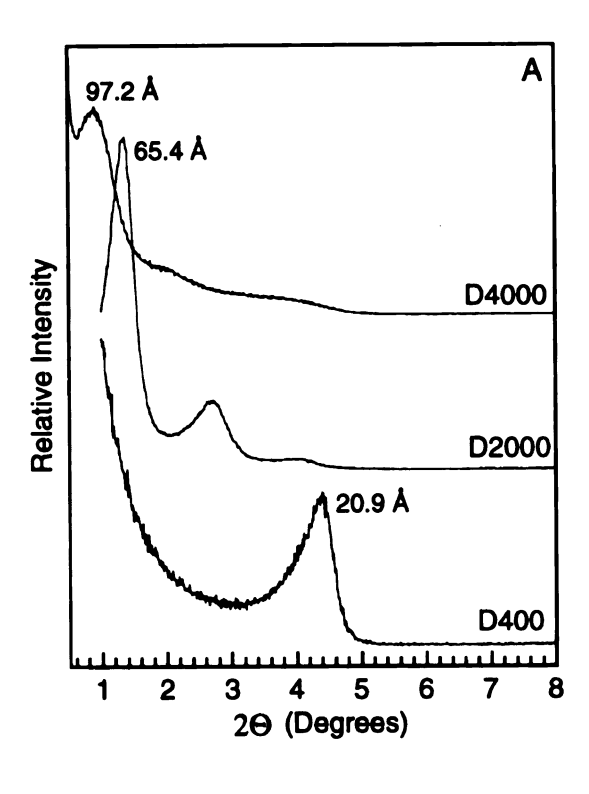


Figure 5.2 XRD patterns for the as-synthesized (unwashed) intercalates formed from H+-magadite and poly(oxypropyleneamines): (A) Jeffamine D-series; and (B) Jeffamine T-series.



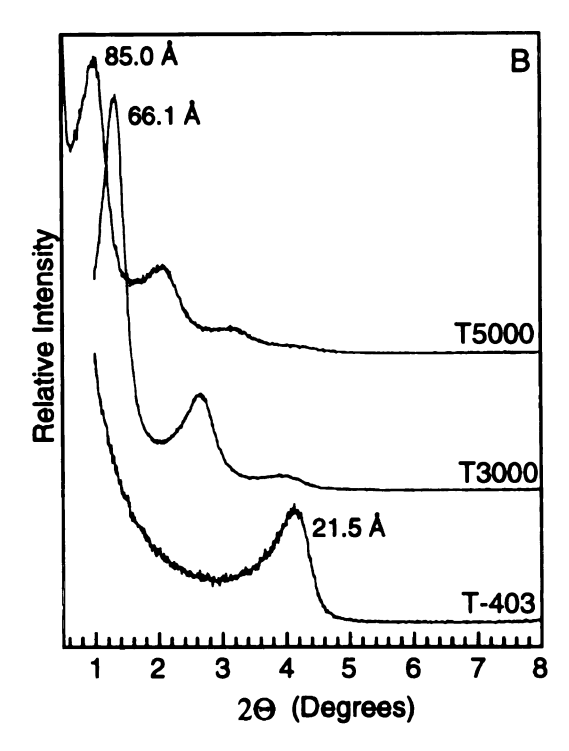


Figure 5.3 XRD patterns for the as-synthesized intercalates (unwashed) formed from H+-kenyaite and poly(oxypropyleneamines): (A) Jeffamine D-series; and (B) Jeffamine T-series.

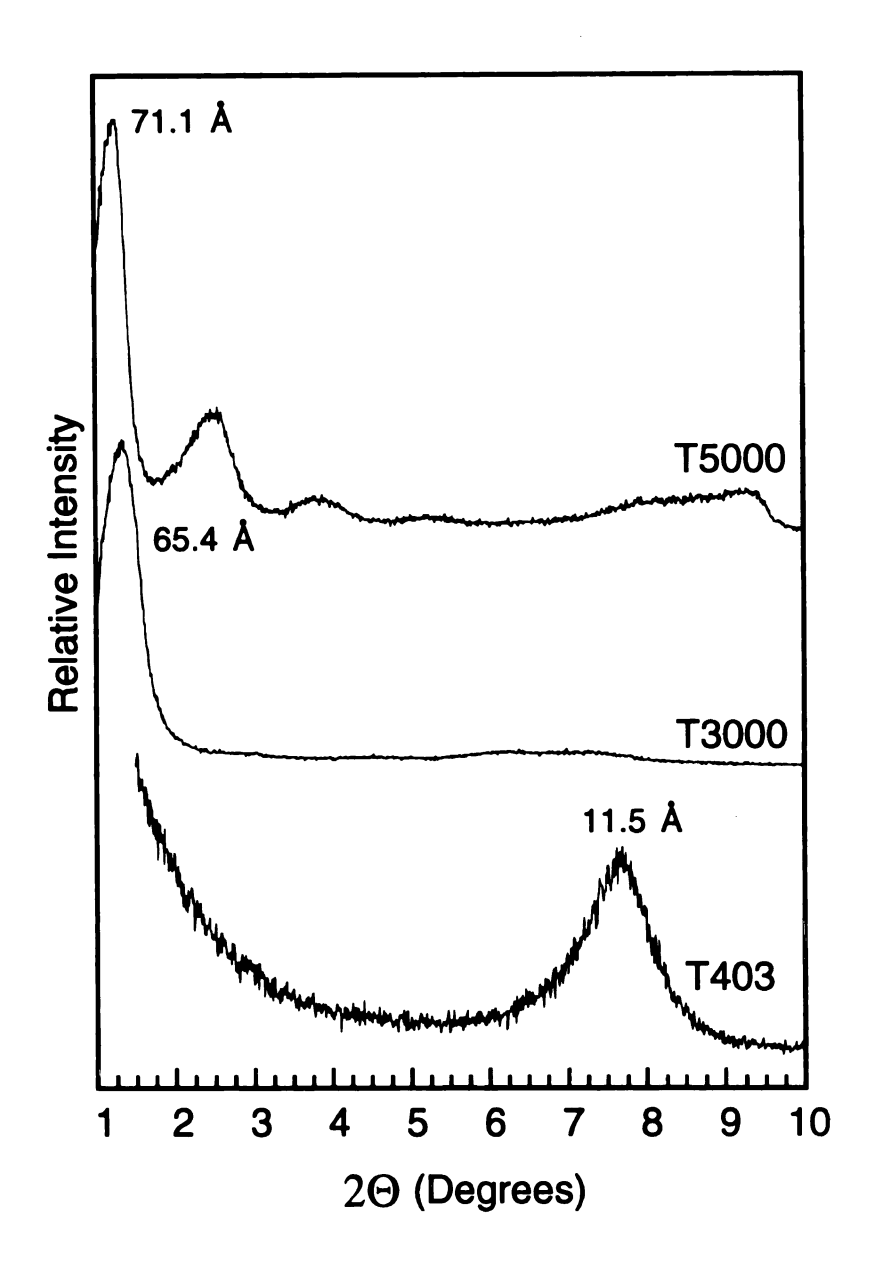


Figure 5.4 XRD patterns for the as-synthesized (unwashed) intercalates formed from H⁺-ilerite and poly(oxypropyleneamines) Jeffamine T-series.

The formation of intercalates using water soluble Jeffamine D230, D400 and T403 exhibited only slightly expanded (~ 4 Å increase) gallery heights. This suggests that only a monolayer of Jeffamine has been intercalated with the amine in a strong electrostatic interaction with the layers.

We have mentioned in the beginning that washing the as-synthesized intercalates can result in a decrease in basal spacing and a powdered physical state. However, the washing process has to be controlled, otherwise, a collapsed gallery can be formed as shown by the XRD results in Figure 5.5. The as-synthesized D4000-H-kenyaite intercalate has a basal spacings of 97.2 Å, whereas an intercalate with a 69.0 Å basal spacing is formed when it is washed by the mixture of ethanol and water (cf. Table 5.3). An intercalate with a 20.9 Å basal spacing is likely to be formed when further washing is applied. This latter intercalate has a lateral monolayer gallery structure which can not be intercalated by any other polymer precursors.

TGA results for a series of intercalate of D4000-H-kenyaite intercalates with different basal spacings are shown in Figure 5.6. The weight loss showed even for the intercalate with the highest basal spacing corresponds to a molar ratio of amino groups to intragallery protons of only about 0.45. It is likely that all of the amino groups have been protonated and that further intercalation by neutral Jeffamine might be possible at higher concentrations, except for the inaccessible intercalate with a 20.9 Å basal spacing.

The basal spacings for each intercalate formed between the layered silicic acids and the Jeffamines are summarized in Table 5.5. An ordered peak was not observed for the intercalate formed between H-magadiite and Jeffamine D4000, suggesting that this product may contain exfoliated silicic acid nanolayers.

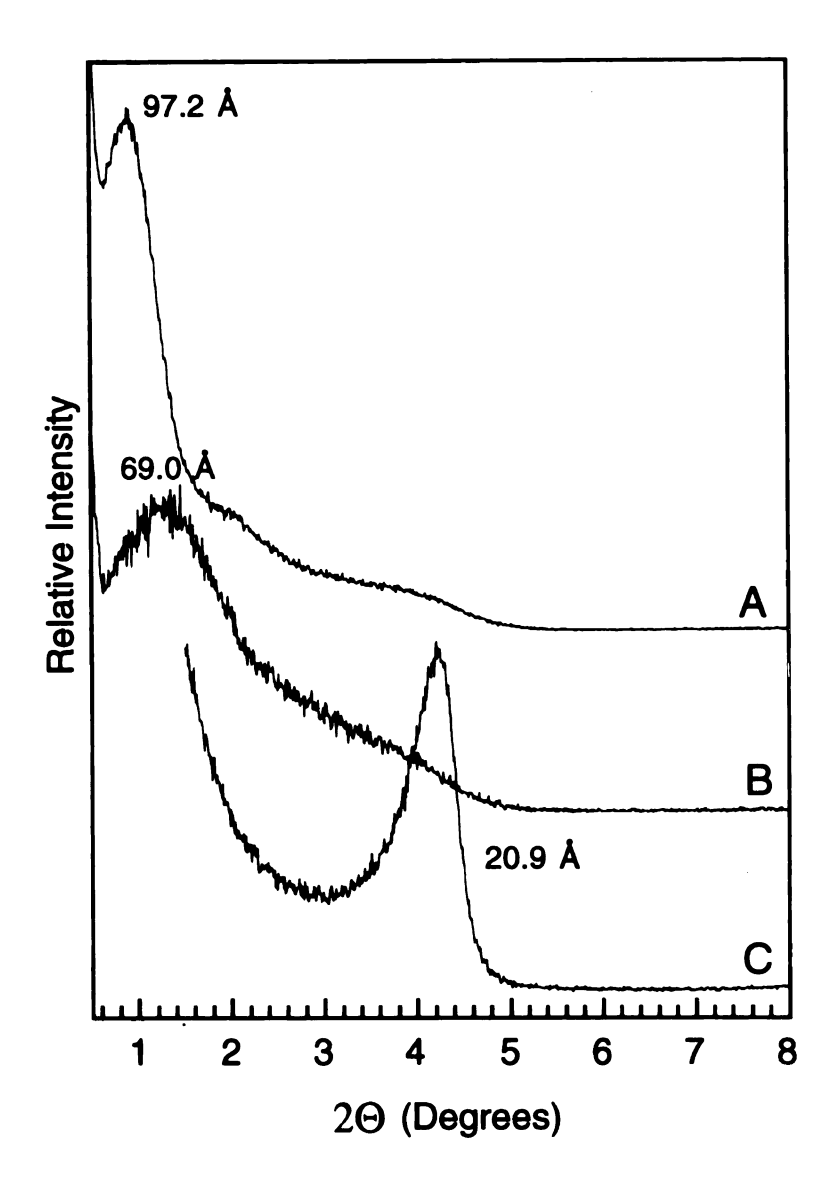


Figure 5.5 XRD patterns of the intercalates formed from H⁺-kenyaite and the poly(oxypropyleneamine) Jeffamine D4000: (A) as-synthesized (unwashed); (B) washed one time with ethanol; and (C) washed multiple times with ethanol.

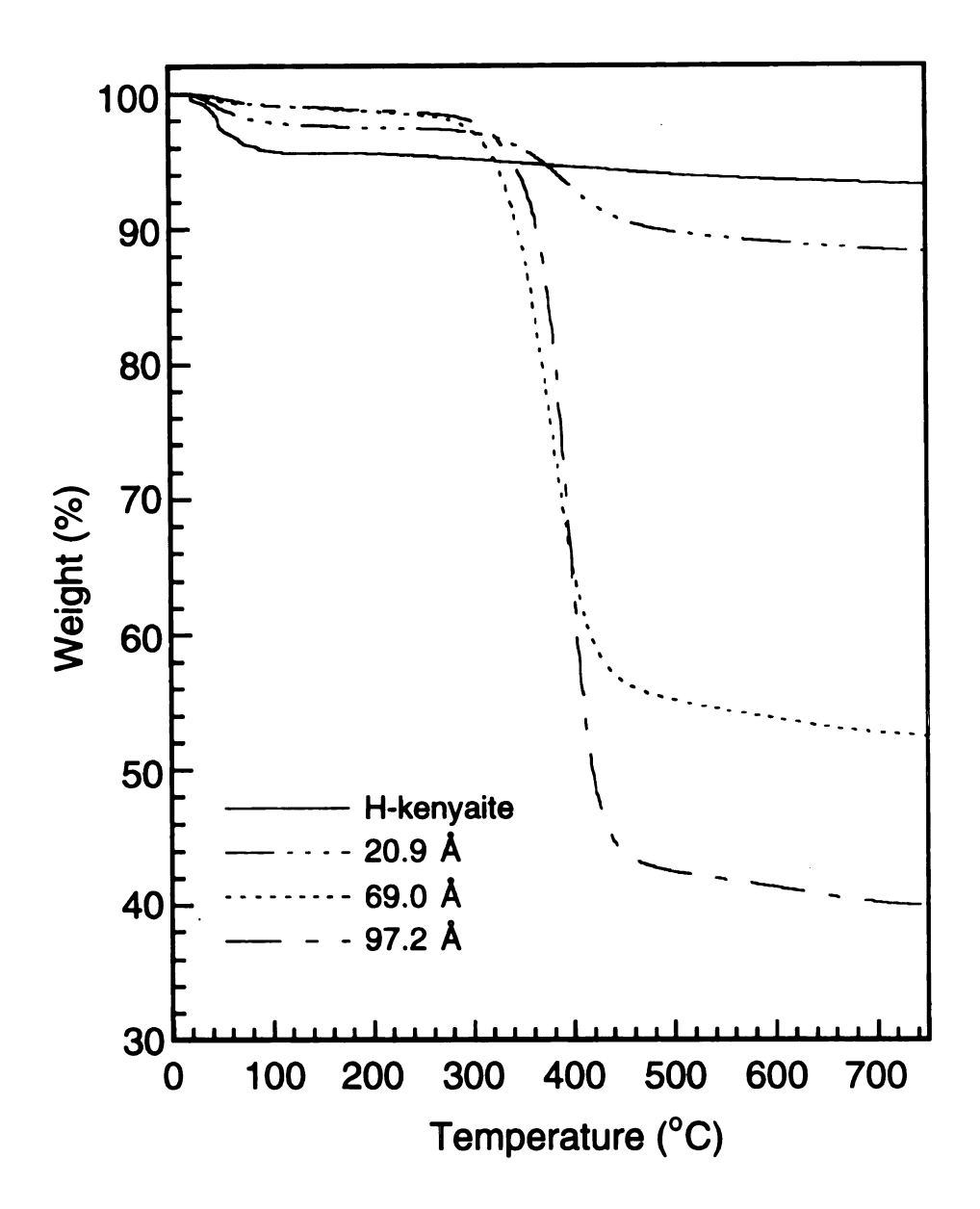


Figure 5.6 TGA curves for H-kenyaite and D4000-H-kenyaite intercalates with different basal spacings (cf. Figure 5.5).

Basal Spacings (Å) of As-Synthesized Intercalates Formed From Layered Silicic Acids and JEFFAMINE D-Series and T-Series Table 5.5

initial silicic	layer		D-Series			T-Series	
acid	thickness (Å) D400 D2000	D400	D2000	D4000	T403	T403 T3000	T5000
H-ilerite	7.0	11.5	11.5 68.0 (52.9) ^a 52.0	52.0	11.5	11.5 65.4	71.1
H-magadiite	11.2	16.1	16.1 54.6 (44.0)	+	16.3	16.3 57.7 (39.4) 80.7 (53.2)	80.7 (53.2)
H-kenyaite	17.7	21.7	65.4 (47.8)	21.7 65.4 (47.8) 97.2 (69.0)	21.3	21.3 66.1 (43.3) 85.0 (59.7)	85.0 (59.7)

^aValues in parenthesis are for the powdered forms of the intercalates obtained after one washing (see Table 5.2-5.4).

Although, the approach developed for the synthesis of Jeffamine-H-layered silicic acid intercalates was successful, most of products required a washing process in order to obtain intercalates in a powdered physical state. The post washing process can cause two problems. First of all, the washing process has to be controlled to avoid the formation of a collapsed lateral monolayer gallery structure or the formation of mixed phases. Secondly, Jeffamine is deintercalated and a significant amount of ethanol have to be used, although both chemicals can be recycled. However, we developed an alternative method that can avoid both problems. In this approach, the precise amount of Jeffamine and the minimum amount of ethanol need to form a powdered intercalate are used. The powdered intercalates are formed directly after the solvent is removed after air drying. Typical experimental conditions are summarized in Table 5.6 for the synthesis of different intercalates wherein Jeffamine D2000 is the intercalate. The intercalation reaction were completed in less than 5 hours. Some of the intercalates may contain less than 3 wt % of water, which can be removed by drying in an oven at 100 °C for overnight. This approach is very general for Jeffamine and other organic species that can react with the proton forms of layered silicic acids. For instances, the preparation of C18-magadiite-PF and C18-kenyaite-PF is easily obtained by this universal approach.

Synthesis Conditions for Formation of Powdered Forms of As-Synthesized JEFFAMINE-H-Layered Silicic Acid Intercalates Table 5.6

intercalates	ф (ў	physical state	Jeffamine (g)/g of H-layered silicic acid	solvent (v/v) r EtOH/H ₂ O	rxn time (h)	rxn temp (°C)
D2000-H-ilerite	52.9	pwd	1.35	20/50	12	09
D2000-H-magadiite	51.3	pwd	0.98	10/20	4.5	09
D2000-H-kenyaite	49.9	pmd	0.51	10/50	4.5	09

5.3.2 Exfoliation of Layered Silicic Acid Nanolayers in an Epoxy Polymer Matrix Using Jeffamine-H-Layered Silicic Acid Intercalates

Except for those intercalates with a lateral monolayer or lateral bilayer structures, the Jeffamine-layered silicic acid intercalates are reactive toward intercalation by the mixture of Jeffamine and epoxide resin. The co-intercalation of D2000-H-magadiite intercalate with a 44.0 Å basal spacing, D2000-H-kenyaite intercalate with a 47.8 Å basal spacing, and D2000-H-ilerite intercalate with a 53.0 Å basal spacing by a stoichiometric mixture of epoxide and D2000 curing agent were investigated by XRD as a function of time (see Figure 5.7, Figure 5.8 and Figure 5.9, respectively). The advantages using powdered forms of these intercalates are that the diffusion process is much quicker and more silicate can be used to form a composite with a high silicate loading. As shown in these figures, the co-interrelation of epoxide and D2000 is very readily achieved. An intercalate with a higher basal spacing is quickly formed even at room temperature with about a 20 Å increase of gallery height for magadiite and kenyaite, and a 12 Å increase for ilerite. We also observed that the diffusion process is much faster for D2000-Hlayered silicic acid intercalates than the alkylammonium exchange analogs, suggesting a more open gallery structure. The initial intercalates were replaced quickly by expanded phases that exhibit only second and third order peaks. In all cases, a rapid intragallery polymerization was observed with the formation of exfoliation (amorphous) phases. The strong intragallery acidity affords a very favorable intragallery environment for delamination of silicate nanolayers.

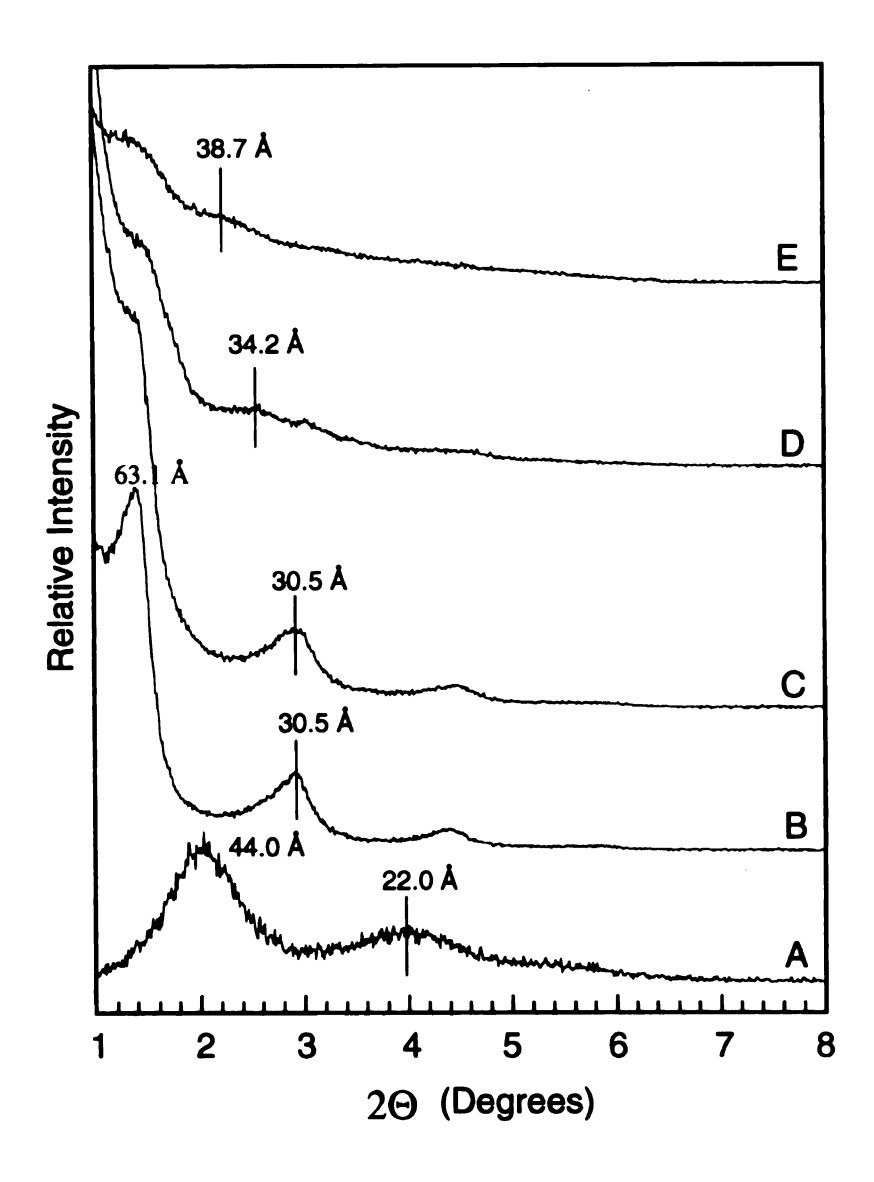


Figure 5.7 XRD patterns of (A) the initial D2000-H-magadiite intercalate and the nanocomposites formed at 20 wt % D2000-H-magadiite intercalate loading by reaction of stoichiometric mixtures of epoxide and the poly(oxypropyleneamine) under the following reaction conditions: (B) 25 °C, 60 min; (C) 75 °C, 60 min; (D) 75 °C, 120 min; (E) 75 °C, 150 min.

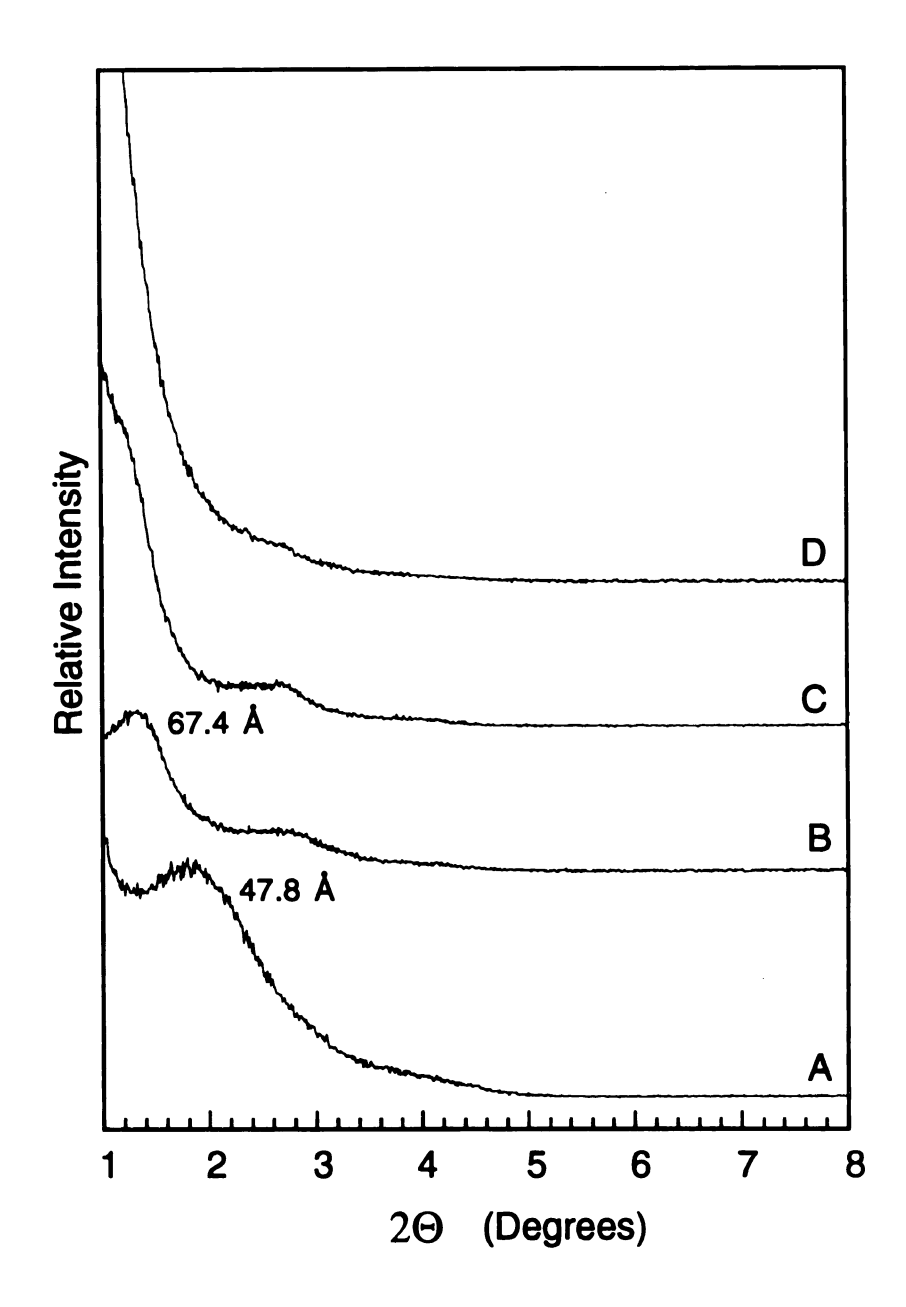


Figure 5.8 XRD patterns of (A) the initial D2000-H-kenyaite intercalate and the nanocomposites formed at 20 wt % D2000-H-kenyaite intercalate loading by reaction of stoichiometric mixtures of epoxide and the poly(oxypropyleneamine) under the following reaction conditions: (B) 25 °C, 2 min; (C) 25 °C, 10 min; (D) 75 °C, 30 min.

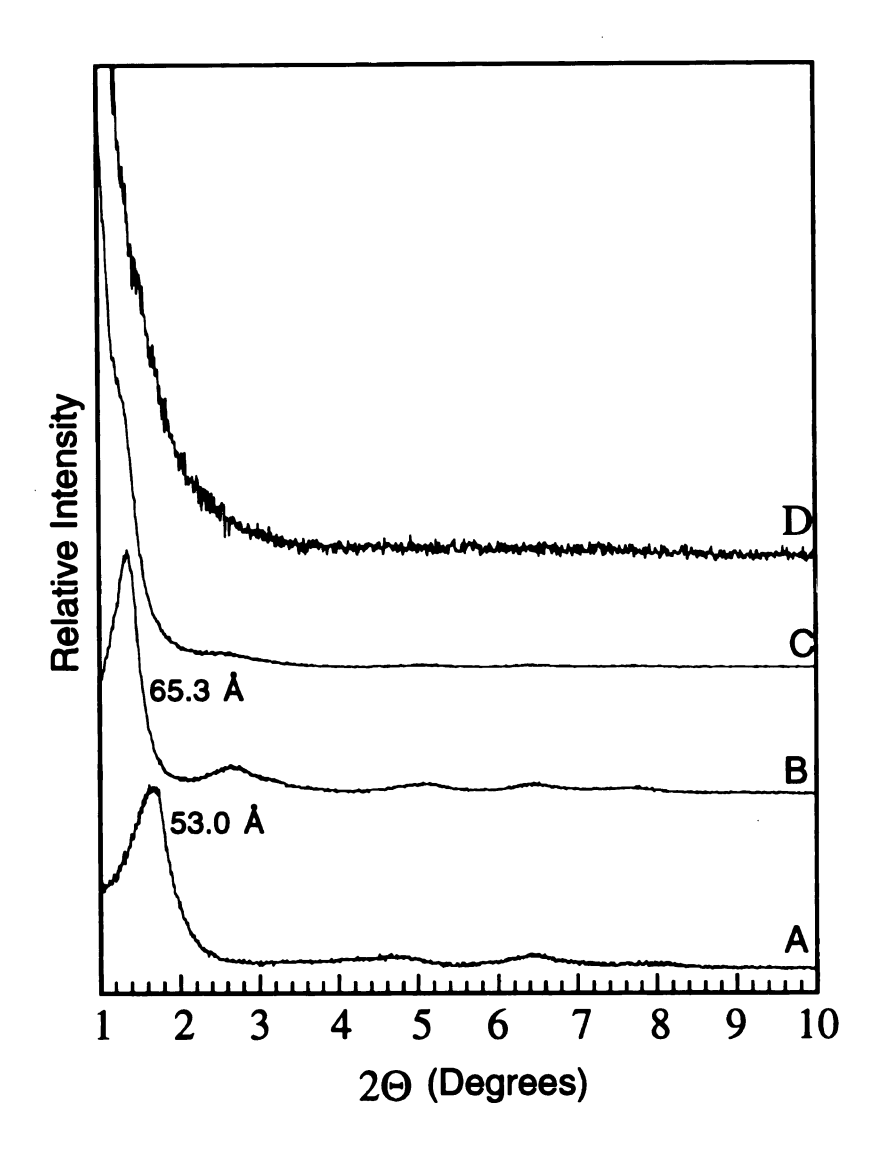
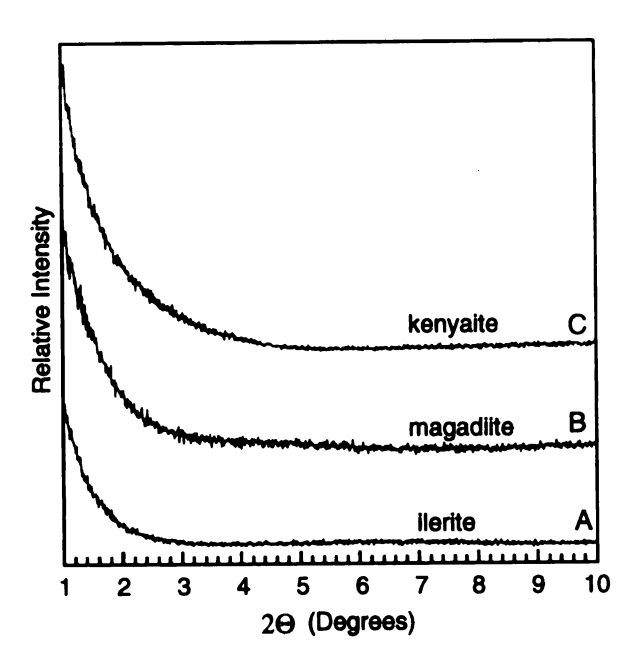


Figure 5.9 XRD patterns of (A) the initial D2000-H-ilerite intercalate and the nanocomposites formed at 20 wt % D2000-H-ilerite intercalate loading by reaction of stoichiometric mixtures of epoxide and the poly(oxypropyleneamine) under the following reaction conditions: (B) 25 °C, 5 min; (C) 75 °C, 5 min; (D) 75 °C, 135 min.

The XRD patterns for the fully cured composites prepared from D2000-H-layered silicic acid intercalates are shown in Figure 5.10. All these patterns are characterized by the absence of XRD peaks at low angle which suggests that the exfoliated epoxy-layered silicic acid nanocomposites have been obtained. The x-ray results also show that the 2-dimensional structures of layered silicic acids are retained for all of these exfoliated nanocomposites, as indicated by the strong in-plane peaks. We point out that the other Jeffamine-H-layered silicic acid intercalates can also undergo very similar intercalation and exfoliation chemistry.

A series of epoxy nanocomposites with different D2000-H-magadiite intercalate loadings were also prepared. The XRD patterns for the nanocomposites are shown in Figure 5.11. Interestingly, as the magadiite loading is increased, broad x-ray reflections appear, which signifies that the average layer separation decreases with increasing loading. The high basal spacing peaks at low 2θ angles are observed when the loading of the intercalate reaches 40 wt %. These results show that the average layer separation is related to the loading of silicate nanolayers. Table 5.7 lists the results of average nanolayer separation expected for the theoretical calculation and the values observed by XRD. The calculated and observed values agree relatively well in the range of high loading for D2000-H-magadiite intercalates. It is noteworthy that peaks at 121 Å and 95 A are of relatively low intensity. So, the magadiite layers may be dispersed in the polymer a mixed disordered and ordered exfoliated fashion. It is not surprising that an ordered exfoliated phase is present, because the synthetic layered silicate normally has a very homogenous distribution of charges. The uniform distribution in layer charge favors uniform polymerization rates and the formation of regularly ordered gallery heights between nanolayers.



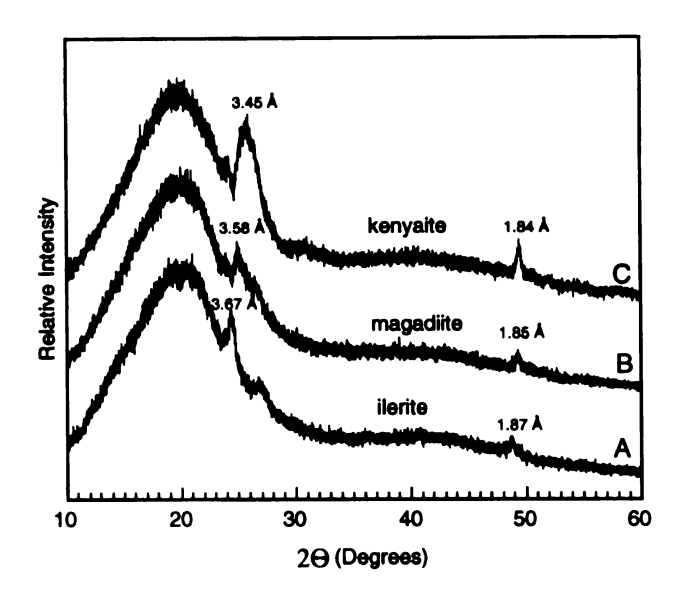


Figure 5.10 XRD patterns for the epoxy-layered silicic acid nanocomposites formed from the following intercalates: (A) D2000-H-ilerite; (B) D2000-H-magadiite; (C) D2000-H-kenyaite. The D2000-layered silicic acid intercalate loadings are 20 wt %, 10 wt % and 15 wt % for ilerite, magadiite and kenyaite, respectively. The intercalated curing agent was counted as contributing to the stoichiometry for epoxide cross-linking.

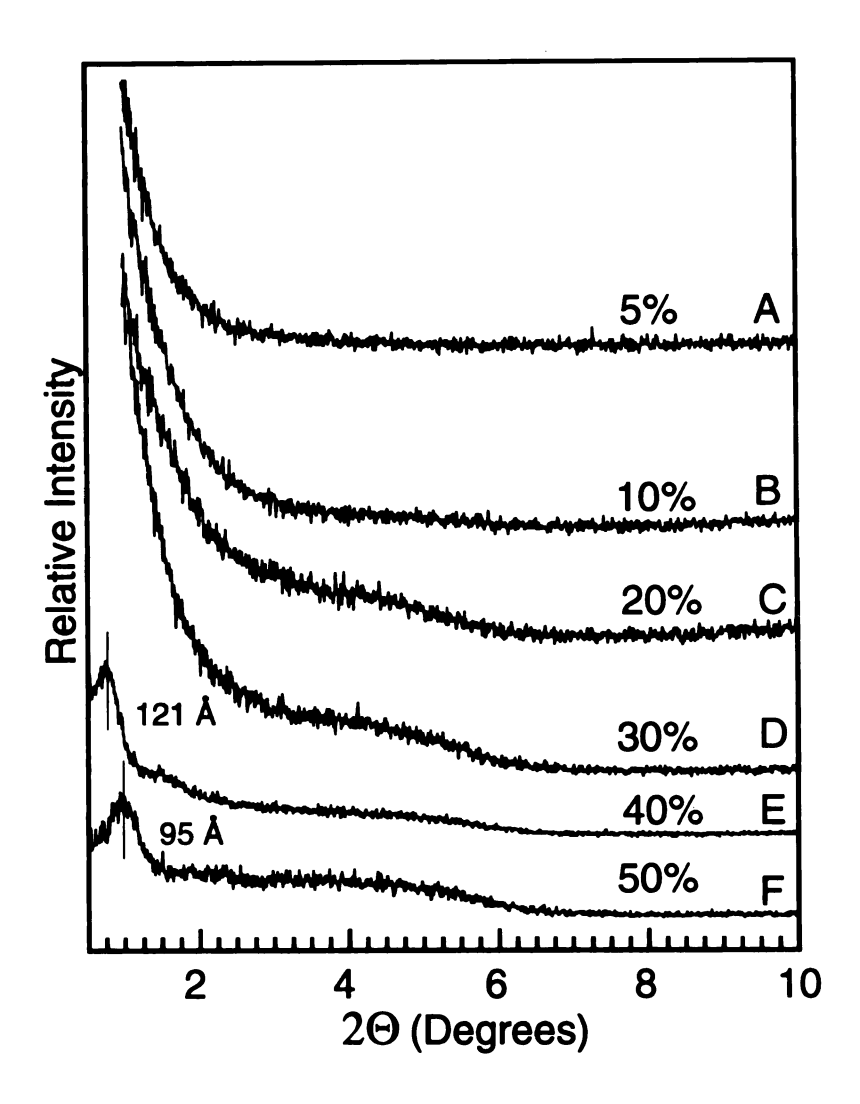


Figure 5.11 XRD patterns of cured epoxy-magadite nanocomposites (curing conditions: at 75 °C for 3 h, and followed by 3 h at 125 °C) prepared from D2000-H-magadite intercalates. The D2000-H-magadite intercalate loadings were as follows: (A) 5 wt %; (B) 10 wt %; (C) 20 wt %; (D) 30 wt %; (E) 40 wt %; and (F) 50 wt %.

Table 5.7 Average Silicate Layer Separation (Å) for Regularly Exfoliated Epoxy-Magadiite Nanocomposites Prepared form D2000-H-magadiite Intercalates

wt % D2000-H- magadiite intercalate	5	10	20	30	40	50
calculated	1360	670	310	205	149	113
observed			_		121	95

It was of interest to investigate the nature of the silica formed upon calcination of the nanocomposites. The morphology of the nanolayers in the nanocomposite should be reflected in the surface area and XRD patterns of the silica recovered upon calcination accordingly, the exfoliated nanocomposite prepared from D2000-H-magadiite intercalate with a 44.0 Å basal spacing was calcined at 650 °C for 4 h to form silica. The D2000-H-magadiite intercalate with a 54.6 Å basal spacing was also calcined at the same conditions. The XRD results are shown in Figure 5.12. Strong in-plane magadiite peaks are observed in both cases. However, the extent of layer restacking upon calcination was quite different in these two cases. The silica formed from the D2000-H-magadiite intercalate shows an intense and narrow d_{001} peak indicative of extensive layer restacking, whereas the d_{001} peak for the silica from the exfoliated nanocomposite is very weak and broad, indicating much less restacking order.

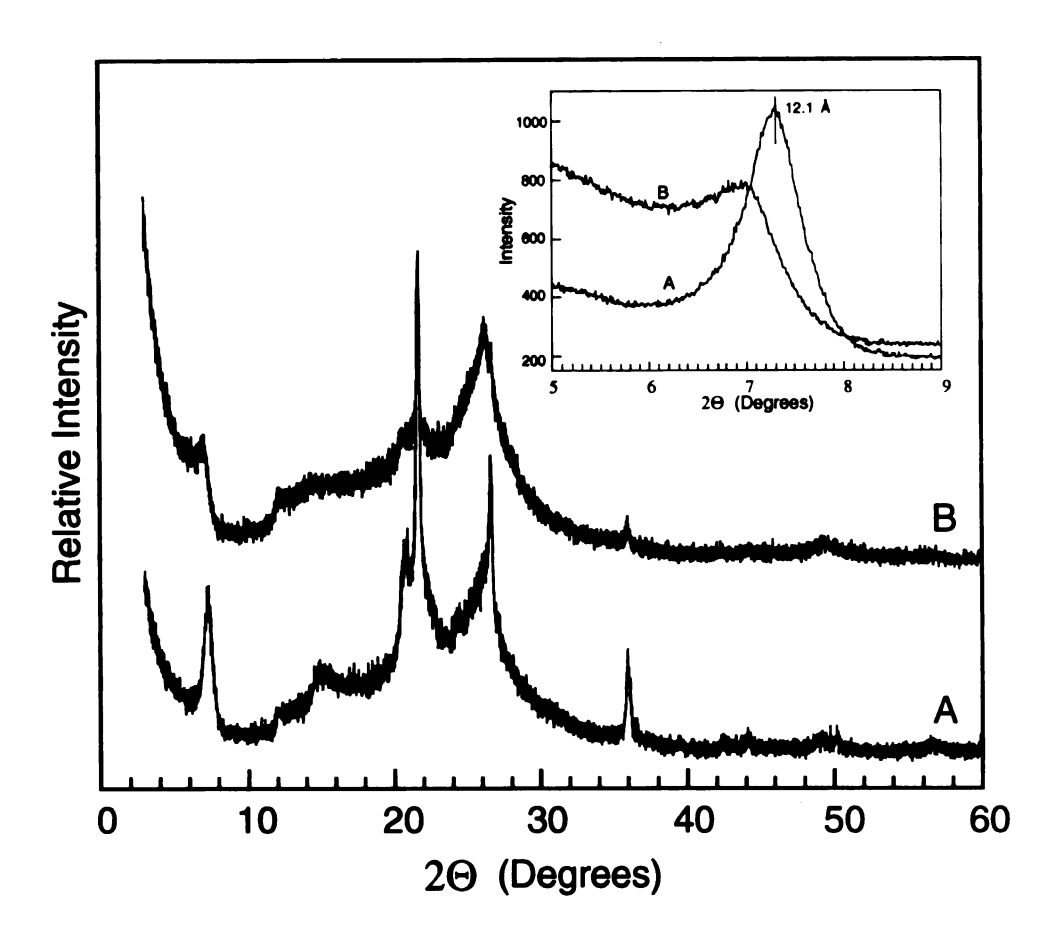


Figure 5.12 XRD patterns for the silica formed from upon calcination of (A) D2000-H-magadiite intercalate with a 54.6 Å basal spacing and containing 50 wt % H-magadiite; and (B) an exfoliated epoxy-magadiite nanocomposite prepared form the D2000-H-magadiite intercalate with a 44.0 Å basal spacing and containing 5 wt % H-magadiite. The expanded insert for the d_{001} peaks was obtained using a step scan mode. The calcinations were carried out at 650 °C for 4 h in air using a heating rate of 2 °C/min.

The N₂ adsorption-desorption measurements for the silica obtained from the exfoliated nanocomposite and D200-H-magadite intercalate, are shown in Figure 5.13. The N₂ adsorption results verify the above XRD results. A much larger texture porosity and surface area are observed for the silica recovered form the exfoliated nanocomposite than from D2000-H-magadiite intercalate. Most of the exfoliated silicate nanolayers in the nanocomposite retain their exfoliated morphology to form the familiar card-house structure upon calcination. The card house structure is schematically illustrated in Figure 5.14 along with the restacked layer aggregation possibilities for the silica obtained by calcination of the D2000-H-magadite intercalate. The card-house structure will result in a significant increase in texture porosity and surface area. In addition a weak and very broad 001 XRD reflection is expected, as observed. Interestingly, the surface area for the exfoliated nanocomposite prepared from D2000-H-magadiite intercalate is about 50% larger than the value obtained by calcination of the exfoliated nanocomposite formed from C18-magadiite-PF, although they have a similar magadiite silicate (SiO₂) loading (cf. Figure 3.17). This result suggests that the extent of magadiite exfoliation is higher for the nanocomposite formed from D2000-H-magadiite than from C18-magadiite-PF. So, it would not be surprising to expect a superior performance properties for the nanocomposite prepared from D2000-H-magadiite intercalate than C18-magadiite-PF.

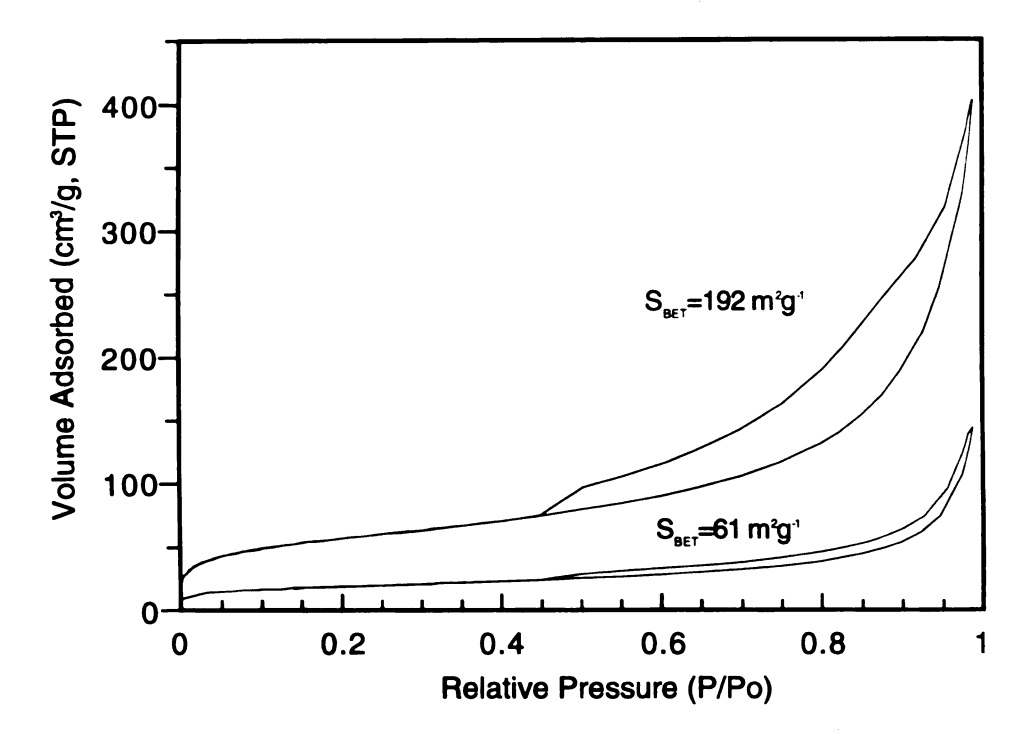
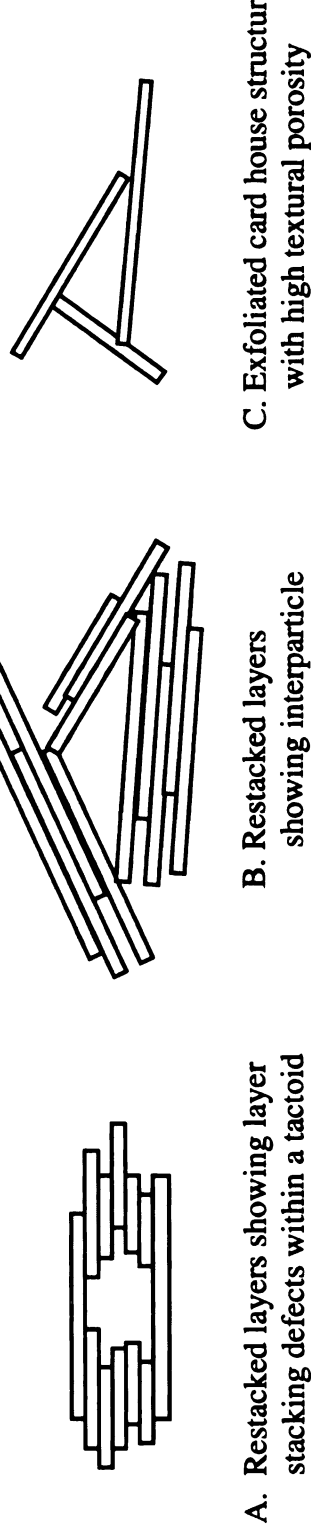


Figure 5.13 N_2 adsorption-desorption isotherms for the silicas obtained by calcination of an epoxy-exfoliated magadiite nanocomposite prepared from D2000-H-magadiite intercalate with a 44.0 Å basal spacing and containing 5 wt % H-magadiite (top curve); and the D2000-H-magadiite intercalate with a 54.6 Å basal spacing containing 50 wt % H-magadiite (bottom curve). The calcinations were carried out at 650 °C for 4 h in air using a heating rate of 2 °C/min.



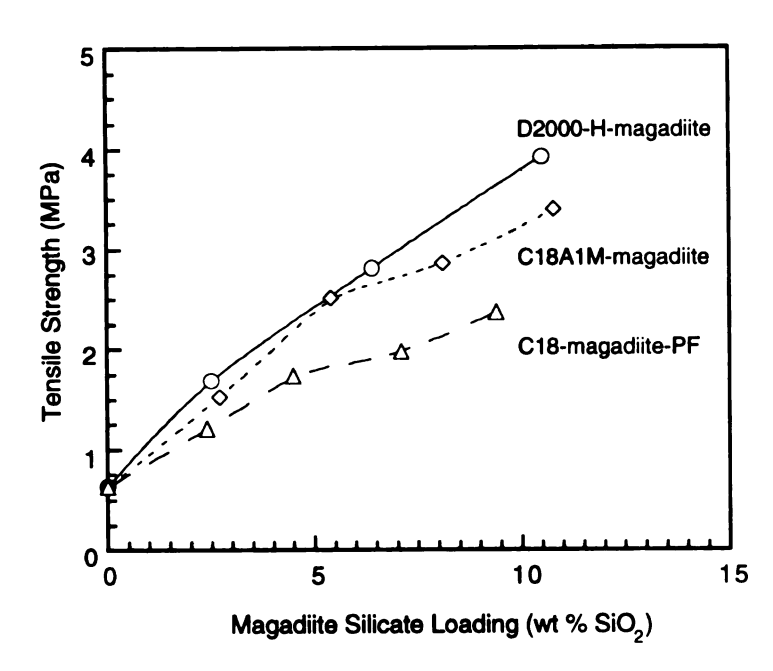
C. Exfoliated card house structure with high textural porosity showing interparticle

house structure is predominant for the magadiite recovered by calcination of an exfoliated epoxy-magadiite Possible types of morphologies for silicate nanolayer aggregates formed upon calcination. The card nanocomposite. Restacked layers are more predominant in the magadiite obtained by calcination of a well ordered D2000-H-magadiite intercalate. **Figure 5.14**

5.3.3 Performance Properties of Exfoliated Epoxy-Layered Silicic Acid Nanocomposites Prepared by the Proton Exchanged Pathway

A comparison of the tensile properties for epoxy-exfoliated magadiite nanocomposites prepared from D2000-H-magadiite intercalates and alkylammonium exchanged magadiite intercalates is shown in Figure 5.15. For both the tensile strength and the tensile modulus, the nanocomposite prepared from D2000-H-magadiite intercalates out-performs the nanocomposites prepared from C18A1M-magadiite and C18-magadiite-PF (cf. Chapter 2 & 3). The increase with loading is nearly linear for the nanocomposites prepared by the new proton-exchange layered silicic acid pathway. On the other hand, the nanocomposites prepared by alkylammonium exchange pathway show a tendency to yield, especially for the tensile modulus.

At least two factors play important roles in the improvement of the mechanical performance of the nanocomposites obtained by proton exchange pathway. The first factor is that the formation of dangling chains has been eliminated by the pathway using Jeffamine intercalated H-layered silicic acids as the starting materials. As was shown in Chapter 2 & 3, the formation of the dangling chains in the polymer matrix compromises the reinforcement advantages of the exfoliated silicate nanolayers, particularly, at high magadiite loading when alkylammonium exchanged magadiite intercalates are used to achieve exfoliation. Secondly, as we have demonstrated in section 5.3.2, the extent of silicate nanolayer exfoliation is superior for the proton-exchange pathway. The degree of exfoliation always play a dominate role in deciding the performance properties of polymer-layered silicate clay nanocomposites.



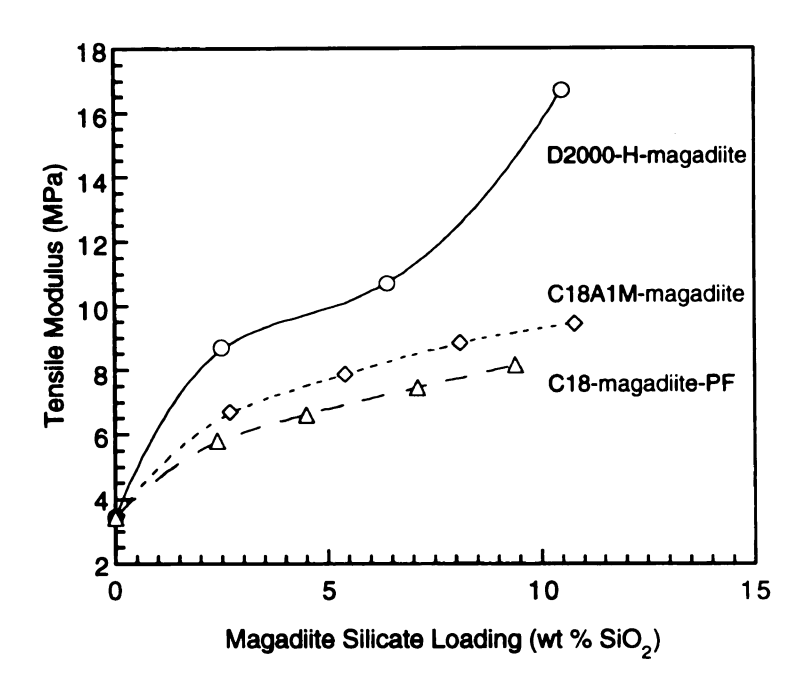
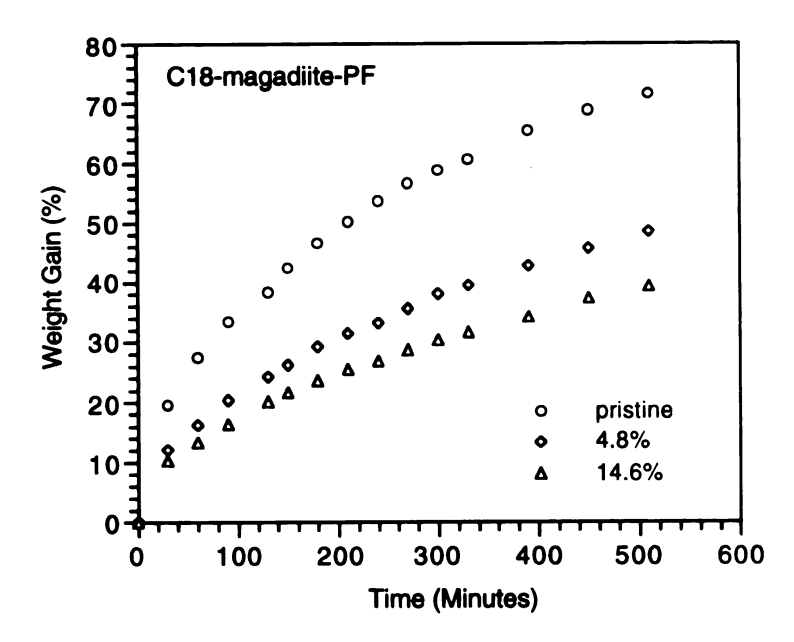


Figure 5.15 Comparison of tensile properties for exfoliated nanocomposites prepared from D2000-H-magadiite intercalates and organo magadiite intercalates with a paraffin structure (C18-magadiite-PF and C18A1M-magadiite).

The exfoliated nanocomposites prepared by this new pathway are superior not only in their tensile properties. We also compared the solvent resistance for the exfoliated nanocomposites prepared from different pathways. The solvent uptake curves are plotted in Figure 5.16 and Figure 5.17 for the nanocomposites prepared from D2000-H-magadiite intercalate and C18-magadiite-PF. The plots of equilibrium uptake value vs. magadiite silicate loading are shown in Figure 5.18. The uptake of methanol and toluene was reduced substantially by both pathways. However, the nanocomposites prepared from this new H-magadiite pathway show a much greater reduction of solvent uptake than those prepared from alkylammonium exchanged magadiites. The formation of dangling chains in the polymer matrix is still a dominant factor in compromising the solvent swelling properties of nanocomposites formed from organo magadiites.

More significantly, we have found that the nanocomposites prepared by this H-magadiite pathway can be almost completely restored to their original strength after solvent swelling. Show in Figure 5.19 are the tensile properties of epoxy-kenyaite composites in the original state and after swelling in toluene and drying. In contrast, the pristine epoxy polymer, as well as most of the nanocomposites prepared by the alkylammonium exchange pathway, are completely disintegrated upon drying, especially at low magadiite silicate loading.

We already discussed in Chapter 4 the effect of nanolayer thickness on the performance properties of nanocomposites prepared by the alkylammonium exchange pathway. However, the effect of alkylammonium and alkylamine in introducing dangling chains in the polymer matrix should not be ignored. This factor has been largely eliminated using the Jeffamine-H-layered silicic acid intercalates as starting materials. A comparison of tensile strength for nanocomposites prepared from different proton-exchange members of the layered silicic acid family is given in Figure 5.20. We only observed marginal differences between each member. This applies to the results of chemical stability and solvent resistance, which are summarized in Table 5.8.



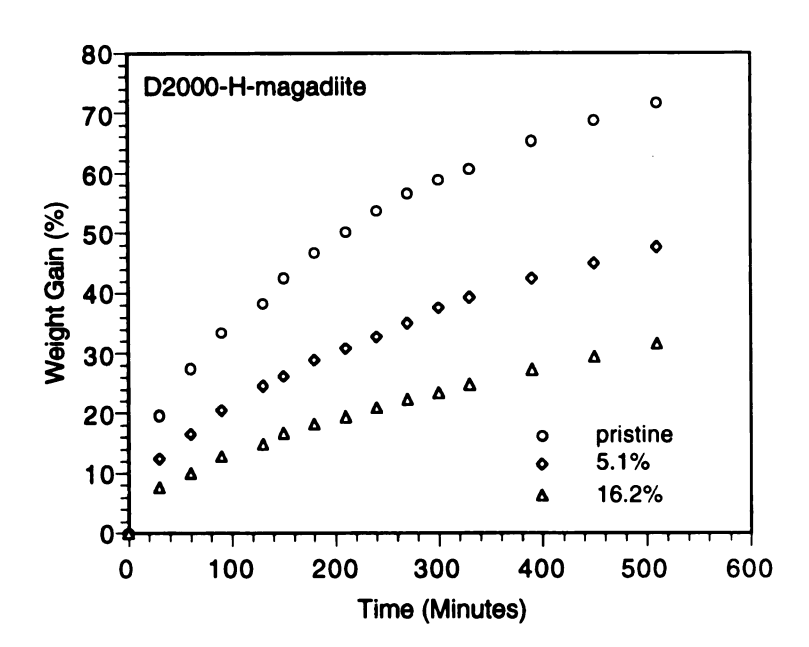
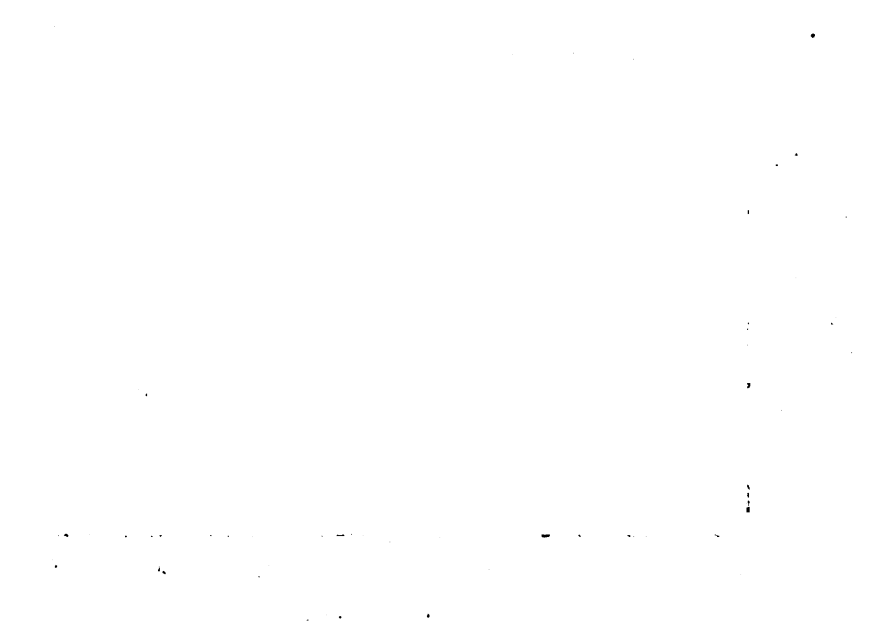
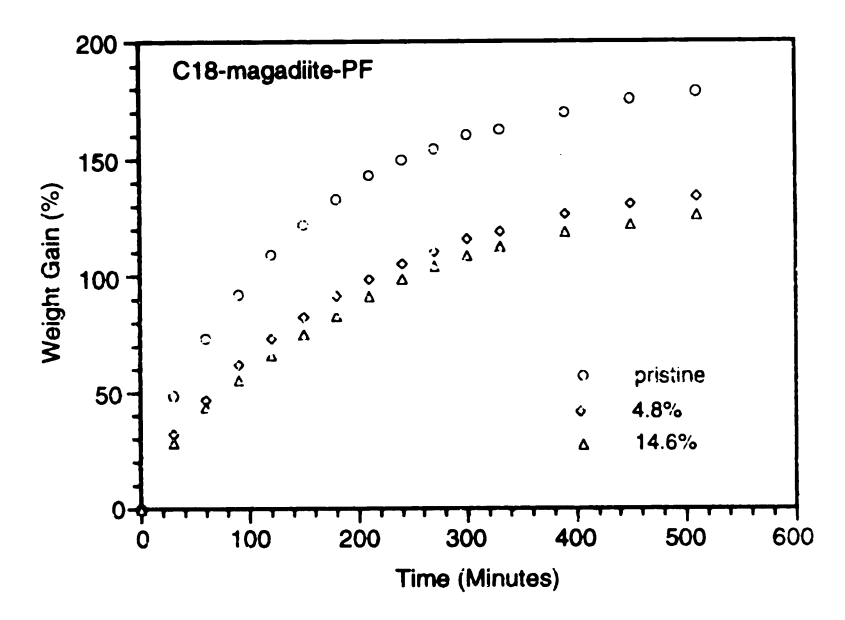


Figure 5.16 Comparison of methanol uptake curves for epoxy-exfoliated magadiite nanocomposites prepared from C18-magadiite-PF intercalates and D2000-H-magadiite intercalates. The tabulated values are the loadings (wt %) of C18-magadiite-PF intercalate and D2000-H-magadiite intercalate for each composite.





(a) The second of the secon



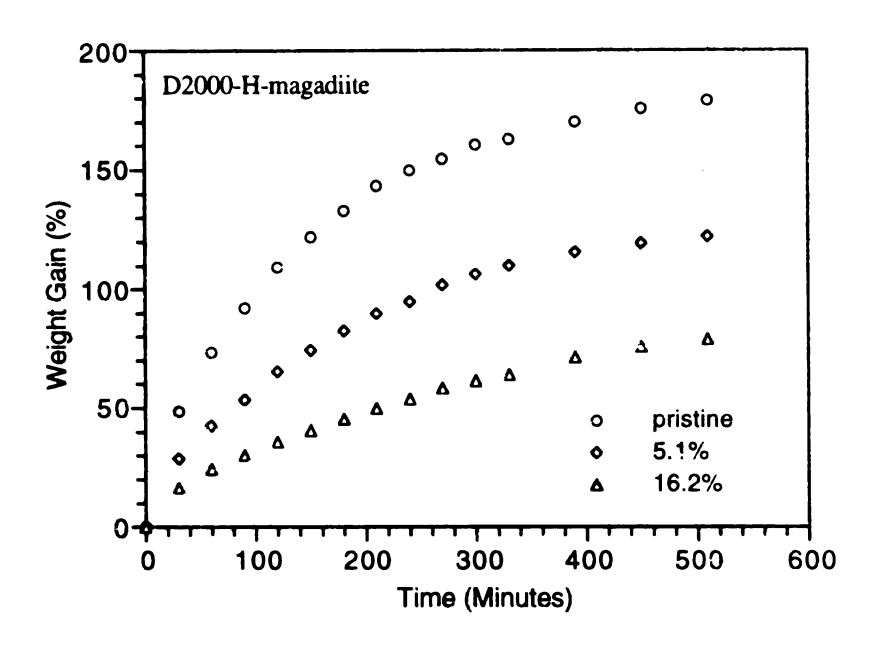
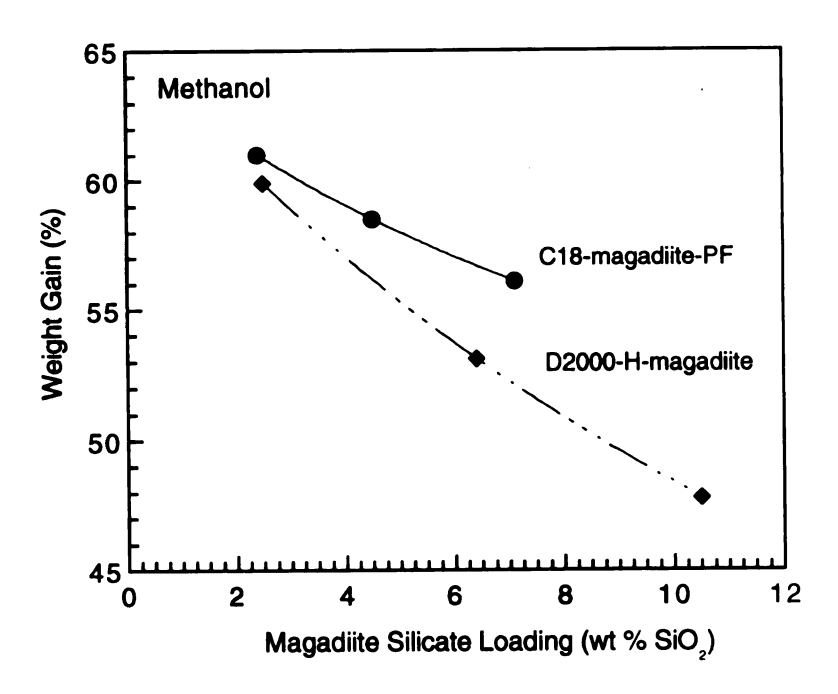


Figure 5.17 Comparison of toluene uptake curves for epoxy-exfoliated magadiite nanocomposites prepared from C18-magadiite-PF intercalates and D2000-H-magadiite intercalates. The tabulated values are the loadings (wt %) of C18-magadiite-PF intercalate and D2000-H-magadiite intercalate for each composite.



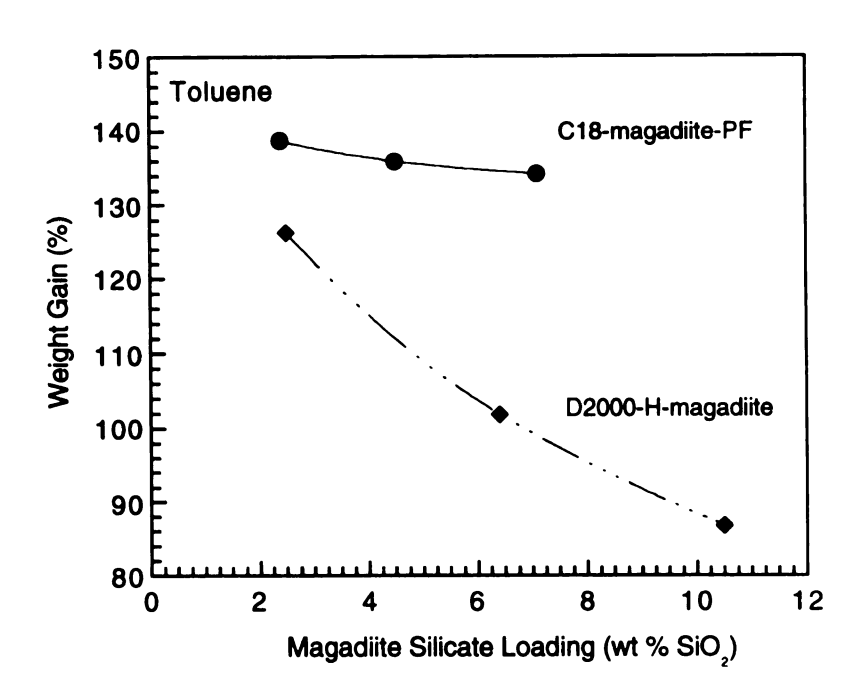
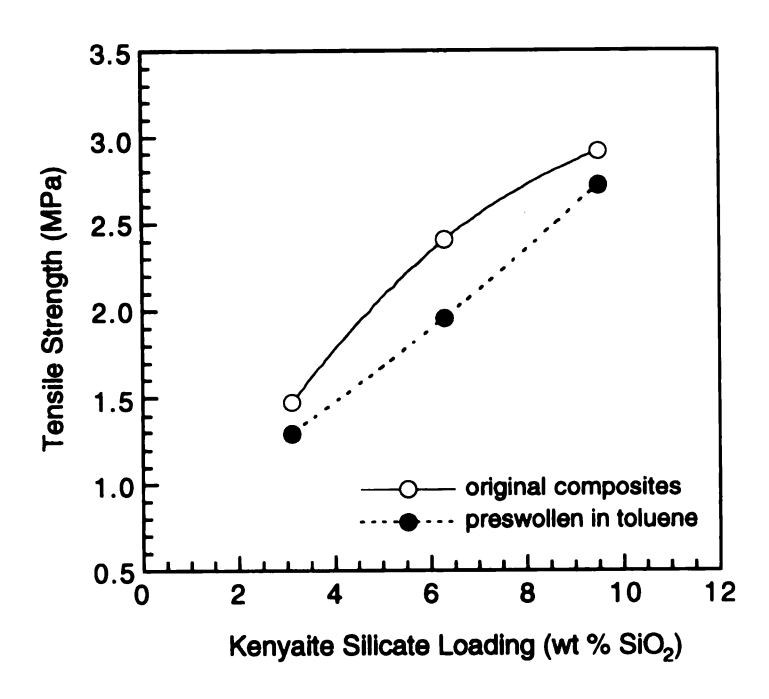


Figure 5.18 Comparison of methanol and toluene uptake at equilibrium vs. magadiite silicate (SiO₂) loading for epoxy-exfoliated magadiite nanocomposites prepared form C18-magadiite-PF and D2000-H-magadiite intercalates.



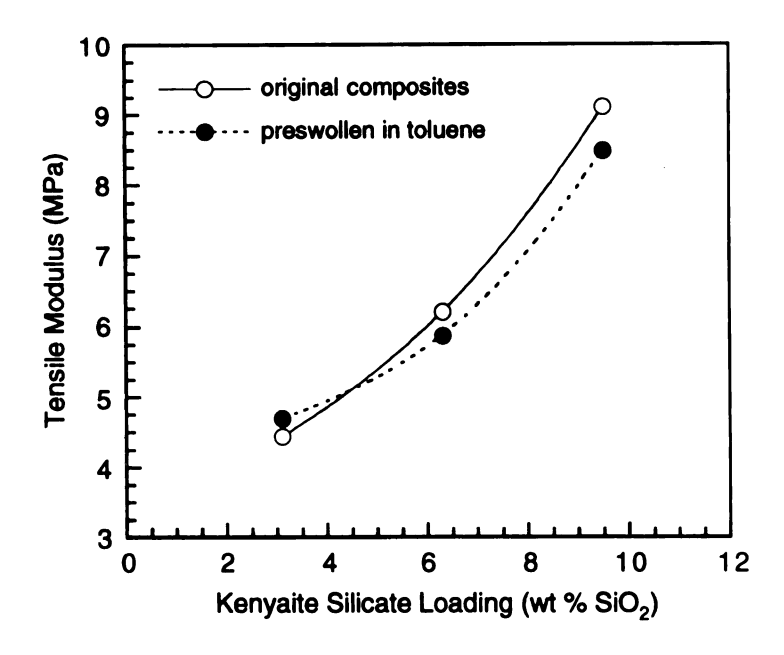


Figure 5.19 Tensile properties for the epoxy-kenyaite nanocomposites prepared from D2000-H-kenyaite intercalates before and after having been swollen in toluene. In the solvent swelling experiment the nanocomposites were soaked in toluene for 12 h, and subsequently dried in air for 24 h before the tensile properties were measured.

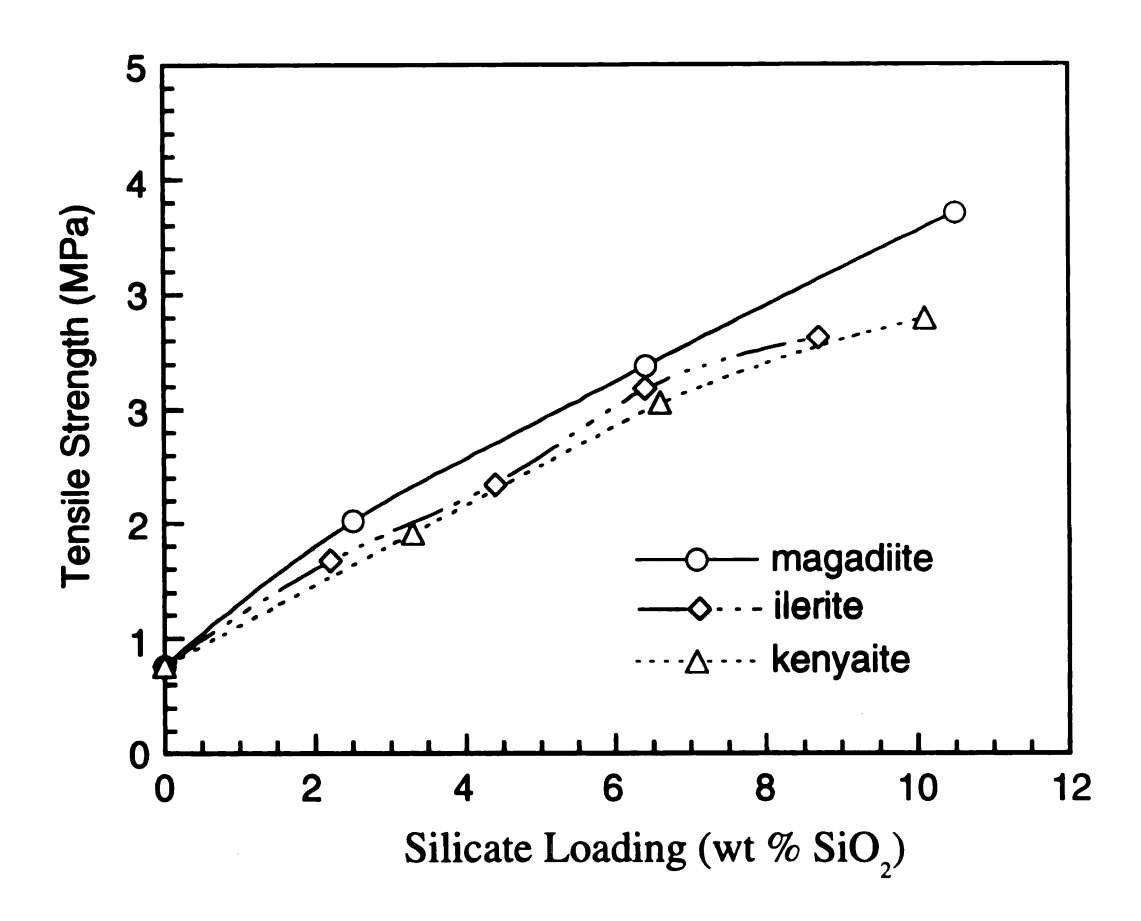


Figure 5.20 A comparison of the tensile strength vs. silicate loading for epoxy-layered silicic acid nanocomposites prepared from D2000-H-layered silicic acid intercalates.

Table 5.8 Chemical and Solvent Resistance of Epoxy-Exfoliated Layered Silicic acid Nanocomposites Prepared From D2000-H-silicic acid intercalates. The silicate (SiO₂) loadings for each composite are 4.4 wt %, 6.4 wt % and 6.6 wt % for ilerite, magadite and kenyaite respectively. Values are the Immersion Weight Gain (wt %) after Certain Uptake Periods.

materials	10%	distilled	30%	5%	methanol ^b	toluenec
	NaOHa	H ₂ Oa	H ₂ SO ₄ ^a	acetic acid	a	
pristine polymer	1.6	2.5	16.7	13.4	76.5	189
ilerite	1.6	2.7	12.4	10.4	58.7	118
magadiite	1.7	2.4	12.5	8.8	53.2	102
kenyaite	1.8	2.4	13.3	9.0	53.7	104

^a Weight gain after 15 days. ^b Weight gain after 48 hr. ^c Weight gain after 24 hr.

Theoretically, the aspect ratios of silicate nanolayers should affect the mechanical properties of each nanocomposite. But, the number of silicate nanolayer presented is varied when the silicate loading is a constant. We already know that the silicate loading has a significant effect on the performance properties. Also, the interfacial properties can also influence the overall performance. The nanocomposites we prepared so far have a relatively weak interface, wherein ionic bonding and van der Waals forces are the main interactions between the polymer matrix and the layered silicate phases. If interfacial interactions are more important than aspect ratios, then we will not see the effect of aspect ratios. Covalent bonding between the polymer and the layered silicate phases could address this issue. However, forming covalent linkages will not be easy. Most silylating agents which can be potentially grafted on interlayer surface of layered silicic acids are not large enough to force formation of the paraffin or lipid bilayer structures that are needed to achieve exfoliation in the final nanocomposite. The more commonly encountered lateral monolayer structure is not swellable by our polymer precursors. Also, the conditions needed for grafting reactions are not suited to our organo layered

silicic acids with a paraffin structure, because most intragallery organo species are desorbed under organic solvent refluxing conditions. Nevertheless, grafting is still an attractive option, provided that the proper reaction conditions and silylating agents, can be formed.

5.4 Conclusions

A new approach has been developed for the preparation of thermoset polymer-layered silicate clay nanocomposites in which curing agents can be directly intercalated into the intragallery without the need for alkylammonium ions on the exchange sites of the clay. This new development has resulted in a greater improvement of the overall properties of the polymer-layered silicic acid nanocomposites. This approach is general and could be applied to a lot of polymer systems when the polymer precursors can react with the intragallery protons of layered silicate clays. Nanocomposites based on both thermoplastic and thermoset polymers should be possible by this method. The interactions between the polymer precursors and protons can lead either to ionic bonding or the hydrogen bonding. The polymer precursors with amino, hydroxyl, amide, urea and urethane end or side groups are all good candidates for intercalation into proton exchanged clays for nanocomposite formation.

5.5 References

- 1. Kojima, Y.; Usuki, A.; Kawasumi, M.; Okada, A.; Fukushima, Y.; Kurauchi, T.; Kamigaito, O. J. Mater. Res. 1993, 8, 1185.
- 2. Kojima, Y.; Fukumori, K.; Usuki, A.; Okada, A.; Kurauchi, T. J. Mater. Sci. Lett. 1993, 12, 889.
- 3. Yano, K.; Usuki, A.; Okada, A.; Kurauchi, T.; Kamigaito, O. J. Polym. Sci., Part A: Polym. Chem. 1993, 31, 2493.
- 4. Messersmith, P. B.; Giannelis, E. P. Chem. Mater. 1993, 5, 1064.
- 5. Wang, M. S.; Pinnavaia, T. J. Chem. Mater. 1994, 6, 468.
- 6. Messersmith, P. B.; Giannelis, E. P. *Chem. Mater.* **1994**, 6, 1719.
- 7 Okada, A.; Usuki, A. *Mater. Sci. Eng.* **1995**, C3, 109.
- 8. Lan, T.; Kaviratna, P. D.; Pinnavaia, T. J. Chem. Mater. 1995, 7, 2144.
- 9. Giannelis, E. P. Adv. Mater. 1996, 8, 29.
- 10. Kurokawa, Y.; Yasuda, H.; Oya, A. J. Mater. Sci. lett. 1996, 15, 1481.
- 11. Usuki, A.; Kato, M.; Okada, A.; Kurauchi, T. J. Appl. Polym. Sci. 1997, 63, 137.
- 12. Pinnavaia, T. J. Science 1983, 220, 365.
- 13. Kato, C.; Kuroda, K.; Misawa, M. Clays Clay Miner. 1979, 27, 129.
- 14. Fukushima, Y.; Inagaki, S. J. Inclusion Phenom. 1987, 5, 473.
- 15. Fukushima, Y.; Okada, A.; Kawasumi, M.; Kurauchi, T.; Kamigaito, O. *Clay Miner.* **1988**, 23, 27.
- 16. Shi, H.; Lan, T.; Pinnavaia, T. J. Chem. Mater. 1996, 8, 1584.
- 17. Usuki, A.; Kojima, Y.; Kawasumi, M.; Okada, A.; Fukushima, Y.; Kurauchi, T.; Kamigaito, O. J. Mater. Res. 1993, 8, 1179.
- 18. Messersmith, P. B.; Giannelis, E. P. J. Polym. Sci., Part A: Polym. Chem. 1995, 33, 1047.
- 19. Pinnavaia, T. J.; Lan, T.; Wang, Z.; Shi, H.; Kaviratna, P. D. ACS Symp. Ser. 1996, 622, 250.
- 20. Vaia, R. A.; Jandt, K. D.; Kramer, E. J.; Giannelis, E. P. Chem. Mater. 1996, 8, 2628.
- 21. Vaia, R. A.; Ishii, H.; Giannelis, E. P. Chem. Mater. 1993, 5, 1694.

- 22. Lagaly, G.; Beneke, K.; Weiss, A. Am. Mineral. 1975, 60, 642.
- 23. Lagaly, G.; Beneke, K.; Weiss, A. Am. Mineral. 1975, 60, 650.
- 24. Pinnavaia, T. J.; Johnson, I. D.; Lipsicas, M. J. Solid State Chem. 1986, 63, 118.
- 25. Rojo, J. M.; Ruiz-Hitzky, E.; Sanz, J. Inorg. Chem. 1988, 27, 2785.
- 26. Beneke, K.; Lagaly, G. Am. Mineral. 1983, 68, 818.
- 27. Beneke, K.; Lagaly, G. Am. Mineral. 1989, 74, 224.
- 28. Kruse, H. H.; Beneke, K.; Lagaly, G. Colloid Polym. Sci. 1989, 267, 844.
- 29. Doring, J.; Lagaly, G. Clay Mineral. 1993, 28, 39.
- 30. Fletcher, R. A.; Bibby, D. M. Clays Clay Miner. 1987, 35, 318.
- 31. Beneke, K.; Kruse, H. H.; Lagaly, G. Z. anorg. allg. Chem. 1984, 518, 65.
- 32. Kosuge, K.; Tsunashima, A. J. Chem. Soc., Chem. Commun. 1995, 2427.

Chapter 6

HYBRID NANOCOMPOSITES FORMED FROM AN ORGANOFUNCTIONAL POLY(DIMETHYLSILOXANE) POLYMER AND PROTON FORMS OF LAYERED SILICIC ACIDS; AND THEIR USE FOR THE FORMATION OF HIGH SURFACE AREA SILICAS

6.1 Introduction

Polymer-clay nanocomposites can exhibit performance properties superior to their parent materials.^{1,2} Two types of nanostructured polymer-clay nanocomposites have been synthesized.^{3,4} Intercalated nanocomposites are formed when one or a few molecular layers of polymer are inserted into the clay galleries with fixed interlayer spacings. Exfoliated nanocomposites are formed only when the silicate nanolayers are exfoliated in the polymer matrix with their average layer separation dependent on the clay silicate loading. The interlayer spacing for the exfoliated nanocomposite may be uniform (regular) or variable (disordered).⁵ Although the intercalated phase of layered silicates can improve some structural properties,⁶ the exfoliated phase of silicate nanolayers is more effective in improving the overall performance properties of the resulting composite materials.⁷⁻⁹

However, organic polymers more readily form intercalated polymer-clay nanocomposites than exfoliated polymer-clay nanocomposites upon intercalation in organo clays. Ever since the nylon 6-clay hybrid material, which is truly an exfoliated polymer-clay nanocomposite, was synthesized by Toyota researchers, 10-13 only a few other polymer systems such as polyimides, 14 acrylonitrile rubber, 15 polyether, 16 epoxy 8.9 and polysiloxane 17 have been successfully used to extend this revolutionary chemistry

over the pass ten years. In most systems, the factors required to facilitate the exfoliation of clay nanolayers were not well understood. The process of exfoliation is most difficult when an extremely hydrophobic polymer is involved, such as polyethylene and polypropylene. 18,19

Polysiloxane polymers are unique polymeric materials because of their special properties in a variety of physical forms (fluids, resins, and elastomers). They exhibit the lowest T_g of (-125 °C) and T_m of (-40 °C) among useful polymers. Siloxane polymers have very low surface tension and good dielectric strength. They possess good thermal stability, oxidative resistance and chemical stability. All of these physical and chemical properties decide that they can be widely used as lubricants, greases, releasing agents, surfactants, water-repellents, adhesives, heat-transfer fluids, sealants and so on.^{20,21}

Polysiloxane elastomers are commonly reinforced by fillers such as silica to improve abrasion resistance, tear strength and tensile properties.²² The technique of *in situ* formation of precipitated silica particles (sol-gel technique) has been recently used in order to achieve the formation of highly dispersed silica fillers.^{22,23} In this method, the inorganic phase is formed by the hydrolysis and condensation of metal oxide precursors such as tetraethylorthosilicates:

$$\mathrm{Si}(\mathrm{OEt})_4 + 2\mathrm{H}_2\mathrm{O} \rightarrow \mathrm{SiO}_2 + 4\mathrm{EtOH}$$

The metal oxide precursors are first absorbed into the polymer network, then the swollen polymer is placed into water containing the catalyst (an acid or base) which can facilitate the above hydrolysis and condensation reaction. The average diameter of the resulted silica particles is about 20 ~ 30 nm. The resulted composites showed improved tensile properties.

Layered silicate nanolayers can be used as alternative inorganic components in the synthesis of polysiloxane-silicate nanocomposites. The clay silicate nanolayers possess high particle aspect ratios comparable to the *in situ* formed silica particles.²⁴ It

has been reported that the dielectric strength of siloxane polymer was improved by simply imbedding the surfactant treated silicate clays such as polygorskite and montmorillonite into the siloxane polymer matrix.²⁵ The intercalation chemistry of layered silicate clays by silicone polymers can play an important role in further improving the performance properties of resulted composite materials, especially when 10 Å-thick nanolayers of clay are exfoliated in the polymer matrix.

The synthesis of a polysiloxane polymer-exfoliated clay nanocomposite was reported recently. ¹⁷ In that synthesis, a silanol terminated poly(dimethylsiloxane) (PDMS) was cross-linked by tetraethylorthosilicate (TEOS) in the presence of an organo clay. The resulting nanocomposite exhibited an improved solvent resistance and thermal stability. However, the organo clay used to achieve silicone intercalation contained long chain quaternary alkylammonium ions on the gallery exchange sites. The introduction of nonfunctional onium ion surfactants is not preferred in this chemistry, because they compromise the performance properties of the polymer.

In the present work, the new approach has been developed for preparing thermoset silicone polymer-layered silicate clay nanocomposites in which curing agents can be directly intercalated into clay galleries and cross-linked without the need of organic onium ions on the clay exchanged sites. We also show that the calcination of the PDMS-layered silicic acid nanocomposites leads to porous, high surface area silicas in which the silicate layers are partially re-stacked with silica separating the layers.

6.2 Experimental

6.2.1 Materials

The organofunctional siloxane precursors (Gelest) used for the cross-linked polymer matrix formation were as follow:

Epoxypropoxypropyl Terminated PDMS (DMSE12)

$$H_2C-CHCH_2O(CH_2)_3$$
 $Si-O+Si-O+Si-O+Si-(CH_2)_3OCH_2CH-CH_2$
 CH_3 CH_3

Aminopropyl Terminated PDMS (DMSA12)

$$H_{2}N(CH_{2})_{3} - Si - O + CH_{3} CH_{3} CH_{3} CH_{2}$$

$$CH_{3} CH_{3} CH_{3} CH_{3} CH_{3}$$

$$CH_{3} CH_{3} CH_{3} CH_{3}$$

$$MW = 900-1000 n = 8.8-10.2$$

The above siloxane precursors were cross-linked by the reaction of epoxy groups with primary amine groups to afford a polysiloxane elastomer matrix.

6.2.2 Synthesis of Layered Silicic Acids

Synthesis of Alkali-Metal Forms of Layered Silicic Acids. Alkali-metal forms of layered silicic acids were synthesized by hydrothermal methods. ²⁶⁻²⁸ In general, a suspension of amorphous silica gel was added to a MOH solution (M = Na or K) and heated at a temperature above 100 °C for a few days with stirring in a Teflon-lined Parr reactor. The suspension containing the alkali-metal form of layered silicic acid was centrifuged, and the solid product was washed with deionized water to remove excess MOH, and air-dried at room temperature. The exact synthesis conditions used for each layered silicic acid were specified previously in Chapter 5 (cf., Table 5.1).

Synthesis of Proton Forms of Layered Silicic Acids. H⁺ forms of layered silicic acids were obtained by titration of synthetic alkali-metal forms of layered silicic acids with dilute hydrochloric acid.²⁹ A 500-mL of aqueous suspension containing 15.0 g of layered silicic acid (magadiite, kenyaite and ilerite) was titrated with 0.1 M HCl at a rate of 3 mL/min to lower the pH to 1.9. For kenyaite the final pH was 1.8. The suspensions

at pH = 1.9 (1.8 for kenyaite) were stirred for 24 hours (48 h for kenyaite). The proton exchange forms of layered silicic acids were separated by centrifugation and washed with deionized water until free of Cl⁻, and then air-dried at room temperature.

Synthesis of DMSA12-H-Layered Silicic Acid Intercalates. An ethanol solution containing the aminopropyl terminated PDMS (DMSA12) was added to an aqueous suspension of the H⁺ form of layered silicic acid and stirred at 60 °C for a certain period. The ratios of DMSA12 to H-layered silicic acid, the solvent composition, reaction time, and post reaction washing process used for each synthesis, along with basal spacing for each intercalate, are specified in Table 6.1. The solid products were obtained by either centrifugation when a washing process was applied or by evaporation of the EtOH/H₂O solvent in hood. The DMSA12-H-layered silicic acid intercalates were dried in an oven at 100 °C for 24 h before they were used for composite preparation.

6.2.3 Preparation of PDMS-Layered Silicic Acid Composites

Stoichiometric amounts of DMSE12 and DMSA12 in the form of the free amine and the DMSA12-H-layered silicate intercalate were mixed at room temperature for 10 min. The desired amount of DMSA12-H-layered silicic acid intercalates was added to the DMSE12-DMSA12 mixture and stirred at room temperature or at 50 °C for an additional 24 h. The DMSA12 in intercalated form was counted as contributing to the stoichiometry for DMSE12-DMSA12 cross-linking. This mixture was outgassed in a vacuum oven and poured into a stainless steel mold for curing at 125 °C for 6 h.

Table 6.1 Synthesis of DMSA12-H-layered Silicic Acid Intercalates

intercalate	d ₀₀₁ (Å) physica	physical state	DMSA12 (g)/g of H-layered silicic acid	solvent (v/v) rxn time rxn temp EtOH/ H_2O (h) (°C)	rxn time (h)	rxn temp (°C)	washings with 1:1 (v/v) EtOH/H ₂ O
DMSA12-H-ilerite	42.6	pwd	2.00	20/30	9	09	none
DMSA12-H-magadiite	56.3	pwd	2.00	20/30	12	9	none
DMSA12-H-kenyaite	63.1	pwd	1.40	35/35	24	99	none
	36.5	pwd	2.00	50/30	24	09	twice

6.2.4 Characterization Methods

X-ray Powder Diffraction (XRD). XRD patterns were recorded on a Rigaku rotaflex 200B diffractometer equipped with a rotating anode, Cu K_{α} x-ray radiation (λ = 1.541838 Å) and a curved crystal graphite monochromator. The x-ray was operated at 45 KV and 100 mA. Diffraction patterns were collected with 0.01° 2θ interval between 1 and 10° 2θ using a scanning rate of 2° 2θ per minute, and DS and SS slit widths of 1/6. For patterns obtained at starting angle of 0.5° 2θ , a SS width of 0.05 was used instead of 1/6. XRD patterns at high angles were collected using DS and SS slit widths of 1. The gel-like samples were prepared by applying thin films on glass slides. Cured composite specimens were prepared by mounting a flat rectangular sample into an aluminum holder.

Surface Area Measurement. N_2 adsorption-desorption isotherms were determined on a ASAP 2010 Sorptometer at liquid N_2 temperature using a static sorption mode. Samples were outgassed at 150 °C and 10⁻⁵ Torr for 12 h. Surface areas were determined using BET plots.

Thermal Analysis. Thermogravimetric analyses (TGA) were performed using a Cahn TG System 121 thermogravimetric analyzer. Samples were heated to 750 °C at a heating rate of 5 °C/min under N₂ atmosphere.

Chemical and Solvent Resistance. Resistance to solvent swelling was obtained according to ASTM procedure D543. The specimens were immersed in the desired reagent and removed periodically to measured the weight gain until equilibrium was reached.

6.3 Results and Discussion

6.3.1 Synthesis of PDMS-H-Layered Silicic Acid Intercalates

We have demonstrated previously that the proton forms of layered silicic acids can react with the polymer precursors with amino end groups. The present work shows

that this approach can be extended to the aminofunctional PDMS siloxane precursors wherein a very hydrophobic system is involved:

The quantitative nature of this reaction is shown by the XRD patterns in Figure 6.1. The intercalates are formed between DMSA12 and H-layered silicic acids. A co-solvent of water and ethanol, however, is still necessary for this intercalation reaction. Generally, a high volume percentage of ethanol has to be applied due to the poor solubility of DMSA12 in water. The typical synthesis conditions along with basal spacings for each intercalate are specified in Table 6.1. Basically, a post reaction washing is not necessary in order to obtain a powdered form of the product, and synthesis conditions can be varied in a certain range without changing the basal spacings of the resulted intercalates.

The washing is applied only when an intercalate with a decreased basal spacing (less PDMS) is desired. As listed in Table 6.1, the basal spacing of the DMSA12-H-kenyaite intercalate decreased from 63.1 Å to 36.5 Å when the as-synthesized product was washed by a 1:1 (v/v) mixture of water and ethanol. Interestingly, both the intercalates of DMSA12-H-kenyaite with different d-spacings can be further swollen by the mixture of DMSA12 and DMSE12, but the structures for the final composites formed by these two intercalates are quite different, as discussed in next section.

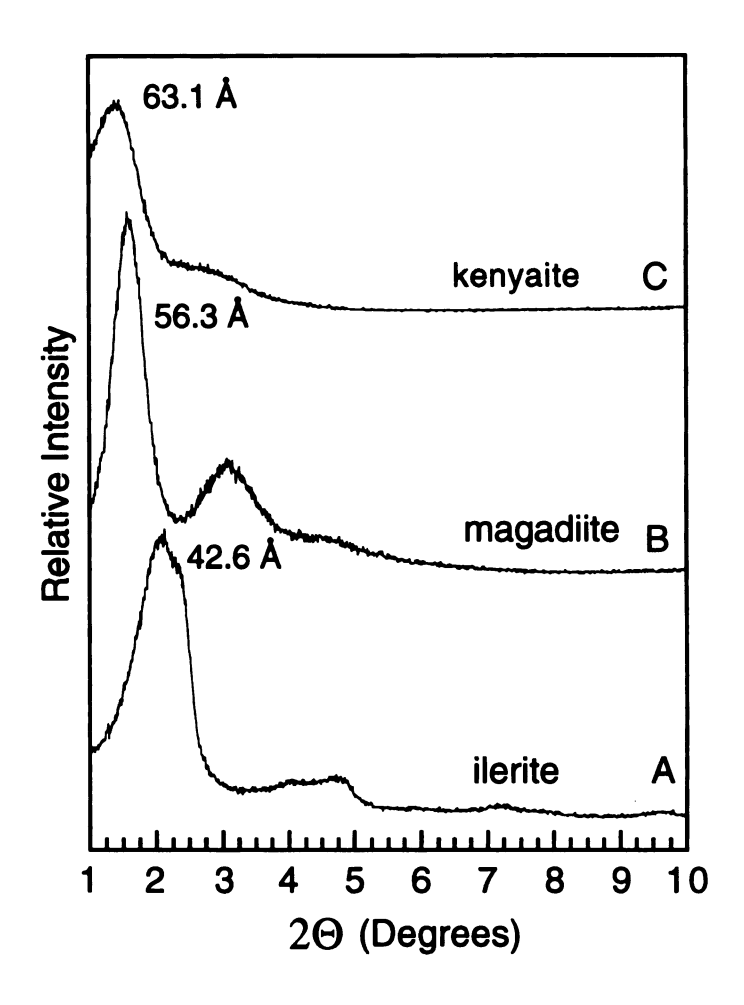


Figure 6.1 XRD patterns of intercalates formed by reaction of aminopropyl terminated polydimethylsiloxane (DMSA12) and (A) H-ilerite; (B) H-magadiite; and (C) H-kenyaite in ethanol/ H_2O (cf. Table 6.1) and air-dried without washing.

6.3.2 Exfoliation of Layered Silicic Acid Nanolayers in a Cured PDMS Matrix

The reaction of DMSA12-H-kenyaite intercalate with a 63.1 Å basal spacing by a stoichiometric mixture of DMSE12 and DMSA12 as a function of time was investigated by XRD (Figure 6.2). At a loading of 15 wt % H-kenyaite, an intercalate with a 75 Å d-spacing was quickly formed at 50 °C, corresponding to about a 12 Å increase of gallery height. Unlike the co-intercalation chemistry observed previously for organo layered silicic acids and mixtures of Jeffamine and epoxide, an even higher d-spacing peak observed with about an additional 9 Å gallery height increase can be achieved by increasing the curing time at 50 °C to 22 h. This is probably due to the slow diffusion process and the low reactivity for these polymer precursors with high molecular weight, consequently, more intermediate intercalates are observed. The absence of a first order peak is observed when the reaction mixture is heated to a higher temperature of 125 °C. Finally, an amorphous XRD pattern is obtained (Figure 6.2E) after a sequential cure at 50 °C and 125 °C, which suggests an exfoliated structure has been achieved in the synthesis of PDMS-kenyaite nanocomposite.

The DMSA12-H-magadiite intercalate undergoes very similar intercalation and exfoliation chemistry under the same reaction condition. The XRD patterns for the cured PDMS-layered silicic acid nanocomposites are shown in Figure 6.3. The retention of the 2-D layered silicate structures upon exfoliation is confirmed by the presence of the inplane peaks. It is noteworthy that the peak intensity for these patterns is lower than the system of epoxy-layered silicic acid nanocomposites. This is probably due to the interference scattering (contrast matching) by the siloxane polymer backbone.

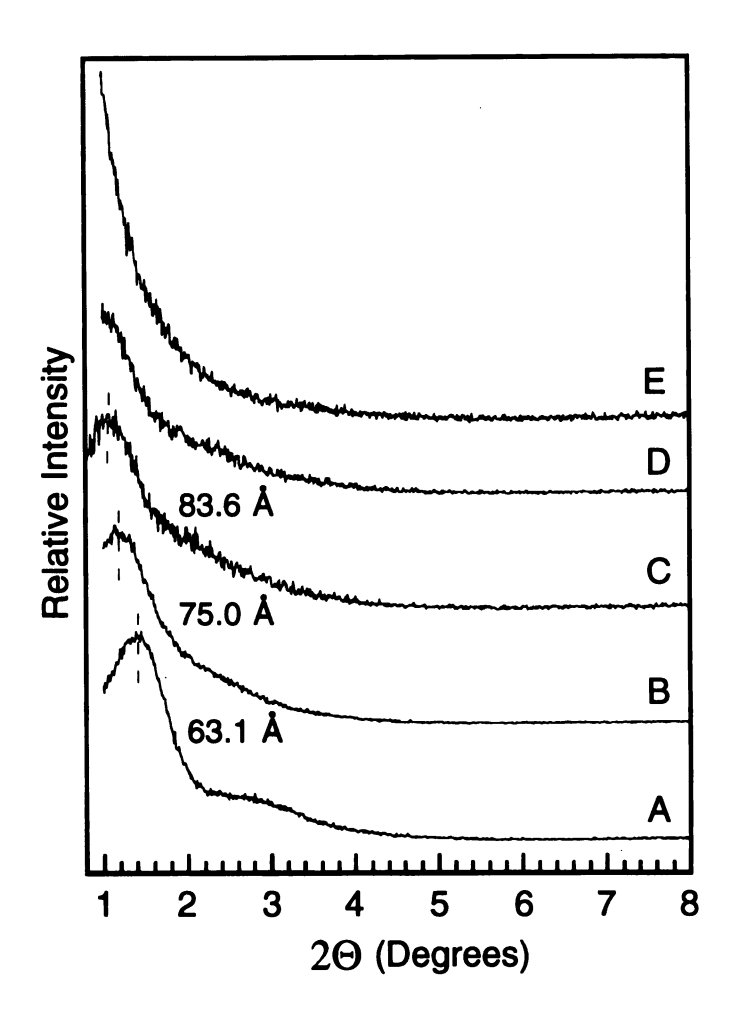
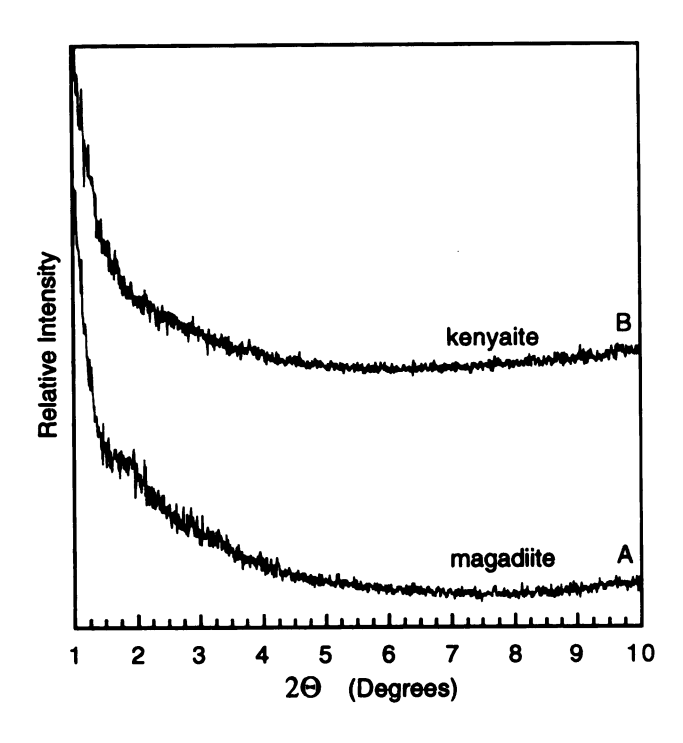


Figure 6.2 XRD patterns of (A) the initial DMSA12-H-kenyaite intercalate and the partially cured composites formed at 15 wt % H-kenyaite loading by reaction of a stoichiometric mixture of DMSA12 and DMSE12 under the following reaction conditions: (B) 50 °C, 30 min; (C) 50 °C, 22 h; (D) 50 °C, 24 h and 125 °C, 10 min. The pattern (E) is for the fully cured PDMS-kenyaite composite that was cured first at 50 °C for 24 h and then at 125 °C for 6 h.



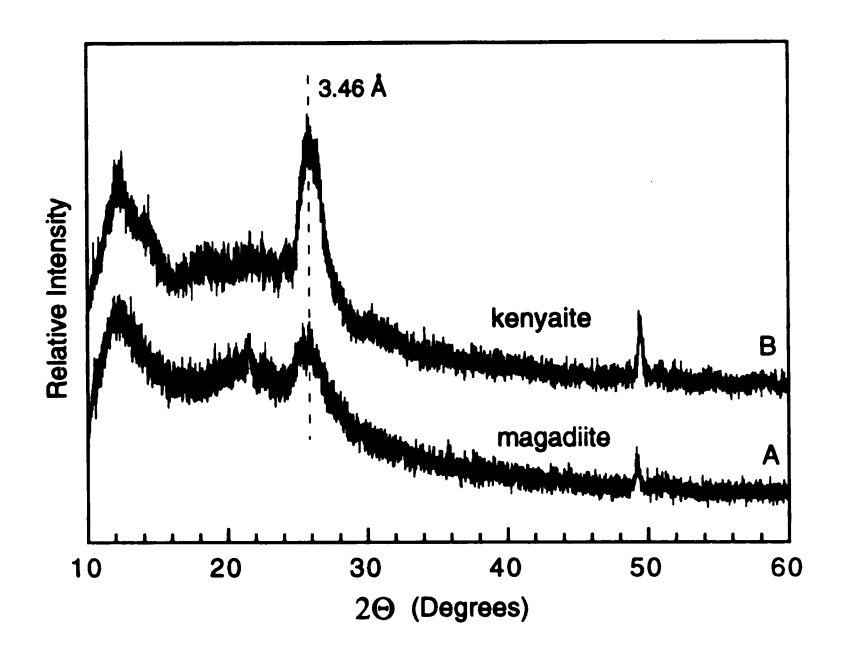


Figure 6.3 XRD patterns of the cured PDMS-exfoliated layered silicic acid nanocomposites prepared from the intercalates formed between DMSA12 and (A) H-magadiite; and (B) H-kenyaite. The H-silicic acid loading for each composite is 10 wt %. Polymer curing was carried out at 50 °C for 24 h, and followed by 6 h at 125 °C.

The exfoliation of silicate nanolayers in the polysiloxane matrix is further proved by the following experiments. The PDMS-kenyaite nanocomposites were calcined at 540 °C for 10 h in order to remove the cured polymer and obtain the calcined silica residue, the DMSA12-H-kenyaite intercalate with a 63.1 Å d-spacing was also calcined as a reference sample. The XRD patterns for these calcined samples are shown in Figure 6.4. Interestingly, the DMSA12-H-kenyaite intercalate shows a strong asymmetric peak with about a 32 Å d-spacing, whereas, the PDMS nanocomposites prepared from this DMSA12-H-kenyaite intercalate show broad peaks at higher spacings with the peak position dependent on the loading of H-kenyaite. Since the composite samples are calcined in air, the polymer matrix is converted into amorphous silica. The kenyaite layers become partially restacked with amorphous silica trapped between the layers. The is supported the weight loss after calcination and by XRD patterns for the calcined samples. The kenyaite galleries are loaded with the different amounts of polysiloxane polymer when the ratio of polymer to H-kenyaite is varied. Therefore, once the intragallery polysiloxane polymer is converted into the amorphous silica phase, the gallery height becomes proportional to the loading of intragallery polymer. The XRD results for these calcined samples ($d_{001} = \sim 100 \text{ Å}$ at 8.2 wt %, $\sim 76 \text{ Å}$ at 15 wt % loading of H-kenyaite) are consisted with this concept, and with the presence of exfoliated silicate nanolayers in the initial composite.

The technique of surface area measurement by N_2 adsorption-desorption was also used to investigate the partial restacking of silicate nanolayers for the silica-intercalated kenyaites formed by calcination. which is shown in Figure 6.5. A large texture porosity and surface area were observed for the silica obtained from the calcined nanocomposite with a 8.2 wt % loading of H-kenyaite (Figure 6.5). This result agrees with the formation of a silica in which some of the kenyaite is re-stacked with amorphous silica between the layers and remainder is exfoliated. This provides a significant increase in texture porosity and surface area, especially when the amorphous silica is presented.

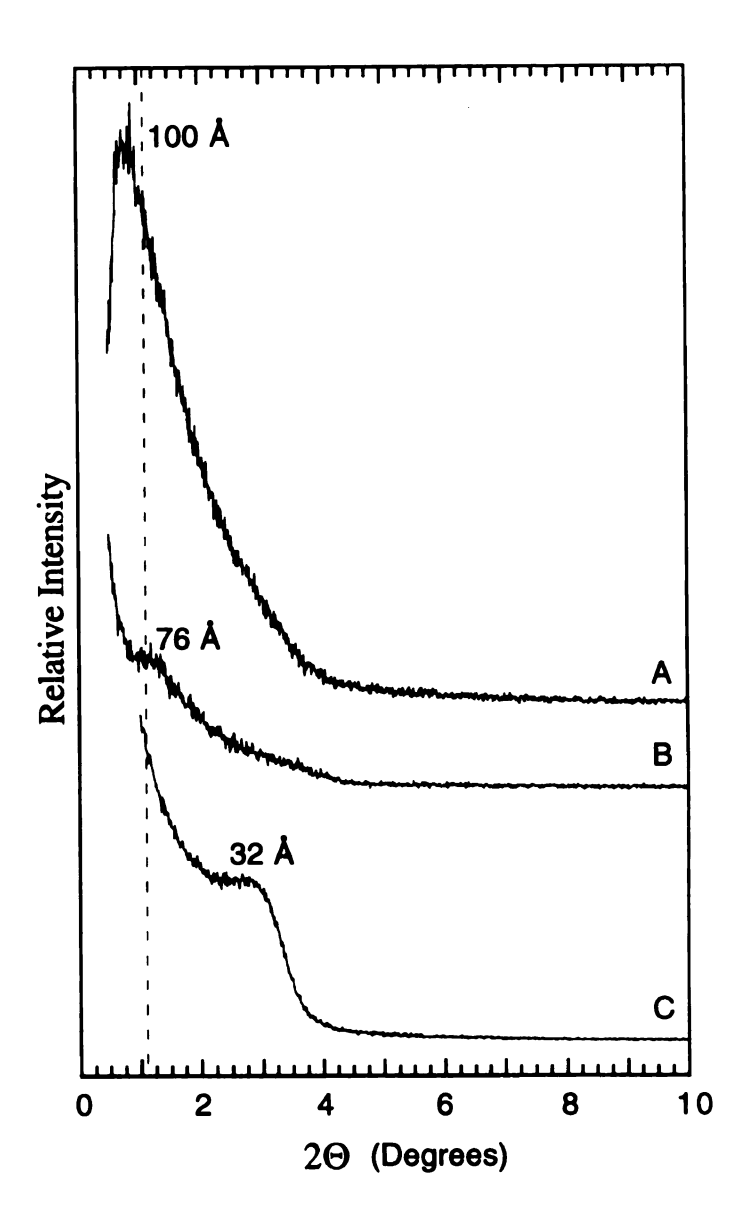


Figure 6.4 XRD patterns for the silica-intercalated kenyaites obtained by calcination of the PDMS-exfoliated kenyaite nanocomposites at 540 °C for 10 h with a heating rate of 1 °C/min. The H-kenyaite loading was (A) 8.2 wt %; and (B) 15 wt %. Pattern (C) is for the DMSA12-H-kenyaite intercalate after the same calcination conditions.

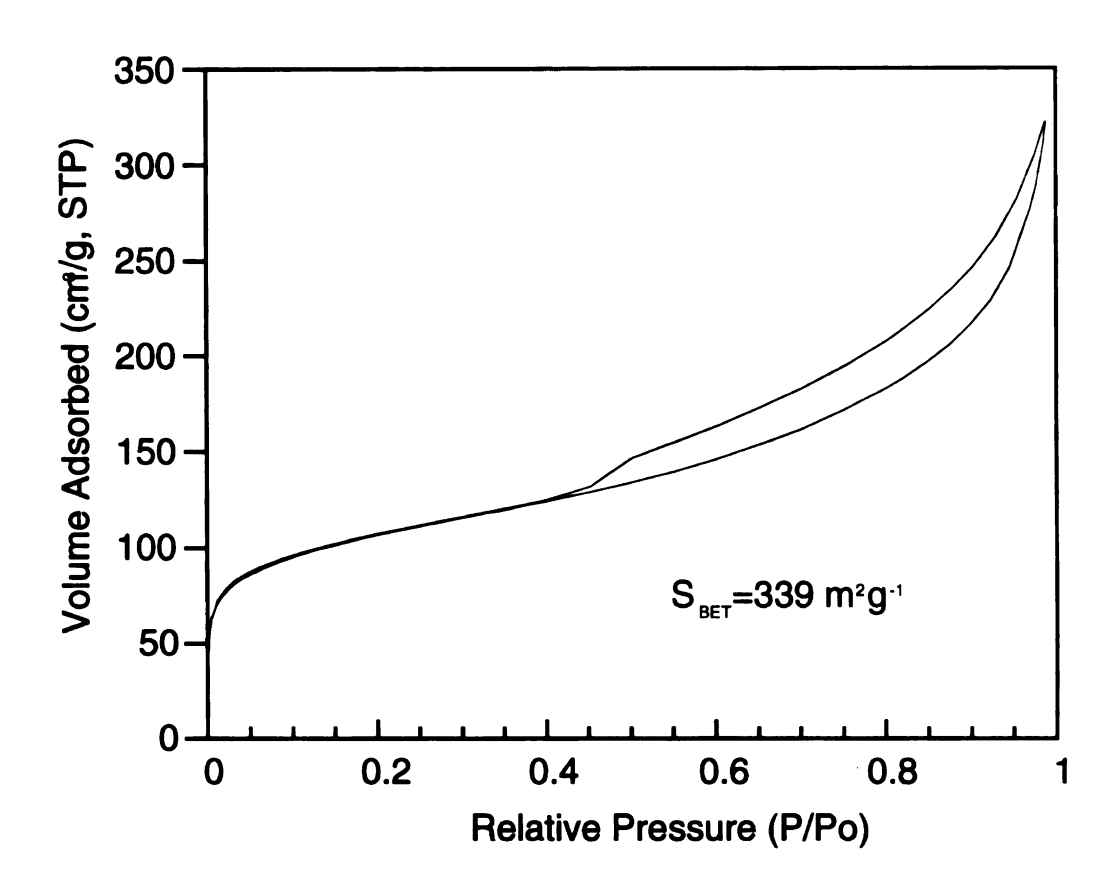


Figure 6.5 N_2 adsorption-desorption isotherm for the silica residue obtained by calcining the PDMS-exfoliated kenyaite nanocomposite prepared from a DMSA12-H-kenyaite intercalate. The H-kenyaite loading was 8.2 wt %. The calcination was carried out at 540 °C for 10 hr in air using a heating rate of 1 °C/min.

As we mentioned in last section, the washed DMSA12-H-kenyaite intercalate with a 36.5 Å d-spacing showed a behavior different from the unwashed 63.1 Å intercalate (see Table 6.1) when swollen by a mixture of DMSE12 and DMSA12. An intercalated nanocomposite with a 72.8 Å d-spacing is formed instead of an exfoliated nanocomposite. Figure 6.6 compares the XRD patterns for the 72.8 Å intercalated nanocomposite and the DMSA12-H-kenyaite intercalate from which the intercalated nanocomposite was prepared. The lower gallery height causes the intragallery diffusion process to be slow and the extragallery cross-linking rate is faster than the intragallery polymerization rate.

The intercalated PDMS-kenyaite nanocomposite with a 72.8 Å d-spacing was used to compare the structural difference between the silica obtained from intercalated and exfoliated nanocomposite phases. A plot of surface area vs. H-kenyaite loading for the silicas obtained from PDMS-exfoliated kenyaite nanocomposites is given in Figure 6.7. Included in the figure is the surface area of the silica obtained by calcination of a PDMS-intercalated kenyaite nanocomposite at 10 wt % loading. At the same 10 wt % H-kenyaite loading, the surface area for the intercalated nanocomposite is substantially lower than the silica obtained from exfoliated analog. The registry of restacked silicate nanolayers is greater in the case of the intercalated nanocomposite, so the fraction of exfoliated structure is limited. On the other hand, the surface area increases with the kenyaite nanolayer loading for the silica obtained from exfoliated nanocomposites. This effect is explained by the formation of a greater fraction of exfoliated kenyaite silica with increased loading.

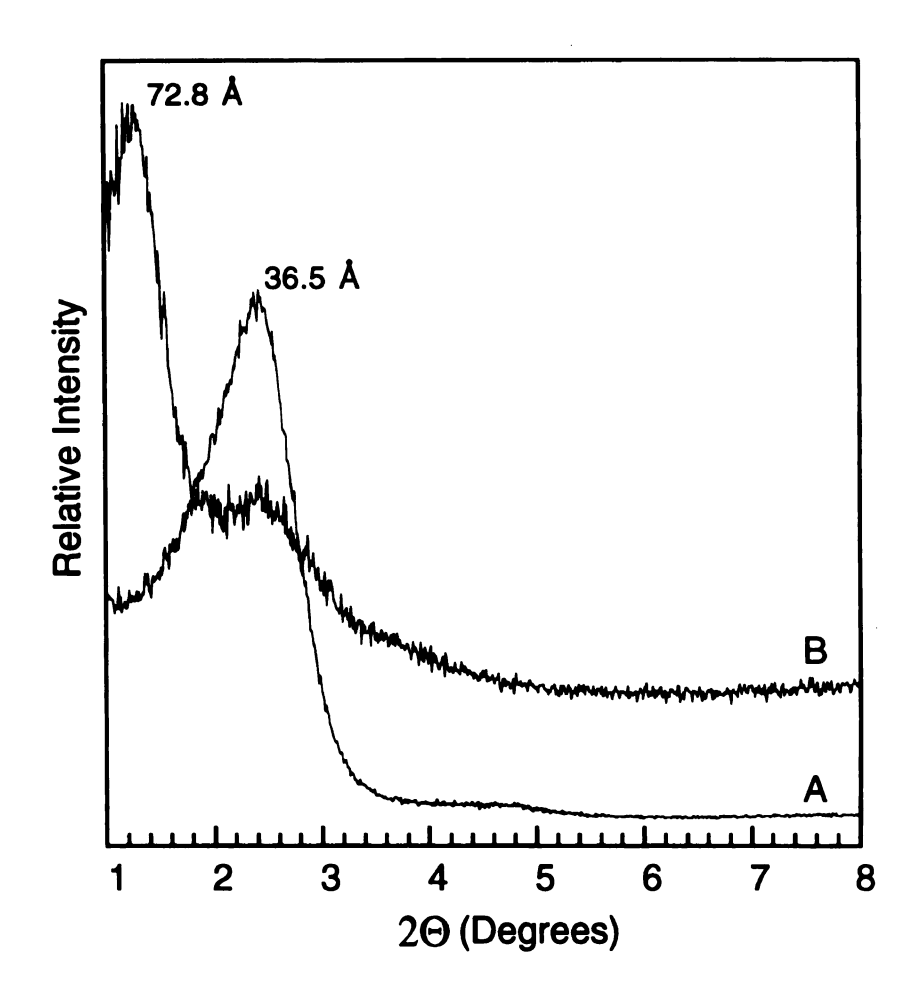


Figure 6.6 XRD patterns of kenyaite intercalates: (A) DMSA12-H-kenyaite (36.5 Å); (B) a PDMS-intercalated kenyaite (10 wt % loading of H-kenyaite) nanocomposite (72.8 Å).

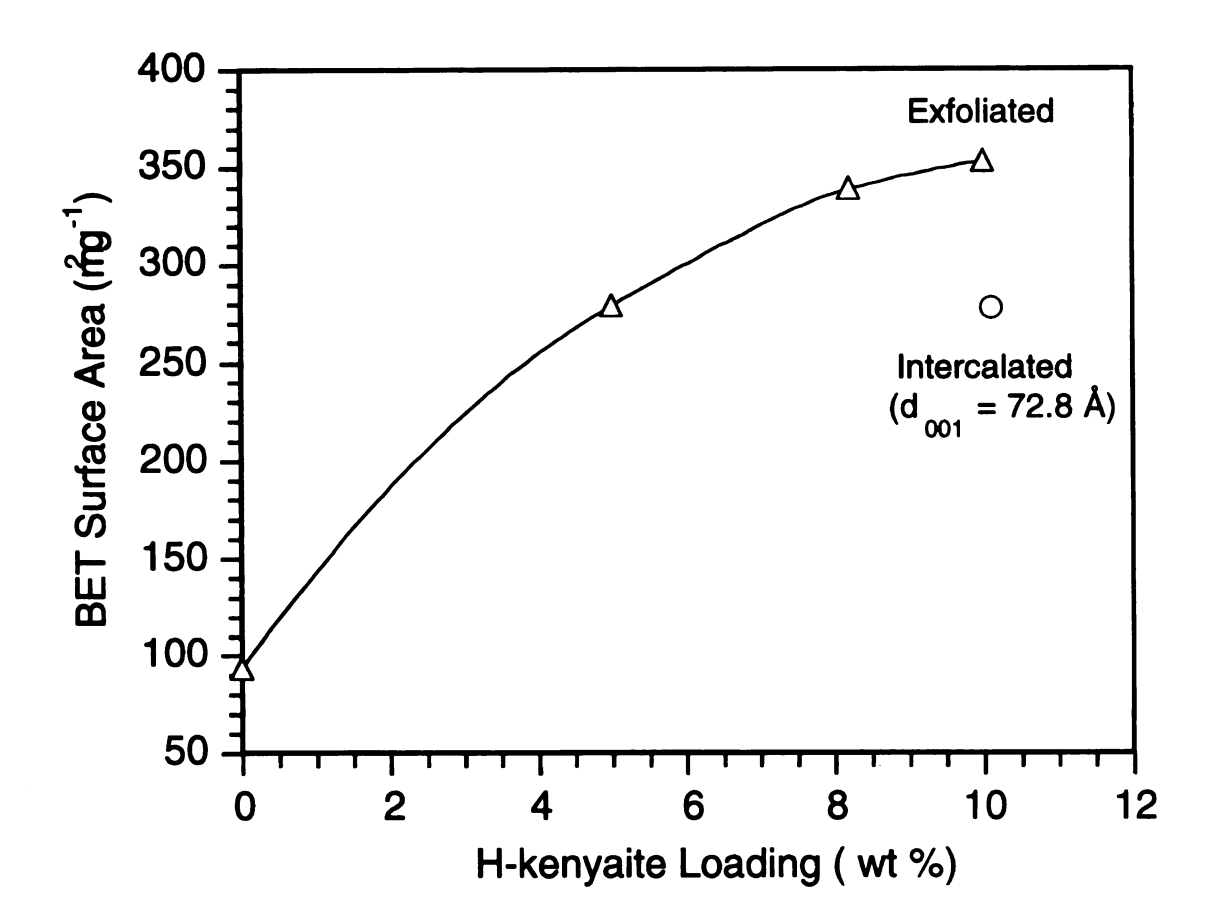


Figure 6.7 Comparison of BET surface area for the silica residues obtained by calcining exfoliated PDMS-kenyaite nanocomposites with different loadings (wt %) of H-kenyaite. The open circle is the surface area for the silica residue obtained by calcining an intercalated PDMS-kenyaite nanocomposite with a 10 wt % loading of H-kenyaite. The calcination was carried out at 540 °C for 10 hr in air using a heating rate of 1 °C/min.

6.3.3 Performance Properties of Exfoliated PDMS-Layered Silicic Acid Nanocomposites

The exfoliated PDMS-kenyaite nanocomposites show superior solvent resistance properties relative to pristine PDMS (see Figure 6.8). With a 10 wt % of H-kenyaite loading, the toluene uptake is substantially reduced by a factor of greater than 2. The effect of kenyaite loading on reduction is very significant. This highly desired improvement in swelling resistance is attributed to the interfacial forces that are higher than the intramolecular forces in the pristine polymer. The polysiloxane polymer has a very low glass transition temperature, so that a large free volume exists in the pristine polymer. The enhanced polymer-kenyaite interactions strengthen the polymer and make it more resistant to solvent swelling. One also would predict an increase in Tg. Future studies will investigate this point.

The thermal stability of the exfoliated nanocomposite is compared with the pristine polysiloxane polymer shown in Figure 6.9. Unlike the result that Burnside and Giannelis has claimed previously for PDMS-smectite clay nanocomposites, ¹⁷ substantial improvement in thermal stability is not observed in this work. The difference behavior is probably due to the introduction of the organic linkages in this system.

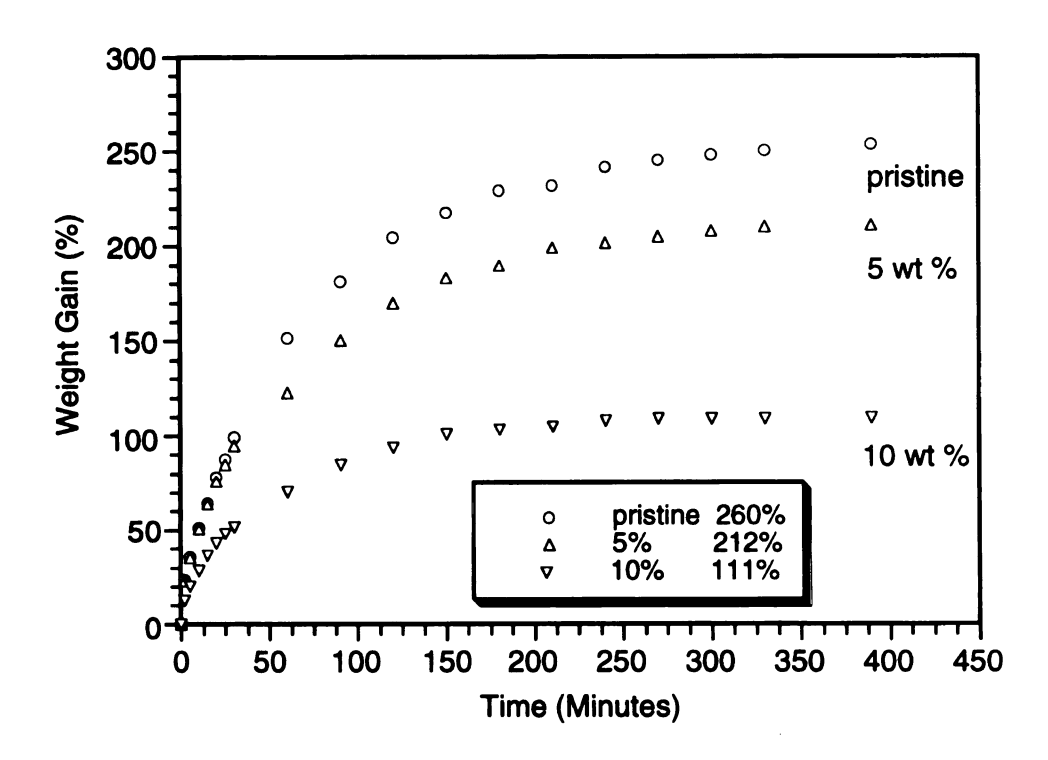


Figure 6.8 Toluene uptake by the exfoliated PDMS-kenyaite nanocomposites prepared from DMSA12-H-kenyaite intercalates. The tabulated values in the insert are equilibrium data determined by the immersion weight gain after 24 hr. The H-kenyaite loadings for the composites are 5 wt % and 10 wt %.

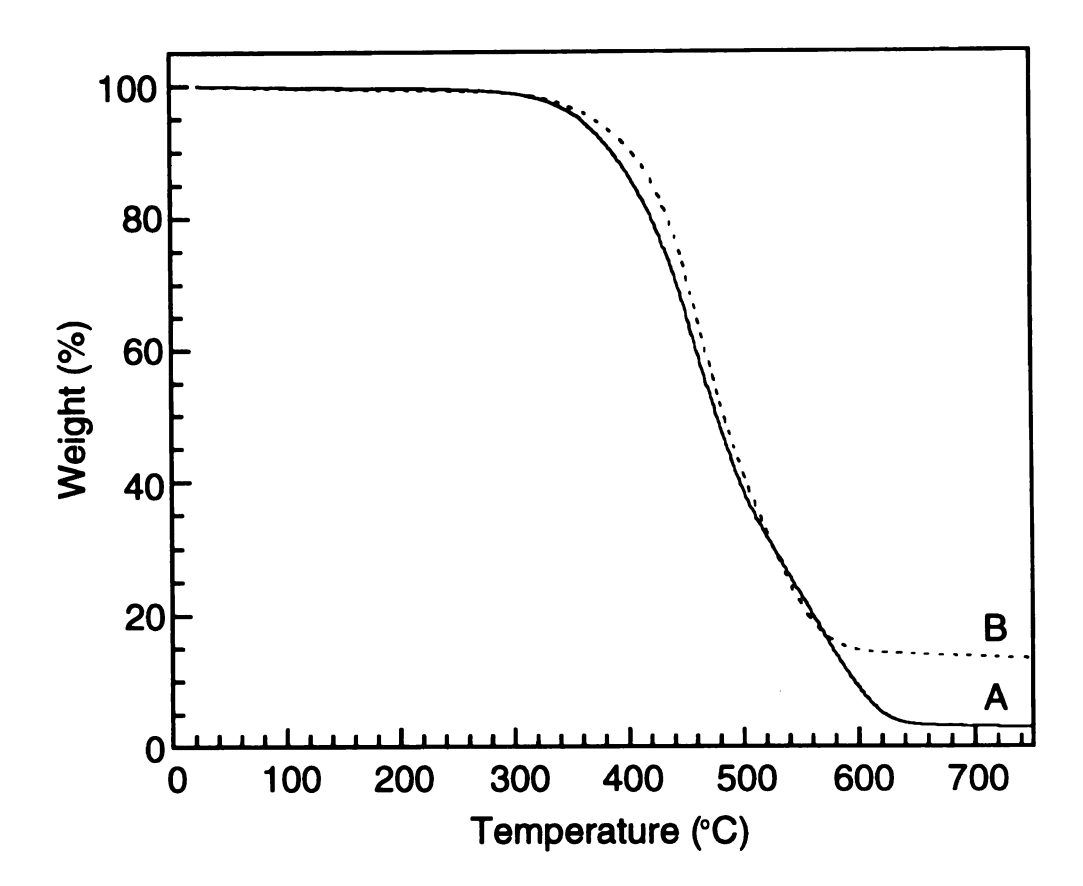


Figure 6.9 Thermogravimetric analysis curves for (A) a pristine PDMS polymer; and (B) an exfoliated PDMS-kenyaite nanocomposite. The loading of H-kenyaite for the composite is 10 wt %. The analysis was carried out in N_2 atmosphere with a heating rate of 5 °C/min.

6.4 Conclusions

The approach developed for the formation of thermoset polymer-layered silicate clay nanocomposites wherein curing agents can be directly intercalated into the clay galleries without the need for chemically inert quaternary alkylammonium ions on the exchange sites is successfully extended to the polysiloxane system. The technique provides nanocomposites with greatly improved solvent resistance with an expected improvement of the mechanical properties. This approach may also be expected to apply to the preparation of nanocomposites form a polysiloxane precursor with hydroxyl end groups. The PDMS-layered silicic acid nanocomposites also are chemically interesting precursors for the preparation of high surface area silica powders for potential adsorption and catalytic applications.

6.5 References

- 1. Giannelis, E. P. JOM 1992, 44, 28.
- 2. Okada, A.; Usuki, A. Mater. Sci. Eng. 1995, C3, 109.
- 3. Giannelis, E. P. Adv. Mater. 1996, 8, 29.
- 4. Pinnavaia, T. J.; Lan, T.; Wang, Z.; Shi, H.; Kaviratna, P. D. ACS Symp. Ser. 1996, 622, 250.
- 5. Lan, T.; Pinnavaia, T. J. Mater. Res. Soc. Symp. Proc. 1996, 435, 79.
- 6. Lan, T.; Kaviratna, P. D.; Pinnavaia, T. J. Chem. Mater. 1994, 6, 573.
- 7. Kojima, Y.; Usuki, A.; Kawasumi, M.; Okada, A.; Fukushima, Y.; Kurauchi, T.; Kamigaito, O. J. Mater. Res. 1993, 8, 1185.
- 8. Lan, T.; Pinnavaia, T. J. Chem. Mater. 1994, 6, 2216.
- 9. Messersmith, P. B.; Giannelis, E. P. Chem. Mater. 1994, 6, 1719.
- 10. Fukushima, Y.; Inagaki, S. J. Inclusion Phenom. 1987, 5, 473.
- 11. Fukushima, Y.; Okada, A.; Kawasumi, M.; Kurauchi, T.; Kamigaito, O. Clay Miner. 1988, 23, 27.
- 12. Usuki, A.; Kawasumi, M.; Kojima, Y.; Okada, A.; Kurauchi, T.; Kamingaito, O. *J. Mater. Res.* **1993**, 8, 1174.
- 13. Usuki, A.; Kojima, Y.; Kawasumi, M.; Okada, A.; Fukushima, Y.; Kurauchi, T.; Kamigaito, O. J. Mater. Res. 1993, 8, 1179.
- 14. Yano, K.; Usuki, A.; Okada, A.; Kurauchi, T.; Kamigaito, O. J. Polym. Sci., Part A: Polym. Chem. 1993, 31, 2493.
- 15. Kojima, Y.; Fukumori, K.; Usuki, A.; Okada, A.; Kurauchi, T. J. Mater. Sci. Lett. 1993, 12, 889.
- 16. Wang, M. S.; Pinnavaia, T. J. Chem. Mater. 1994, 6, 468.
- 17. Burnside, S. D.; Giannelis, E. P. Chem. Mater. 1995, 7, 1597.
- 18. Kurokawa, Y.; Yasuda, H.; Oya, A. J. Mater. Sci. lett. 1996, 15, 1481.
- 19. Usuki, A.; Kato, M.; Okada, A.; Kurauchi, T. J. Appl. Polym. Sci. 1997, 63, 137.
- 20. Clarson, S. J.; Semlyen, J. A. Siloxane Polymers; PTR Prentice Hall: Englewood Cliffs, NJ, 1993; p 315.
- 21. Odian, G. Principles of Polymerization, John Wiley & Sons, Inc. 1993; pp 138-140.

- 22. Mark, J. E.; Eisenberg, A.; Graessley, W. W.; Mandelkern, L.; Samulski, E. T.; Koenig, J. L.; Wignall, G. D. *Physical Properties of Polymers*, ACS, Washington, DC, 1993; pp 48-49.
- 23. Clarson, S. J.; Semlyen, J. A. *Siloxane Polymers*; PTR Prentice Hall: Englewood Cliffs, NJ, 1993; pp 637-638.
- 24. Pinnavaia, T. J. Science 1983, 220, 365.
- 25. Terlikovskii, E. V.; Kruglitskii, N. N. kompoz. Polim. Mater. 1982, 14, 18.
- 26. Fletcher, R. A.; Bibby, D. M. Clays Clay Miner. 1987, 35, 318.
- 27. Beneke, K.; Kruse, H. H.; Lagaly, G. Z. anorg. allg. Chem. 1984, 518, 65.
- 28. Kosuge, K.; Tsunashima, A. J. Chem. Soc., Chem. Commun. 1995, 2427.
- 29. Lagaly, G.; Beneke, K.; Weiss, A. Am. Mineral. 1975, 60, 650.

